
# STUDY ON DIMENSIONAL STABILITY OF ULTRA-HIGH PERFORMANCE CONCRETE (UHPC)

A Thesis submitted by

Linmei WU

For the award of

Doctor of Philosophy

2020

# Abstract

Ultra-high performance concrete (UHPC), a new cement-based material, has character of superior mechanical properties and excellent durability. Especially, it possesses compressive strength higher than 150 MPa, which is approximately 3 times as that of conventional concrete. UHPC is nearly impermeable to carbon dioxide, chlorides and sulphates. The superior durability leads to long service life with significantly reduced maintenance.

This thesis focuses on the dimensional stability of UHPC, which is one of the most significant factors of the material. Unlike in normal concretes which are mixed at a regular water/cement ratio (w/c = 0.32-0.5), UHPC usually consists of extremely low w/c (0.14-0.24). At the conditions of ultra-low w/c and high dose of superplasticizer, the hydration process of cement particles is different, resulting in the occurrence of high early age shrinkage. High autogenous shrinkage correlated with high binder content makes UHPC highly vulnerable to shrinkage cracking, which requires urgent resolution for its engineering application. On the other hand, at the conditions of ultra-low w/c, abundant amounts of un-hydrated cementitious materials in the matrix may affect the long-term performance of UHPC. The ongoing hydration of cement particles in UHPC has a retrieving effect on physicochemical properties of UHPC, also known as "autogenous/self-healing" products, which plays an important role in determining the microstructure of finally obtained UHPC. This project is proposed to conduct fundamental research on the dimensional stability (early age shrinkage and long-term stability) of cement with partial replacement of ultra-fine fly ash (UFA) under the UHPC condition, especially long-term stability of UHPC in different exposure conditions (the seawater, tap water or outdoors).

Results show that the addition of 30% UFA significantly improved the early-age as well as later-age compressive strengths of ordinary and high-volume fly ash concretes. The effectiveness of UFA in the blended system lies in producing high packing density and in accelerating the pozzolanic activity to produce more C–S–H gel by consuming calcium hydroxide (CH) in HVFA concretes. In the case of UHPC specimens exposed to seawater, the CH was efficiently even after 1080 days. TGA/DTG results indicated that the CH was consumed, which was accompanied by the formation of $CaCO_3$ (calcite), due to the

carbonation effect at outdoor conditions. Whereas for the water and seawater immersion conditions, the CH was transformed into other reaction products including $Mg(OH)_2$ and ettringite. Fiber addition improved the performance of fly ash based UHPC, because of the formation of a denser microstructure, as evidenced by the dramatic decrease in the diffusion coefficient and porosity. XRD and SEM analyses imply that the UHPC sample exposed to outdoor and seawater condition underwent less deterioration compared to fly ash (FA) containing UHPCs, more calcite was formed than the calcite formed in water condition. The surface layer of the sample immersed in seawater had some brucite and calcite formation as well as Friedel's salt and sulfoaluminates. However, under the outdoor condition, the surface pH dropped due to the penetration of $CO_2$ into the binder neutralizing the pore solution. As time passed, either large or small sized pores were formed in the seawater because of the expanding effect induced by ettringite, whereas for outdoor environments, the formation of calcites tended to promote the development of medium-sized pores.

Keywords: ultra-high performance concrete (UHPC); autogenous shrinkage; dimensional stability; microstructure development; steel fiber; ultra-fine fly ash; seawater; outdoors

## Certification of Thesis

This Thesis is entirely the work of **Linmei WU** except where otherwise acknowledged, with the majority of the authorship of the papers presented as a Thesis by Publication undertaken by the student. The work is original and has not previously been submitted for any other award, except where acknowledged.

Principal Supervisor: _____

Associate Supervisor: _____

Student and supervisors' signatures of endorsement are held at the University.

# Publications

## Journal papers

1. **Linmei Wu**, Nima Farzadnia, Caijun Shi, Zuhua Zhang, Hao Wang. Autogenous shrinkage of high performance concrete: A review, Construction and Building Materials, 149, 62-75 ***(Chapter 2)***
2. **Linmei Wu**, Z Zhang, H Wang. Combine tube test and ring test ultra-high performance concrete to predict the autogenous shrinkage of ultra-high performance concrete, Proceedings of the 1st RILEM International Conference on UHPC Materials and Structures, pp46-52, Oct 27-30, 2016, Changsha, China ***(Chapter 3)***
3. **Linmei Wu,** Caijun Shi, Zuhua Zhang, Hao Wang. Effects of Steel Fiber on Drying Shrinkage of Ultra High Performance Concrete. Materials Review, 23:007. September 2017 ***(Chapter 4)***
4. **Linmei Wu**, Zuhua Zhang, Hao Wang. Effects of ultra-fine fly ash (UFA) content on hydration mechanisms and microstructure development of ultra-high strength cement-based materials (UHSC), Proceedings of the International Conference on Construction Materials and Structure, Czech Republic, 2019. ***(Chapter 5)***
5. **Linmei Wu**, Zuhua Zhang, Hao Wang. Carbonation and chloride ingression depths in ultra-high performance concrete after long term exposure to different conditions, Construction and Building Materials, under review ***(Chapter 6)***
6. **Linmei Wu**, Nima Farzadnia, Caijun Shi, Zuhua Zhang, Hao Wang, Long-term performance of ultra-high performance concrete (UHPC) in different exposure conditions, Construction and Building Materials, under review ***(Chapter 7)***
7. **Linmei Wu,** Peng Liu, Zuhua Zhang, DeJu Zhu, Hao Wang. Multiscale modeling for high-performance concrete: a review. International Journal for Multiscale Computational Engineering 16.1 (2018).

# Statement of Contribution

The following detail is the agreed share of contribution for candidate and co-authors in the presented publications in this thesis:

- **Article I:** Wu, Linmei, Nima Farzadnia, Caijun Shi, Zuhua Zhang, and Hao Wang. "Autogenous shrinkage of high performance concrete: A review." Construction and Building Materials 149 (2017): 62-75. Impact Factor: 3.485 and SNIP: 2.309). DOI: https://doi.org/10.1016/j.conbuildmat.2017.05.064

  The overall contribution of ***Linmei Wu*** was 65% to the concept development, analysis, drafting and revising the final submission; ***others*** contributed the other 35% to concept development, analysis, editing and providing important technical inputs.

- **Article II:** Wu, Linmei, Peng Liu, Zuhua Zhang, DeJu Zhu, and Hao Wang. "Multiscale modeling for high-performance concrete: a review." International Journal for Multiscale Computational Engineering 16, no. 3 (2018). (Impact Factor: 1.016 and SNIP: 0.68). DOI:https://10.1615/IntJMultCompEng.2018022827

  The overall contribution of ***Linmei Wu*** was 60% to the concept development, analysis, drafting and revising the final submission; ***others*** contributed the other 40% to concept development, analysis, editing and providing important technical inputs.

- **Article III:** Linmei Wu, Caijun Shi, Zuhua Zhang, Hao Wang. Effects of Steel Fiber on Drying Shrinkage of Ultra High Performance Concrete. Materials Review, 23:007. September 2017. (Impact Factor: 0.992 and SNIP0.531).

  The overall contribution of ***Linmei Wu*** was 65% to the concept development, analysis, drafting and revising the final submission; ***others*** contributed the other 35% to concept development, analysis, editing and providing important technical inputs.

- **Article IV:** Linmei Wu, Peng Liu, Caijun Shi, Zuhua Zhang, Tinh Quoc Bui, and Dengwu Jiao. "Edge-based smoothed extended finite element method for dynamic fracture analysis." Applied Mathematical Modelling 40, no. 19-20 (2016): 8564-8579. (Impact Factor: 2.617 and SNIP: 1.394).
  DOI: https://doi.org/10.1016/j.apm.2016.05.027

  The overall contribution of ***Linmei Wu*** was 60% to the concept development, analysis, drafting and revising the final submission; ***others*** contributed the other 40% to concept development, analysis, editing and providing important technical inputs.

- **Article V:** Xiaoluo Cao, Linmei Wu and Z.henming Li, "Behaviour of steel-reinforced concrete columns under combined torsion based on ABAQUS FEA." Engineering Structures 40, no. 19-20 (2019): 8564-8579. (Impact Factor: 3.084 and SNIP: 2.089).
  DOI: https://doi.org/10.1016/j.engstruct.2019.109980

  The overall contribution of ***Linmei Wu*** was 60% to the concept development, analysis, drafting and revising the final submission; ***others*** contributed the other 40% to concept development, analysis, editing and providing important technical inputs.

# Acknowledgements

I would like to thank the following people, without whom I would not have been able to complete this research and make it through my PhD degree. Firstly, I want to thank the Centre for Future Materials (CFM) team at University of Southern Queensland (USQ). I would like to acknowledge my principal supervisor professor Hao Wang whose Jobs inspired my interest in the development of innovative technologies; and my associate supervisor Dr. Zuhua Zhang whose insight and knowledge into the subject matter steered me through this research. And I would also like to show my special thanks to Professor Caijun Shi, for his guidance through each stage of the process. Their invaluable advices and supports greatly smooth the path to accomplishing my research project. They are the ultimate role models. I am extremely grateful.

I would like to acknowledge the financial support received from the University of Southern Queensland for conducting the background work for this research. I would also like to thank my colleagues at the CFM for their moral, technical, and financial support. I also would like to thank all the people who create a research-conductive atmosphere in the laboratories. The support of the School of Civil Engineering of Hunan University is also highly appreciated.

Finally, I wish to show my gratitude to Damon who provided unending inspiration, and my family for their continuous support and encouragement.

# Table of Contents

**ABSTRACT** ..... **1**
**CERTIFICATION OF THESIS** ..... **3**
**PUBLICATIONS** ..... **4**
**STATEMENT OF CONTRIBUTION** ..... **4**
**ACKNOWLEDGEMENTS** ..... **7**
**TABLE OF CONTENTS** ..... **8**
**LIST OF FIGURES** ..... **13**
**LIST OF TABLES** ..... **17**
**CHAPTER 1 INTRODUCTION** ..... **19**
**1.1 Background** ..... **19**
**1.2 Introduction** ..... **23**
**1.3 Aim and objectives of the research** ..... **25**
1.3.1 Research gap ..... 25
1.3.2 Objectives of the research ..... 26
**1.4 Outline of the thesis** ..... **27**
**1.5 The Technology Road map** ..... **30**
**1.6 References** ..... **34**
**CHAPTER 2 LITERATURE REVIEW** ..... **37**
**2.1 Introduction** ..... **37**
**2.2 Hydration of UHPC** ..... **38**
2.2.1 The influence of ultra-fine fly ash on hydration ..... 40
2.2.2 Benefits of UFFA in UHPC ..... 42
**2.3 Microstructure of UHPC** ..... **44**
**2.4 Shrinkage of concrete** ..... **46**
2.4.1 Autogenous shrinkage ..... 47
2.4.2 Chemical shrinkage ..... 47
2.4.3 Thermal shrinkage ..... 50
2.4.4 Carbonation shrinkage ..... 51
**2.5 Mechanism of autogenous shrinkage** ..... **51**
2.5.1 Pore Structure ..... 53
2.5.2 Relative humidity ..... 54

2.5.3 Self-stress ..... 55
2.5.4 Degree of hydration ..... 56
**2.6 Interface structure ..... 56**
**2.7 Influential factors on autogenous shrinkage ..... 57**
2.7.1 Cement ..... 57
2.7.2 Supplementary cementitious materials ..... 59
2.7.3 Fibers67
2.7.4 Chemical admixtures ..... 71
**2.8 Conclusions and Outlook ..... 75**
2.8.1 Concluding remarks ..... 75
2.8.2 Research needs ..... 76
**2.9 References ..... 77**
**CHAPTER 3 EVALUATION OF FIBRE ON AUTOGENOUS SHRINKAGE OF ULTRA-HIGH PERFORMANCE CONCRETE BY RING TEST .....** ERROR! BOOKMARK NOT DEFINED.
**3.1 Introduction ..... 87**
**3.2 Test program ..... 90**
3.2.1 Raw materials ..... 90
3.2.2 Mixture proportions ..... 91
3.2.3 Mixing procedure and sample preparation ..... 91
**3.3 Test procedures ..... 92**
3.3.1 Unrestrained autogenous shrinkage test: autogenous shrinkage corrugated tube measurement ..... 92
3. 3. 2 Restrained autogenous shrinkage test: ring test ..... 92
**3.4 Results and discussion ..... 94**
3.4.1 Unrestrained autogenous shrinkage ..... 94
3.4.2 Restrained autogenous shrinkage ..... 95
3.4.3 Comparison of the two testing methods ..... 96
**3.5 Theoretical models of autogenous shrinkage ..... 98**
**3.6 Conclusion ..... 106**
**3.6 References ..... 107**
**CHAPTER 4 EFFECTS OF STEEL FIBER ON DRYING SHRINKAGE OF ULTRA HIGH PERFORMANCE CONCRETE ..... 110**
**4.1 Introduction ..... 111**
**4.2 Experimental program ..... 113**

4.2.1 Raw materials....113
4.2.2 UHPC Mixture proportions....114
4.2.3 Mixing procedure and specimen preparation....115
4.2.4 Workability test....115
4.2.5 Drying shrinkage test....116
4.2.6 Mass change....116
4.2.7 Scanning electron microscopy....116
**4.3 Experimental results....117**
4.3.1 Effect of steel fiber content on the workability of UHPC....117
4.3.2 Effect of steel fiber content on the drying shrinkage of UHPC....118
4.3.3 SEM images of interface between fiber and UHPC matrix....119
**4.4 Discussion....122**
4.4.1 The evolution of drying shrinkage against curing age for UHPC....122
4.4.2 The comparisons between different equations....123
4.4.3 UHPC Drying shrinkage mechanism....125
**4.5 Conclusion....129**
**4.6 References....130**
**CHAPTER 5 CHAPTER 5EFFECTS OF ULTRA-FINE FLY ASH UFA CONTENT ON EARLY AGE SHRINKAGE AND MICROSTRUCTURE DEVELOPMENT OF ULTRA-HIGH STRENGTH CEMENT BASED MATERIALS..... .....**ERROR! BOOKMARK NOT DEFINED.
**5.1 Introduction....136**
**5.2 Test program....138**
5.2.1 Raw materials....138
5.2.2 Mixture proportions....139
5.2.3 Test procedures....139
5.2.4 FTIR spectrum analysis....142
**5.3 Results and Discussion....142**
5.3.1 Effect of UFA content on flowability of fresh UHSC....142
5.3.2 Effect of UFA content on compressive strength of UHSC....143
5.3.3 Effect of UFA content on micro hardness of UHSC....144
5.3.4 Autogenous shrinkage....145
5.3.5 XRD of UFA....146

5.3.6 Effect of UFA content on heat of hydration of UHSC....147
5.3.7 FTIR of UHSC Mixtures....148
5.3.8 SEM of UHSC Mixtures....150
**5.4 Conclusion....151**
**5.5 References....152**
**CHAPTER 6 MICROSTRUCTURE DEVELOPMENT OF ULTRA-HIGH PERFORMANCE CONCRETE AFTER LONG TERM EXPOSURE TO DIFFERENT CONDITIONS....155**
**6.1 Introduction....156**
**6.2 Experimental program....158**
6.2.1 Raw materials....158
6.2.2 Mixture proportions....159
6.2.3 Mixing procedure and specimen preparation....159
6.2.4 Exposure conditions....160
6.2.5 Testing methods....162
**6.3 Results and discussion....164**
6.3.1 Effect of steel fiber content on flowability of fresh UHPC....164
6.3.2 Carbonation degree of UHPC....164
6.3.3 TG/DTG analyses....165
6.3.4 CH content....170
6.3.5 Analysis of XRDA test results....171
6.3.6 Pore structure characteristics....173
6.3.7 SEM/EDX....177
**6.4 Conclusion....179**
**6.5 References....180**
**CHAPTER 7 LONG-TERM PERFORMANCE OF ULTRA-HIGH PERFORMANCE CONCRETE (UHPC) UNDER DIFFERENT EXPOSURE CONDITIONS....184**
**7.1 Introduction....184**
**7.2 Experimental program....187**
7.2.1 Raw materials....187
7.2.2 Mixture proportions....187
7.2.3 Mixing procedures and specimen preparation....188
7.2.4 Exposure conditions....188
**7.3 Testing methods....190**
7.3.1 Workability....190

7.3.2 Compressive strength....190
7.3.3 Nitrogen adsorption and desorption (NAD) analysis....190
7.3.4 Dimensional stability....190
7.3.5 Mass change....191
7.3.6 Thermogravimetric analysis (TGA)....191
7.3.7 X-ray diffractometry (XRD)....192
7.3.8 Scanning electron microscopy (SEM)....192
**7.4 Experimental results....192**
7.4.1 Workability....192
7.4.2 Porosity....193
7.4.3 Compressive strength development....194
7.4.4 Dimensional stability....197
7.4.5 Mass change....201
**7.5 Discussion....203**
**7.6 Conclusion....210**
**7.7 References....211**
**CHAPTER 8 CONCLUSIONS AND FUTURE WORK....218**
**8.1 General discussion....218**
**8.2 Conclusions....219**
**8.3 Future work....222**
**REFERENCES.....223**
**APPENDIX....254**
***A1. The bending failure morphology of the UHPC samples*....254**
***A2. Three point bending load displacement curve of slag containing UHPC*....254**
***A3. Three point bending load displacement curve of fly ash containing UHPC*....255**
***A4. Steel fibres (3%) distribution of the sample F4*....255**

# List of Figures

Chapter 1

**Figure 1-1.** The Sherbrook Bridge in Quebec. ..... 22
**Figure 1-2.** The frame of the thesis. ..... 32
**Figure 1-3.** Process-microstructure-property relationship. ..... 33

Chapter 2

**Figure 2-1.** Time dependent phase development in OC and UHPC (Korpa et al., 2009). ..... 39
**Figure 2-2.** Q0 to Q4 percentages for samples with heat treatment at 90℃, 200℃, 250℃ for 8 hours (Zanni et al., 1996). ..... 40
**Figure 2-3.** SEM image in UHPC (C. Wang et al., 2012). ..... 46
**Figure 2-4.** The relationship between chemical shrinkage and autogenous shrinkage (L. Wu et al., 2017b). ..... 48
**Figure 2-5.** Autogenous and drying shrinkage of mortars with a) limestone powder b) slag (Itim et al., 2011). ..... 50
**Figure 2-6.** Schematic diagram of capillary water tension. ..... 52
**Figure 2-7.** Effect of the fineness of cement on a) relative humidity b) autogenous shrinkage (Dale P Bentz et al., 1999). ..... 58
**Figure 2-8.** Effect of silica fume content on autogenous shrinkage of concrete with low water-to- cement ratio from (M. Zhang et al., 2003). ..... 60
**Figure 2-9.** Effect of slag content on autogenous shrinkage of concrete with low water to binder ratio adopted from (K. M. Lee et al., 2006). ..... 61
**Figure 2-10.** Effect of water-to-binder ratio on autogenous shrinkage of high performance concrete from (M. Zhang et al., 2003). ..... 64
**Figure 2-11.** Schematic diagram of shrinkage crack in the interface area from (Ling Qi, 1996). ..... 65
**Figure 2-12.** Autogenous shrinkage resulting with addition of aggregate from mortar (paste volume = 57%) to concrete (paste volume = 34%) at w/c ratio = 0.30 from (Holt, 2005) . ..... 65
**Figure 2-13.** Comparison of autogenous shrinkage of lightweight aggregate concrete and normal concrete (LWC: lightweight concrete; NWC: normal weight concrete; SSD: saturated surface dry; AD: air dry. ..... 67
**Figure 2-14.** Autogenous shrinkage of plain and steel fiber-reinforced concrete specimens (CRC : compact reinforced composite) from (Loukili, Khelidj, & Richard, 1999). ..... 68

**Figure 2-15.** The effect of PP and carbon fibres on the autogenous shrinkage of pastes form (Kaufmann et al., 2004). 70
**Figure 2-16.** Linear autogenous deformation of mortar specimens with and without cellulose fiber addition (Zeroed to time of final set) from (Kawashima & Shah, 2011). 71
**Figure 2-17.** Autogenous shrinkage of paste specimens containing various contents of MEA and AEA under non-wet curing condition. 74

Chapter 3

**Figure 3-1.** Test steel ring (Note: Dimensions are in millimetres). 89
**Figure 3-2.** Ring test. 93
**Figure 3-3.** Development of autogenous shrinkage of UHPC. 95
**Figure 3-4.** The development of strain along circle direction at middle location of the surface of the steel ring with age. 96
**Figure 3-5.** Free and restraint Autogenous shrinkage deformation of chart of UHPC bar. 98
**Figure 3-6.** Circular ring under surface pressure 101
**Figure 3-7.** Decomposing of concrete-steel composite ring. 102
**Figure 3-8.** Comparison between effective shrinkage strain and free shrinkage of UHPC. 105

Chapter 4

**Figure 4-1.** Effect of steel fiber content on workability of slag containing (K) and fly ash containing (F) UHPC mixtures. 118
**Figure 4-2.** Effect of steel fiber content on drying shrinkage of UHPC. 118
**Figure 4-3.** Effect of steel fiber content on mass loss of UHPC. 119
**Figure 4-4.** SEM images of the slag containing sample with 2% steel fiber at 3 days. 120
**Figure 4-5.** SEM images of the fly ash containing sample with 2% steel fiber at 3 days. 121
**Figure 4-6.** SEM images of the slag containing sample with 2% steel fiber at 120 days. 122
**Figure 4-7.** SEM images of the fly ash containing sample with 2% steel fiber at 120 days. 122
**Figure 4-8.** A typical graph of drying shrinkage of hardened cement paste (Courtial et al., 2013). 127

Chapter 5

**Figure 5-1.** Effect of UFA Content on Flowability of Fresh UHSC Mixtures. 143
**Figure 5-2.** Effect of UFA Content on mechanical properties of Fresh UHSC 144

**Figure 5-3.** Effect of UFA Content on micro hardness of UHSC Mixtures.....145
**Figure 5-4.** Effect of UFA Content on autogenous shrinkage of UHSC Mixtures.....146
**Figure 5-5.** XRD pattern of UHSC Mixtures.....147
**Figure 5-6.** Effect of UFA Content on rate of hydration of UHSC Mixtures. .....148
**Figure 5-7.** Effect of UFA Content on FTIR of U0 and U2.....149
**Figure 5-8.** Effect of UFA Content on FTIR of UHSC Mixtures. .....150
**Figure 5-9.** SEM images of UHSC Mixtures specimen.....151

Chapter 6

**Figure 6-1.** The mixing and preparation procedure of UHPC specimens. .....160
**Figure 6-2.** Slicer. .....160
**Figure 6-3.** Mean values of temperature and humidity change of Changsha during the exposure time.....161
**Figure 6-4.** Effect of steel fiber contents on flowability of slag containing (K) and fly ash containing (F) UHPC mixtures. .....164
**Figure 6-5.** Sectional colour image of UHPCs sprayed with a phenolphthalein solution. .....165
**Figure 6-6.** TG and DTG curves of UHPCs exposure to different environment after 28 d. .....166
**Figure 6-7.** TGA curves of UHPCs after exposure to different conditions after 360d and 1080d.....168
**Figure 6-8.** TGA curves of UHPCs with steel fiber after exposure to different conditions after 90d and 1080d. .....169
**Figure 6-9.** TGA curves of UHPCs after exposure to different conditions.....170
**Figure 6-10.** Amount of CH formed in UHPC samples with age. .....171
**Figure 6-11.** XRD patterns of F-0 after exposure to different conditions.....172
**Figure 6-12.** Effects of different environment on porosity and pore size distribution of UHPCs.....174
**Figure 6-13.** The pore analysis of K0 and F0, respectively after 1080-day immersion in seawater.....176
**Figure 6-14.** SEM images of specimens after exposure. .....178
**Figure 6-15.** Surface appearance and internal fibers of specimen F-3 exposed to seawater after 1080 days.....179

Chapter 7

**Figure 7-1.** Mean values of temperature and humidity change of Changsha during the exposure time.....189
**Figure 7-2.** Effect of steel fiber contents on flowability of slag containing (K) and fly ash containing (F) UHPC mixtures. .....193

**Figure 7-3.** Cumulative pore volume and Pore size distributions in K0 and F0 as calculated by the BJH method with desorption data.....194
**Figure 7-4.** Compressive strength development of UHPCs under the three exposure conditions. .....195
**Figure 7-5.** Length change of UHPCs under different exposure conditions: (a), (c), (e) slag containing UHPC specimens; (b), (d), (f) fly ash containing UHPC specimens. ....200
**Figure 7-6.** Mass change of UHPCs under different exposure conditions: (a), (c), (e) slag containing UHPC specimens; (b), (d), (f) fly ash containing UHPC specimens. .....202
**Figure 7-7.** Surface appearance and internal fibers of specimen F-3 exposed to seawater after 720 days. .....205
**Figure 7-8.** SEM images of specimens after exposure. .....206
**Figure 7-9.** TGA curves of UHPCs after exposure to different conditions.....207
**Figure 7-10.** XRD patterns of F-0 after exposure to different conditions at 720 d. ....207

# List of Tables

Chapter 3

**Table 3-1:** Physical properties of Portland cement P.I 42.5 ..... 90
**Table 3-2:** Chemical compositions of cementitious materials (%) ..... 90
**Table 3-3:** Mixture proportions of UHPC ..... 91
**Table 3-4:** The shrinkage strain rate α of mixes by the corrugated tube test ..... 97

Chapter 4

**Table 4-1:** Chemical composition of material (mass %) ..... 114
**Table 4-2:** Physical and mechanical properties of cement ..... 114
**Table 4-3:** Sieve analysis of river sand ..... 114
**Table 4-4:** Mixture ratio of UHPC ..... 115
**Table 4-5:** Comparison of experiment data with the calculated results ..... 123
**Table 4-6:** Regression results for the relationship between drying shrinkage and time of UHPC ..... 124

Chapter 5

**Table 5-1:** Physical properties of cement. ..... 138
**Table 5-2:** Chemical composition of materials (%). ..... 138
**Table 5-3:** Mixture proportions of UHSC. ..... 139

Chapter 6

**Table 6-1:** Physical properties of Portland cement P.I 42.5 ..... 158
**Table 6-2:** Chemical composition of cementitious materials (weight %), LOI is loss on ignition. ..... 158
**Table 6-3:** Mixture proportions of UHPCs. ..... 159
**Table 6-4:** The compositions of the natural seawater in the Gulf of China (NS), the ASTM D-14 specified artificial seawater (AS1) and the artificial seawater used in this study (AS2) (g/L). ..... 161
**Table 6-5:** MIP results of UHPC. ..... 174
**Table 6-6:** Characteristic properties of UHPC specimens. ..... 177

Chapter 7

**Table 7-1:** Physical properties of Portland cement P.I 42.5 ..... 187
**Table 7-2:** Chemical composition of cementitious materials (weight %), LOI is loss on ignition. ..... 187
**Table 7-3:** Mixture proportions of UHPCs. ..... 188

**Table 7-4:** The compositions of the natural seawater in the Gulf of China (NS), the ASTM D-14 specified artificial seawater (AS1) and the artificial seawater used in this study (AS2) (g/L). .....190

# CHAPTER 1 INTRODUCTION

## 1.1 Background

Nowadays, cement and concrete are building materials most widely-used in a variety of applications, such as hydroelectric project, constructional engineering, high-speed rail, nuclear power project, freeway, marine engineering, and large-scale bridge.(Fowler, 1999). However, the safety of those structure is under influences of both the natural and the man-made factors. In addition, natural disasters, including marine corrosion, typhoon, earthquake, and environmental effects, such as freezing and thawing, alkali-aggregate reaction, salt physical attack, can also cause serious damage to present concrete structure and construction. As concrete is the basic material for mega infrastructures, the diversification and complication of modern structures pose high requirements for concrete(Rip & Kemp, 1998), which cannot be fulfilled with traditional concrete technology. Therefore, to prolong the service life of concrete buildings, the concrete having high strength (small component size), superb toughness and durability is needed

UHPC is a steel fiber reinforced concrete, consisting of an optimized gradation of fine powders and a very low water to cementitious materials ratio (R Yu, P Spiesz, & HJH Brouwers, 2014). It exhibits enhanced strength, durability and ductility properties when compared to normal concrete or high-performance concrete. UHPC can cope with the challenges from modern structures (C. Shi, Wu, Xiao et al., 2015a). UHPC is regarded as the most promising and manipulable material. As a new cement-based material, UHPC has advantages over traditional concrete because of its superior mechanical properties and excellent durability. UHPC usually possesses compressive strength higher than 150 MPa, which is approximately 3 times stronger than the conventional concrete. Due to incorporation of steel fibre, the ductility and energy absorption capacity of UHPC are typically 300 times greater than that of high-performance concrete. UHPC is nearly impermeable to carbon dioxide, chlorides and sulphates(Z. Wu, Shi, He, & Wu, 2016). The superior durability performance of UHPC leads to a long service life, which significantly reduces the maintenance frequency. In addition, UHPC could easily meet the

requirements for different structural applications, it has the potential of being the most suitable building materials for modern buildings.

However, the UHPC also has drawbacks, especially the large shrinkage and cracking occurred in the early-age, owing to the autogenous shrinkage and drying shrinkage. Besides, large amounts of un-hydrated cementitious materials in the matrix also affect the long-term performance of UHPC (D. Wang et al., 2016). The ongoing hydration of cement particles in UHPC has a retrieving effect on physicochemical properties of UHPC, also known as "autogenous/self-healing" products, which plays an important role in determining the microstructure of finally obtained UHPC. Until now, only little experience has been gathered concerning the application of UHPC in practice. Hence its long-term behaviour remains unclear.

Unlike normal concrete (NC), UHPC behaves differently under long-term efforts, especially creep, shrinkage or long-term deflections. It is reported that– the UHPC reinforced with steel-fibres has properties, like compressive strength higher than 150 MPa and tensile strength higher than 20 MPa (Su, Li, Wu, Wu, & Li, 2016). It is reported that (Bărbos, 2016) the creep of UHPC samples is significantly reduced if the concrete is subjected to heat treatment or contains steel-fibre reinforcement (V. Garas, Kurtis, & Kahn, 2012; V. Y. Garas, Kahn, & Kurtis, 2009). It is important to know the structural elements made of this type of concrete work in service life under long-term loadings. The results obtained on UHPC samples, regarding creep straining from tension or compression efforts may not be researched when UHPC was used as structural elements (e.g. beams, slabs, columns) and subjected to bending(Smith et al., 2014; Van Damme, 2018). To solve this problem, Caijun Shi recommended to understand the influence of the heat treatment and steel-fiber addition on the rheological phenomena of UHPC bended beams(C. Shi, Wu, Lv, & Wu, 2015).

After 50 years of research, the development of fibre reinforced concrete has matured to the stage, where UHPC has found increasing application in practice and acquired true technological significance. In the U.S. and many European countries, standards are developed for the structural applications of UHPC. In Australia, the rationale behind standards rules for development of structural application in UHPC has been discussed. UHPC is produced by mixing cement, slag, silica fume, and/or fly ash, with superplasticizer. At the conditions of ultra-low w/c and high dose of superplasticizer, the

hydration of cement particles differs from the cement hydration in normal concrete (C. Shi, Wu, Wang, & Wu, 2014; XIANG, SHI, WU, & CHONG, 2015).

In addition, high strength of UHPC reduces the cross-sectional area of structural components and materials consumption (Fehling, Schmidt, Walraven, Leutbecher, & Fröhlich, 2014), UHPC displayed the extremely low permeability and excellent durability, which could apply to the severe environment, UHPC has no chloride penetration depth after 96 hours of non-steady state migration test, UHPC has no mass loss after 1000 cycles of freezing and thawing test. UHPC can meet most of the demands of modern structure, such as: high-rise building with a height above 1000m, super large-span thin structure, offshore oil production platform, wind power generation bar, wind turbine blade, etc.

UHPC can show compressive strength over 150 MPa, approximately three times as that of conventional concrete, high ductility and excellent durability(I. H. Yang, Joh, & Kim, 2010). Use of ultrafine fly ash and superplasticizer can help to achieve this performance. The French firm Bouygues SA developed the reactive powder concrete originally(Oliver Bonneau, Poulin, Dugat, & Tcin, 1996), which is engineered to be a highly compacted concrete with a small, disconnected pore structure that helps to minimize many of the limitations of typical UHPCs. These advancements are achieved through a combination of finely ground powders and the elimination of coarse aggregates. The addition of small steel fibers to the mix is responsible for much of the tensile strength and toughness of the material.

Numerous other countries already employed UHPC in different structural applications. Canada and South Korea have used UHPC for pedestrian bridges: the Sherbrooke Bridge in Quebec (Blais & Couture, 1999a) (Figure 1-1), Canada, was built in 1997, a pedestrian bridge of 190 ft. with a deck thickness of only 1.25 int.; and the footbridge of Peace in Seoul, Korea, was built in 2002. The span of this bridge is 400 ft. and its deck thickness are 1.25 in. Portugal has employed it for seawall anchors, Australia has committed to its use in a vehicular bridge, and France has used it in building power plants. In all of these cases, the material was chosen for its ability to stand up to high stress, both environmental and load-related. The increasing deployment of UHPC worldwide and results of FHWA's testing of the product bode well for its future use.

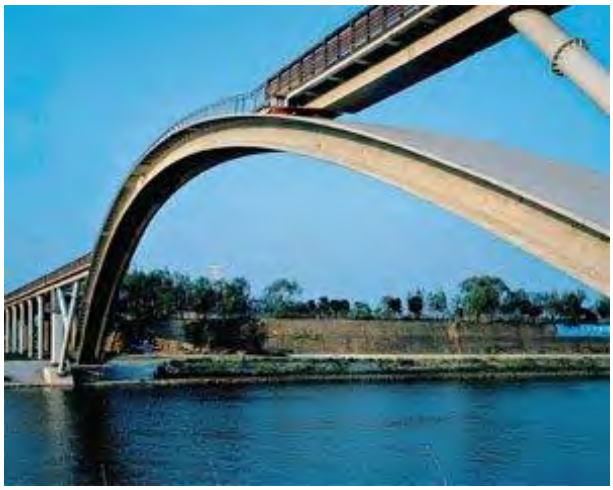

**Figure 1-1.** The Sherbrook Bridge in Quebec.

Pioneering fundamental research in Australia has led to the success in the advanced manufacturing of UHPC. Several construction projects adopted UHPC, such as the opening of Shepherd's Gully Bridge 150 km north of Sydney in 2005, Australia was amongst the leaders in the world in the utilization of ultra-high performance UHPC for road bridge construction. These activities have put Australia in a leading position of UHPC manufacturing in the world, and boost the interests of using this green material in construction and building sectors. It is glad to see that the standardization and regulatory barriers are being removed step by step through the domestic and international collaboration efforts from both academic and industrial sectors in the past 20 years. However, a critical technical issue still barriers today's large-scale production: how to control the durability of UHPC which is formed by using intrinsically variable industrial by-products as raw materials?

This question is of critical importance in enabling the wider uptake of UHPC, and in particular its attractiveness to designers and specifiers, who require fundamentally-based information regarding the likely service life of a material or structural element before they can confidently recommend its use to a client. Embarrassingly, the long-term performance of UHPC has been subjected to detailed investigation only very recently. And there is a lack of understanding of the autogenous shrinkages of UHPC, thus very few approaches available that can convincingly guild the early age cracking and long-term stability towards a more desirable direction. There is an urgency to find solutions to this question to turn the economic and environmental potentials of using UHPC into realistic benefits in industry and our life.

## 1.2 Introduction

The study of UHPC has become an interest of many researchers owing to its high strength, low permeability, and outstanding performance. Due to the use of superplasticizer, low water to cement ratio, highly fine sand and absence of coarse aggregate, the amount of cement used in UHPC is relatively high (commonly over 900 kg/m$^3$) (C. Shi, Wang, Wu, & Wu, 2015b; Van Tuan, Ye, Van Breugel, & Copuroglu, 2011; R Yu, Przemek Spiesz, & HJH Brouwers, 2014). Currently, the global concrete producing makes up more than five percent of anthropogenic carbon dioxide emissions each year, namely from the production of cement (Van den Heede & De Belie, 2012). To minimize the $CO_2$ emissions, researchers are making constant efforts to reduce the cement content in UHPC by adding various supplementary cementitious materials (SCMs) as a substitute. Therefore, how to produce UHPC with less cement and lower emission while providing the equivalent properties remains an open issue (Lothenbach, Scrivener, & Hooton, 2011).

UHPC can provide great structure reliability even under overload conditions or earthquakes (Blais & Couture, 1999b; Dauriac, 1997; Dowd, 1999). UHPC is nearly impermeable to carbon dioxide, chlorides and sulphates. Its superior durability leads to long service life with reduced maintenance. The enhanced abrasion resistance provides extended life for bridge decks and industrial floors(Dauriac, 1997), while the enhanced corrosion resistance provides protection to areas with bad or harsh climate conditions(Tam, Tam, & Ng, 2012). A significant amount of unhydrated cement in the finished product provides a self-healing potential under cracking conditions (Dauriac, 1997). UHPC structures weigh only one-third or one-half of the corresponding conventional concrete structures. This weight reduction has benefit in producing more slender structures, increasing usable floor space in high-rise buildings and reducing overall costs (Blais & Couture, 1999b; Dauriac, 1997; Ng, Tam, & Tam, 2010). Elimination of steel reinforcement bars reduces labor costs and provides greater architectural freedom, allowing nearly limitless structural member shapes and forms for architects and designers (Blais & Couture, 1999b; Dauriac, 1997; Dowd, 1999). Although UHPC possesses many outstanding properties, they also have some weaknesses. High binder content of about 800-1000 kg/m$^3$ affects not only the production costs, but also high heat of hydration, causing shrinkage problems(Yazıcı, Yardımcı, Aydın, & Karabulut, 2009).

Moreover, UHPC is generally costly and cannot replace the conventional concrete in most applications where the conventional concrete can economically meet the performance criteria. the main reason limiting their broader use is the high cost coming from a number of expensive components used in UHPC mixes, particularly the cement and silica fume, and the steel fibers. A typical strain hardening UHPFRC, has 1100-1300 kg/m$^3$ of cement, and 200-350 kg/m$^3$ of silica fume which is 18-26% of the mass of the binder (Kazemi Kamyab, 2013; Park, Kim, Ryu, & Koh, 2012; Rossi, 2013). Due to the ultra-low water content in UHPC (W/B=0.14-0.20), the hydration degree of cement is only 30-40% (Korpa, Kowald, & Trettin, 2009), and the reaction degree of silica fume is also low, approximately 30% (Kazemi Kamyab, 2013; Schachinger, Hilbig, Stengel, & Fehling, 2008), which means a significant quantity of unhydrated cement clinker and unreacted silica fume particles serve as expensive fillers.

Therefore, it is of great interest to study the possibility of using other materials to partially replace the cement in UHPC mixes. Much attention has been devoted to reducing the cement content in UHPC. For instance, Ghafari et al. (Ghafari, Costa, Júlio, Portugal, & Durães, 2014)utilized about 950 kg/m$^3$ cement and 250 kg/m$^3$ silica fume to produce UHPC. El-Dieb (A. S. El-Dieb, 2009) produced ultra-high performance fiber reinforced concrete (UHPFRC) with about 775 kg/m$^3$ cement and 135 kg/m$^3$ silica fume. Hassan et al. (Hassan, Jones, & Mahmud, 2012) exhibited mechanical investigation with 657 kg/m$^3$ cement, 418 kg/m3 Ground Granulated Blast Furnace Slag (GGBS) and 119 kg/m$^3$ silica fume. Aldahdooh et al. (Aldahdooh, Bunnori, & Johari, 2013) utilized 638 kg/m$^3$ cement to produce UHPC with compressive strength of 120 MPa. Yu et al. (Jisong Zhang & Zhao, 2016)presented an experimental study of compressive strengths that reach around 100 MPa with 620 kg/m$^3$ cement content.

With the application of fly ash concrete for more than ten years history, the concrete mixed with fly ash, not only can partially replace cement, reduce the project cost, but also can improve and enhance the performance of concrete. So, fly ash is the ideal concrete admixture. The use of fly ash is accepted in recent years primarily because of resulting economy from saving cement, secondly because of consuming industrial wastes and thirdly because of making durable materials. Fly ash has larger output and critical contamination in China, the development of ultrafine fly ash used in HPC is the first

priority. The replacement of cement by ultrafine fly ash can not only improve the properties of concrete, but also increase the green degree of concrete.

## 1.3 Aim and objectives of the research

### 1.3.1 Research gap

Over the last twenty years, remarkable advances have taken place in the research and application of UHPC which exhibits excellent rheological behaviours that include workability, self-placing and self-densifying properties, improved in mechanical and durability performance with very high compressive strength, and non-brittleness behaviour. These excellent properties of UHPC will lead to reduction in size and self-load of structural elements, increase in their resistance to earthquake and seawater attack. Thus, it is a concrete material that is very suitable for engineering construction in Australia. Unlike in normal concretes which are mixed at a regular water/cement ratio (w/c = 0.32-0.5), the mix of UHPC usually consists of extremely low w/c (0.14-0.24), high dose of superplasticizer and supplementary cementitious materials (SCMs), such as silica fume. At the conditions of ultra-low w/c and high dose of superplasticizer, the hydration of cement particles differs from the normal hydration (C. Shi, Wang et al., 2015b; XIANG et al., 2015). High autogenous shrinkage correlated with high binder content makes UHPC highly vulnerable to shrinkage cracking, which requires urgent addressment for its engineering application(L. Wu, Farzadnia, Shi, Zhang, & Wang, 2017b). A comprehensive understanding of the influence of affecting factors on autogenous shrinkage of UHPC is of great significance to evaluate early-age cracking potential. On the other hand, abundant amounts of un-hydrated cementitious materials in the matrix may affect the long-term performance of UHPC. Due to ongoing hydration, it has a retrieving effect on physicochemical properties of UHPC, also known as “autogenous/self-healing” products and microstructure are determined. However, the eager industry still faces a question: Are UHPC stable and durable? This is widely concerned because the construction industry needs to ensure a service life of decades, even longer. The difficulties to answer this question result from (1) early-age shrinkage and cracking, (2) long-term stability (3) the uncertainty of whether the existing durability tests for Portland cement concrete are still valid in assessing UHPC.

The ultimate aim of this project is proposed to conduct fundamental research on the early-age shrinkage and long-term stability of UHPC, their micromechanics, formation kinetics and stability, to ensure highly durable products. Based on systematic experimental studies on setting and hardening process, microstructure development, deformation, increase of toughness, constitutive relationships and durability, it will clarify the mechanisms of setting and hardening, the features of microstructure development, and the relationships between microstructure and macro-properties of UHPC. The effects of fibers on toughness of UHPC will be explained. The constitutive relationships and failure criteria will be established. Based on the migration of chloride ion in UHPC, the requirements for cover design of rebar reinforced UHPC structure in marine environments will be proposed. The research will provide scientific base for production and application of UHPC in Australia.

### 1.3.2 Objectives of the research

Based on the above research gap identified in the literature, there are three objectives of the project, as following:

- Proposed to conduct fundamental research on the hydration of cement with partial replacement of ultra-fine fly ash under the UHPC conditions. This part focused on the early age hydration process, fly ash with different chemical compositions and particle sizes are examined and hydration products and microstructure are determined.
- At the conditions of ultra-low w/c, abundant amounts of un-hydrated cementitious materials in the matrix may affect the long-term performance of UHPC. Due to ongoing hydration, it has a retrieving effect on physicochemical properties of UHPC, also known as “autogenous/self-healing” products and microstructure are determined. This part is proposed to investigate the effects of slag, fly ash, and fiber contents on long-term strength development, dimensional stability, and mass change in three exposure conditions: water, seawater, and outdoor, for a duration of more than 1080 days.
- Ending part is understanding the micromechanism of autogenous shrinkage and drying shrinkage from pore structure, mechanical, moisture lose and chemical stability; Implement the micromechanics, kinetic, micromechanics and phase

transformation knowledge on commercial raw materials to build a mathematical or physical model to predict autogenous shrinkage and drying shrinkage of UHPC. Study the long-term performance of UHPC under three different exposure conditions.

## 1.4 Outline of the thesis

***CHAPTER 1:*** **Introduction** *(about the background and objective of early age shrinkage, microstructure development and dimensional stability of ultra-high performance concrete).*

***CHAPTER 2:*** **Review.** In chapter 2, the mechanism of early age shrinkage of UHPC and influential factors in its development are discussed. In general, autogenous shrinkage is more pronounced in UHPC/HPC, albeit, using low heat cement, fly ash, shrinkage reducing agents, lightweight aggregates, and fibers can effectively reduce it. The effects of SCMs on autogenous shrinkage, relationship between different types of shrinkage and autogenous shrinkage as well as the effect of internal curing on autogenous shrinkage need to be further studied.

***CHAPTER 3:*** **Evaluation of fibre on autogenous shrinkage of ultra-high performance concrete by ring test.** Due to high content of cementitious materials and low water-to-binder ratio (w/b), UHPC has high autogenous shrinkage. In chapter 3, the effects of steel fiber on the autogenous shrinkage of UHPC were evaluated by using ring tests and corrugated tube method under plastic film sealed conditions. The results indicated that the development of autogenous shrinkage of UHPC was mainly during the first 24 hours. The autogenous shrinkage of UHPC is significant reduced by adding steel fiber. The optimal fiber content was found to be 3% where UHPC exhibited highest strength (107 MPa at 3 day) and lowest autogenous shrinkage (750×10-6μm at 3 day, which was only 30% of that of the specimens without steel fiber).

***CHAPTER 4:*** **Effects of steel fiber on drying shrinkage of ultra high performance concrete.** Chapter 4 reports the study of the influence of steel fibers on drying shrinkage of UHPC at fiber volume content of 0%, 1%, 2% and 3%, temperature of 20 ± 2°C and relative humidity of 50 ± 5%. The results showed that during the first 7 days, the drying

shrinkage rate of UHPC was very fast, while after 7 days it gradually decreased. The interfacial bonding of steel fiber and the physical properties of steel fiber can effectively reduce the drying shrinkage. However, when the steel fiber exceeds an optimal volume, the effect of steel fiber on drying shrinkage can decrease. Compared with the steel fiber content at 2%, the drying shrinkage of the UHPC with 3% steel fiber was decreased by only 1.5%. The reason is that the increase in the steel fiber leads to an increase in the interface layer, the interface transition zone is usually more porous than the matrix, which easily leads to shrinkage, and consequently reducing the beneficial effect of steel fiber on drying shrinkage control. It was also found that the inhibition of fly ash on the drying shrinkage of UHPC was higher than slag.

***CHAPTER 5:*** **Early age of hydration mechanisms and microstructure development of ultra-high strength cement-based materials (UHSC).** In chapter 5, the effects of UFA content on flowability, heat of hydration, mechanical properties and early age shrinkage properties were determined for ultra-high strength cement-based materials (UHSC) containing 0-75% UFA by the mass of binder. Thermal gravimetry (TG) and mercury intrusion porosimetry (MIP) were used to quantitatively determine the calcium hydroxide (CH) content and pore structure, respectively. The results indicated that the optimal UFA content could be in the range of 15%-30% in terms of flowability, mechanical properties, CH content, porosity, and interfacial bonding properties. The TG analysis revealed that the use of 15%-30% UFA efficiently consumed the CH, transforming it to C-S-H gel. The CH content in those samples at 28 d was reduced by 50% in comparison with that in the reference sample. From MIP results, the total porosity of UHSC with 15%-30% UFA was only 5%-8%, in which more gel micro-pores but less capillary pores could be observed. The enhancement of mechanical properties and fiber bonding strength of UHSC was mainly due to the increased C-S-H content, and reduced CH content and porosity due to the addition of UFA.

***CHAPTER 6:*** **Carbonation and chloride ingression depths in ultra-high performance concrete after long term exposure to different conditions.** In chapter 6, carbonation and chloride ingression in UHPC after the exposure to three different conditions: water, seawater, and outdoor for a duration of 1080 days, were studied to examine the effects of SCMs, including slag and fly ash on the long-term durability of UHPC. In addition, steel fibers were also added into some UHPC-based systems to improve the related properties.

The results indicated that the optimal steel fiber content was 2% when considering the flowability, mechanical properties, CH content and porous networks. Fiber addition improved the performance of fly ash based UHPC, while it had little impact on the slag-based counterpart. Moreover, the UHPC specimens exposed to seawater for 1080 days also efficiently consumed CH. It was also found that the CH was consumed with the formation of $CaCO_3$ (calcite) due to the carbonation effect in outdoor conditions whereas for the water and seawater immersion conditions, the CH was transformed into other reaction products including $Mg(OH)_2$ and ettringite. Furthermore, because slag based UHPCs have a denser microstructure evidenced by diffusion coefficient and porous characteristics, seawater and water conditions led to a decrease in C-S-H content, which was particularly evident after 28 days. XRD and SEM analysis also implies that for the sample exposed to outdoor and seawater condition, slag-based UHPC underwent less deterioration than fly ash (FA) containing counterparts. Finally, it revealed that the chemical reactions and microstructure properties of the UHPCs varied significantly when comparing the seawater and outdoor exposure conditions.

***CHAPTER 7:*** **Long-term performance of ultra-high performance concrete (UHPC) in different exposure conditions.** Chapter 7 investigated the effects of slag, fly ash, and fiber contents on long-term strength development, dimensional stability, and mass change in three exposure conditions: water, seawater, and outdoor, for a duration of 720 days. Thermogravimetric analysis (TGA), X-ray diffractometry (XRD) and scanning electron stereoscopy (SEM) were applied to examine the hydration phases during this exposure period. The results showed that the specimens in water and outdoor conditions experienced a shrinking behavior, while in contrast, the specimens exposed to seawater expanded slightly with a higher rate of mass gain. The compressive strength of specimens under seawater and outdoor expose conditions were lower than those in water and the main hindering mechanism to strength development was the shortage of calcium hydroxide from the matrix, which led to lower reaction extent of SCMs.

***CHAPTER 8:*** **Conclusions and future work.** Chapter 8 draws the conclusions of the research undertaken in this thesis. Some problematic issues that have been noted in the UHPC application are mentioned. Detailed suggestions to the future work are presented for UHPC application.

## 1.5 The technology road map

In autogenous shrinkage and drying shrinkage aspects, I used traditional method (corrugated tube measurement) and ring test to test the autogenous shrinkage, based on the results I developed a thermochemical model to quantify the shrinkage. This method is testified to be useful and can be applied in understanding more complex systems, however, what was happed at the beginning time of autogenous shrinkage still remains unknown. In the drying shrinkage aspect, I investigated the effects of steel fiber on it, the results showed that during the first 7 days, the drying shrinkage rate of UHPC was very fast, while after 7 days it gradually decreased(Linmei Wu, Caijun Shi et al., 2018). The interfacial bonding of steel fiber and the physical properties of steel fiber can effectively reduce the drying shrinkage. The reason is that the increase in the steel fiber leads to an increase in the interface layer, the interface transition zone is usually more porous than the matrix, which easily leads to shrinkage, and consequently reducing the beneficial effect of steel fiber on drying shrinkage control. It was also found that the inhibition of fly ash on the drying shrinkage of UHPC was higher than slag.

In dry shrinkage part of UHPC, I will mainly concentrate in the shrinkage and cracks induced by early drying and hydration. Even though this subject has been widely studied, there are still some points which are staying unclear, e.g. the competition between hydration and early drying, and the combination of shrinkage and creep etc. Shrinkage occurred when water content reduces caused by hydration (autogenous shrinkage) and by drying results in a deformation in function of water content / HR. There are two hydraulic effects on the solid phase, increasing capillary pressure while decreasing of water content, another Gradient of hydraulic pressure (maintained before cavitation, Darcy's law) induces a tension in liquid which is balanced by a compression in solid matrix. So is the shrinkage deformation reversible or irreversible? Is it in elastic range or

extending to plastic range? Now it is widely known that the hydra strain could be induced by three kinds of effects. In a high water content range, disjoining pressure and capillary pressure are the main driving force of hydric strain. The surface energy change would be responsible for a low water content range situation. If we consider the solid matrix as an elastic system, try to understand the mechanism of the drying induced shrinkage. In transcend structure, the project will focus on relationship between shrinkage and early drying, by offering experimental data in order to validate predictive models(L. Wu et al., 2016; L. Wu, Liu, Zhang, Zhu, & Wang, 2018).

In the long-term stability of UHPC aspect, I doubt the state-of-the-art rule 'the crystallization only takes place in the hollows left by reacted ash, instead of in the binder itself'. In my proof-of-concept experiment, this study investigated the effects of slag, fly ash, and fiber contents on long-term strength development, dimensional stability, and mass change in three exposure conditions: water, seawater, and outdoor, for a duration of 720 days. Thermogravimetric analysis (TGA), X-ray diffractometry (XRD) and scanning electron stereoscopy (SEM) were applied to examine the hydration phases during this exposure period. I found that the specimens in water and outdoor conditions experienced a shrinking behavior, while in contrast, the specimens exposed to seawater expanded slightly with a higher rate of mass gain. The compressive strength of specimens under seawater and outdoor expose conditions were lower than those in water and the main hindering mechanism to strength development was the shortage of calcium hydroxide from the matrix, which led to lower reaction extent of SCMs. More importantly, the formation of only 5-7% zeolite can cause compressive strength loss, which must be prevented to ensure the durability. It hypothesise that strength loss also results from pore structure evolution besides crystallization. To prove this, it must remove the difficulty of

characterizing the reaction products due to the complexity induced by the residual fly ash particles. Figure 1-2 shows the frame of the thesis.

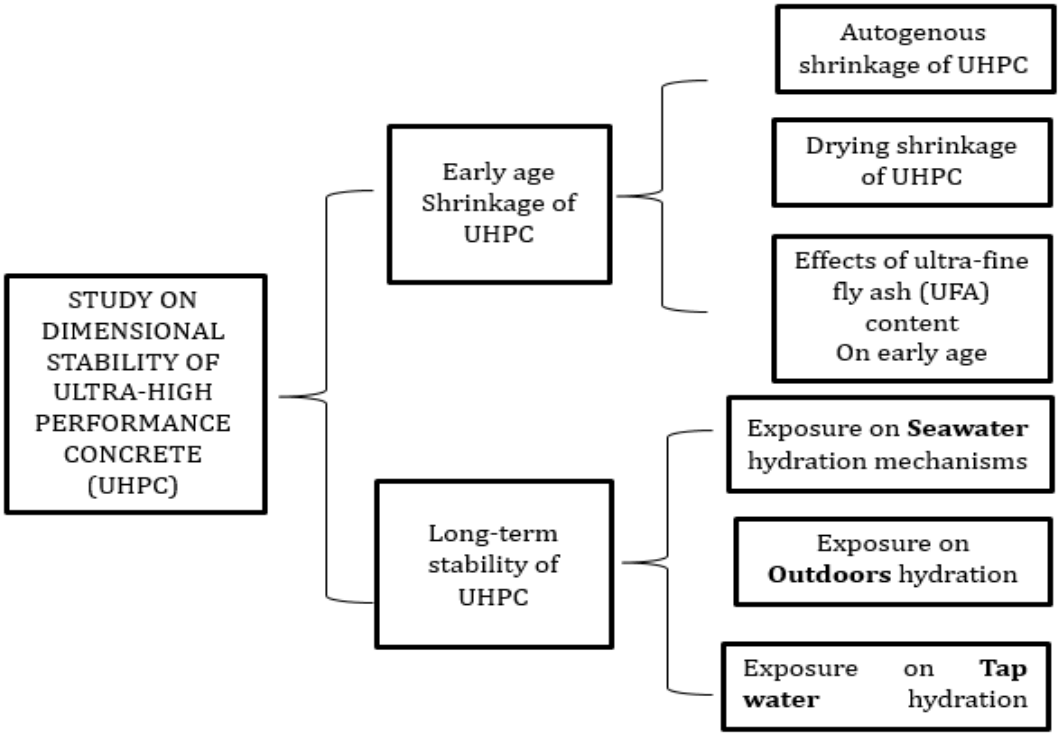


**Figure 1-2.** The frame of the thesis.

### 3.1. Conceptual framework

The two major work packages of the thesis have been developed to achieve the ultimate aim, the following figure shows the technology road map of the project, about the Process-microstructure-property relationship:

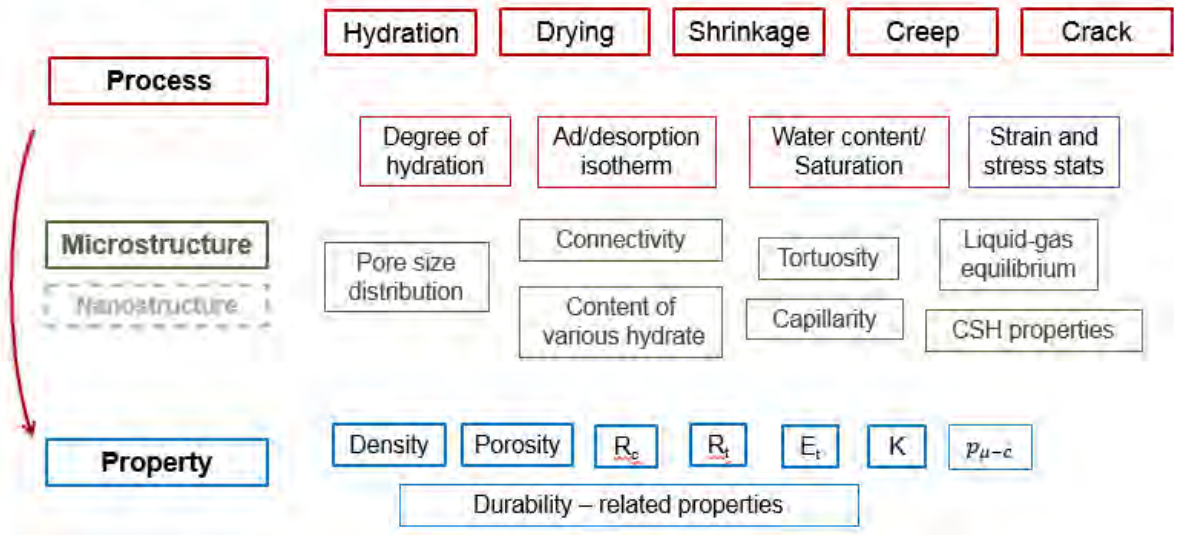


**Figure 1-3.** Process-microstructure-property relationship.

## 1.6 References


D.W. Fowler, Polymers in concrete: a vision for the 21st century, Cement and concrete composites, 21 (1999) 449-452.

A. Rip, R. Kemp, Technological change, Human choice and climate change, 2 (1998) 327-399.

E. Fehling, M. Schmidt, J. Walraven, T. Leutbecher, S. Fröhlich, Ultra-high performance concrete UHPC: Fundamentals, design, examples, John Wiley & Sons2014.

R. Yu, P. Spiesz, H. Brouwers, Effect of nano-silica on the hydration and microstructure development of Ultra-High Performance Concrete (UHPC) with a low binder amount, Construction and Building Materials, 65 (2014) 140-150.

C. Shi, Z. Wu, J. Xiao, D. Wang, Z. Huang, Z. Fang, A review on ultra-high performance concrete: Part I. Raw materials and mixture design, Construction and Building Materials, 101 (2015) 741-751.

I.H. Yang, C. Joh, B.-S. Kim, Structural behavior of ultra-high performance concrete beams subjected to bending, Engineering Structures, 32 (2010) 3478-3487.

O. Bonneau, C. Poulin, M. Dugat, P.-C.A. Tcin, Reactive powder concretes: from theory to practice, Concrete international, 18 (1996) 47-49.

P.Y. Blais, M. Couture, precast, prestressed pedestrian bridge-world's first reactive powder concrete bridge, PCI journal, 44 (1999).

N. Van Tuan, G. Ye, K. Van Breugel, O. Copuroglu, Hydration and microstructure of ultra-high performance concrete incorporating rice husk ash, Cement and Concrete Research, 41 (2011) 1104-1111.

R. Yu, P. Spiesz, H. Brouwers, Mix design and properties assessment of ultra-high performance fibre reinforced concrete (UHPFRC), Cement and Concrete Research, 56 (2014) 29-39.

C. Shi, D. Wang, L. Wu, Z. Wu, The hydration and microstructure of ultra-high strength concrete with cement–silica fume–slag binder, Cement and Concrete Composites, 61 (2015) 44-52.

P. Van den Heede, N. De Belie, Environmental impact and life cycle assessment (LCA) of traditional and ‘green’concretes: literature review and theoretical calculations, Cement and Concrete Composites, 34 (2012) 431-442.

B. Lothenbach, K. Scrivener, R. Hooton, Supplementary cementitious materials, Cement and Concrete Research, 41 (2011) 1244-1256.

P.Y. Blais, M. Couture, Precast, prestressed pedestrian bridge: World's first Reactive Powder Concrete structure, PCI journal, 44 (1999) 60-71.

C. Dauriac, Special concrete may give steel stiff competition, The Seattle Daily Journal of Commerce, 1997.

W. Dowd, Reactive powder concrete: ultra-high performance cement based composite, United States: Construction Innovation Forum, 1999.

C.M. Tam, V.W. Tam, K.M. Ng, Assessing drying shrinkage and water permeability of reactive powder concrete produced in Hong Kong, Construction and Building Materials, 26 (2012) 79-89.

K.M. Ng, C.M. Tam, V.W. Tam, Studying the production process and mechanical properties of reactive powder concrete: a Hong Kong study, Magazine of Concrete Research, 62 (2010) 647-654.

H. Yazıcı, M.Y. Yardımcı, S. Aydın, A.Ş. Karabulut, Mechanical properties of reactive powder concrete containing mineral admixtures under different curing regimes, Construction and building materials, 23 (2009) 1223-1231.

M. Kazemi Kamyab, Autogenous Shrinkage and Hydration Kinetics of SH-UHPFRC under Moderate to Low Temperature Curing Conditions, (2013).

P. Rossi, Influence of fibre geometry and matrix maturity on the mechanical performance of ultra-high-performance cement-based composites, Cement and Concrete Composites, 37 (2013) 246-248.

S.H. Park, D.J. Kim, G.S. Ryu, K.T. Koh, Tensile behavior of ultra-high performance hybrid fiber reinforced concrete, Cement and Concrete Composites, 34 (2012) 172-184.

A. Korpa, T. Kowald, R. Trettin, Phase development in normal and ultra-high performance cementitious systems by quantitative X-ray analysis and thermoanalytical methods, Cement and Concrete Research, 39 (2009) 69-76.

I. Schachinger, H. Hilbig, T. Stengel, E. Fehling, Effect of curing temperature at an early age on the long-term strength development of UHPC, 2nd International Symposium on Ultra High Performance Concrete, 2008, pp. 205-213.

E. Ghafari, H. Costa, E. Júlio, A. Portugal, L. Durães, The effect of nanosilica addition on flowability, strength and transport properties of ultra-high performance concrete, Materials & Design, 59 (2014) 1-9.

A.S. El-Dieb, Mechanical, durability and microstructural characteristics of ultra-high-strength self-compacting concrete incorporating steel fibers, Materials & Design, 30 (2009) 4286-4292.

A. Hassan, S. Jones, G. Mahmud, Experimental test methods to determine the uniaxial tensile and compressive behaviour of ultra-high performance fibre reinforced concrete (UHPFRC), Construction and building materials, 37 (2012) 874-882.

M. Aldahdooh, N.M. Bunnori, M.M. Johari, Evaluation of ultra-high-performance-fiber reinforced concrete binder content using the response surface method, Materials & Design, 52 (2013) 957-965.

J. Zhang, Y. Zhao, The mechanical properties and microstructure of ultra-high-performance concrete containing various supplementary cementitious materials, Journal of Sustainable Cement-Based Materials, (2016) 1-13.

M. Frías, R.V. la Villa, M. Rojas, C. Medina, A. Juan Valdés, Scientific aspects of kaolinite based coal mining wastes in pozzolan/Ca $(OH)_2$ system, Journal of the American Ceramic Society, 95 (2012) 386-391.

J. Resplendent, F. Toutlemonde, The UHPFRC revolution in structural design and construction, Proceedings of International Symposium on Ultra-High Performance Fiber-Reinforced Concrete, Marseille, France, 2013, pp. 791-804.

F.C.o. Concrete, Condensed silica fume in concrete, Thomas Telford1988.

H.G. Russell, B.A. Graybeal, Ultra-high performance concrete: A state-of-the-art report for the bridge community, 2013.

# CHAPTER 2 LITERATURE REVIEW

Note: this chapter is based on the manuscript entitled "Autogenous shrinkage of high performance concrete: A review", by Linmei Wu, N Farzadnia, C Shi, Z Zhang and H Wang, published in journal of **Construction and Building Materials**, 2017.

**Abstract**: Autogenous shrinkage is a major concern in early age cracking of high performance concrete (HPC). Low water-to-binder ratio and incorporation of supplementary cementitious materials (SCMs) can remarkably affect the pore structure, relative humidity, self-stress, degree of hydration, and interface structure, hence increasing the shrinkage in the matrix. In this chapter, the mechanism of autogenous shrinkage of HPC and influential factors in its development are discussed. In general, autogenous shrinkage is more pronounced in HPC, albeit, using low heat cement, fly ash, shrinkage reducing agents, lightweight aggregates, but can be effectively reduce by introducing fibers. The effects of SCMs on autogenous shrinkage, relationship between different types of shrinkage and autogenous shrinkage, as well as the effects of internal curing on autogenous shrinkage need to be further studied.

## 2.1 Introduction

Autogenous shrinkage refers to reduction of apparent volume or length of cement-based materials under sealed and isothermal conditions (Williams, Markandeya, Stetsko, Riding, & Zayed, 2016). It is found that autogenous shrinkage is caused by further hydration of cement after the formation of initial structure of the cement matrix and can be best explained by capillary tension theory (Lura, Jensen, & van Breugel, 2003). In concrete with water-to-cement ratio lower than 0.40, the internal moisture is insufficient to fully hydrate cement particles; thus, the occurrence probability of autogenous shrinkage may increase (LE, 2013). Therefore, autogenous shrinkage is a major concern in early age cracking of high performance concrete (HPC) (D. Wang et al., 2015). Generally, the early-stage autogenous shrinkage occurs within the first 24 hours after mixing with water. The matrix

is more prone to cracking during the first 12 hours (Van Breugel & Van Tuan, 2015). During this time period, tensile strength of concrete is too low to resist the crack propagation caused by shrinkage stresses. Addition of some supplementary cementitous materials (SCMs) such as silica fume to the mixture may further increase the autogenous shrinkage, as the hydration and pozzolanic reactions accelerates the water consumption at early ages (W. Li et al., 2015). Autogenous shrinkage leads to micro-cracks in the matrix and lowers the durability of the structure. Ineffective curing of concrete in dry environments may cause simultaneous occurrence of drying shrinkage and autogenous shrinkage (Henkensiefken, Bentz, Nantung, & Weiss, 2009).

In general, shrinkage can be measured based on changes in volume and length. Regardless of test methods, the measured shrinkage is a combination of autogenous shrinkage, dry shrinkage, and chemical shrinkage (Recommendation & DE LA RILEM, 1995). The autogenous shrinkage of HPC is a complex phenomenon influenced by many factors including: fineness of cement, cement type, SCMs, aggregate, fiber, water-to-cement ratio, admixtures, and curing. No uniform mechanism has yet explicated the autogenous shrinkage, albeit, the capillary pressure was introduced as the main driving force (Bazant & Chern, 1985). A thorough understanding of the mechanism is indispensable in order to apply methods to reduce the autogenous shrinkage and to improve the early-age cracking resistance of cement-based materials.

In this chapter, the autogenous shrinkage mechanism is discussed and its different nature in comparison to other shrinkage types is elaborated. Furthermore, the influential factors in autogenous shrinkage of HPC are discussed. Meanwhile, problems involved in autogenous shrinkage of HPC and possible solution are also deliberated.

## 2.2 Hydration of UHPC

The hydration of cementitious materials in UHPC is similar to that in ordinary concrete (OC). First, Portland cement hydrates to form calcium silicate hydrate and calcium hydroxide, then mineral admixtures (such as silica fume) react with calcium hydroxide to form calcium silicate hydrate (C-S-H). Figure 2-1 shows the time dependent phase

development in OC and UHPC at room temperature (Korpa et al., 2009). It can be seen that the content of crystalline phases was considerably higher in normal concrete, whereas less amorphous phases in the UHPC are measured. The difference arises from the pozzolanic reactions associated with the relatively high amounts of silica fume and fly ash. The consumption of portlandite becomes remarkable after the second hydration day, and is much lower than that in the normal concrete after 28 days, indicating that the pozzolanic reactions are still incomplete. The fact that no calcite was detected in the XRD analysis in the UHPC specimen even after 28 days may be interpreted as indication of no considerable phase carbonation in this specimen. The variations of ettringite content development between the first and second hydration day indicate that conversion of ettringite to monosulphate phase is possible, and that significant amount of aluminate may enter the X-ray amorphous C-S-H phases (Korpa et al., 2009).

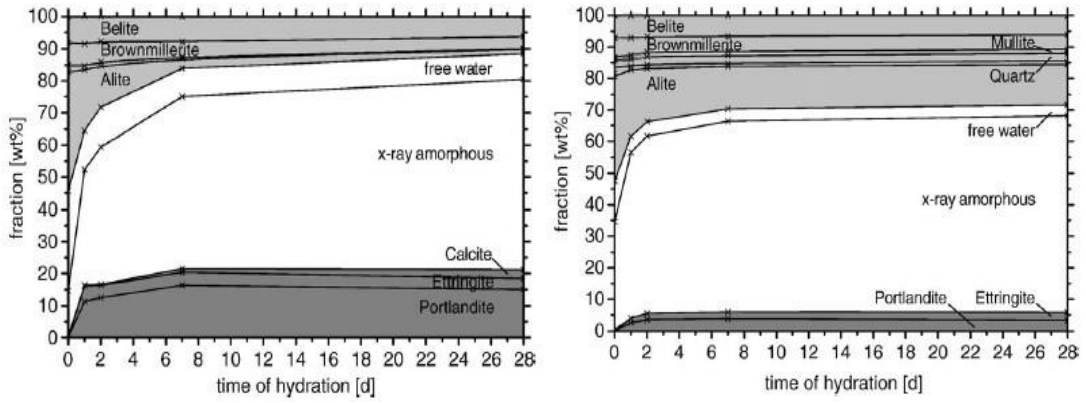


(a) OPC (b) UHPC

**Figure 2-1.** Time dependent phase development in OC and UHPC(Korpa et al., 2009).

The increase of curing temperature accelerates the hydration of cement and promotes secondary hydration between mineral admixtures and $Ca(OH)_2$ (C. Yang, Lai, & Xu, 2012). Hydration products at 90 ℃ remain amorphous. Under the autoclave curing, the hydration of $C_3S$ and $C_2S$ leads to the formation of crystalline α-dicalcium silicate hydrate in the absence of an external $SiO_2$ source. Tricalcium aluminate ($C_3A$) and tetracalcium alumino-ferrite ($C_4AF$) yield a hydrogarnet phase. The bonding characteristics of these two phases are rather unfavorable. In the presence of finely ground quartz and/or other $SiO_2$ sources, a pozzolanic reaction takes place, yielding crystalline 1.1nm tobermorite

($C_5S_5H_5$) as the main production of reaction at temperatures between about 150 and 200℃. Xenolith C-S-H (I), C-S-H (II) and α-$C_2SH$ may also be formed at even higher temperature(Yazıcı, Yiğiter, Karabulut, & Baradan, 2008). It was also found that at 150 ℃, Crystalline $Ca(OH)_2$ and some unidentified hydration products appeared in 1-day Portland cement (PC) paste. Crystalline $C_2SH$ (A) could be detected in 5-day PC paste. Only $Ca(OH)_2$ and $C_2SH$(A) could be detected in the 15-day PC paste. The main hydration products for alkali-blast furnace slag cement (ABSC) paste were C-S-H (B) and xonotlite. The $3CaO{\cdot}MgO{\cdot}2SiO_2$ in the slag disappeared after 5 days. Only C-S-H (B) and tobermorite could be detected in APSC paste (C. Shi, Wu, & Tang, 1991). The formation of both 1.1 nm tobermorite and xonolite is favorable for strength development of autoclaved material (Odler, 1998). Xonotlite formed with a $Q^3$ peak at 250℃, as shown in Figure.2-2 (Philippot et al., 1996; Zanni, Cheyrezy, Maret, Philippot, & Nieto, 1996). The H/C ($H_2O$ to CaO) ratio of C-S-H of OC is approximately one, while the H/C of xonotlite is 1/6, and the xonotlite is only formed in the inner part of concrete specimen (Cheyrezy, Maret, & Frouin, 1995). The formation of xonotlite in heat-cured UHPC was due to local, large water vapor pressures. However, lower (3Pa) dynamic equilibrium vapor pressures could totally suppress the formation of crystalline hydration products, even no xonotlite or other crystalline hydration products formed even at 250℃ (Feylessoufi et al., 1997).

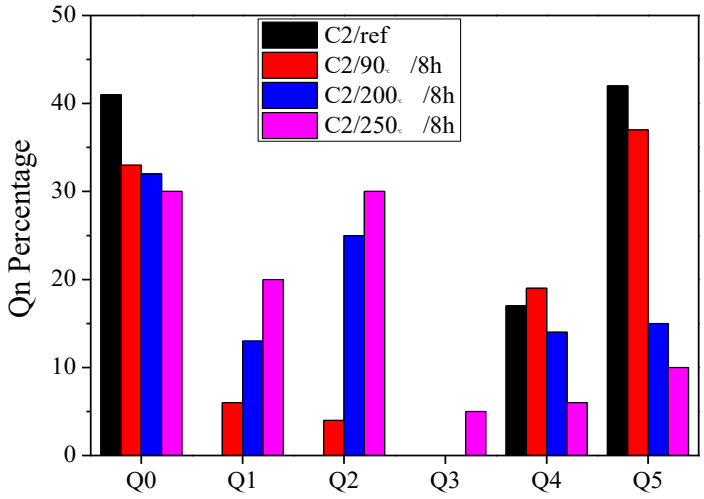


**Figure 2-2.** Q0 to Q4 percentages for samples with heat treatment at 90℃, 200℃, 250℃for 8 hours (Zanni et al., 1996).

### 2.2.1 The influence of ultra-fine fly ash on hydration

At present，Fly Ash has been widely used as a kind of mineral admixture in the production

of cement and concrete. As a matter of fact, the excitation of its chemical activity is still worth studying. With the method of mechanical grinding, a large part of vitreous has been ground up. Thus the ultra-fine fly ash (UFA) has been got, of whose specific surface area is 651 $m^2$/kg, and particle sized distribution is mainly under 71 μm (B. Liu, Xie, Zhou, & Yuan, 2000). Although the chemical composition of UFA and the ordinary fly ash are the same, the particle size distribution and morphology of UFA have been greatly changed, so as to the physical and chemical function of ultra-fine fly ash. The performance of ultra-fly ash is different from the ordinary fly ash during the hydration process of the complex binders.

The UFA helps to improve the mechanical properties of composite cement mortar .The physical filling effect of UFA helps to increase the flexural strength 3 days before; the activity of the ultra-fine fly ash began to emerge 3 days later. The flexural strength after 14 days and compressive strength after 60 days improved significantly; compared with the compressive strength, the UFA helps to increase the flexural strength, the more dosage, the greater the flexural strength increased; compared with the ordinary fly Ash, the activity of the UFA is greater, the pozzolanic reaction started earlier, the UFA contributes a lot to the strength of the middle and later time(Potgieter-Vermaak, Potgieter, Kruger, Spolnik, & Van Grieken, 2005).

The UFA promotes the hydration of the composite gel materials, in the early stage, the ultra-fine fly ash makes the second moment of exothermic peak appeared slightly ahead of time, the bigger the dosage is, the more obvious in advance; the activity of UFA appeared at 3 days, it also Can be proved through the result of XRD and the content of the CH, the first hydration dominants 28 days before, the reaction of fly ash increases. 28 days later, then the second hydration reaction dominants(Subramaniam, Gromotka, Shah, Obla, & Hill, 2005).

The UFA improves the microstructure of the hardened pastes (E.-H. Yang, Yang, & Li, 2007a), the UFA helps to decreases the threshold aperture and most probable aperture of the hardened pastes, the most probable aperture of the hardened paste is about l00nm

because of the UFA，which is near that of the pure cements system．As the curing time going，the most probable aperture of each group decreases，the holes whose diameter is above 200nm decreases．

Hydration shrinkage generated by cement hydration is the cause of autogenous shrinkage of high strength concrete. It may result in the volume change and even cracking of mortar and concrete. According to the data analysis in a series of previous studies, it is found that ultra-fine fly ash can reduce the hydration shrinkage of cement paste effectively, and the more the ultra-fine fly ash, the less the hydration shrinkage. Compared with cement paste without the ultra-fine fly ash, the shrinkage ratio of cement paste reduces from 23.4% to 39.7% when the ultra-fine fly ash replaces cement from 20% to 50% .Moreover, the hydration shrinkage can be restrained to a certain degree because the ultra-fine fly ash does not participate in the hydration at the early stage and the secondary hydration products are different at the later stage.

### 2.2.2 Benefits of UFFA in UHPC

Extensive laboratory and field-testing research has been published during the last 50 years on the properties of UFFA, and its beneficial performance in a wide range of cementitious mixtures is well documents(Aldred et al., 2006).

For UHPC applications, two key characteristics of UFFA are highlighted:

Small round particles (typically 0.1 to 0.3 μm) and a corresponding high specific surface area. These factors contribute to particle packing and to internal cohesion in the concrete mixture. Figure 1 shows the dramatic difference in size and shape of a typical UFFA particle, compared to a Portland cement particle. When UFFA first became commercially available, in Scandinavia in the 1970s, it coincided with the development of the first commercial UHPC products. For example, in Denmark, Hans Henrik Bache (Aalborg Portland Cement) developed the 'Densified System of homogeneously arranged ultrafine Particles (DSP)'. Based on the principle of optimum particle packing, Bache used UFFA as ultra-fine powder in mortars to achieve compressive strength in the order of 250 – 300 MPa. A summary of his early work was published in 1981(Aftcin, Bédard, Plumat, & Haddad, 1984).

High content of amorphous, and therefore reactive, silicon dioxide. The high specific surface area and reactive SiO2 makes UFFA an extremely efficient pozzolan – it consumes calcium hydroxide and reacts with alkalis in the concrete. This leads to less alkali in the pore solution and less calcium hydroxide in the matrix. Consequently, more calcium silicate hydrate binder is present and less calcium hydroxide.

**High strength**

As already mentioned, UFFA helps to optimize the particle packing of aggregates and powders in the concrete mix design, helping to minimize the number of voids and increasing the density of the concrete. By improving packing, concrete properties including strength can be improved. To help design a concrete mixture with optimal particle packing, computer programs are now commonly used. For example the EMMA grading curve program, based on the Andreasen and Andersen mathematical model (Andreasen & Andersen, 1930).

Well-dispersed UFFA particles which have packed around aggregate particles during concrete mixing and placing will modify the interfacial transition zone between the cementitious paste and the particles of aggregate. In conventional concrete, the microstructure of the transition zone is significantly different from that of the bulk paste. Modification of this transition zone is a major benefit of the addition of UFFA, as it gives increased strength to the concrete(Güneyisi, Gesoğlu, & Özturan, 2004).

**High durability**

A wide range of research has confirmed the high durability of UHPC concrete mixtures against durability parameters such as chloride penetration, sulfate attack and freeze-thaw cycling. For example Pierard et al (J. Piérard, Dooms, & Cauberg, 2012), who concluded that the highly dense hardened state of UHPC, due to low water/cement ratio and high powder content, is the primary reason for this enhanced durability.

UFFA concrete can be significantly more resistant than conventional concretes towards degradation caused by the ingress of aggressive ions or by leaching from the concrete. This is a consequence of an improved, more homogeneous, pore system giving reduced permeability to water and aggressive ions and improved resistance to leaching. In

addition, UFFA can also cause a significant reduction in the electrical conductivity of concrete. This is beneficial because active corrosion (of steel within the concrete) is an electrochemical process, governed by the resistivity of the concrete. The practical consequence of these factors is that UFFA significantly reduces the risk of chloride-initiated corrosion, especially in concrete exposed to severe environments.

**Sustainability**

Fly ash arises as an industrial co-product and generally it has a far lower embodied carbon emissions value than Portland cement. In this regard it is comparable to UFFA and ground granulated blast furnace slag. For example, a UK Concrete Society report (Ramezanianpour, 2014)suggested typical values of 930 kg/ton carbon dioxide for Portland cement and 28 kg/ton carbon dioxide for UFFA powder, delivered to site in the UK. In theory, the partial replacement of Portland cement by fly ash in an optimized UHPC mix design could reduce the environmental impact of the mixture. However in practice, the whole life cycle of the UHPC building or structure is the key measure of its sustainability.

## 2.3 Microstructure of UHPC

UHPC has a very dense and uniform microstructure due to following fundamental effects: (1) close packing of raw materials; (2) hydration and pozzolanic reactions in cementitious materials; (3) improvement of the interfacial transition zone between aggregates and bulk matrix. The internal microstructure of hardened UHPC is mainly comprised of unhydrated cement clinker particles, quartz sand and hydration products such as C-S-H(Jinchang & Ronggui, 2016). Low w/b in UHPC results in low porosity that restricts the space available for the growth of Ca $(OH)_2$ (CH) crystals. Use of elevated temperature curing accelerates the hydration of cement and promotes the pozzolanic effects of mineral admixtures. There were almost no pores observed in the Nano porous range with pore sizes up to 100 nm, and no significant CH was detected by XRD (Sayari, Yang, Kruk, & Jaroniec, 1999). The C-S-H in UHPC has high density characterized by higher intrinsic stiffness and hardness than those of low density C-S-H that dominates in conventional concrete.

The interfacial transition zone (ITZ) between aggregates and paste matrix has high porosity and CH content, and is the weakest part in conventional concrete. ITZ in conventional cement mortars and UHPC from SEM observations are shown in Figure.5 (Jinchang & Ronggui, 2016; Sayari et al., 1999). It can be seen that ITZ in conventional Portland cement mortar is very porous. However, owing to the low w/b and pozzolanic reactions between CH and reactive mineral admixture, which consumes most of the CH crystals and converts them to C-S-H (Jinchang & Ronggui, 2016; Yazıcı et al., 2009), the ITZ in UHPC seems as dense as the matrix. The homogenous structure is important for the excellence performance of UHPC.

UHPC is designed by close packing density and use of pozzolanic mineral admixtures. Therefore, it has a very low porosity, especially continuous porosity. For UHPC at W/C=0.20, its capillary pores become discontinuous when only 26% of cement has hydrated, instead of 54% for HPC (W/C=0.33) (Olivier Bonneau, Vernet, Moranville, & Aïtcin, 2000). The pore size of UHPC basically concentrates between 2 to 3 nm, the most probable pore diameter is 2.0 nm, and its total porosity is 2.23% (Long, 2003). It is nil in the range of 3.75 nm to 100 μm for UHPC when it is cured between 150~200℃ (Cheyrezy et al., 1995).

UHPC is composed of aggregate and compact matrix phase, which is composed of hydration products and unhydrated cement clinker particles and powder particles. A reactive interface is formed between incompletely hydrated core and hydration products. The core plays a role in skeleton to matrix, and enhances the properties of matrix phase greatly (D. F. Zhao, Liu, & Zhang, 2014). Scanning electron microscope (SEM) observation, as shown in Figure.2-3a, indicated that the structure of hardened paste was very dense due to the very low W/B and the hydration of cement and the pozzolanic effect of SF and GGBS. The main hydration product was homogeneous C–S–H gel, no $Ca(OH)_2$ and ettringite could be found (Alaee, 2002) (C. Wang, Yang, Liu, Wan, & Pu, 2012). The picture in Figure 2-3b indicated that UHPC had a very compact interfacial transitional zone with no obvious pores (C. Wang et al., 2012).

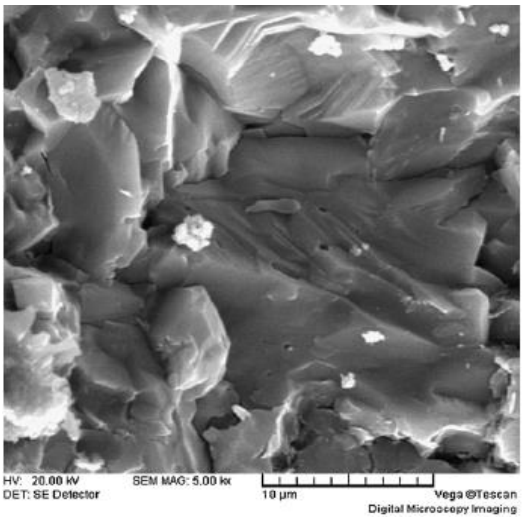


a) SEM image of hardened paste in UHPC (C. Wang et al., 2012).

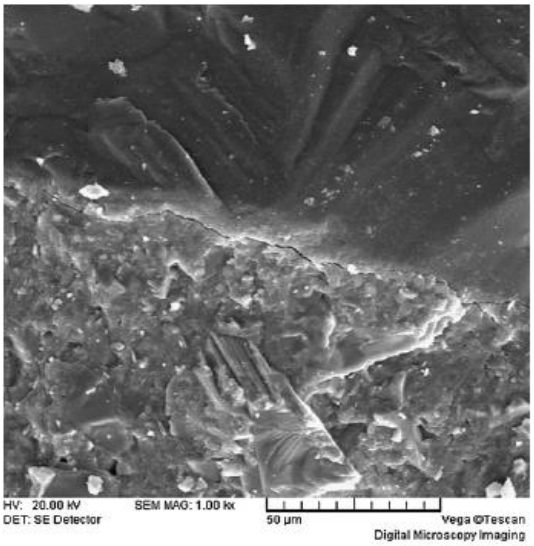


b) SEM image of ITZ structure in UHPC (C. Wang et al., 2012).

**Figure 2-3.** SEM image in UHPC (C. Wang et al., 2012).

The use of rice husk ash (RHA) increased the degree of cement hydration at later ages, even higher than that in the sample containing silica fume (SF) at 91 days. The total porosity of the RHA modified sample was higher than that of the SF modified sample but lower than that of the control sample because both filler effect and pozzolanic reaction of RHA were less significant than those of SF. Both RHA and SF strongly reduced the calcium hydroxide content where the effect of SF was greater than that of RHA at later ages(Van Tuan et al., 2011).

## 2.4 Shrinkage of concrete

Shrinkage of concrete can occur in two different stages: early and later ages. The first stage (within the first 24 hours) is defined as a duration in which concrete is setting and starting to harden. Second stage, on the other hand, refers to the age beyond 24 hours. Shrinkage at both stages mainly include autogenous shrinkage, drying shrinkage and thermal shrinkage which have overlapping results but with different mechanisms. In long term, the carbonation shrinkage is also added which has an accumulated effect. It was observed that autogenous shrinkage accounts for the most significant volume change in HPC at early ages compared to other types of shrinkage(Lura, 2003). A quick glance at differences can help to better elaborate the mechanism and influential factors in the autogenous

shrinkage of HPC.

### 2.4.1 Autogenous shrinkage

In general, the part of shrinkage which does not include any volume change due to loss or ingress of substances, temperature variation, and application of an external force and restraint can be considered as autogenous shrinkage. Therefore, it is also referred to as self-desiccation shrinkage. A technical committee on autogenous shrinkage at the Japan Concrete Institute (JCI) defined autogenous shrinkage as the macroscopic volume reduction of cementitious materials when cement hydrates after initial setting (E. Tazawa, 1996). However, Mehta and Monteiro referred to it as the measured deformation of cement paste in a closed system(P. K. Mehta, 1986). Some studies consider the critical influence of autogenous shrinkage only limited to high and ultra-high performance concrete in which high amount of cementitious materials and low water-to-binder ratio are applied and the self-desiccation is highly triggered in the paste (Holt, 2005; C. Jiang, Yang, Wang, Zhou, & Ma, 2014; Maruyama & Teramoto, 2013).

### 2.4.2 Chemical shrinkage

Chemical shrinkage refers to the volume change during the early ages of hydration resulted by formation of hydration products with lower volume in comparison with the volume of the initial reactants (water and cement) during the hardening process (Bullard et al., 2011). Chemical shrinkage, as a measurement of the absolute internal volume reduction, is considered as the driving force of autogenous shrinkage which represents the external, bulk volume change of concrete(Mounanga, Khelidj, Loukili, & Baroghel-Bouny, 2004). Figure.2-4 depicts a general relationship between the definition of chemical and autogenous shrinkage in concrete. After the formation of initial structure of slurry (roughly referred to as the early coagulation), further hydration causes voids within the matrix. At this stage, the autogenous shrinkage value is less than the chemical shrinkage as the former measures the apparent volume of reduction; the accumulated volume of voids is considered in measurement of chemical shrinkage value.

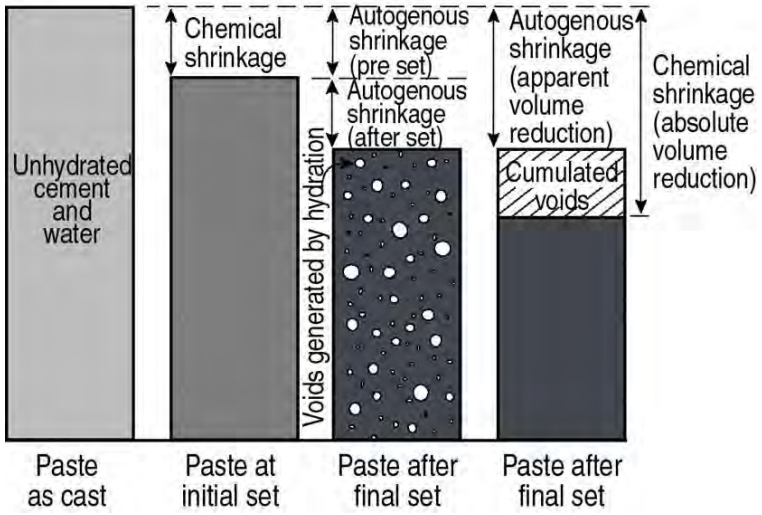


**Figure 2-4.** The relationship between chemical shrinkage and autogenous shrinkage (L. Wu et al., 2017b).

In the plastic stage, the terms "autogenous shrinkage" and "chemical shrinkage" may be used interchangeably. In a study by Holt (Holt, 2005), however, it was shown that the early age autogenous shrinkage and chemical shrinkage were not equivalent in concrete specimens when water-to-binder ratio as low as 0.3 was used. Besides, the addition of superplasticizer with presence of low water-to-binder ratio increased the chemical and autogenous shrinkage values at different rates. It should be noted that with presence of water at the w/b of 0.45 no autogenous shrinkage was observed while chemical shrinkage was noticeable.

### 2.3 Drying shrinkage

Drying shrinkage is caused by internal water evaporation from the matrix due to the low external environment humidity of the cement-based materials (Toledo Filho, Ghavami, Sanjuán, & England, 2005). The development of drying shrinkage of concrete is lengthy relative to the autogenous shrinkage. Accurate measurement of drying shrinkage is a challenge as the autogenous shrinkage deformation of the sealed specimens should be deducted from the total measured deformation of the concrete due to their distinct physical definition. The drying shrinkage value measured by traditional method contains part of autogenous shrinkage, however, it is not a simple superposition, since the drying condition has a serious effect on the hydration of cement. Addition of supplementary cementitious materials as in HPC can have different effects on drying shrinkage and autogenous shrinkage based on their reactivity and influence on the hydration. Itim et al.

(Itim, Ezziane, & Kadri, 2011) studied the effect of different contents on SCMs on autogenous shrinkage and drying shrinkage. Figure 2-5 illustrates the effect of content and type of limestone powder and slag on shrinkage values. As can be seen, there is a reverse relationship between drying shrinkage and autogenous shrinkage as the slag content increased. On the contrary, the limestone powder with almost inert properties influenced the autogenous shrinkage merely at early ages and had almost minor effect on the drying shrinkage. This can be related to higher reactivity of slag which can accelerate the hydration and increase self-desiccation of the matrix. However, a direct relationship between drying shrinkage and autogenous shrinkage were recorded when silica fume was used. It is reported that the increase in silica fume content increased autogenous and drying shrinkage of concrete especially at early ages (G. Rao, 1998; G. A. Rao, 2001; M. Zhang, Tam, & Leow, 2003).

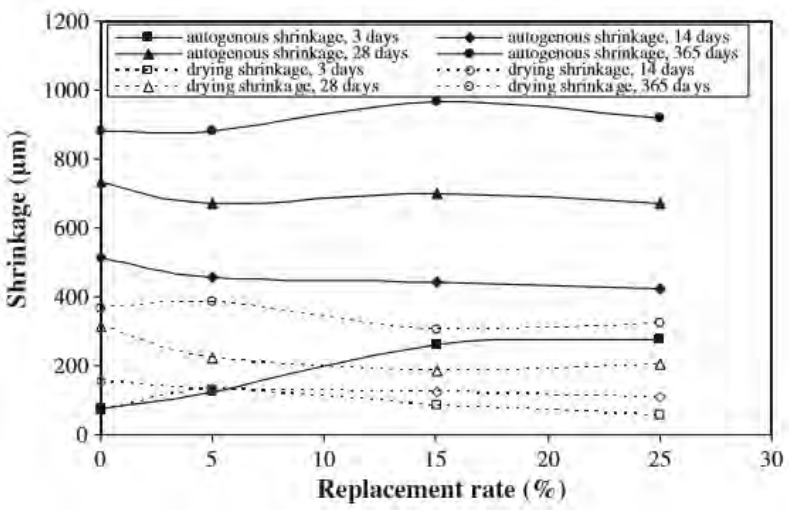


(a) Limestone powder

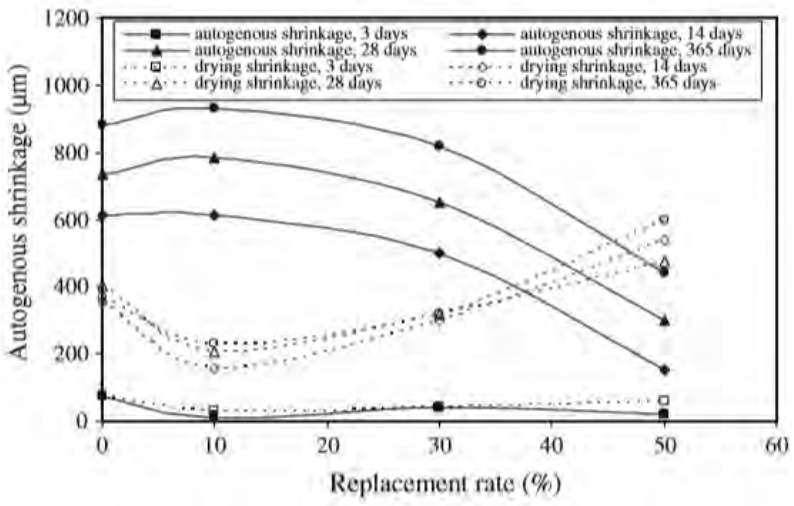


(b) Slag

**Figure 2-5.** Autogenous and drying shrinkage of mortars with (a) limestone powder (b) slag (Itim et al., 2011).

### 2.4.3 Thermal shrinkage

Field experience with HPC mixtures showed that concrete with high early age strength is prone to cracking at early-age from high autogenous shrinkage and high thermal shrinkage (P. K. Mehta, 1986). Thermal shrinkage indicates reduction of volume triggered by excessive temperature gradient between the inner and outer layers or temperature descending in the early stage of concrete hardening(Schrefler, Majorana, Khoury, & Gawin, 2002). The temperature difference predominantly owes to the temperature rise above environment temperature induced by heat evolution in the cement hydration process. Heat of hydration can affect the autogenous shrinkage as it increases the self-desiccation of the system. In a study by Maruyama and Teramoto (Maruyama & Teramoto, 2013) , the temperature change induced by hydration was simulated and its effect on autogenous shrinkage was studied. The results showed an inflection point by which the shrinking trend was divided in two stages. The autogenous shrinkage of the specimens before the inflection point, showed a larger increase when subjected to lower temperatures while after the inflection point, the shrinkage increased when subjected to higher temperatures. In the initial stage, the autogenous shrinkage strain developed without relative humidity change, while it developed with a decrease in relative humidity after the inflection point. In some cases, the release of heat is accompanied by thermal expansion which is concurrent with the onset of autogenous shrinkage. It is observed that concrete with a

very low water to binder ratio swells as long as the thermal expansion is larger than autogenous shrinkage. But, generally, the autogenous shrinkage overtakes the expansion rapidly and concrete shrinks after the initial swelling phase(Kaufmann, Winnefeld, & Hesselbarth, 2004). If the concrete temperature decreases quickly, the thermal contraction can be accumulated to that of autogenous shrinkage (P. Aitcin, 1999).

### 2.4.4 Carbonation shrinkage

Carbonation shrinkage is caused by carbonation of concrete when exposed to $CO_2$. Carbonation may occur by permeation of available $CO_2$ in the atmosphere and its reaction with calcium hydroxide as well as destabilization of calcium silicate hydrates(Ramachandran, 1996). The decline in concentration of $Ca(OH)_2$, the low integrity of C-S-H along with moisture loss may trigger the carbonation shrinkage. At later ages of concrete (after 24 hr.), the carbonation shrinkage and autogenous shrinkage may occur concurrently, however, the occurrence of carbonation shrinkage is low in HPC (Aïtcin, 2003; Wong et al., 2007). In a study by Persson (Persson, 2002), a good comparison was made between carbonation and autogenous shrinkage in HPC. It was stated that carbonation shrinkage was concomitant with an increase in weight of specimens, while no loss of weight was observed with the occurrence of autogenous shrinkage. Furthermore, there was a correlation among inner relative humidity and water-to-binder ratio of specimens and the autogenous shrinkage. No carbonation shrinkage took place when water-to-binder ratio reduced to less than 0.3 and 10% silica fume was applied. This was in agreement with his previous study where water-to-binder ratio was less than 0.25(Persson, 1998). In the same study, he reported that the carbonation shrinkage caused no decline in the internal relative humidity of the specimens which is different from autogenous shrinkage mechanism.

## 2.5 Mechanism of autogenous shrinkage

Different approaches and driving forces are used to explain autogenous shrinkage mechanism such as surface tension, disjoining pressure, and capillary tension. The capillary tension approach is advantageous, as it is based on sound mechanical and thermodynamically studies(Lura, Jensen, & van Breugel, 2003). The capillary tension

theory in general explicates the autogenous shrinkage using pore structure, relative humidity, self-stress, degree of hydration, and interface structure (Ye & Radlińska, 2016). Over time, free water in the matrix gradually decreases due to progressive hydration of cement, and the internal relative humidity reduces. Consequently, a large number of pores are formed in the hardened cement paste and the saturation of water in the pores declines. With the change in the saturation state of capillary pore from saturated to unsaturated, the inner concave surface of pore is subjected to an internal pressure. In order to make the concave surface in a state of equilibrium, the capillary tension increases by which autogenous shrinkage takes place(Fisher & Israelachvili, 1981). The schematic mechanism of autogenous shrinkage is shown in Figure 2-6.

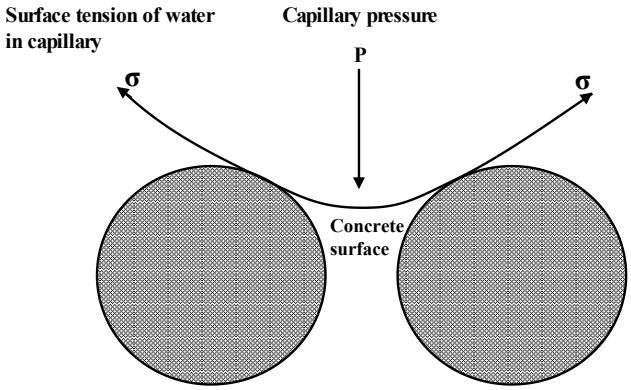


**Figure 2-6.** Schematic diagram of capillary water tension.

Capillary pressure can be calculated by the Laplace equation (eq.2-1) and Kelvin equation (eq. 2-2):

$$P_C - P_V = \Delta P = \frac{2\sigma \cos\theta}{r} \tag{2-1}$$

$$\frac{M}{\rho} \cdot \frac{2\sigma}{r} \cdot \cos\theta = RT \ln \frac{P_0}{P_r} \tag{2-2}$$

Where,

σ -surface tension of gas- liquid interface, mN/m;

θ - liquid-solid contact angle, rad;

$P_C$ - water pressure, Pa;

$P_V$ - water vapor pressure, Pa;

$P_0$- actual vapor pressure, Pa;

$P_r$- the saturated vapor pressure, Pa;

r - Hydraulic radius of capillary, Pa;

M - Molecular weight of water, $nm^3$;

ρ - Density of water;

R - ideal gas constant;

T - Absolute temperature, K.

Li and Li (Y. Li & Li, 2014) established a prediction method of early autogenous shrinkage of self- consolidating concrete based on the capillary tension theory and pore structure of concrete. In their study, negative pressure of capillary and autogenous shrinkage was determined by means of capillary tension theory. The computational model of the autogenous shrinkage determined by the capillary pores was expressed as $\epsilon = \frac{1-2\mu}{Es} . \frac{2\gamma}{r}$, where r is the critical capillary diameter, μ is the Poisson's ratio and $E_S$ is the modulus of elasticity of concrete with capillary tension. They showed that as time increased, the median pore diameter decreased and micro-pore porosity content increased which ultimately increased the autogenous shrinkage.

The capillary tension theory can well elaborate the accentuated influence of low water-to-cement ratio and SCMs in autogenous shrinkage of HPC as they remarkably affect the pore structure, relative humidity, and self- stress, degree of hydration, and interface structure. Although some studies have addressed the effects of pore structure and relative humidity in particular on autogenous shrinkage, the roles of self-stress, degree of hydration and interface structure are mostly discussed through influence of cement, SCMs, aggregates, and etc.

### 2.5.1 Pore Structure

Pore structure, which includes porosity, pore size distribution (pore gradation) and the morphology of pores, plays an important role in the autogenous shrinkage of cement based materials. The shrinkage stresses induced by consumption of water in pores of different sizes are dissimilar. The connectivity of pores also directly affects the migration of moisture from saturated to unsaturated pores, thus influences the development of shrinkage(Meddah & Tagnit-Hamou, 2009). Research on pore size has a crucial role in revealing the intrinsic laws of shrinkage and deformation.

In HPC, the decreasing rate of the critical hydraulic radius of capillary is accelerated due to the refinement of pore structure of bulk cement paste(Meddah & Tagnit-Hamou, 2009). The improved chemical reactions and the corresponded chemical shrinkage also increase the water consumption and triggers an additional surface tension. The increase in surface tension enlarges the capillary tension, and further promotes shrinkage stresses in HPC (Kong, Zhang, & Lu, 2015). The growth of volume ratio of bulk paste in HPC also increases the autogenous shrinkage (Huy, 2013). The increase of creep further accelerates the shrinkage of bulk paste in the presence of macro shrinkage stress. In a study by Li et al (Y. Li, Bao, & Guo, 2010), the effect of silica fume, slag and fly ash on pore structure were studied and the correlation with the autogenous shrinkage was elaborated. In their study, water-to-binder ratio was kept constant at a rate of 0.3. The results showed different influences on the autogenous shrinkage. Fly ash reduced the autogenous shrinkage while silica fume and slag markedly increased it. However, the effect of slag was reported to be reliant on the content. As for pore structure, both silica fume and slag refined the micro-pore structure, reduced the porosity and the pore mean diameter. They increased specific surface and the volumetric percentage of pores with diameter between 5 and 50 nm. It was concluded that the volumetric percentage was the main factor influencing the autogenous shrinkage. The refinement of pore structure led to an increase in the capillary tension and hence the autogenous shrinkage increased.

### 2.5.2 Relative humidity

Relative humidity is another influential factor in autogenous shrinkage which is more underscored in HPC. Hydration of cement induces the reduction of internal relative humidity of concrete and ultimately increases the internal pore pressure. Accordingly, the initial free water in the matrix (water-to-cement ratio) plays an important role (A. El-Dieb, 2007; J.-K. Kim & Lee, 1999). The relationship between the relative humidity and pore structure was discussed by Grasley and Lange(Grasley & Lange, 2007; Grasley, Lange, & D'Ambrosia, 2006). They measured the relative humidity at various locations inside concrete and also the thermal expansion and internal relative humidity changes of hardened cement paste. The results were indicative that the number of saturated pores governed the relative humidity changes inside concrete. Jiajun (Jiajun, Shuguang, Fazhou, Yufei, & Zhichao, 2006) investigated the effect of pre-wetting degree of aggregate on internal relative humidity of lightweight aggregate concrete. A measuring instrument was

utilized to monitor the relative humidity of the central part of concrete specimens. The results showed that the internal relative humidity of concrete reduced with the curing period. The humidity gradient from 1 to 7 days was particularly evident; however, incorporation of saturated lightweight aggregate delayed the reduction of internal relative humidity of concrete. The internal relative humidity and water introduced to the system by lightweight aggregate presented good linear relationship with autogenous shrinkage. Jiang at al. (Z. Jiang, Sun, & Wang, 2006; Z. Wu Z. Sun et al., 2003) further determined the relationship between internal relative humidity changes and autogenous shrinkage by measuring the effect of water-to-cement ratio and mineral admixtures on internal relative humidity of concrete in dry adiabatic conditions. From the point of thermodynamics, the reduced content of evaporative water in capillary pores by progressive hydration of cement compounds was reported to be responsible for reduction of relative humidity in concrete. Quanbing (Q. Yang, 1999) investigated the internal relative humidity and maturity of high performance concrete. The results showed that with the decrease of water-to-cement ratio and increase of silica fume quantity, the internal relative humidity of high performance concrete decreased; the relative humidity and the maturity value of outer layers of concrete were higher than that of the inner ones. This can increase the autogenous shrinkage in HPC where low water-to-cement ratio and SCMs are applied.

### 2.5.3 Self-stress

Based on the Hook law ($\sigma=E\varepsilon$), strain and elastic modulus are physical variables determining the shrinkage stress in high performance concrete. As mentioned earlier, Li and Li (Y. Li & Li, 2014) established a relationship between the elastic modulus of the micro-matrix around the capillary and the autogenous shrinkage. They reported that both compressive strength and elastic modulus increased rapidly at the early age and then the development rate slowed down which affected the autogenous shrinkage. As a result, any factors affecting the slurry structure of the matrix at the early age can induce autogenous shrinkage stresses. These factors can be divides into external and internal factors. Internal factors are the type of aggregate and cement, mix ratio, water-to-cement ratio, admixture, component size, etc.; external factors are temperature, humidity, sealing condition, the degree of restraint and etc.

### 2.5.4 Degree of hydration

The degree of hydration is largely influenced by cement type and content, SCMs, water-to-binder ratio and temperature. Many works have applied different techniques such as microstructural analysis or thermodynamics to measure or model the hydration degree. Detailed information can be found in works of Lothenbach et al. (Lothenbach et al., 2011) and Damidot et al. (Damidot, Lothenbach, Herfort, & Glasser, 2011) on degree of hydration and formation of C-S-H. However, previous studies mostly on autogenous shrinkage addressed the relationship between degree of hydration and autogenous shrinkage in HPC through effects of concrete major constituents or curing methods on autogenous shrinkage, which will be discussed in section 4. In a study by Pietro et al. (Lura, Jensen, & van Breugel, 2003) degree of hydration in the first week of hydration was specifically addressed and used to model the autogenous shrinkage using capillary tension method. The calorimetric data and Powers' volumetric model were used to calculate the development of the degree of hydration and saturation fraction, respectively. The simulated shrinkage curves were in good agreement with the experiments in the higher relative humidity range.

## 2.6 Interface structure

Concrete is a multiphase composite material and the type, quantity, size, shape and distribution of each phase constitute the structure of concrete. The cross section of concrete displays an evident two-phase structure; different sizes and shapes of aggregates, and cementitious hydrated cement paste. But, the microstructure of hardened cement paste next to coarse aggregate has noticeable inconsistency with hardened cement paste or mortar in the matrix, and major properties of concrete can only be illustrated when the cement paste-aggregate interface is regarded as the third phase of microstructure. Therefore, the concrete can be divided into aggregate, transition zone bonding to aggregate and the hardened cement paste. The structure of concrete depends on the combination of the three components after molding, the development of age, and hydration degree of cement in certain circumstances which can affect the autogenous shrinkage. Previous studies referred to the effect of pozzolanic reaction of silica fume that

consumed the calcium hydroxide (CH) crystals and removed the internal restraints in the paste and further induced shrinkage(mejlhede Jensen & Freiesleben Hansen, 1996). The effectiveness of calcium hydroxide in passive restraining the shrinkage can be supported by results from Carde and Francois (Carde & François, 1997) indicating loss in mechanical properties of cement paste due to leach out of calcium hydroxide. The carbonation shrinkage can also well explain the restraining effect of calcium hydroxide as its degradation leads to a volume change (J. J. Brooks, 2015).

## 2.7 Influential factors on autogenous shrinkage

### 2.7.1 Cement

#### 2.7.1.1 Composition of cement

Cement is the core component in cement-based materials with major constituent compounds namely, tricalcium silicate ($C_3S$), calcium silicate ($C_2S$), tricalcium aluminate ($C_3A$) and tetra calcium aluminate ferrite ($C_4AF$). A study by Tazawa (E.-i. Tazawa & S. Miyazawa, 1995) showed that the autogenous shrinkage of cement based materials can be predicted by the composition of cement. Hydration rate of $C_3S$ and $C_3A$ is rapid, and the heat release of hydration is enormous and concentrated, so the concrete structure is prone to generate cracks caused by temperature gradient in the early stage. Later, the consumption of interlayer water as well as volume reduction of hydration products during the transformation process promote larger shrinkage (E.-i. Tazawa, 1999; E.-i. Tazawa & S. Miyazawa, 1995; E. Tazawa & Miyazawa, 1997). In hydration of $C_3A$ , results showed that the heat release was even further with a rapid heat evolution, and a fast condensation speed, which would not only make large temperature deformation, but also would cause increase in autogenous and drying shrinkage of concrete (R. W. Burrows, 1998; P. K. Mehta & Burrows, 2001). Overall, the impact of $C_3A$ is the most dominant followed by $C_3S$, $C_4AF$ and $C_2S$ (Van Breugel & Van Tuan, 2015).

The effect of different types of cement on the autogenous shrinkage is essentially due to its different composition. For instance, higher contents of $C_3A$ and $C_3S$ in high-early-strength cements cause more autogenous shrinkage than that of low to moderate heat

generating cements in which higher contents of $C_2S$ are used. The autogenous shrinkage rate can also be affected when composite cement is used. A study by Neto et al. showed that the autogenous shrinkage of slag cement was more frequent than that of ordinary Portland cement (Neto, Cincotto, & Repette, 2008).

#### 2.7.1.2 Cement fineness

Along with demand for high strength concrete in the engineering construction, the fineness of modern cement has unceasingly increased. However, a study by Bullard et al. [9] showed that the increased fineness and larger specific surface area of cement decreased the relative humidity at a higher pace, and the corresponding autogenous shrinkage deformation was greater. It can be attributed to the accelerated cement hydration, and consequent water consumption in the matrix. This can lead to a decline in relative humidity, so as to intensify the capillary pressure and autogenous shrinkage deformation. In works by Bentz et al. (Dale P Bentz, Garboczi, Haecker, & Jensen, 1999; D. P. Bentz, M. R. Geiker, & K. K. Hansen, 2001), it was showed that higher fineness of Portland cement contributed to a faster reaction rate, caused more contraction phase of C-S-H gel. It displayed stronger ability for refinement of pores in the matrix and shrank the pore structure in the first 3 days of curing age. Following the extension of hydration period after 14 days, the hydration rate gradually slowed down and the autogenous shrinkage of the cement stopped. Figure 2-7 shows the effect of cement fineness on relative humidity and autogenous shrinkage.

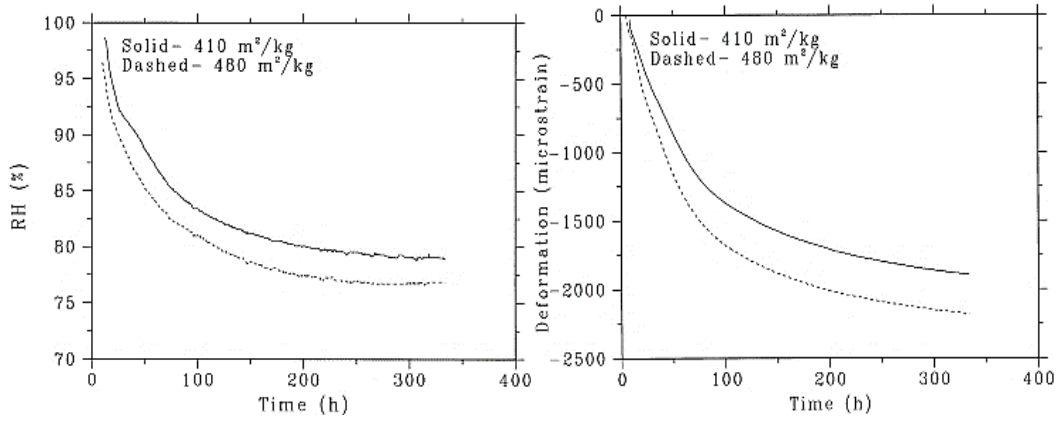


(a) Relative humidity (b) Autogenous shrinkage

**Figure 2-7.** Effect of the fineness of cement on (a) relative humidity (b) autogenous shrinkage (Dale P Bentz et al., 1999).

Therefore, the fineness of cement should be set appropriately in order to decrease the autogenous shrinkage. It was suggested by Bentz and Haecker (Dale P. Bentz & Haecker, 1999) that using coarse cement in high performance concrete may imbibe water for a longer period of time, and results in an increase in the long-term degree of hydration and a reduction in autogenous shrinkage.

Furthermore, sufficient attention should be paid to morphology of cement particles. Spherical cement particles have smaller contact area and larger pore radius, which is very conducive to reduce the autogenous shrinkage of concrete (Turcry, Loukili, Barcelo, & Casabonne, 2002). Thus, to reasonably control the cement particles composition, advanced technology and equipment should be applied.

## 2.7.2 Supplementary cementitious materials

### 2.7.2.1 Silica fume

Jensen et al. (mejlhede Jensen & Freiesleben Hansen, 1996) showed that the rate of autogenous shrinkage of high performance concrete at early stage of hydration correlated positively with the content of silica fume. They reported that the autogenous shrinkage of cement paste (w/b of 0.23) increased with the cumulative content of silica fume within content range of 0%-20%. With presence of 10% silica fume, the autogenous shrinkage of specimens was about 3 times of the plain paste at 28 days. A similar trend was observed in a study by Zhang et al.(M. Zhang et al., 2003). Figure 2-8 illustrates the effect of 5% and 10% silica fume at two different water to cement ratios. As can be seen, the autogenous shrinkage increased with the increase of silica fume content which was further affected when lower water-to-cement ratio was used. The increasing effect of silica fume on autogenous shrinkage were also reported in (Ghafari et al., 2016; Holt, 2005; Maruyama & Teramoto, 2013; Yang Yang, Sato, & Kawai, 2005).

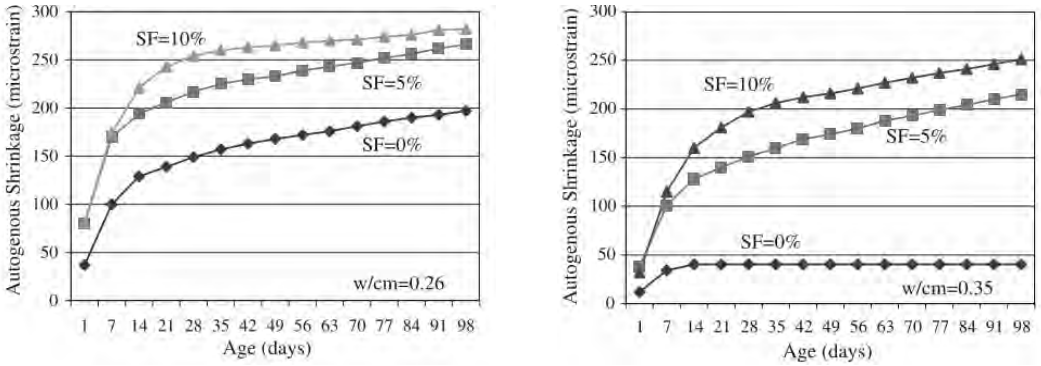


(a) (b)

**Figure 2-8.** Effect of silica fume content on autogenous shrinkage of concrete with low water-to- cement ratio from (M. Zhang et al., 2003).

Three mechanisms can be used to explain the results: (1) the richer contents of silica fume refined the pore structure to a certain extent, and the number of small pores increased, resulting in serious autogenous shrinkage of the specimens. (2) During the hydration of clinker, the formed CH was partly distributed into interlayer pores of C-S-H gel and restrained the chain. The addition of silica fume consumed the CH and the porous structure of C-S-H was formed. The empty pores caused by consumption of CH weakened their restraining effect on the C-S-H structure and increased the shrinkage of hardened cement paste (Mazloom, Ramezanianpour, & Brooks, 2004). In a study by Igarashi et al. (Igarashi, Bentur, & Kovler, 2000), the specimens with silica fume showed a greater creep tendency than that of a plain concrete in restrained shrinkage conditions. (3) In the third view, silica fume acted as a superfine active admixture, which accelerated the hydration reaction of cement. Large surface area of silica fume caused fast combination of silica fume and mixing water, accelerated the water shortage in the pore space of cement paste, reduced the relative humidity inside the cement matrix, and intensified the self-desiccation process (Paillere, Buil, & Serrano, 1989; G. A. Rao, 2001).

#### 2.7.2.3 Slag

In a study by Tazawa et al. (E. Tazawa & Miyazawa, 1997), it was showed that the autogenous shrinkage of concrete was proportional to the amount of slag with specific surface area over 400m$^2$/kg. With presence of excessive amounts higher than 75%, the autogenous shrinkage of concrete began to decrease. The inflection point decreased to 60% when fineness increased to 836 m$^2$/kg. The effect of slag fineness on autogenous shrinkage comes from the significant effect of fineness on its reactivity. The autogenous

shrinkage had negative correlation when slag with fineness of 338m$^2$/kg. In another study by Lee et al.(K. M. Lee, Lee, Lee, & Kim, 2006), it was also reported that the inclusion of slag especially at higher contents increased the autogenous shrinkage when compared with plain concrete specimens. Figure 2-9 shows the increasing effect of 30% and 50% cement replacement with slag on the autogenous shrinkage with water to binder ratio of 0.27 and 0.32. The results were indicative of higher increase in the autogenous shrinkage as the water-to-binder ratio decreased. The higher autogenous shrinkage was related to higher chemical shrinkage as a driving force in slag concrete than that of plain specimens. However, reportedly, the increasing effect of slag on autogenous shrinkage is less than that of silica fume due to less volume of fine pores and higher volume of coarser pores in slag concrete which contribute to lower capillary pressure in the paste and hence reduction of the autogenous shrinkage (Ghafari et al., 2016).

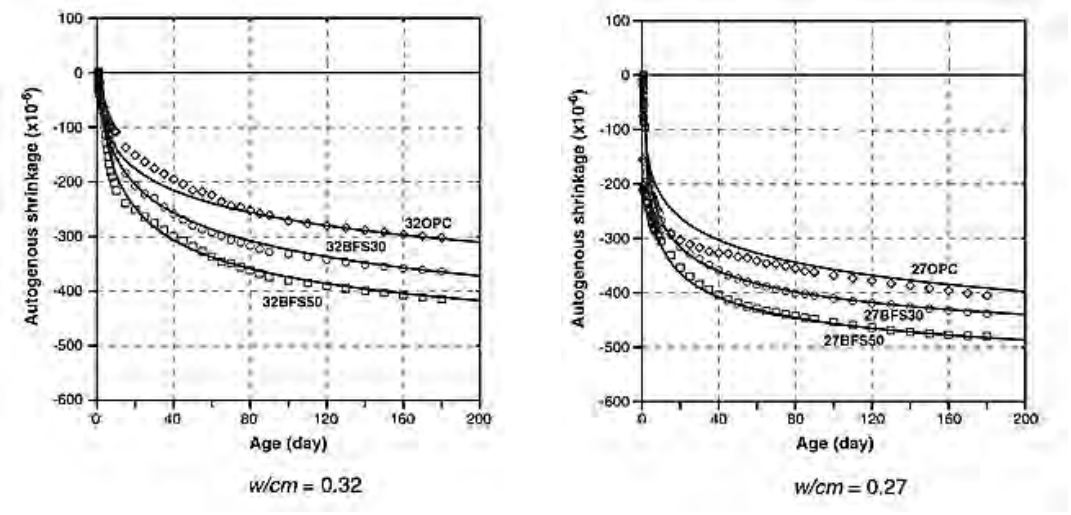


(a) (b)

**Figure 2-9.** Effect of slag content on autogenous shrinkage of concrete with low water to binder ratio adopted from (K. M. Lee et al., 2006).

Nevertheless, other researchers debated the increasing effect of slag on the autogenous shrinkage of concrete (Y. Li et al., 2010). For instance, in a study by Huang et al. (K. Huang, Deng, Mo, & Wang, 2013), volume expansion was observed when ground blast furnace slag cement was used. The analysis of literature shows that there is yet a great controversy on the effect of slag on autogenous shrinkage. The existing research results are based on the conclusions drawn from limited materials, thus the role of slag in autogenous shrinkage is still unknown.

#### 2.7.2.4 Fly ash

Previous work by Malhotra (Malhotra, 2002) showed that fly ash had an inhabiting effect on autogenous shrinkage due to deceleration of the reduction of internal humidity in the matrix. It was reported that the internal relative humidity of concrete specimens declined when fly ash was used which slowed down as the mixing amount of fly ash increased from 15% to 60% in a sealed condition with water-to-binder ration of 0.3. When the mixing amount of fly ash exceeded 40%, the reduction of internal relative humidity within 120 days exhibited less than 13%. This amount was more than 20% when plain cement was used. The addition of more than 60% fly ash maintained the internal relative humidity of concrete up to 7 days. Termkhajornkit et al. (Termkhajornkit, Nawa, Nakai, & Saito, 2005) also showed that the replacement of more than 50% fly ash remarkably reduced the autogenous shrinkage of concrete specimens with water-to-binder ratio of 0.3. They related the autogenous shrinkage partly to the hydration reactions of Portland cement and reactions of $Al_2O_3$ to form ettringite, and partly to hydration of fly ash; the latter brought about the slowdown of shrinking process. Huang and Hui (Guoxing Huang, 1990) measured the autogenous shrinkage of mass concrete with fly ash. It was reported that the incorporation of up to 20% fly ash reduced the autogenous shrinkage by half; while inclusion of 40% lowered the autogenous shrinkage as low as one tenth of plain specimens. The increased fineness and content of fly ash further decreased the autogenous shrinkage and prolonged the initial cracking time (P. K. Mehta, 1986). The reason lies in the slow hydration of fly ash in comparison to cement, which adds to the effective water-to-binder ratio by dilution effect, thereby reduces the early autogenous shrinkage. Nevertheless, the low content of fly ash does not inevitably reduce the autogenous shrinkage. Zhengwu et al. (Termkhajornkit et al., 2005)found that when the amount of fly ash was 10%, a portion of fly ash contributed to reduction of the autogenous shrinkage, while the rest had an adverse effect. Moreover, the early crack formation could not be avoidable by adding fly ash alone (Subramaniam et al., 2005) (Gdoutos, Shah, & Dattatraya, 2003). Fly ash showed to be the most effective in reduction of autogenous shrinkage comparing to that of silica fume and slag (Ghafari et al., 2016).

Overview of the above, it is understood that the effect of SCMs on autogenous shrinkage of HPC with low water-to-binder ratio is still controversial. On one hand, a comprehensive

understanding is restricted by lack of efficient testing instruments and methods, however, systematic research on the influence of these materials on shrinkage under low water-binder-ratio condition is indispensable. More importantly, it is not possible to fundamentally elucidate the influence without an in-depth study on the mechanism. The above problems seriously hinder the application of SCMs in the high-performance concrete in engineering practices.

#### 2.7.2.5 Water-to-binder ratio

Water-to-binder ratio has a remarkable influence on high performance concrete. HPC with low water-to-binder ratio below 0.4 is more prone to the autogenous shrinkage (M. Zhang et al., 2003). Figure 2-10 depicts the influence of water-to-binder ratio in HPC. They showed that a reduction of w/b from 0.35 to 0.30 resulted in a significant increase in the autogenous shrinkage, whereas a further reduction of w/c lowered the increasing effect. The effect of water-to-binder ratio was less pronounced when silica fume was also used. The role of water-to-binder ratio in autogenous shrinkage with presence of slag and silica fume was also studied by Jiang et al. (Z. Jiang, Sun, & Wang, 2005) which was in agreement with (M. Zhang et al., 2003). It was reported that addition of slag to the binary mix of cement and silica fume decreased the autogenous shrinkage especially at early ages. Wang et al. (Chong Wang, et al., 2008) utilized a segmental screw micrometer to investigate autogenous shrinkage characteristics of cement based materials with ultra-low water-to-binder ratio. The results indicated that water-to-binder of 0.25 was a critical ratio. When water-to-binder ratio was higher than 0.25, the autogenous shrinkage dropped with the increasing of water-to-binder ratio; on the contrary, the water-to-binder ratio lower than 0.25 declined the autogenous shrinkage as it increased. The pore structure and low degree of hydration of cement based materials with ultra-low water-to-binder ratio were regarded as main reasons, albeit, further study is still needed.

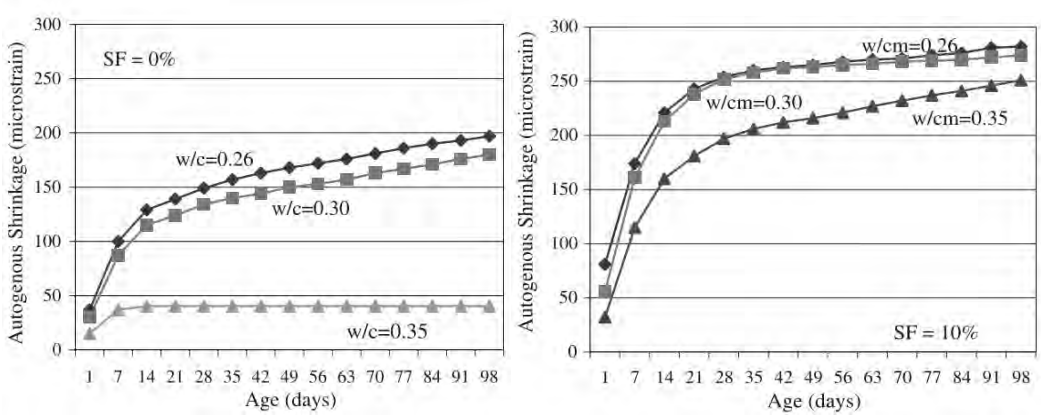


(a) (b)

**Figure 2-10.** Effect of water-to-binder ratio on autogenous shrinkage of high performance concrete from (M. Zhang et al., 2003).

In a study by Tian (Qian Tian, 2006), it was showed that the reduction of water-to-binder ratio decreased internal relative humidity of cement slurry, particularly at the early age; and significant increase of self-desiccation effect was observed. However, further reduction of internal humidity depended on the hydration progress, and did not decrease with the reduction of water-to-binder ratio. It was explained that as water-to-binder ratio decreased, the total pore volume of high performance concrete reduced as well, and pore structure was refined. This induced water redistribution toward the inside of finer micro pores, accelerated the reduction of critical radius and enlarged the capillary negative pressure and autogenous shrinkage. Critical radius is defined as the minimum size that must be formed by atoms or molecules clustering together (in a gas, liquid or solid matrix) before a new-phase inclusion (a bubble, a droplet, or a solid particle) is stable and begins to grow.

#### 2.7.2.6 Aggregate

Autogenous shrinkage of concrete is also controlled by aggregates. The aggregates provide constraints during shrinkage of bulk paste and hence a bearing pressure is formed on the paste and aggregate surface interface in the normal and tangent directions (Figure 2-11). The stress field is gradually transferred from the aggregate surface to the bulk paste, and the interface surface goes under the maximum stress. If shrinkage stress is large enough, cracks along the aggregate surface in the normal direction are first appeared on the

interface (Ling Qi, 1996).

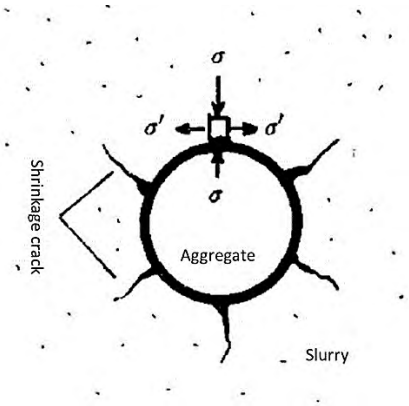


**Figure 2-11.** Schematic diagram of shrinkage crack in the interface area from (Ling Qi, 1996).

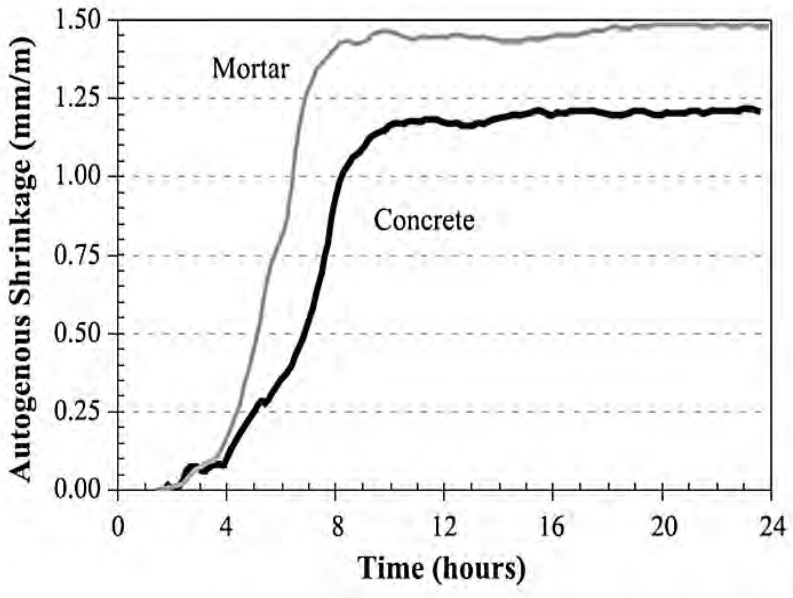


**Figure 2-12.** Autogenous shrinkage resulting with addition of aggregate from mortar (paste volume = 57%) to concrete (paste volume = 34%) at w/c ratio = 0.30 from (Holt, 2005) .

In the HPC, owing to the limited effect of aggregate on the deformation of cement, the autogenous shrinkage of concrete is inferior to that of bulk paste. Holt (Holt, 2005) studied the effect of mix design including aggregate on concrete with low water-to-binder ratio of 0.3. The effect of aggregate on autogenous shrinkage is shown in Figure 2-12 in which mortar and concrete specimens are compared. The restraining effect of aggregate on autogenous shrinkage is well elaborated as explained earlier. The results of Tazawa's research (E.-i. Tazawa & S. Miyazawa, 1995) showed that for high performance concrete with high workability and durability, reduction in amount of cementitious materials and

increase in volume of aggregate with larger elastic modulus can decrease the autogenous shrinkage of concrete.

Besides, incorporation of lightweight aggregates can further reduce the autogenous shrinkage in the HPC. Compared with ordinary dense aggregates, the lightweight aggregates are porous, with high water absorption (Bentur, Igarashi, & Kovler, 2001; Kohno, Okamoto, Isikawa, Sibata, & Mori, 1999). The water absorbed by lightweight aggregate offers a decent internal curing environment during hardening process of concrete. Under the action of capillary tension, the water in lightweight aggregate migrates to the cement paste and provides internal water for unhydrated cement particles, and maintains the gradually decreasing internal relative humidity of concrete. Higher water content of lightweight aggregate and more water available for migration make stronger compensation for the autogenous shrinkage. This characteristic was employed to reduce the shrinkage and cracking tendency of concrete with low water-to-cement ratio in early stages (Ji, Zhang, Zhuang, & Wu, 2015). Accordingly, lightweight aggregate and ordinary dense aggregate compounded into a composite aggregate matrix to reduce the autogenous shrinkage (Figure 2-13) in order to meet the requirements of high performance of concrete. The same trend was observed when low quality recycled aggregates were used (Gonzalez-Corominas & Etxeberria, 2016). Additionally, lightweight aggregates are composed of silicate and aluminosilicate glass phase with a surface sheltered with a layer of hard glass shell, which has potential chemical reactivity, and can react with cement hydration products mainly CH. So, the interaction between lightweight aggregates and cement is not only a physical function, but also a certain degree of chemical action. Moreover, owing to open pores on the lightweight aggregate surface, the structure of lightweight aggregate is relatively rough, and it has a strong mechanical action with the cement paste. Besides, the internal soluble ions of lightweight aggregate have a certain degree of influence on the formation process of the interface structure, so as to effectively improve the interface between lightweight aggregate and cement paste.

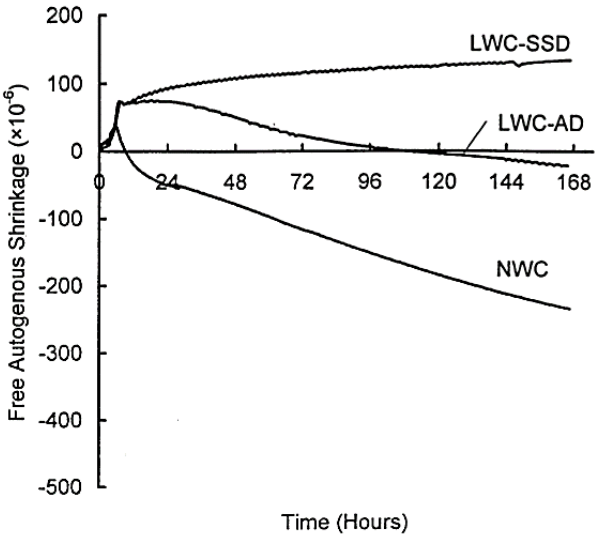


**Figure 2-13.** Comparison of autogenous shrinkage of lightweight aggregate concrete and normal concrete (LWC: lightweight concrete; NWC: normal weight concrete; SSD: saturated surface dry; AD: air dry.

## 2.7.3 Fibers

### 2.7.3.1 Steel fibers

Previous works showed that addition of steel fibers markedly suppressed the shrinkage of concrete (K. Huang, Deng et al., 2013; Miao, Chern, & Yang, 2003). In general, the positive effect of steel fibers on the reduction of autogenous shrinkage in HPC can be explained with the following mechanism. In the mixing process of steel fiber and concrete, a few micron water film is formed on steel fiber surface, so calcium hydroxide crystals grow with no constraints and arrange on the surface of steel fiber directionally, which forms loose reticular structure in the interface of steel fiber and matrix (Wei Sun, 1987). Besides, high elastic modulus of steel fiber can support the skeleton in the process of free shrinkage of concrete (Amin Noushini, Vessalas, Arabian, & Samali, 2014). Due to the tensile stress of fiber, a range of bond stress distribution is created around the fiber close to the cracks, and the development of crack tip will be inhibited due to constraints and barriers of fiber. Hence, the steel fibers can reduce the shrinkage and deformation of the high-performance concrete. Figure 2-14 illustrates the effect of steel fibers on autogenous shrinkage in high performance concrete with water-to-binder ratio of 0.2. The steel fibers were 12 mm long and 0.4 mm in diameter at a volume of 6%.

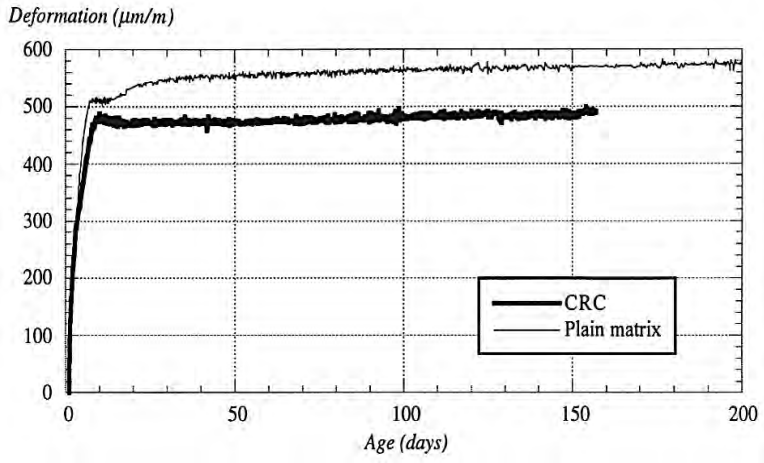


**Figure 2-14.** Autogenous shrinkage of plain and steel fiber-reinforced concrete specimens (CRC : compact reinforced composite) from (Loukili, Khelidj, & Richard, 1999).

Both the autogenous shrinkage and the total shrinkage of HP-SFRC are less than the values corresponding to the comparable HPC. By gradually adding longer steel fibres (l=30 mm) up to 1 % of the composite volume, the shrinkage of the HP-SFRC can be significantly reduced, whereas if the fibre content is further increased, only a relatively small reduction in the composite shrinkage can be achieved. When using shorter steel fibres (l=16 mm), the shrinkage of the composite can, with an increase in the fiber content, be noticeably reduced only up to a fiber content of 0.75 % by volume of the composite. When the volume content of the steel fibers is higher than 1 %, the workability of the composite becomes significantly poorer, especially when longer fibers are used (Bandelj, Branko, et al, 2011, Paillere, A_M, M. Buil, and J. J. Serrano 1989).

Reportedly, as the steel fiber content exceeded a certain amount, the cohesiveness increased and the mobility of high performance concrete was reduced in return. This decreased the compactness of high performance concrete and resulted in the growth of pores and autogenous shrinkage in the concrete (Habel, Viviani, Denarié, & Brühwiler, 2006; H. Lee, Lee, & Kim, 2003; A. Turatsinze, H. Farhat, & J.-L. Granju, 2003). Lin (Hongbin Lin, 2011) reported that steel fiber contents below 0.6% reduced the autogenous shrinkage of high performance concrete. The positive effect of steel fibers increased with the increase of steel fiber content by up to 0.65%. They stated that the reduction of autogenous shrinkage was due to the smaller interspace between the micro steel fiber and concrete matrix, denser filling, stronger bonds between fiber and concrete matrix, and

more excellent interface structure with the presence of low content of micro steel fibers. The incorporation of higher contents of steel fiber to 0.9% had an adverse effect on the autogenous shrinkage. Yu and Zhao (Junchao Yu & Xinqing Zho, 2013) also reported a reduced beneficial effect of steel fibers on shrinkage as excessive contents were used. The results showed that with the increasing content of micro steel fiber volume, the workability of concrete decreased, accompanied by fibers agglomeration, which greatly influenced the performance of concrete. Thus, in engineering practice, a reasonable amount of micro fiber needs to be considered. They also reported that the influence of steel fiber content on shrinkage was lower after the hardening of concrete. With the growth of the age, the elastic modulus of the matrix increased, and the influence of the steel fiber content on shrinkage declined accordingly.

#### 2.7.3.2 Synthetic fibers

Among fibers other than steel, Polypropylene fibers (PP) are more widely used in HPC (Pakravan, Latifi, & Jamshidi, 2017). However, the available studies mostly targeted the plastic shrinkage and a distinct effect of fibers on autogenous shrinkage needs to be investigated. PP fibers added into cement paste can be adhered to the cement particles, convert the granular cement into coarse particles, and enlarge interparticle friction, shear stress, and tensile strength, which can ultimately reduce the shrinkage at the plastic stage(S. Jian, W. Kong et al., 2014). Furthermore, due to the presence of fibrous materials on polypropylene fiber surface, water migration is challenged and the rate of water evaporation is minimized; leading to lower capillary tension caused by the water loss from the capillary voids. On the other hand, the mixture of polypropylene fiber shrinks the cracks generated by the inner stress of high performance concrete, especially for the cracks formed by dewatering of concrete in plastic stage (J. Sun, F. Luan & Yu Zhang, 2000). Extensive research on effects of PP fibers on plastic shrinkage and early age cracking is available in (Mazzoli, Monosi, & Plescia, 2015; S. Jian, et al., 2014) which is not within the scope of this study. A study by Kaufmann et al. (Kaufmann et al., 2004), explicitly compared the effect of PP and carbon fibers on autogenous shrinkage when 20% fine cement was used with a low water-to-cement ratio of 0.19. Figure 2-15illustrates the length change of the paste specimens as well as heat of hydration at the first 30 hrs. of hydration. As can be seen, the effect of 1% PP was remarkable on the reduction of

autogenous shrinkage. Swelling was also observed at times corresponded to the major peak of hydration which reduced the autogenous shrinkage.

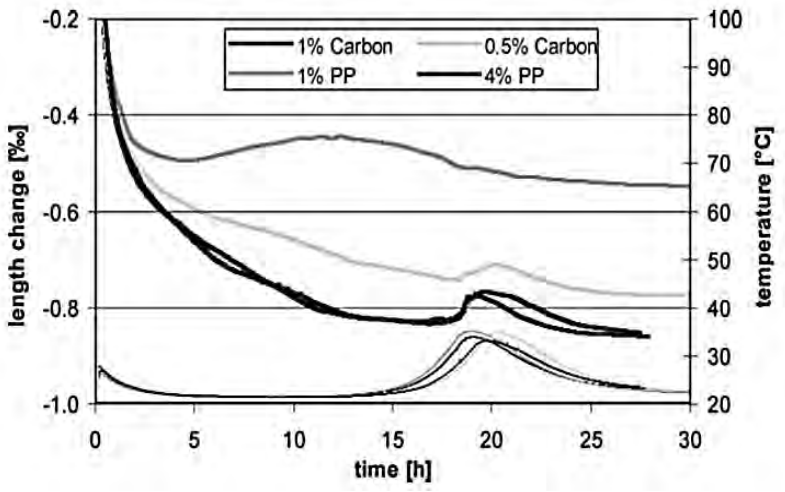


**Figure 2-15.** The effect of PP and carbon fibres on the autogenous shrinkage of pastes form (Kaufmann et al., 2004).

Another synthetic fiber used in concrete is Polyvinyl alcohol (PVA) fiber with high strength and high modulus of elasticity. A uniform distribution of disorientated fibers can block micro-cracks in the matrix during the hardening process, and prevent them to grow into harmful cracks, and hence increase the cracking resistance at early ages. Incorporation of PVA fibers in concrete also increases the number of bubbles, pores and the porosity. In addition, polyvinyl alcohol fiber is hydrophilic, so it can adsorb water in the fresh concrete. A research by Shujin Li (Shujin Li, Hongping Qian & Zhengcheng Xu, 2014) showed that the addition of polyvinyl alcohol fiber decreased the initial free shrinkage of self-compacting concrete, but the reduction range was limited.

### 2.7.3.3 Cellulose fibers

Cellulose fibers are other types of fibers being used in some applications in concrete industry. Cellulose is a natural polymer consisting of D-anhydro-glucose ($C_6H_{11}O_5$) repeating units joined by $\beta$-1, 4-glycosidic linkages. Each repeating unit contains three hydroxyl groups which play an important role in directing the crystalline packing and the physical properties of cellulose by forming hydrogen bonds (Nevell & Zeronian, 1985). The reinforcing effectiveness of cellular fiber is due to the nature of cellulose and its crystallinity. In a study by Kawashima and Shah (Kawashima & Shah, 2011), the effect of

cellulose fibers on autogenous shrinkage of mortar with water-to-binder ratio of 0.28 was investigated. They reported that the addition of 1% cellulose fiber significantly inhibited the cracks caused by autogenous shrinkage due to the internal solidification of the matrix. It was stated that incorporation of cellulose fibers especially at higher contents had internal curing capabilities, however, it might cause an adverse effect on the workability. So, the improvement of dispensability could improve the applicability fibers to be used in concrete. Figure 2-16 shows the reducing effect of cellulose fibers on autogenous shrinkage during the first 7 days of hydration.

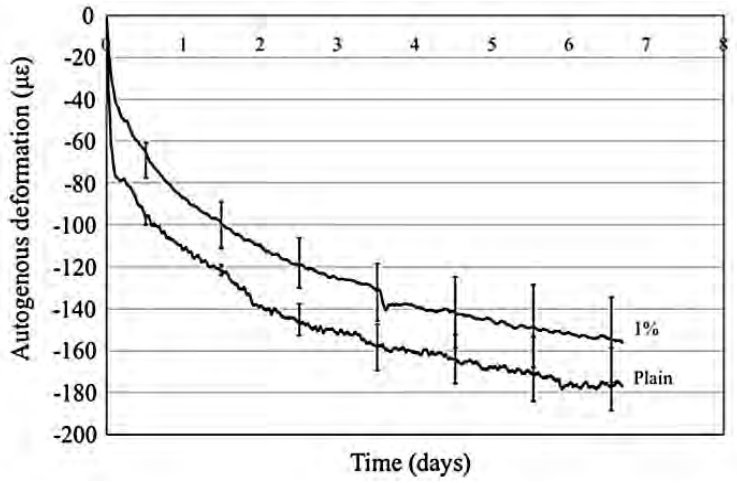


**Figure 2-16.** Linear autogenous deformation of mortar specimens with and without cellulose fiber addition (Zeroed to time of final set) from (Kawashima & Shah, 2011).

## 2.7.4 Chemical admixtures

### 2.7.4.1 Water reducing agents

In the premise of maintaining the liquidity, the addition of water reducing agents decreases the water-to-cement ratio and hence increases the possibility of autogenous shrinkage occurrence(Tam et al., 2012). Holt (Holt, 2005) reported that the addition of 1% superplasticizer to mortar with w/c of 0.3 increased the autogenous shrinkage by almost 30%. They related the greater autogenous shrinkage of mortar specimens with SP to the improved cement dispersion and faster rate of hydration reactions in the matrix. On the other hand, the lower shrinkage of specimens with no added water reducing agent was attributed to increased heterogeneities, such as cluster formations between aggregates and their internal restraining effect. The acceleration of hydration rate and its subsequent

increase in autogenous shrinkage was also reported in (Beltzung & Wittmann, 2002).

#### 2.7.4.2 Shrinkage reducing agents

The effects of shrinkage reducing agents on the autogenous shrinkage were reported by some workers (Dale P Bentz, 2008; D. P. Bentz et al., 2001; Lura, Pease, Mazzotta, Rajabipour, & Weiss, 2007; Rongbing & Jian, 2005). In order to explore the possibility of cracking by shrinkage in HPC, Yoo (D.-Y. Yoo, Banthia, & Yoon, 2015; D.-Y. Yoo, Kang, Lee, & Yoon, 2013) adopted three shrinkage reducing agent contents (0%, 1% and 2%) and three different reinforcement ratio (1.3%, 2.9% and 8.0%). Based on the hydration degree model, experimental and predicted results of tensile strength were obtained. Also, the effect of shrinkage reducing agents on autogenous shrinkage of fiber reinforced HPC in free and constrained state was explored. The results revealed that the content of shrinkage reducing agent had positive correlation with the tensile strength, but negative correlation with the autogenous shrinkage. It was observed that the high shrinkage reducing agent contents led to an increase in porosity of the interface transition zone between fiber and matrix. At higher reducing agent contents and lower reinforcement ratio, the autogenous shrinkage behavior was better suppressed. In another study by Rongbing and Jian (Rongbing & Jian, 2005), it was shown that for a shrinkage reducing agent content of 2%, the autogenous shrinkage of mortar declined by 30-40% in the first 60 days, and 20~30% when duration extended to 90 days. The shrinkage reducing agents efficiently delayed the development of capillary pressure on the concave surface, and lessened the shrinkage cracking of concrete at the plastic stage, especially for the high-strength concrete(Bullock & Foltz, 1995). However, shrinkage reducing agents also have a potential risk of early strength drop in concrete, extension of the aggregating time, and sometimes adverse interactions with other admixtures such as air entraining agent(Tam et al., 2012).

#### 2.7.4.3 Expansive agents

The macroscopic expansion of system by inclusion of expansive agents can be utilized to partially compensate the autogenous shrinkage generated in the early stage. Liu et al. (Jiaping Liu, Qian Tian & Mingshu Tang, 2006) studied the effect of expansive agents on shrinkage cracking of concrete with high volume mineral admixtures. It was showed that under the sealed or sufficient curing conditions, concrete mixed with expansive agents

eliminated the autogenous shrinkage, and prompted self-expansion. At the same time, the initial cracking time was elongated and the ability of shrinkage cracking resistance was enhanced. In the dry environments, however, the initial crack time was half an hour earlier, and the crack width increased correspondingly. In a study by Mo et al. (L. Mo, Deng, & Wang, 2012), they compared the expansive effect of aluminate (AEA) and MgO (MEA) based expansive agents. It was reported that MEAs were more efficient in cement based materials with low water to binder ratio. Figure 2-17 shows the effect of two expansive agents on the autogenous shrinkage in comparison with the reference under non-wet curing condition. The higher effectiveness of MgO based agent was attributed to the relatively low water requirement for the hydration of MgO and its slow hydration rate, while aluminate based agents need higher amount of water to compensate the shrinkage cause by the self-desiccation of the system. To further reduce the autogenous shrinkage, some efforts have been made to combine expansive and shrinking reducing agents. Meddah et al. (Meddah, Suzuki, & Sato, 2011) studied combined effect of the admixtures on HPC with 10% silica fume and water-to-binder ratio of 15, 23, and 30%. Their results showed a remarkable reduction of 50% in autogenous shrinkage and self-tensile stress induced in concrete specimens with w/c of 0.15 when combination of agents was used. The hybrid mixture of agents was more effective on concrete with a w/b higher than 0.23 by which the shrinkage was almost eliminated. The shrinkage reduction was related to the simultaneous action of the agents and their synergistic effect. However, it was reported that the inclusion of a combination of admixtures caused a slight decrease in the early age compressive and splitting tensile strengths as well as the modulus of elasticity. Oliveira et al. (Oliveira, Ribeiro, & Branco, 2014) also confirmed the advantageous combination of shrinkage reducing and expansive agents on autogenous shrinkage. They attributed that to a lower degree of restraint of the solid body with presence of shrinkage reducing agents when the expansive action occurred. They, however, suggested to formulate mixtures to have a desired autogenous shrinkage.

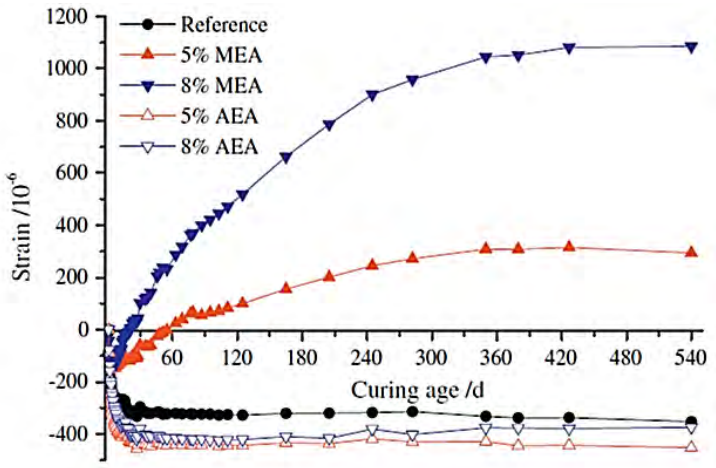


**Figure 2-17.** Autogenous shrinkage of paste specimens containing various contents of MEA and AEA under non-wet curing condition.

#### 2.7.4.4 Curing methods

For high performance concrete with compact pore structure, external curing has little effect on lowering the autogenous shrinkage. Internal curing, though, can compensate the weak role of external curing on early shrinkage cracking of HPC. An extensive literature review is recently available on internal curing and its effects on early age shrinkage of HPC(J. Liu et al., 2017). The internal curing of concrete refers to the introduction of extra water by adding absorbent materials in concrete. When the internal relative humidity drops, the imbibed water can gradually be released into the matrix to compensate water consumption inside cement paste, hence, the concrete internal humidity can be maintained at a high level. By this mechanism self-desiccation can be suppressed, and the autogenous shrinkage can be effectively reduced. Commonly used materials for internal curing include porous shale, ceramic aggregate and polymer materials with high water absorption. Super absorbent polymers (SAPs) are new polymer materials with very high water absorbency and spatial network structure. SAPs are ideal internal curing materials with high adsorption rate and little influence on the strength; and easy to dehydrate(Ole Mejlhede Jensen & Hansen, 2001, 2002). Some scholars discussed the effects of adding SAP on mechanical properties and autogenous shrinkage deformation of low water-to-cement ratio concrete (Craeye, Geirnaert, & De Schutter, 2011; McDermott, Chen, Williams, Markley, & Payne, 2004; Pang, Ruan, & Cai, 2011; F. Wang, Zhou, Peng, Liu, & Hu, 2009; Xinwei Ma, Xueying Li & Hejun Jiao, 2009). Nevertheless, so far, a convincing explanation

for mechanism of shrinkage rules of SAP has not been provided and sufficient theoretical support for making SAP as a curing agent in concrete engineering application is missing, which restricts its development and application. Jensen (Ole Mejlhede Jensen & Hansen, 2001) was first to put forward the use of SAP as an inside curing materials. He investigated the possibility of using super absorbent polymer for self-curing from theoretical and experimental aspects. Bentz et al (Schlitter, Bentz, & Weiss, 2013) showed that incorporation of SAP could form a stable internal water supply source inside the bulk paste. Because of its sufficient fineness, it could be evenly distributed in concrete to inhibit uneven expansion and shrinkage and reduced the formation of micro cracks. Besides. It had no adverse effects on workability of mixture. The addition of SAP had a significant effect on reduction of the autogenous shrinkage of high performance concrete. Results showed that the autogenous shrinkage rate after 28 days was 32% ~ 46% of that of specimens without SAP. It should be stated that the addition of SAP had an undesirable effect on the strength and performance of high performance concrete.

## 2.8 Conclusions and Outlook

### 2.8.1 Concluding remarks

Autogenous shrinkage is an unavoidable volume reduction due to the self-desiccation of concrete, especially when low water-to-cement ratio is applied. In this chapter, through the analysis of autogenous shrinkage research results of high performance concrete, the following conclusions can be drawn:

(1) Capillary tension theory well explicates the autogenous mechanism in concrete. This theory can elaborate the accentuated influence of low water-to-cement ratio and SCMs in autogenous shrinkage of HPC as they remarkably affect the pore structure, relative humidity, self- stress, degree of hydration, and interface structure.

(2) Although some studies have addressed the effects of pore structure and relative humidity in particular on autogenous shrinkage, the role of self-stress, degree of hydration and interface structure are mostly discussed through influence of cement, SCMs, aggregates, and etc.

(3) The utilization of low temperature and spherical shape cement can properly reduce autogenous shrinkage. Appropriate contents of fly ash can inhibit autogenous shrinkage of concrete, while silica fume increases autogenous shrinkage. The effect of slag on autogenous shrinkage, though, depends on its fineness.

(4) Internal curing is an effective means to reduce the autogenous shrinkage of high performance concrete. Lightweight aggregate and high water absorbent polymers can considerably reduce the autogenous shrinkage of high performance concrete

(5) The impact of steel fiber is associated with the content; low amount of steel fibers can restrain the autogenous shrinkage of concrete, while excessive contents increase cohesiveness and decrease workability of high performance concrete, which can lead to furthered autogenous shrinkage.

### 2.8.2 Research needs

Although meaningful results have been achieved in the research field of autogenous shrinkage of concrete with low water-to-cement ratio, the following aspects of the efforts also need to be carried out:

(1) The definition of shrinkage is not entirely unified, and the established test methods also lack uniform standards, which restricts the further development of this field.

(2) The effect of supplementary cementitious materials on shrinkage deformation behavior is still controversial, and its mechanism shows absence of an in-depth study.

(3) Researches mostly intend for a single shrinkage behavior, but ignore the connection between various shrinkage mechanisms, which is difficult to grasp the characteristics of shrinkage and deformation of concrete.

(4) The researches on mechanism of autogenous shrinkage are mainly limited to the capillary theory, and some factors have not been taken into account, such as temperature

and the type of supplementary cementitious materials. Moreover, effects of mixing content on shrinkage strain rate and ultimate shrinkage value are also unclear. Simultaneously, the influence mechanism of internal curing agents on autogenous shrinkage should be further reconnoitered.

## 2.9 References


A. Williams, A. Markandeya, Y. Stetsko, K. Riding, A. Zayed, Cracking potential and temperature sensitivity of metakaolin concrete, Construction and Building Materials 120 (2016) 172-180.

P. Lura, O.M. Jensen, K. van Breugel, Autogenous shrinkage in high-performance cement paste: An evaluation of basic mechanisms, Cement and Concrete Research 33(2) (2003) 223-232.

U.D.S.L.P. LE, the use of lightweight sand for internal curing and its effect on performance of hpc used for concrete infrastructures, (2013).

D. Wang, C. Shi, Z. Wu, J. Xiao, Z. Huang, Z. Fang, A review on ultra high performance concrete: Part II. Hydration, microstructure and properties, Construction and Building Materials 96 (2015) 368-377.

K. Van Breugel, N. Van Tuan, Autogenous Shrinkage of HPC and Ways to Mitigate it, Trans Tech Publ2015.

W. Li, Z. Huang, T. Zu, C. Shi, W.H. Duan, S.P. Shah, Influence of nanolimestone on the hydration, mechanical strength, and autogenous shrinkage of ultrahigh-performance concrete, Journal of Materials in Civil Engineering 28(1) (2015) 04015068.

R. Henkensiefken, D. Bentz, T. Nantung, J. Weiss, Volume change and cracking in internally cured mixtures made with saturated lightweight aggregate under sealed and unsealed conditions, Cement and Concrete Composites 31(7) (2009) 427-437.

R.D. Recommendation, P.D.R. DE LA RILEM, Creep and shrinkage prediction model for analysis and design of concrete structures-model B3, Mater. Struct 28 (1995) 357-365.

Z. Bazant, J. Chern, Concrete creep at variable humidity: constitutive law and mechanism, Materials and structures 18(1) (1985) 1.

P. Lura, Autogenous deformation and internal curing of concrete, TU Delft, Delft University of Technology, 2003.

E. Tazawa, Technical committee report on Autogenous shrinkage, Proceedings of JCI 18 (1996) 29-38.

P.K. Mehta, Concrete. Structure, properties and materials, (1986).

I. Maruyama, A. Teramoto, Temperature dependence of autogenous shrinkage of silica fume cement pastes with a very low water–binder ratio, Cement and Concrete Research 50 (2013) 41-50.

C. Jiang, Y. Yang, Y. Wang, Y. Zhou, C. Ma, Autogenous shrinkage of high performance concrete containing mineral admixtures under different curing temperatures, Construction and Building materials 61 (2014) 260-269.

E. Holt, Contribution of mixture design to chemical and autogenous shrinkage of concrete at early ages, Cement and Concrete Research 35(3) (2005) 464-472.

J.W. Bullard, H.M. Jennings, R.A. Livingston, A. Nonat, G.W. Scherer, J.S. Schweitzer, K.L. Scrivener, J.J. Thomas, Mechanisms of cement hydration, Cement and Concrete Research 41(12) (2011) 1208-1223.

P. Mounanga, A. Khelidj, A. Loukili, V. Baroghel-Bouny, Predicting Ca $(OH)_2$ content and chemical shrinkage of hydrating cement pastes using analytical approach, Cement and Concrete Research 34(2) (2004) 255-265.

R.D. Toledo Filho, K. Ghavami, M.A. Sanjuán, G.L. England, Free, restrained and drying shrinkage of cement mortar composites reinforced with vegetable fibres, Cement and Concrete Composites 27(5) (2005) 537-546.

A. Itim, K. Ezziane, E.-H. Kadri, Compressive strength and shrinkage of mortar containing various amounts of mineral additions, Construction and Building Materials 25(8) (2011) 3603-3609.

M. Zhang, C. Tam, M. Leow, Effect of water-to-cementitious materials ratio and silica fume on the autogenous shrinkage of concrete, Cement and Concrete Research 33(10) (2003) 1687-1694.

G.A. Rao, Long-term drying shrinkage of mortar—influence of silica fume and size of fine aggregate, Cement and concrete research 31(2) (2001) 171-175.

G. Rao, Influence of silica fume replacement of cement on expansion and drying shrinkage, Cement and concrete research 28(10) (1998) 1505-1509.

B.A. Schrefler, C.E. Majorana, G.A. Khoury, D. Gawin, Thermo-hydro-mechanical modelling of high performance concrete at high temperatures, Engineering Computations 19(7) (2002) 787-819.

J. Kaufmann, F. Winnefeld, D. Hesselbarth, Effect of the addition of ultrafine cement and short fiber reinforcement on shrinkage, rheological and mechanical properties of Portland cement pastes, Cement and Concrete Composites 26(5) (2004) 541-549.

P. Aitcin, Autogenous shrinkage measurement, Autogenous shrinkage of concrete: proceedings of the international workshop, organised by JCI (Japan Concrete Institute), Hiroshima, June 13-14, 1998, Taylor & Francis, 1999, p. 257.

V.S. Ramachandran, Concrete admixtures handbook: properties, science and technology, William Andrew1996.

P.C. Aïtcin, The durability characteristics of high performance concrete: a review, Cement and Concrete Composites 25(4–5) (2003) 409-420.

A.C.L. Wong, P.A. Childs, R. Berndt, T. Macken, G.-D. Peng, N. Gowripalan, Simultaneous measurement of shrinkage and temperature of reactive powder concrete at early-age using fibre Bragg grating sensors, Cement and Concrete Composites 29(6) (2007) 490-497.

B. Persson, Eight-year exploration of shrinkage in high-performance concrete, Cement and Concrete Research 32(8) (2002) 1229-1237.

B. Persson, Experimental studies on shrinkage of high-performance concrete, Cement and Concrete Research 28(7) (1998) 1023-1036.

H. Ye, A. Radlińska, A review and comparative study of existing shrinkage prediction models for portland and non-portland cementitious materials, Advances in Materials Science and Engineering 2016 (2016).

L.R. Fisher, J.N. Israelachvili, Experimental studies on the applicability of the Kelvin equation to highly curved concave menisci, Journal of colloid and Interface Science 80(2) (1981) 528-541.

Y. Li, J. Li, Capillary tension theory for prediction of early autogenous shrinkage of self-consolidating concrete, Construction and Building Materials 53 (2014) 511-516.

M.S. Meddah, A. Tagnit-Hamou, Pore structure of concrete with mineral admixtures and its effect on self-desiccation shrinkage, ACI Mater J 106(3) (2009) 241-250.

X.-m. Kong, Z.-l. Zhang, Z.-c. Lu, Effect of pre-soaked superabsorbent polymer on shrinkage of high-strength concrete, Materials and Structures 48(9) (2015) 2741-2758.

Q. Huy, Modelling properties of cement paste from microstructure: porosity, mechanical properties, creep and shrinkage, ÉCOLE POLYTECHNIQUE FÉDÉRALE DE LAUSANNE, 2013.

Y. Li, J. Bao, Y. Guo, The relationship between autogenous shrinkage and pore structure of cement paste with mineral admixtures, Construction and Building Materials 24(10) (2010) 1855-1860.

J.-K. Kim, C.-S. Lee, Moisture diffusion of concrete considering self-desiccation at early ages, Cement and Concrete Research 29(12) (1999) 1921-1927.

A. El-Dieb, Self-curing concrete: Water retention, hydration and moisture transport, Construction and Building Materials 21(6) (2007) 1282-1287.

Z.C. Grasley, D.A. Lange, M.D. D'Ambrosia, Internal relative humidity and drying stress gradients in concrete, Materials and Structures 39(9) (2006) 901-909.

Z.C. Grasley, D.A. Lange, Thermal dilation and internal relative humidity of hardened cement paste, Materials and Structures 40(3) (2007) 311-317.

Y. Jiajun, H. Shuguang, W. Fazhou, Z. Yufei, L. Zhichao, Effect of pre-wetted light-weight aggregate on internal relative humidity and autogenous shrinkage of concrete, Journal of Wuhan University of Technology-Mater. Sci. Ed. 21(1) (2006) 134-137.

Z. Jiang, Z. Sun, P. Wang, Internal relative humidity distribution in high-performance cement paste due to moisture diffusion and self-desiccation, Cement and Concrete Research 36(2) (2006) 320-325.

Q. Yang, Inner relative humidity and degree of saturation in high-performance concrete stored in water or salt solution for 2 years, Cement and Concrete Research 29(1) (1999) 45-53.

B. Lothenbach, K. Scrivener, R. Hooton, Supplementary cementitious materials, Cement and Concrete Research 41(12) (2011) 1244-1256.

D. Damidot, B. Lothenbach, D. Herfort, F. Glasser, Thermodynamics and cement science, Cement and Concrete Research 41(7) (2011) 679-695.

O. mejlhede Jensen, P. Freiesleben Hansen, Autogenous deformation and change of the relative humidity in silica fume-modified cement paste, ACI Materials Journal 93(6) (1996) 539-543.

C. Carde, R. François, Effect of the leaching of calcium hydroxide from cement paste on mechanical and physical properties, Cement and Concrete Research 27(4) (1997) 539-550.

J.J. Brooks, 6 - Shrinkage of Concrete, Concrete and Masonry Movements, Butterworth-Heinemann2015, pp. 137-185.

E.-i. Tazawa, S. Miyazawa, Influence of cement and admixture on autogenous shrinkage of cement paste, Cement and Concrete Research 25(2) (1995) 281-287.

E. Tazawa, S. Miyazawa, Influence of constituents and composition on autogenous shrinkage of cementitious materials, Magazine of Concrete Research 49(178) (1997) 15-22.

E.-i. Tazawa, Autogenous shrinkage of concrete, CRC Press1999.

R.W. Burrows, The visible and invisible cracking of concrete, American Concrete Institute, 1998.

P.K. Mehta, R.W. Burrows, Building durable structures in the 21 st century, Indian Concrete Journal 75(7) (2001) 437-443.

A.A.M. Neto, M.A. Cincotto, W. Repette, Drying and autogenous shrinkage of pastes and mortars with activated slag cement, Cement and Concrete Research 38(4) (2008) 565-574.

D.P. Bentz, E.J. Garboczi, C.J. Haecker, O.M. Jensen, Effects of cement particle size distribution on performance properties of Portland cement-based materials, Cement and Concrete Research 29(10) (1999) 1663-1671.

D.P. Bentz, O.M. Jensen, K.K. Hansen, J.F. Olesen, H. Stang, C.J. Haecker, Influence of Cement Particle‐Size Distribution on Early Age Autogenous Strains and Stresses in Cement‐Based Materials, Journal of the American Ceramic Society 84(1) (2001) 129-135.

D.P. Bentz, C.J. Haecker, An argument for using coarse cements in high-performance concretes, Cement and Concrete Research 29(4) (1999) 615-618.

P. Turcry, A. Loukili, L. Barcelo, J.M. Casabonne, Can the maturity concept be used to separate the autogenous shrinkage and thermal deformation of a cement paste at early age?, Cement and Concrete Research 32(9) (2002) 1443-1450.

E. Ghafari, S.A. Ghahari, H. Costa, E. Júlio, A. Portugal, L. Durães, Effect of supplementary cementitious materials on autogenous shrinkage of ultra-high performance concrete, Construction and Building Materials 127 (2016) 43-48.

Y. Yang, R. Sato, K. Kawai, Autogenous shrinkage of high-strength concrete containing silica fume under drying at early ages, Cement and Concrete Research 35(3) (2005) 449-456.

M. Mazloom, A. Ramezanianpour, J. Brooks, Effect of silica fume on mechanical properties of high-strength concrete, Cement and Concrete Composites 26(4) (2004) 347-357.

S.-i. Igarashi, A. Bentur, K. Kovler, Autogenous shrinkage and induced restraining stresses in high-strength concretes, Cement and Concrete Research 30(11) (2000) 1701-1707.

A.M. Paillere, M. Buil, J. Serrano, Effect of fiber addition on the autogenous shrinkage of silica fume, Materials Journal 86(2) (1989) 139-144.

K.M. Lee, H.K. Lee, S.H. Lee, G.Y. Kim, Autogenous shrinkage of concrete containing granulated blast-furnace slag, Cement and Concrete Research 36(7) (2006) 1279-1285.

K. Huang, M. Deng, L. Mo, Y. Wang, Early age stability of concrete pavement by using hybrid fiber together with MgO expansion agent in high altitude locality, Construction and Building Materials 48 (2013) 685-690.

V. Malhotra, High-performance high-volume fly ash concrete, Concrete International 24(7) (2002) 30-34.

P. Termkhajornkit, T. Nawa, M. Nakai, T. Saito, Effect of fly ash on autogenous shrinkage, Cement and Concrete Research 35(3) (2005) 473-482.

R.H. Guoxing Huang, The shrinkage of concrete China railway publishing house1990.

Jiang Zhengwu etc., The drying effects of high performance concrete research. Journal of building materials, 2004. 7(1): Page19-24.

K.V. Subramaniam, R. Gromotka, S.P. Shah, K. Obla, R. Hill, Influence of ultrafine fly ash on the early age response and the shrinkage cracking potential of concrete, Journal of materials in civil engineering 17(1) (2005) 45-53.

M.K. Gdoutos, S. Shah, D. Dattatraya, Relationships between engineering characteristics and material properties of high strength-high performance concrete, Role of Concrete In Sustainable Development: Proceedings of the International Symposium dedicated to Professor Surendra

Shah, Northwestern University, USA held on 3–4 September 2003 at the University of Dundee, Scotland, UK, Thomas Telford Publishing, 2003, pp. 37-46.

Z. Jiang, Z. Sun, P. Wang, Autogenous relative humidity change and autogenous shrinkage of high-performance cement pastes, Cement and Concrete Research 35(8) (2005) 1539-1545.

Wang Chong, Low water-binder ratio the hydration process of cement paste material test. Journal of materials science and engineering, 2008, 26 (6): pp. 857-852.

Tian Qian, low water/cement ratio of cement base material with high content mineral admixtures is shrinking and its mechanism research [D], 2006. Nanjing: southeast university school of materials science and engineering.

Qi Ling, some mechanical properties of concrete in the interface. Journal of guangxi institute of technology, 1996. 7 (1) : page 26 to 30.

K. Kohno, T. Okamoto, Y. Isikawa, T. Sibata, H. Mori, Effects of artificial lightweight aggregate on autogenous shrinkage of concrete, Cement and concrete research 29(4) (1999) 611-614.

A. Bentur, S.-i. Igarashi, K. Kovler, Prevention of autogenous shrinkage in high-strength concrete by internal curing using wet lightweight aggregates, Cement and concrete research 31(11) (2001) 1587-1591.

T. Ji, B.-b. Zhang, Y.-Z. Zhuang, H.-C. Wu, Effect of Lightweight Aggregate on Early-Age Autogenous Shrinkage of Concrete, ACI Materials Journal 112(3) (2015).

A. Gonzalez-Corominas, M. Etxeberria, Effects of using recycled concrete aggregates on the shrinkage of high performance concrete, Construction and Building Materials 115 (2016) 32-41.

B. Miao, J.C. Chern, C.A. Yang, Influences of fiber content on properties of self‐compacting steel fiber reinforced concrete, Journal of the Chinese Institute of Engineers 26(4) (2003) 523-530.

Sun Wei, steel fiber reinforced concrete interface research. Concrete and cement products, 1987 (02): 3-7

A. Noushini, K. Vessalas, G. Arabian, B. Samali, Drying shrinkage behaviour of fibre reinforced concrete incorporating polyvinyl alcohol fibres and fly ash, Advances in Civil Engineering 2014 (2014).

A. Loukili, A. Khelidj, P. Richard, Hydration kinetics, change of relative humidity, and autogenous shrinkage of ultra-high-strength concrete, Cement and Concrete Research 29(4) (1999) 577-584.

K. Habel, M. Viviani, E. Denarié, E. Brühwiler, Development of the mechanical properties of an ultra-high performance fiber reinforced concrete (UHPFRC), Cement and Concrete Research 36(7) (2006) 1362-1370.

H. Lee, K. Lee, B. Kim, Autogenous shrinkage of high-performance concrete containing fly ash, Magazine of Concrete Research 55(6) (2003) 507-515.

A. Turatsinze, H. Farhat, J.-L. Granju, Influence of autogenous cracking on the durability of repairs by cement-based overlays reinforced with metal fibres, Materials and Structures 36(10) (2003) 673-677.

Lin Hongbin, the preparation and properties of steel fiber reinforced self-compacting high-strength concrete research, 2011, Chongqing university.

Yu junchao, Zhao qingxin, steel fiber on the properties of concrete creep effects. Journal of silicate, 2013 (8): 1093-1087.

H.R. Pakravan, M. Latifi, M. Jamshidi, Hybrid short fiber reinforcement system in concrete: A review, Construction and Building Materials 142 (2017) 280-294.

Shouwei Sai, Wei Sun, Baoguo Ma, Lvdong Zhang, Fiber influence on thin layer mortar early plastic shrinkage, material review 28(22) (2014) 109-113.

Jiaying sun, Feng ruan and Yu Zhang, reticulate polypropylene fiber on the properties of high performance concrete durability. Journal of silicate, 2000. 28: pp. 64-62.

A. Mazzoli, S. Monosi, E.S. Plescia, Evaluation of the early-age-shrinkage of Fiber Reinforced Concrete (FRC) using image analysis methods, Construction and Building Materials 101 (2015) 596-601.

T.P. Nevell, S.H. Zeronian, Cellulose chemistry and its applications, (1985).

S. Kawashima, S.P. Shah, Early-age autogenous and drying shrinkage behavior of cellulose fiber-reinforced cementitious materials, Cement and Concrete Composites 33(2) (2011) 201-208.

C.M. Tam, V.W. Tam, K.M. Ng, Assessing drying shrinkage and water permeability of reactive powder concrete produced in Hong Kong, Construction and Building Materials 26(1) (2012) 79-89.

F. Beltzung, F. Wittmann, Influence of cement composition on endogenous shrinkage, Self-desiccation and Its Importance in Concrete Technology. Report TVBM3104. ISBN 573185343 (2002) 113-126.

D.P. Bentz, A review of early-age properties of cement-based materials, Cement and Concrete Research 38(2) (2008) 196-204.

B. Rongbing, S. Jian, Synthesis and evaluation of shrinkage-reducing admixture for cementitious materials, Cement and Concrete Research 35(3) (2005) 445-448.

P. Lura, B. Pease, G.B. Mazzotta, F. Rajabipour, J. Weiss, Influence of shrinkage-reducing admixtures on development of plastic shrinkage cracks, ACI Materials Journal 104(2) (2007) 187.

D.-Y. Yoo, N. Banthia, Y.-S. Yoon, Effectiveness of shrinkage-reducing admixture in reducing autogenous shrinkage stress of ultra-high-performance fiber-reinforced concrete, Cement and Concrete Composites 64 (2015) 27-36.

D.-Y. Yoo, S.-T. Kang, J.-H. Lee, Y.-S. Yoon, Effect of shrinkage reducing admixture on tensile and flexural behaviors of UHPFRC considering fiber distribution characteristics, Cement and Concrete Research 54 (2013) 180-190.

R.E. Bullock, S.D. Foltz, REMR Management Systems-Navigation and Reservoir Structures, Condition Rating Procedures for Concrete in Gravity Dams, Retaining Walls, and Spillways, DTIC Document, 1995.

Jia-ping liu, Tian Qian and ming-shu tang, expansive agent and shrinkage-reducing agent for the influence of shrinkage cracking of high performance concrete [J]. Journal of southeast university: natural science edition, 2006 (2): 199-195.

L. Mo, M. Deng, A. Wang, Effects of MgO-based expansive additive on compensating the shrinkage of cement paste under non-wet curing conditions, Cement and Concrete Composites 34(3) (2012) 377-383.

M.S. Meddah, M. Suzuki, R. Sato, Influence of a combination of expansive and shrinkage-reducing admixture on autogenous deformation and self-stress of silica fume high-performance concrete, Construction and Building Materials 25(1) (2011) 239-250.

M.J. Oliveira, A.B. Ribeiro, F.G. Branco, Combined effect of expansive and shrinkage reducing admixtures to control autogenous shrinkage in self-compacting concrete, Construction and Building Materials 52 (2014) 267-275.

J. Liu, C. Shi, X. Ma, K.H. Khayat, J. Zhang, D. Wang, An overview on the effect of internal curing on shrinkage of high performance cement-based materials, Construction and Building Materials 146 (2017) 702-712.

O.M. Jensen, P.F. Hansen, Water-entrained cement-based materials: I. Principles and theoretical background, Cement and concrete research 31(4) (2001) 647-654.

O.M. Jensen, P.F. Hansen, Water-entrained cement-based materials: II. Experimental observations, Cement and Concrete Research 32(6) (2002) 973-978.

L.F. Pang, S.Y. Ruan, Y.T. Cai, Effects of internal curing by super absorbent polymer on shrinkage of concrete, Key Engineering Materials, Trans Tech Publ, 2011, pp. 200-204.

B. Craeye, M. Geirnaert, G. De Schutter, Super absorbing polymers as an internal curing agent for mitigation of early-age cracking of high-performance concrete bridge decks, Construction and Building Materials 25(1) (2011) 1-13.

Ma xinwei, Li Xueying, Jia Hejun, The application of super absorbent polymers in mortar and concrete. Journal of Wuhan University of technology, 2009(2).

F. Wang, Y. Zhou, B. Peng, Z. Liu, S. Hu, Autogenous shrinkage of concrete with super-absorbent polymer, ACI Materials Journal 106(2) (2009) 123.

M.K. McDermott, T. Chen, C.M. Williams, K.M. Markley, G.F. Payne, Mechanical properties of biomimetic tissue adhesive based on the microbial transglutaminase-catalyzed crosslinking of gelatin, Biomacromolecules 5(4) (2004) 1270-1279.

J. Schlitter, D. Bentz, W. Weiss, Quantifying stress development and remaining stress capacity in restrained, internally cured mortars, ACI Materials Journal 110(1) (2013) 3.

# CHAPTER 3 EVALUATION OF FIBRE ON AUTOGENOUS SHRINKAGE OF ULTRA-HIGH PERFORMANCE CONCRETE BY RING TEST

Note: this chapter is based on the manuscript entitled “Combine tube test and ring test ultra-high performance concrete to predict the autogenous shrinkage of ultra-high performance concrete”, by Linmei Wu, Z Zhang and H Wang, published in Proceedings of the 1st RILEM International Conference on UHPC Materials and Structures, pp46-52, Oct 27-30, 2016, Changsha, China

**ABSTRACT**: Due to high content of cementitious materials and low water-to-binder ratio (w/b), ultra-high performance concrete (UHPC) have high autogenous shrinkage. In this study, the effects of steel fibre on the autogenous shrinkage of UHPC was evaluated by using ring tests and corrugated tube method under plastic film sealed conditions. The results indicated that the development of autogenous shrinkage of UHPC was mainly during the first 24 hours. The autogenous shrinkage of UHPC is significant reduced by adding steel fibre. The optimal fibre content was found to be 3% where UHPC exhibited highest strength (107 MPa at 3 day) and lowest autogenous shrinkage (750×10-6μm at 3 day, which was only 30% of that of the specimens without steel fibre).

## 3.1 Introduction

Autogenous shrinkage of cement based materials is an important factor causing cracking of early-age cement(Pei, Li, Zhang, & Ma, 2014). It is defined as sum of chemical shrinkage and autogenous drying shrinkage (Dale P Bentz, 2008; L. Wu et al., 2017b). Nowadays, there are many methods to measure autogenous shrinkage. Autogenous shrinkage of

cement based materials is an important factor of cracking of early-age cement. There are different definitions of autogenous shrinkage and testing methods recently. Autogenous shrinkage should be defined as the summary of chemical shrinkage and autogenous drying shrinkage, not just refers one of them. Wherever all testing methods can be divided into two categories: direct and indirect measurement methods. The direct methods usually measure volumetric or one dimensional changes. The indirect methods usually measures porosity or humidity change of cement-based materials, which can reflect the autogenous shrinkage change. Indirect methods need to establish correlations between autogenous shrinkage and porosity or humidity. And all of the current testing methods for recording autogenous shrinkage can be divided into direct and indirect methods. Buoyancy method and corrugated tube measurement as the oldest and most common method of direct method, are mainly used for cement paste and mortar test, (R. Burrows, Kepler, Hurcomb, Schaffer, & Sellers, 2004; O Mejlhede Jensen & Hansen, 1995). but the testing result of usually buoyancy method shows poor repeatability (Turcry et al., 2002).Corrugated tube measurement (Dale P Bentz & Peltz, 2008)combines the advantages and disadvantages of the measure volumetric and the one dimensional changes at the same time, starting from casting, it can avoid the influence of environment, but if you add fiber in UHPC , it is difficult to operate(Ole Mejlhede Jensen & Hansen, 2002). Even so, corrugated tube measurement is as the first selection for autogenous shrinkage so for(Bao, Meng, Chen, Chen, & Khayat, 2015; Hu et al., 2013).

To reduce the magnitude of early-age shrinkage and cracking potential, several mitigation strategies have been proposed including the use of steel fiber. To appropriately utilize steel fiber, it is important to have a complete understanding of the driving forces behind early-age volume change and how steel fiber work from a materials science perspective to

reduce shrinkage under unrestrained and restrained conditions. Autogenous shrinkage of cement based materials is an important factor governs cracking at early-age of hydration.

Tensile stress can develop in concrete when constraint prevents the concrete from shrinking freely in response to drying, chemical reaction, or temperature reduction. When these tensile stresses exceed the tensile strength of the concrete, visible cracking may be expected to occur. While several test methods have been developed to assess a material's potential for early-age shrinkage cracking, this chapter describes the use of the 'ring-test' (Figure 3-1) for assessing the performance of a fiber reinforced concrete.

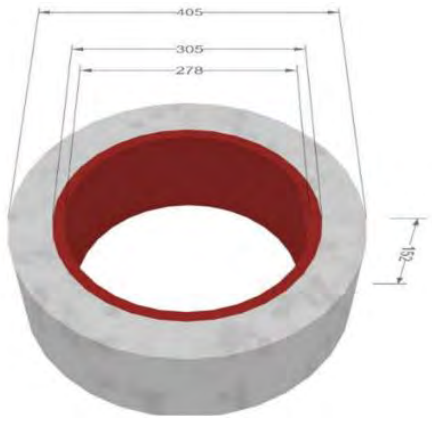


**Figure 3-1.** Test steel ring (Note: Dimensions are in millimetres).

Through a large number of documents, you can see that there are a lot of people did ring experiment, but are used for the experiment and the resistance to cracking, and the drying shrinkage test, in this chapter, the circle is applied to the autogenous shrinkage of UHPC, compared with the traditional method of corrugated pipe, and also got good result.

In this chapter, the cracking sensitivity was evaluated when the UHPC was under concrete shrinkage stress. Steel-UHPC composite ring tests was used to evaluate comparatively. Measuring the compressive strain along circle direction in the steel ring and observation of cracking status on the ring specimen.

## 3.2 Test program

### 3.2.1 Raw materials

Portland cement P.I 42.5 complying with the Chinese Standards GB175-2007 was used. Table 1 summarizes the physical properties of the cement. Fly ash and ground furnace slag were used to partially replace cement in concrete mix, with the specific surface area were 427 $m^2$/kg and 446 $m^2$/kg, respectively. Silica fume with 63%particle of 0.1~0.5 μm and specific surface area of 18500 $m^2$/kg was used. Table 2 presents the chemical properties of the cement and these supplementary cementitious materials. The natural river sand with maximum particle size of 2.36 mm and fineness modulus of 3.0. It has apparent density and packing density of 2550 kg/$m^3$ and 1570 kg/$m^3$, respectively. The straight steel fiber with the diameter of 0.2 mm and length of 13 mm was used. A polycarboxylate based super-plasticizer (SP) with solid content of 21% was used.

**Table 3-1:** Physical properties of Portland cement P.I 42.5

| Density (kg/$m^3$) | 80 μm-residue on sieve (%) | Specific surface area ($m^2$/kg) | Setting time(h) | | Flexural Strength (MPa) | | Compressive Strength (MPa) | |
|---|---|---|---|---|---|---|---|---|
| | | | Initial | Final | 3d | 28d | 3d | 28d |
| 3.15 | 0.3 | 380 | 2.5 | 3.4 | 6.4 | 9.0 | 33.0 | 60.0 |

**Table 3-2:** Chemical compositions of cementitious materials (%)

| Chemical Composition | $SiO_2$ | $Al_2O_3$ | $Fe_2O_3$ | CaO | MgO |
|---|---|---|---|---|---|
| Cement | 25.26 | 6.38 | 4.05 | 64.67 | 2.68 |
| Silica fume | 90.82 | 1.03 | 1.50 | 0.45 | 0.83 |
| Slag | 33 | 13.91 | 0.82 | 39.11 | 10.04 |
| Fly ash | 54.29 | 22.55 | 5.53 | 1.34 | 2.56 |

### 3.2.2 Mixture proportions

Mixture proportion of UHPC with w/b of 0.18 and binder-to-aggregate ratio of 1.1 was used, as shown in Table 3. The SP dosage was fixed at 2% by the mass of the binder. Steel fiber contents were 0, 1%, 2%, and 3% by the volume of concrete.

**Table 3-3:** Mixture proportions of UHPC

| No. | Cement (%) | Silica fume (%) | Slag (%) | Fly Ash (%) | SP (%) | w/b | binder-aggregate ratio | Steel fiber content (V %) |
|---|---|---|---|---|---|---|---|---|
| K1 | 55 | 20 | 25 | 0 | 2 | 0.18 | 1：1.1 | 0 |
| K2 | 55 | 20 | 25 | 0 | 2 | 0.18 | 1：1.1 | 1 |
| K3 | 55 | 20 | 25 | 0 | 2 | 0.18 | 1：1.1 | 2 |
| K4 | 55 | 20 | 25 | 0 | 2 | 0.18 | 1：1.1 | 3 |
| F1 | 55 | 20 | 0 | 25 | 2 | 0.18 | 1：1.1 | 0 |
| F2 | 55 | 20 | 0 | 25 | 2 | 0.18 | 1：1.1 | 1 |
| F3 | 55 | 20 | 0 | 25 | 2 | 0.18 | 1：1.1 | 2 |
| F4 | 55 | 20 | 0 | 25 | 2 | 0.18 | 1：1.1 | 3 |

### 3.2.3 Mixing procedure and sample preparation

In mixing procedure, dry powders, including cement, silica fume, slag or fly ash, and natural river sand, were first mixed for 3 min at high speed. Then water and super-plasticizer were added and mixed for approximately 6 min at a low speed. Afterwards, steel fibers were added through passing a sieve with size of 5 mm and mixed for another 6 min until the mixtures were uniformly distributed. Then UHPC mixtures were casted into molds and vibrated to consolidate the mixtures.

## 3.3 Test procedures

### 3.3.1 Unrestrained autogenous shrinkage test: autogenous shrinkage corrugated tube measurement

Fresh mixtures were filled into corrugated polyethylene tubes with 10 mm inner diameter using a hopper and rodded with a glass rod in order to eliminate the air and ensure their complete consolidation. After that, the free end was immediately sealed with a stainless steel head. Original lengths of specimen were measured as references. Then the gauge head was fixed at a distance of 2 mm to the free end. The experimental data were recorded immediately after the sensor was connected to the data acquisition system. The data record interval was 5 min and the measurement period were 72 hours. The experiment was conducted in a room at 20±2 °C and with precision of 0.0001 mm. The autogenous shrinkage was calculated as follows:

$$\varepsilon_{st} = \frac{a_t - a_0}{l_0} \qquad (3\text{-}1)$$

where, $\varepsilon_{st}$ is the autogenous shrinkage of concrete at time t (h); $a_t$ is the distance between the sensor head and the steel free head (mm) at time t; $a_0$ is the initial distance between the sensor head and the steel free head (mm); $l_0$ is the original length of the specimens (mm).

### 3.3.2 Restrained autogenous shrinkage test: ring test

Figure3-2 shows an overview of the ring restraint test. Based on the procedures for the ring restraint test suggested by ASTM C 1581-04, a steel ring with outer diameter of 330 ±3.3 mm and the inner diameter of 406±3 mm was used in the tests. The height of ring was 152±6 mm and the thickness of concrete was 38±3mm. Each ring specimen was equipped with four strain gauges that were placed at mid-height on the inner

circumference of the steel ring. The strain gauges were zeroed before concrete ring cast and the strains were automatically recorded every one minute after finishing the specimen surface. The fresh concrete material was cast into the ring mold in two layers and was consolidated by a vibrating table. After finishing the surfaces, the casting face was sealed with soft plastic sheet to prevent moisture exchange with its surroundings. All tests were carried out in the same laboratory where the autogenous shrinkage tests were carried out.

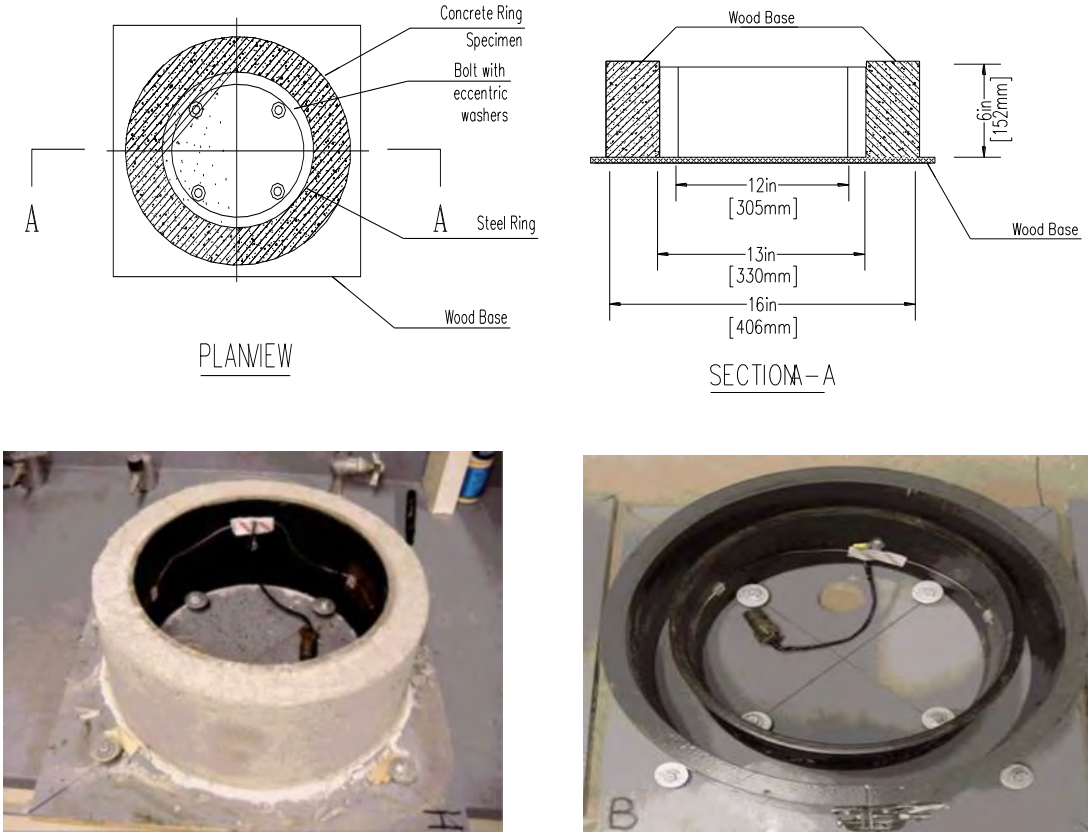


**Figure 3-2.** Ring test.

## 3.4 Results and discussion

### 3.4.1 Unrestrained autogenous shrinkage

The experimental results of the development of autogenous shrinkage of UHPC with ages since material casting are shown in Figure 3-3(a) and (b) respectively for slag added UHPC and fly ash added UHPC under the plastic film sealing conditions. The development of autogenous shrinkage strain with age roughly obeys two-stage pattern, i.e. a fast developing stage within the first 12 h since the specimen cast followed by an increasing stage with a gradually reducing rate. The magnitudes of autogenous shrinkage strains in each stage are different for the slag and fly ash UHPCs with different fiber contents. The absolute value of autogenous shrinkage strains in the observed period are 2420 μm/m and 1320 μm/m respectively for non-fiber reinforced slag and fly ash added UHPCs, respectively. The autogenous shrinkage strain in second stage of non-fiber reinforced slag added UHPC is larger than that of non-fiber reinforced fly ash added UHPC and the development of autogenous shrinkage strain of non-fiber reinforced slag added UHPC is much faster than that of non-fiber reinforced fly ash based UHPC. The autogenous shrinkage strain of fiber-reinforced slag added UHPC is comparable with the autogenous shrinkage of similar fiber-reinforced fly ash added UHPC under the sealing conditions.

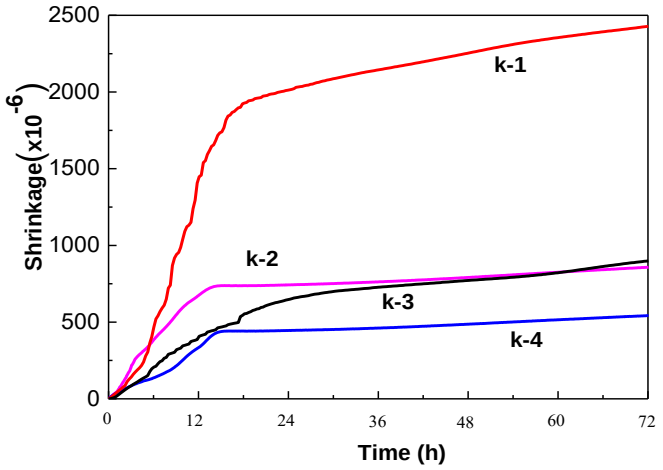


(a) Slag added UHPC

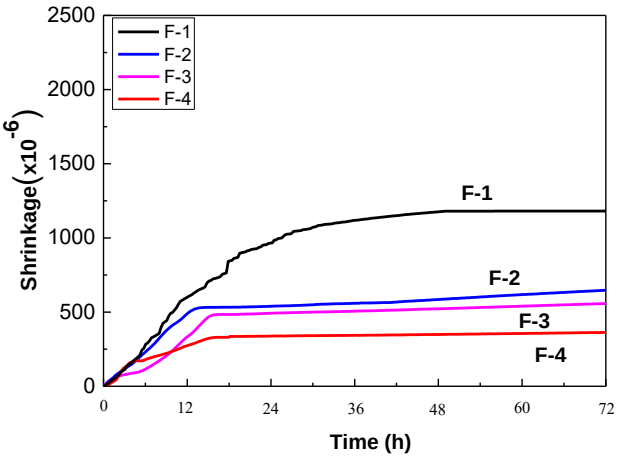


(b) Fly ash added UHPC

**Figure 3-3.** Development of autogenous shrinkage of UHPC.

In the first 14 hours after specimen cast, the development of autogenous shrinkage of the slag UHPC and fly ash UHPC are very similar. When the specimens are starting to dry, an increased rate on the autogenous shrinkage will occur. The autogenous shrinkage strain of slag added UHPC is noted to be larger than that of the fly ash added UHPC. At 72 h, the autogenous shrinkage non-fiber reinforced UHPC is about 4 times larger than that containing 3% fiber. It is evident that the autogenous shrinkage of both the slag and fly ash added UHPC are greatly reduced after using the fiber.

### 3.4.2 Restrained autogenous shrinkage

The development of compressive strain along circle direction at middle location of the inner surface of the steel ring with age since casting of the slag and fly ash added UHPC are presented in Figure 3-4. The compressive strain increases with age after material casting. After the material cast, due to autogenous shrinkage of the concrete, a compressive circle strain along circle direction of the steel ring is formed and gradually increases. The circle strain with age firstly increases with a decelerated rate then gradually goes into a relative stable stage at which a steady strain value is achieved. For the non-

fiber reinforced slag and fly ash added UHPCs, the circle strain are 1300 and 1280 μm/m respectively at 24 hours after casting, which become stable (almost constant).

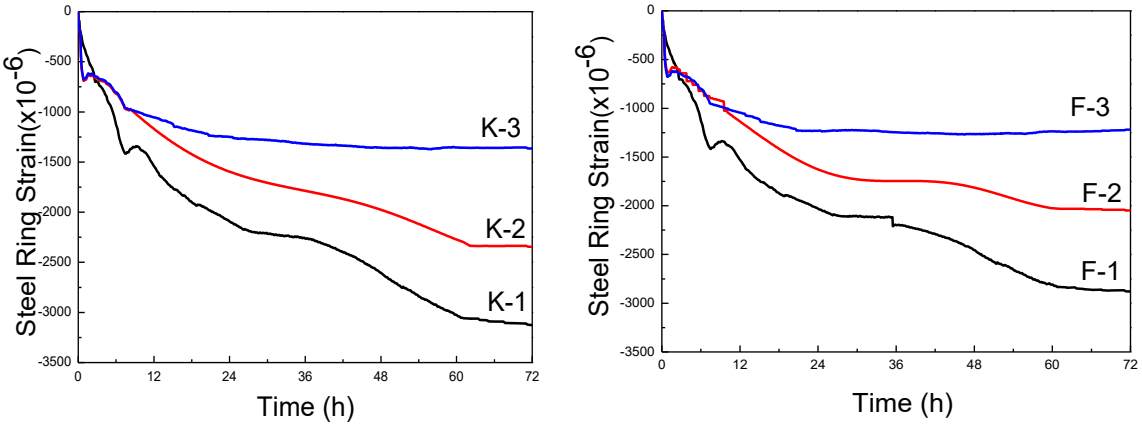


(a) Slag added UHPC (b) Fly ash added UHPC

**Figure 3-4.** The development of strain along circle direction at middle location of the surface of the steel ring with age.

The development of compressive strain of the slag and fly ash added UHPCs are in a similar manner. It is noticed that the compressive strains of fiber reinforced UHPC (both slag and fly ash added) exhibit a higher development rate compared to non-fiber reinforced UHPC. At 72 h, the compressive strain under the sealing conditions for the slag and fly ash added UHPCs are 1410, 2750 and 3728 μm/m for the slag added UPHC and 1272, 2379, and 3225 μm/m respectively for the fly ash added UHPC at fiber contents of 0%, 1% and 2%. The compressive strain of 2% fiber reinforced UHPC is 2.5 times larger than non-fiber reinforced UHPCs for both the slag and fly ash added UHPC. Apparently, the compressive strain of both slag based UHPC and fly ash based UHPC are greatly increased after using the fiber.

### 3.4.3 Comparison of the two testing methods

There was a great linear relationship between the shrinkage of steel ring $\varepsilon_{net}$ and the square root of age $t$ by ring test, and the slope of the fitting line is the shrinkage strain rate

α, as shown in Eq. (3-2). The ring test is used to calculate the stress grow rate of concrete ring by ASTM C1581. Actually, there is also a linear relationship through the prism test method.

$$\varepsilon_{net} = \alpha\sqrt{t} + k \tag{3-2}$$

Where $\varepsilon_{net:}$ is strain development value (m/m);

α is coefficient of Strain development value (m/m)/$d^{1/2}$;

*t* is the time of Strain development value

*k* is Random variable of linear regression.

The shrinkage strain rate α of mixtures can be calculated by Eq. (3-2).(C. Shi, B. Tong & F. He, 2011) Table3-4 and Table 3-5 show the shrinkage strain rate of different mixes by the corrugated tube test and ring test, respectively.

**Table 3-4:** The shrinkage strain rate α of mixes by the corrugated tube test

| **Title.** | K-1 | K-2 | K-3 | K-4 | F-1 | F-2 | F-3 | F-4 |
|---|---|---|---|---|---|---|---|---|
| **Autogenous shrinkage** | 38.64 | 8.76 | 14.34 | 6.86 | 20.19 | 7.28 | 7.03 | 3.42 |

**Table 3-5:** The shrinkage strain rate α of mixes by the ring test

| **Title.** | K-1 | K-2 | K-3 | F-1 | F-2 | F-3 |
|---|---|---|---|---|---|---|
| **Autogenous shrinkage** | 348.3 | 250.2 | 106.9 | 313.2 | 216.2 | 85.99 |
| **Autogenous and dry shrinkage** | 416.8 | 264.8 | 130.4 | 375.7 | 238.2 | 107.5 |

As can be seen from Table 3-4 and Table 3-5, the shrinkage strain rates by ring test are significantly higher than those of corrugated tube test. This result can be contributed to the restriction and higher elasticity modulus of steel ring. The shrinkage strain rate by the prism test, unrestrained ring test and restrained ring test. The maximum and minimum

rate of shrinkage are respectively the result by unrestrained tube test and restrained ring test. Comparing with the shrinkage strain rate and cracking time of concrete, the ring test is more reasonable and satisfactory to characterize the actual shrinkage strain rate than unrestrained ring test.

## 3.5 Theoretical models of autogenous shrinkage

At one point, assuming that free Autogenous shrinkage deformation $\varepsilon_{sh}$ will occur at the early UHPC bar since autogenous shrinkage. It can be argued that the Autogenous shrinkage deformation that develop in the restrained UHPC bar can be considered as a combination of two components as shown in Figure 3-5 (i.e., restrained Autogenous shrinkage deformation $\varepsilon_{sh,r}$ and restrained stretch deformation $\varepsilon_t$.

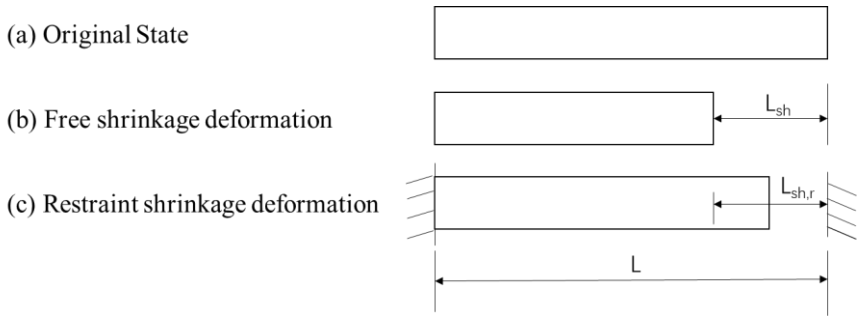


**Figure 3-5.** Free and restraint Autogenous shrinkage deformation of chart of UHPC bar.

Defined the initial length of the UHPC bar as $L$, if no constraint exists, the free Autogenous shrinkage strain can be expressed as $\varepsilon_{sh} = \Delta L / L$. On the contrary, if the UHPC bar is restrained, the restrained autogenous shrinkage strain is $\varepsilon_t = \Delta L - \Delta L_{sh,r} / L$ and the stretch deformation is $\varepsilon_t = \Delta L - \Delta L_{sh,r} / L$. In general, the degree of constrained deformation can be described as constraint degree $R$ ($R=\varepsilon_t/\varepsilon_{sh}$). When $R=0$, there are only free Autogenous shrinkage deformation will occur of the UHPC bar due to no restraint;

When *R=1*, the deformation of the UHPC bar is completely limited by the constraint and the free Autogenous shrinkage deformation $\varepsilon_{sh}$ is equal to the restrained stretch deformation $\varepsilon_t$; When *R=0~1*, the UHPC bar is limited by some constraint and both restrained Autogenous shrinkage deformation and restrained stretch deformation exist, while the restrained stretch deformation is $\varepsilon_t=R\cdot\varepsilon_{sh}$.

In reinforced concrete, for example, assuming that the sectional area of concrete and rebar are $A_c$ and $A_s$, respectively. The free Autogenous shrinkage deformation is $\varepsilon_{sh}(t)$ at the age of $t$ days and the restrained deformation is $\varepsilon_{sh\text{-}s}(t)$ when the concrete is restrained by the internal rebar. The strain of concrete at $t$ days can be expressed as Eq. (3-3).

$$\varepsilon_{c,t}(t)=\varepsilon_{sh}(t)-\varepsilon_{sh,s}(t) \tag{3-3}$$

If the elastic modulus of rebar and concrete are $E_s$ and $E_c$, by the elastic mechanics, the compressive stress by the rebar and tensile stress of concrete are expressed as Eq. (3-4) and Eq. (3-5), respectively.

$$\sigma_s(t)=E_s(t)\cdot\varepsilon_{sh,s}(t) \tag{3-4}$$

$$\sigma_c(t)=E_c(t)\cdot\varepsilon_{c,t}(t) \tag{3-5}$$

Assuming that the deformation is compatible between the inner surface of concrete and the outside surface of steel ring, and then

$$E_s(t)\cdot\varepsilon_{sh,s}(t)=E_c(t)\cdot\varepsilon_{c,t}(t)\cdot A_c \tag{3-6}$$

The compressive strain of steel ring and the tensile strain of concrete are expressed as Eq. (3-7) and Eq. (3-8), respectively.

$$\varepsilon_s(t) = \varepsilon_{sh}(t)\frac{E_c(t)A_c}{E_sA_s + E_c(t)A_c} \tag{3-7}$$

$$\varepsilon_{c,t}(t) = \varepsilon_{sh}(t)\frac{E_sA_s}{E_sA_s + E_c(t)A_c} = R\cdot\varepsilon_{sh}(t) \tag{3-8}$$

Thus, it was demonstrated that the constraint degree is not only associated with the elastic modulus, but also related to the sectional area of bar.

The restrained ring test of concrete is a conventional method used for evaluation of Autogenous shrinkage induced cracking performance of fiber reinforced concrete, which has been used for several decades. The restrained ring test consists of a cement material annulus that is cast around a steel ring. As the outer cement material, such as UHPC in present work shrinks, the steel ring limits the Autogenous shrinkage resulting in tensile stresses in UHPC ring and surface pressure stresses on the outer surface of the steel ring. The following section begins with a stress analysis of Steel Fiber-UHPC composite ring under surface pressure before analyzing the Autogenous shrinkage induced cracking performance of SFUHPC and traditional UHPC.

First we consider a thin circular ring surfers external and internal surface pressure stress, $q_1$ and $q_2$, see Figure 3-6 E and μ are the elastic modulus and Poisson's ratio of the material. *a* and *b* are the inner and outer radius of the ring. Now assume the material undergoes autogenous shrinkage strain $\varepsilon_{sh}$. In polar coordinate, the stress for plane stress can be expressed as:

$$\sigma_r = -\frac{E}{r^2}\int_a^r \varepsilon_{sh} r dr + \frac{EC_1}{2(1-\mu)} - \frac{EC_2}{1+\mu}\frac{1}{r^2} \tag{3-9}$$

$$\sigma_\theta = \frac{E}{r^2}\int_a^r \varepsilon_{sh} r dr - E\varepsilon_{sh} + \frac{EC_1}{2(1-\mu)} + \frac{EC_2}{1+\mu}\frac{1}{r^2} \tag{3-10}$$

Where $C_1$ and $C_2$ are constants which can be determined by the boundary conditions. From boundary condition that $\sigma_r = q_1$ at $r = a$ and $\sigma_r = q_2$ at $r = b$, we obtain:

$$C_1 = \frac{2(1-\mu)}{E}\frac{1}{b^2-a^2}(b^2q_2 - a^2q_1 + E\int_a^b \varepsilon_{sh} r dr) \tag{3-11}$$

$$C_2 = \frac{1+\mu}{E}\frac{a^2b^2}{b^2-a^2}(q_2 - q_1 + \frac{E}{b^2}\int_a^b \varepsilon_{sh} r dr) \tag{3-12}$$

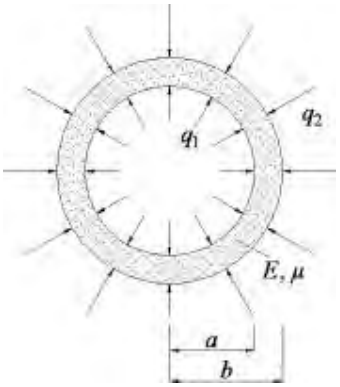


**Figure 3-6.** Circular ring under surface pressure.

The two-layer Steel Fiber-UHPC composite ring can be separated into a steel ring and a UHPC ring with an external interfacial pressure stress and an internal interfacial pressure stress acted on the UHPC and steel interface respectively, as shown in Figure 3-7 for UHPC ring, we have $q_2 = 0$ and $q_1 = q$. For steel ring, we have $q_2 = q$, $q_1 = 0$ and $\varepsilon_{sh} = 0$. Using above conditions in (3-2), we obtain the constants of $C_1$ and $C_2$ for UHPC ring as:

$$C_1 = \frac{2(1-\mu_1)}{E_1}\frac{1}{r_3^2-r_2^2}(r_2^2q_2 + E_1\int_{r_2}^{r_3} \varepsilon_{sh} r dr) \tag{3-13}$$

$$C_2 = \frac{1+\mu_1}{E_1}\frac{r_2^2r_3^2}{r_3^2-r_2^2}(q + \frac{E_1}{r_3^2}\int_{r_2}^{r_3} \varepsilon_{sh} r dr) \tag{3-14}$$

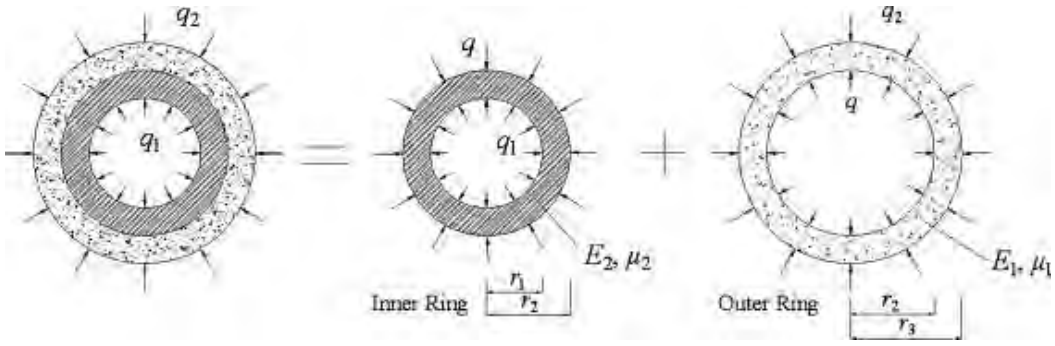


**Figure 3-7.** Decomposing of concrete-steel composite ring.

Clearly, the Autogenous shrinkage resulted stresses in UHPC ring are generated from volume change of UHPC layer and is a function of $\varepsilon_{sh}$ as displayed in (3-3). In ring test, Autogenous shrinkage of UHPC is restraint by steel ring and tensile stress is created in the UHPC ring. Creep of cementitious material then immediately takes place as UHPC ring is loaded in tension. Then part of the Autogenous shrinkage strain is counteracted by the creep strain, behaving as the Autogenous shrinkage tress decreasing with age. Assume the creep factor is $k$, then the effective Autogenous shrinkage strain that actually be used for generation of Autogenous shrinkage stress in UHPC ring as $\varepsilon_{sh\text{-}e}$ then we have:

$$\varepsilon_{sh-e}(t) = k\varepsilon_{sh}(t) \tag{3-15}$$

Replace $\varepsilon_{sh}$ with $\varepsilon_{sh\text{-}e}$ in (3-3), we can obtain the tensile stress along circular direction at outer ($r = r_3$) and inner ($r = r_2$) surface as:

$$\sigma_\theta = \frac{r_2^2}{r_3^2 - r_2^2}\left(\frac{r_3^2}{r_2^2} + 1\right)q \tag{3-16}$$

$$\sigma_r = \frac{r_2^2}{r_3^2 - r_2^2}\left(1 - \frac{r_3^2}{r_2^2}\right)q \tag{3-17}$$

And the interfacial stress $q$ can be expressed as:

$$q = \frac{-k\varepsilon_{sh}}{\frac{1}{E_1}\frac{(1-\mu_1)r_2^2+(1+\mu_1)r_3^2}{r_3^2-r_2^2}+\frac{1}{E_2}\frac{(1-\mu_2)r_1^2+(1+\mu_2)r_2^2}{r_2^2-r_1^2}} \quad (3\text{-}18)$$

On another hand, the interfacial stress $q$ can be related with the inner surface strain on the steel ring, $\varepsilon_\theta$ as

$$q = -\left[1-\left(\frac{r_1}{r_2}\right)^2\right]E_2\varepsilon_\theta \quad (3\text{-}19)$$

The compressive strain $\varepsilon_\theta$ can be measured from experiments. Thus, replace $q$ in Equations (3-5) and (3-6) by Equation (3-7) respectively, we can calculate the shrinkage induced stresses in UHPC ring and the effective shrinkage strain used for generating the stress, $k\varepsilon_{sh}$. After comparing with the shrinkage stress, the shrinkage status of the ring under shrinkage load can then be evaluated.

The following three figures are plotted according to the formulas (3-18) and (3-19). In Figure 3-8 (a), the relationship of UHPC shrinkage strain and time series is described, in which K is extracted by the results of corrugated tube measurement. From the graph, we can see that steel fiber has remarkable effects on both slag based and fly ash based. With the enhancement of fiber mixing amount, shrinkage strain decreases fast, with strain value holding an increasing tendency in the following 72 hours, which is unconformable to the variation of strain. This phenomenon is resulted by shrinkage resistance force due to the regasification of concrete.

Because of the high activity of slag, early stage shrinkage of slag based exceeds that of fly ash based. In Figure 3-8 (b) and (c), the unrestrained autogenous shrinkage of slag based and fly ash based is compared with their restrained shrinkage, respectively. It is showed that two kinds of strains have appropriate correlation and the accuracy of ring method

applied in testing autogenous shrinkage of UHPC is proved. The ring method is suitable for measuring early stage shrinkage of concrete, especially autogenous shrinkage. Guaranteeing the perfect seal of test specimens is a crucial factor to obtain accurate experimental data. However, two problems are expected for deeper research. The first is influence of the stiffness of the steel ring? Another is how can we measure the evolution of the Modulus?

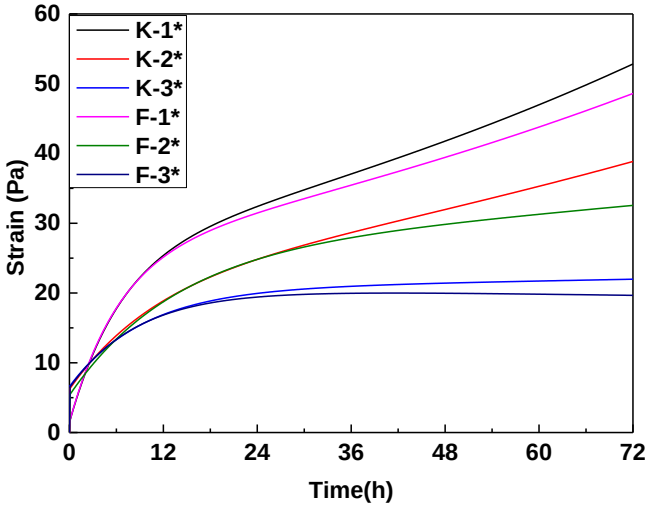


(a) Free shrinkage of UHPC

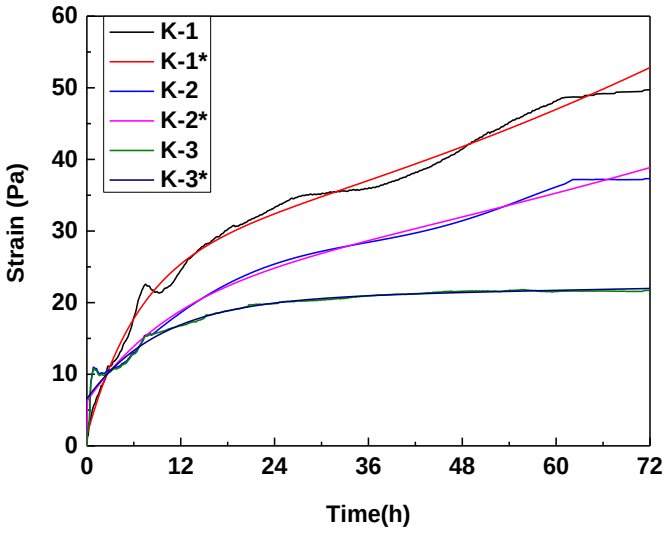


(b) Slag based UHPC

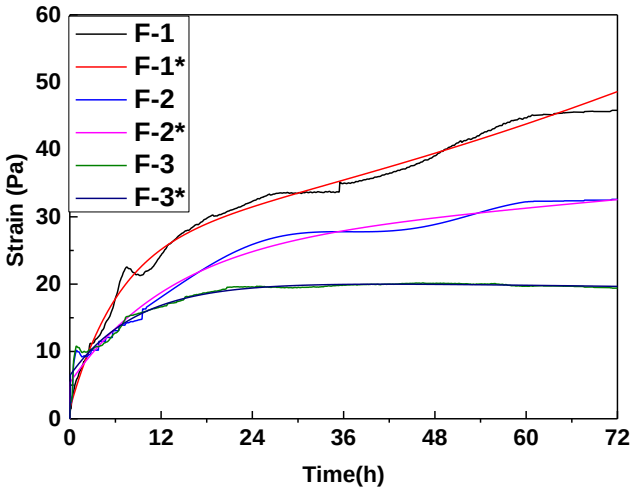


(c) Fly ash based UHPC

**Figure 3-8.** Comparison between effective shrinkage strain and free shrinkage of UHPC.

The elastic modulus and cracking strength of UHPC with fiber and non-fiber, which should be used in the model, were obtained from references (Attiogbe, Weiss, & See, 2004) (Jun Zhang, Gao, & Wang, 2013),in which the tensile performance of UHPC with fiber and non-fiber were investigated in details. The test results of elastic modulus and cracking strength of UHPC with fiber and non-fiber as a function of material age are presented in Figure 3-8 respectively. Typical tensile stress–strain relationship of UHPC with fiber and non-fiber used in the present paper is presented in Figure 3-8, in which the determination of cracking strength is illustrated by the small graph displayed in the figure. Clearly, both materials have displayed strain-hardening and multiple cracking performances under tension and a similar ultimate tensile strain is obtained. The cracking strength of UHPC with fiber is higher than that of UHPC non-fiber. Figs. 8 present the relationship between average shrinkage stress along circle direction calculated from (18) and cracking strength versus time diagrams of UHPC with fiber and non-fiber respectively. From the results, first we can find that the shrinkage stress increases with age following the variation law of shrinkage versus time. As surface drying starts, the shrinkage stress increases suddenly also as shrinkage does at this moment. By comparing the development of shrinkage stress

between UHPC with fiber and non-fiber, we may find that the shrinkage stress keeps continuously increasing with age in UHPC ring. By contrast, the shrinkage stress in UHPC with fiber ring first increases with age then goes into a steady state without increasing with age. The above results mean that it is possible to build UHPC structures without shrinkage induced cracking during service un-der general environments. However, under rigorous environmental conditions, even the cracking cannot be prevented, the crack width can be controlled within a certain magnitude of opening. Such conclusion may enhance the applications of UHPC in practice, especially in the cases of shrinkage induced cracking should be avoided. Apart from shrinkage stress, the effective shrinkage strain, $k\varepsilon_{sh}$ can be calculated from Eq. (3-19). The comparison between effective shrinkage strain and free shrinkage strain of UHPC with fiber and non-fiber are presented in Figure 3-8 respectively, in which the two strains within the initial few days since specimen cast is displayed in the small figure. As expected, the effective shrinkage strain is lower than that of free shrinkage strain for given age. Such difference may due to creep and development of micro cracks if cracking already occurs in the ring specimen. Before cracking, the creep relaxation parameters of the tested material may be estimated by analyzing the difference between free shrinkage strains the effective shrinkage strain as displayed above.

## 3.6 Conclusion

Based on the results from this study, the following conclusions can be drawn:

(1) The experimental results shown that the shrinkage of UHPC with fiber is significantly reduced due to the use of low shrinkage cement matrix comparing with UHPC non-fiber materials. Under the same restraint and environmental drying condition, UHPC with fiber presents super anti-cracking performance behaving as without visible cracks on the ring

specimen. The mechanisms of super anti-cracking performance of UHPC with fiber are interpreted by shrinkage induced stress analyses with UHPC-steel composite ring specimen. The model results show that much lower shrinkage stress is created in UHPC with fiber ring compared with that of UHPC non-fiber ring. This study indicates that it is possible to develop UHPC structures without shrinkage induced cracking during its service. However, the structures still remain the unique crack opening control and strain hardening performance in the case of cracking may not be avoided under rigorous environmental conditions.

(2) The ring method is suitable for measuring early stage shrinkage of concrete, especially autogenous shrinkage. Guaranteeing the perfect seal of test specimens is a crucial factor to obtain accurate experimental data. However, two problems are expected for deeper research. The first is influence of the stiffness of the steel ring? Another is how can we measure the evolution of the Modulus?

## 3.7 References

H. Pei, Z. Li, B. Zhang, H. Ma, Materials Letters 2014;131: 370-372.

D.P. Bentz, Cement and Concrete Research 2008;38(2): 196-204.

L. Wu, N. Farzadnia, C. Shi, Z. Zhang, H. Wang, Construction and Building Materials 2017;149: 62-75.

R. Burrows, W. Kepler, D. Hurcomb, J. Schaffer, J. Sellers, Cement and Concrete Composites 2004;26(5): 509-519.

O.M. Jensen, P.F. Hansen, Advances in Cement Research 1995;7(25): 33-38.

P. Turcry, A. Loukili, L. Barcelo, J.M. Casabonne, Cement and Concrete Research 2002;32(9): 1443-1450.

D.P. Bentz, M.A. Peltz, ACI Materials Journal 2008;105(4): 414.

O.M. Jensen, P.F. Hansen, Cement and Concrete Research 2002;32(6): 973-978.

Z. Hu, C. Shi, Z. Cao, Z. Ou, D. Wang, Z. Wu, L. He, Journal of Sustainable Cement-Based Materials 2013;2(2): 161-171.

Y. Bao, W. Meng, Y. Chen, G. Chen, K.H. Khayat, Materials Letters 2015;145: 344-346.

M. Briffaut, F. Benboudjema, J.M. Torrenti, G. Nahas, Cement and concrete research 2011;41(1): 56-63.

E.K. Attiogbe, W. Weiss, H.T. See, A look at the stress rate versus time of cracking relationship observed in the restrained ring test, The Advances in Concrete Through Science and Engineering, a Rilem International Conference, 2004.

J. Zhang, Y. Gao, Z. Wang, Composites Part B: Engineering 2013;52: 21-29.

Lynam CG: Growth and movement in Portland cement concrete, London, 1934.

Powers TC: A working hypothesis for further studies of frost resistance of concrete: ACI journal Proceedings, ACI, 1945, 41,

Powers TC, Helmuth RA: Theory of volume changes in hardened portland-cement paste during freezing: Highway research board proceedings, 1953, 32,

Fagerlund G: Prediction of the service life of concrete exposed to frost action. Studies on concrete technology 1979:249-276.

Zhang J, Gao Y, and Wang Z: Evaluation of Autogenous shrinkage induced cracking performance of low Autogenous shrinkage engineered cementitious composite by ring tests. Composites Part B: Engineering 2013; 52:21-29.

Briffaut M, Benboudjema F, Torrenti JM, Nahas G: Numerical analysis of the thermal active restrained Autogenous shrinkage ring test to study the early age behavior of massive concrete structures. ENG STRUCT 2011; 33:1390-1401.

Zhu H, Li H, Zhu X: On concrete restrained UHPCentric ring and squared UHPCentric ring Autogenous shrinkage test methods. CONSTR BUILD MATER 2015; 84:239-244.

Choi H, Lim M, Kitagaki R, Noguchi T, Kim G: Restrained Autogenous shrinkage behavior of expansive mortar at early ages. CONSTR BUILD MATER 2015; 84:468-476.

Attiogbe, Emmanuel K., Heather T. See, and Matthew A. Miltenberger. "Potential for restrained shrinkage cracking of concrete and mortar." Cement, concrete and aggregates 26, no. 2 (2004): 1-8.

Lomboy, Gilson, Kejin Wang, and Chengsheng Ouyang. "Shrinkage and fracture properties of semiflowable self-consolidating concrete." Journal of Materials in Civil Engineering 23, no. 11 (2010): 1514-1524.

Moon JH, Weiss J: Estimating residual stress in the restrained ring test under circumferential drying. Cement and Concrete Composites 2006; 28:486-496.

Zhang J, Gong CX, Guo ZL, Ju XC. Mechanical performance of low shrinkage engineered cementitious composite in tension and compression. J Compos Mater 2009; 43(22):2571–84.

# CHAPTER 4 EFFECTS OF STEEL FIBER ON DRYING SHRINKAGE OF ULTRA HIGH PERFORMANCE CONCRETE

Note: this chapter is based on the manuscript entitled ". Effects of Steel Fiber on Drying Shrinkage of Ultra High Performance Concrete." by Linmei Wu, C. Shi, Z. Zhang & H Wang, published in journal of Materials Review, 23:007. September 2017.

**Abstract:** This chapter reports the study of the influence of steel fibers on drying shrinkage of ultra-high performance concrete (UHPC) at fiber volume content of 0%, 1%, 2% and 3%, temperature of 20 ± 2°C and relative humidity of 50 ± 5%. The results showed that during the first 7 days, the drying shrinkage rate of UHPC was very fast, while after 7 days it gradually decreased. The interfacial bonding of steel fiber and the physical properties of steel fiber can effectively reduce the drying shrinkage. However, when the steel fiber exceeds an optimal volume, the effect of steel fiber on drying shrinkage can decrease. Compared with the steel fiber content at 2%, the drying shrinkage of the UHPC with 3% steel fiber was decreased by only 1.5%. The reason is that the increase in the steel fiber leads to an increase in the interface layer, the interface transition zone is usually more porous than the matrix, which easily leads to shrinkage, and consequently reducing the beneficial effect of steel fiber on drying shrinkage control. It was also found that the inhibition of fly ash on the drying shrinkage of UHPC was higher than slag. The experiment also tested the classic dry shrinkage models: the ACI model and the Wang Tiemeng model. Based on the two models and the experimental fitting, a new mathematical model (a combined index model) has been proposed. The results showed that the combined index model fitted better than the two models mentioned above.

## 4.1 Introduction

Drying shrinkage of concrete is the shrinkage caused by evaporation of internal water in hardened concrete. Creep and drying shrinkage are very important time-dependent properties of UHPC, they are in direct relation to the performance of UHPC in concrete structures(P Acker, 2004). With the rapid development of UHPC in the world, more and more attention has been paid to the creep and drying shrinkage behavior of UHPC. In China, there are many research projects at present concentrating on raw materials, mixture design, properties and construction technology of HPC(V. Y. Garas et al., 2009; Z. Li, 2016). The drying shrinkage of cement-based materials is induced by the difference of moisture contents between the interior of the sample and surrounding environments. It was reported that the highest drying shrinkage occurs at the surface of samples and it gradually decreases when approaching to the inner part of the sample(Gilbert, 1988). Warping and cracks may take place when the relative humidity difference between the interior and outside is large enough, leading to the issues of durability(Barr, Hoseinian, & Beygi, 2003; L. Wu et al., 2017b). Worse still, drying shrinkage is to some extent irreversible, indicating that samples including specimens and structural components after first-time drying shrinkage are not able to recover to their initial dimensions when exposed to humidity again (FISCHER & Shuxin, 2003; Monteiro, 2006).

Many influential factors can lead to drying shrinkage of concrete, including concrete compositions, types of mineral admixtures, curing time and temperature, relative humidity and water contents (Barr et al., 2003; H. Chen et al., 2012; FISCHER & Shuxin, 2003; W. Zhang, Zakaria, & Hama, 2013). As a commonly used mineral additive for replacing ordinary Portland cement, mineral admixtures have a great effect on the shrinkage properties of OPC-based materials. However, the issue of specific effects still remains controversial(Chern & Chan, 1989; Khatri, Sirivivatnanon, & Gross, 1995). Shrinkage reducing admixtures can reduced the surface tension of water in the pores of concrete and the corresponding capillary pressure, leading to a decrease in the drying shrinkage of concrete(Mora-Ruacho, Gettu, & Aguado, 2009). It was reported that the 28-day drying shrinkage was reduced by 50-80% for the concrete with the addition of shrinkage reducing agent compared to the one without addition(D. Bentz, M. R. Geiker, & K. K. Hansen, 2001). However, the usage of shrinkage reducing admixture may result in a

series of problems such as a reduced compressive strength during early curing stage, a prolonged setting time and complex reactions with other chemical admixtures (J. Brooks & Jiang, 1997; Folliard & Berke, 1997; Rodden & Lange, 2004). It was also reported that a prolonged curing time can also decrease the final drying shrinkage effectively (Dang et al., 2013; Y. Huang, 2006; Jin & Al-Tabbaa, 2015).

Many types of mineral admixture such as fly ash and limestone powder are used in concrete. However, there is limited information on the drying shrinkage behavior of concrete containing these mineral admixtures. Some researchers (Tongaroonsri, S., & Tangtermsirikul, S. 2009) studied the cracking behavior of concrete with low fly ash content (20% replacement). However, in real application fly ash is used to replace cement from 10% up to 50%. Mixture with lower water to binder ratio (w/b = 0.35) shows shorter cracking age than the mixture with higher water to binder ratio (w/b = 0.55). Fly ash and limestone powder significantly increase cracking age of concrete. The cracking age increases with the increase of the replacement ratio of fly ash. The higher shrinkage rate, when exposed to drying, of mixture with longer curing period leads to shorter cracking age.

UHPC is an ultra-strength cement-based material with a good ductility and durability. According to the foreign standards, the compressive strength of UHPC should not be lower than 150 MPa. Compared to high performance concrete, UHPC has an increased ductility by more than 300 times which is comparable to some metals, making it more structurally reliable when the concrete structures are under loading or seismic conditions (PierreMounanga et al., 2012; C. Shi & Mo, 2015; Tarolli, 1997). UHPC is more likely to shrinkage due to a large amount of binder used in the system. Under the standard curing conditions, the rate of shrinkage gradually decreases as time proceeds (GARAS et al., 2009; Koh, Ryu, Kang, Park, & Kim, 2011). According to Guangcheng Long et al. (M. Ba, Qian, & Hui, 2013), the drying shrinkage of UHPC after one-day casting is relatively small and can reach up to 800 μm/m after 120 days. It was also reported that the shrinkage of UHPC increases as the water/binder ratio increases (M. Ba et al., 2013; Cwirzen, Penttala, & Vornanen, 2008) and the usage of coarse aggregate can reduce the shrinkage of UHPC (Cwirzen et al., 2008) . In addition, it is found that 2% addition of steel fibers was able to reduce the shrinkage of UHPC by 57% after 14 days (GARAS et al., 2009). Moreover, the

shrinkage of sample with 14-day heat curing was significantly reduced compared to the normal curing condition (Xian et al., 2013). Furthermore, there is no significant effect of polymers on the shrinkage of UHPC at the water bath curing condition with temperature at 90 ℃(P. Chen, Liu, & Mingwei, 2011; Dai, Ng, Zhou, Kreiger, & Ahlborn, 2012; GARAS et al., 2009). The addition of a certain amount of steel fibers can significantly reduce the autogenous shrinkage and drying shrinkage of UHPC (BuquanMiao, Jenn‐ChuanChern, & Chen‐AnYang, 2003; Dai et al., 2012). Moreover, it was found by Yoo et al. (BuquanMiao et al., 2003) that an addition within 3% of steel fibers led to a reduced shrinkage of concrete whereas little change was observed when the amount of addition was more than 3%. It is thus apparent that there still remain uncertainty regarding the optimized amount of steel fiber addition. The drying shrinkage strength was highly dependent on fibbers' modules of elasticity, and the steel fibres showed the best performance due to their hook-shaped tail (Yousefieh, Negin, et al., 2017).

This study investigates the effect of different amount of steel fibers, 0%, 1%, 2% and 3% on the drying shrinkage of UHPC and the related mechanisms of the effect of binder components and steel fibers are also analyzed. In addition, different equations of time were developed to fit the experimental results.

## 4.2 Experimental program

### 4.2.1 Raw materials

Portland cement P.I 42.5, complying with the Chinese Standards GB175-2007(Jinfeng Wu, Ligang Yu & Xi Cai, 2009) was used. Table 4-1 summarizes the physical properties of the cement. Fly ash and ground furnace slag were used to partially replace cement in the concrete mixture, with the specific surface area of 427 m2/kg and 446 m2/kg, respectively. Silica fume with 63% particle size of 0.1-0.5 μm and specific surface area of 18500 m2/kg was used. Table 4-2 shows the chemical properties of cement, fly ash and slag. Natural river sand with a fineness modulus of 3.0 was used. Particles with size greater than 2.36 mm were removed by sieving, apparent particle density is 2550 kg/m3，bulk density is 1570 kg/m3，clay content is 1.0%，fineness modulus is 3.0，Screening results shows in

Table 7-3. The straight steel fiber with diameter of 0.2 mm and length of 13 mm was used. Lf=13 mm，df=0.2 mm，Tensile strength is 800 MPa，density is 7 850 kg/m3，elasticity modulus is 200 GPa. A polycarboxylene based super plasticizer (SP) was used. Its water-reducing capacity was greater than 30%. The dosage of SP in the all mixture was 2 % by the mass of cementitious materials.

**Table 4-1:** Chemical composition of material (mass %)

| Materials | SiO2 (%) | Al2O3 (%) | CaO (%) | MgO (%) | SO3 (%) | Fe2O3 (%) | Na2O (%) | K2O (%) | Loss (%) |
|---|---|---|---|---|---|---|---|---|---|
| Cement | 21.53 | 4.60 | 64.09 | 1.50 | 2.32 | 3.37 | 0.12 | 0.32 | 1.80 |
| Fly ash | 52.37 | 32.13 | 2.16 | 0.47 | 0.33 | 4.13 | 0.25 | 0.61 | 1.30 |
| Slag | 31.64 | 13.16 | 38.62 | 10.85 | 3.14 | 1.03 | 0.31 | 0.40 | 0.98 |
| Silica fume | 94.80 | 0.56 | 0.52 | — | 0.88 | 0.24 | — | — | 3.15 |

**Table 4-2:** Physical and mechanical properties of cement

| Cement | Density (kg/m3) | 80μm-residue on sieve (%) | Specific surface area (m2/kg) | Setting time (h:m) | | Flexural strength (MPa) | | Compressive strength (MPa) | |
|---|---|---|---|---|---|---|---|---|---|
| | | | | Initial | Final | 3 d | 28 d | 3 d | 28 d |
| P.I | 3.15 | 0.3 | 340 | 2:30 | 3:24 | 6.4 | 9.0 | 33.0 | 60.0 |

**Table 4-3:** Sieve analysis of river sand

| Sieve Size(mm) | Retained (%) | Cumulative retained (%) |
|---|---|---|
| 1.18 | 11.5 | 11.5 |
| 0.63 | 17.9 | 29.4 |
| 0.315 | 36.3 | 65.8 |
| 0.16 | 32.3 | 98.1 |
| < 0.16 | 1.9 | 100 |

### 4.2.2 UHPC Mixture proportions

The mixture proportions of UHPCs were designed based on a previous study (Bazant & Baweja, 1995). In brief, the w/b of 0.18 and binder-to-aggregate ratio of 1:1.1 were selected and kept constant throughout the study. The SP was used at 2% by mass ratio of

the binder. Steel fiber contents were 0, 1 %, 2 % and 3 % of the concrete by volume. Table 4-4 shows the mixture proportions of UHPCs based on mass of ingredients.

**Table 4-4:** Mixture ratio of UHPC

| No. | Cement (%) | Silica fume (%) | Slag (%) | Fly Ash (%) | SP (%) | w/b | binder-to-aggregate ratio | Steel fiber (% by volume) |
|---|---|---|---|---|---|---|---|---|
| K1 | 55 | 20 | 25 | 0 | 2 | 0.18 | 1:1.1 | 0 |
| K2 | 55 | 20 | 25 | 0 | 2 | 0.18 | 1:1.1 | 1 |
| K3 | 55 | 20 | 25 | 0 | 2 | 0.18 | 1:1.1 | 2 |
| K4 | 55 | 20 | 25 | 0 | 2 | 0.18 | 1:1.1 | 3 |
| F1 | 55 | 20 | 0 | 25 | 2 | 0.18 | 1:1.1 | 0 |
| F2 | 55 | 20 | 0 | 25 | 2 | 0.18 | 1:1.1 | 1 |
| F3 | 55 | 20 | 0 | 25 | 2 | 0.18 | 1:1.1 | 2 |
| F4 | 55 | 20 | 0 | 25 | 2 | 0.18 | 1:1.1 | 3 |

*SP means the total mass of liquid-based SP.

### 4.2.3 Mixing procedure and specimen preparation

In mixing, dry powders, including cement, silica fume, slag or fly ash, and natural river sand, were firstly dry mixed for 3 min in a high-speed drum mixer. Then, water and superplasticizer were added and mixed for 6 min at low speed. Afterwards, steel fiber was added through passing a sieve with size of 5 mm and mixed for another 6 min until the mixtures were homogeneous. The obtained UHPC mixtures were then cast into molds and vibrated for consolidation. The cubic specimen size for the compressive strength test was 40 × 40 × 40 mm3. The specimen size for long-term dimension stability test was 75 × 75 × 275 mm3.The specimens were demolded 1 day after casting and then cured in lime saturated water at the temperature of 20 ± 2°C for 28 days. Then the properties of the hardened concrete such as compressive strength and initial length were measured before exposure to different conditions.

### 4.2.4 Workability test

The fresh mortar was filled into a mini cone placed on an automatic jump table as described in Chinese standard of GB2419-2005. The mini cone has an upper diameter of 70 mm, a lower diameter of 100 mm, and a height of 60 mm. After mini cone was vertically lifted, the mortar was vibrated automatically for 25 times. Two diameters perpendicular to each other were then determined and mean value was reported.

### 4.2.5 Drying shrinkage test

The surface area in contact with air is large and this could accelerate drying shrinkage due to water evaporation, and consequently increase the risk of cracking. Mould cast 75 × 75 × 275 mm beams complying with BS EN 12617–4:2002 were monitored over six months in curing conditions in a climatic chamber (20 °C and 60% relative humidity). Each group comprised five specimens.

The drying shrinkage was monitored based on the length change of the specimens according to Chinese standard GBJ82-85. The two measuring heads were embedded in the two sides of each specimen. The measurements were carried out at exposure ages of 1, 7, 28, 56, 90, 120, 216, 448, 630 and 720 days. The length was measured by a digital micrometer (BC-300) and calculated by Eq. (4-1):

$$\varepsilon'_{st} = \frac{L_0 - L_t}{L_b} \tag{4-1}$$

Where ε'st is the length change index of concrete at t days;

Lb is the standard length of specimen, which is the length of concrete subtracted the two times of the embedded depth of the measuring heads;

Lt is the measured length at t days;

L0 is the initial reading of the specimen.

The reported result was the mean value of the length change of three specimens calculated accurate to 1×l0-6.

### 4.2.6 Mass change

The mass change was recorded concomitantly to the length change measurements. The mass was measured by electronic balance and mass change ratio was calculated by Eq. (4-2):

$$\varepsilon = \frac{m_0 - m_t}{m_0} \tag{4-2}$$

Where m0 is the initial weight of the specimens after 28 days of standard curing (day 0); and mt is the weight of specimens at measured day t after exposure.

### 4.2.7 Scanning electron microscopy (SEM)

Scanning electron microscopy (SEM) was employed to study the microstructure of UHPC.

SEM samples were taken from freshly broken specimens, cut into small fragments and soaked in ethanol prior to testing, to stop the hydration of cement. Subsequently, the samples were dried at 65°C and sputtered with gold before analyzing using ION SPUTTER E-1045.

## 4.3 Experimental results

### 4.3.1 Effect of steel fiber content on the workability of UHPC

Figure 4-1 shows the effect of the fiber content on the flowability of UHPC. It can be seen that the flowability of UHPC was significantly reduced as the fiber content increased regardless of slag-based or fly ash-based systems. The flowability of UHPC for the slag-based system without fiber addition was satisfactory which 218 mm was. However, the flowability decreased almost linearly after the addition of fibers. It is apparent that the flowability decreased by 30% when the addition level was 3%. With the same amount of fiber addition, the flowability of UHPC with fly ash addition was obviously higher than that of the UHPC with slag addition. This can be due to two reasons: 1) the most of the fly ash are round particles and the frictions between particles can be reduced because of its ball-bearing effect; 2) some ultra-fine fly ash particles can fill in the voids among cement particles, thus increasing the bulk density. At the same time, the water content in cluster structures can also be reduced which leads to an increase in the amount of 'free' water with high mobility in the paste systems. The aforementioned two effects finally result in a satisfactory flowability of UHPC containing fly ash.

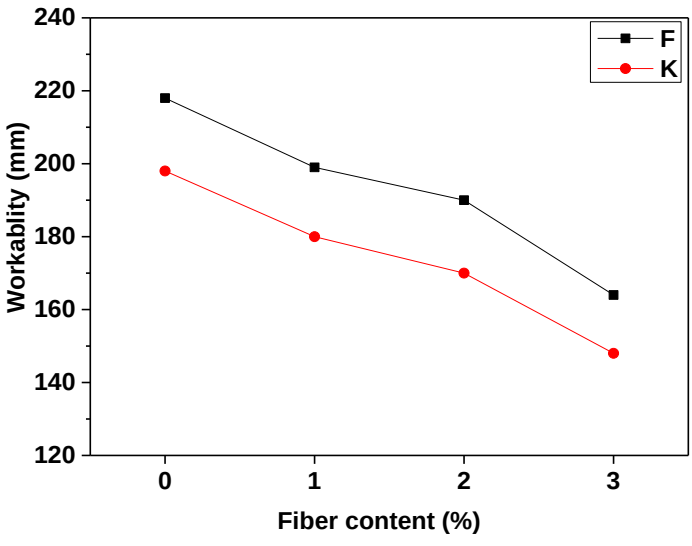

**Figure 4-1.** Effect of steel fiber content on workability of slag containing (K) and fly ash containing (F) UHPC mixtures.

### 4.3.2 Effect of steel fiber content on the drying shrinkage of UHPC

Figure 4-2 shows the drying shrinkage value changes up to 120 days of curing for slag-based UHPC. It shows that the drying shrinkage gradually increases as time proceeds followed by little change at the end of 120 days. It can also be seen that samples with the addition of FA has a more pronounced beneficial effect in limiting shrinkage than slag. This can be explained by considering the replacement of cement by fly ash which reduced the amount of hydrated phase, thus leading to a decreased shrinkage. Another possible reason is that fly ash can fill in the voids in the hydrated matrix as fine aggregates and then reduce the shrinkage. According to Figure 4-2, it is obvious that as the addition level increases, the shrinkage of concrete decreases accordingly. For instance, the drying shrinkage was reduced by 3%, 19% and 30% when the steel fiber addition was 1%, 2% and 3% respectively. In comparison, the shrinkage reduction for the UHPC with FA addition was 29%, 47% and 52% respectively for the same addition levels. It is obvious that the reduction in the drying shrinkage is less significant when the steel fiber addition increases for FA-based UHPC. In addition, the reduction of drying shrinkage was much higher for FA-based UHPC than that for slag-based UHPC when the steel fiber addition was 0% and 1%. When the fiber addition is 2% and 3%, however, the reduction in the drying shrinkage is similar for both slag and FA-based UHPC. The drying shrinkage was decreased by about 75% and about 85% for the FA-based UHPC with 2% and 3% steel fiber addition respectively, compared to the control UHPC.

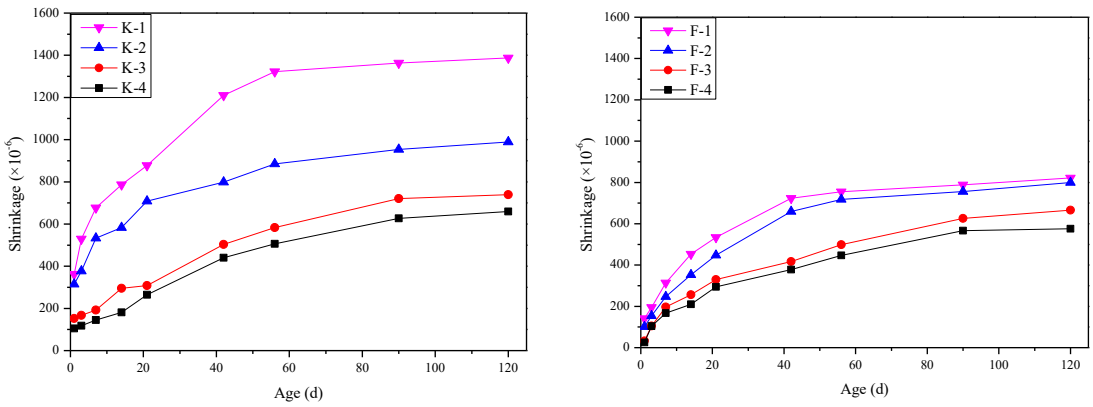


(a) Slag-based UHPC (b) Fly ash-based UHPC

**Figure 4-2.** Effect of steel fiber content on drying shrinkage of UHPC.

Figure 4-3(a) and (b) shows the mass changes (%) of UHPC during the drying test with

different additions of steel fibers for slag-based and FA-based respectively. It can be seen that the percentage mass loss increases as the curing age increases regardless of slag or FA-based binders and no significant changes occurred after 14 days. For the slag-based UHPC, the addition of steel fibers is able to reduce the mass loss of UHPC effectively and the mass loss is decreasing with an increasing amount of fiber addition. However, it is found that the mass loss was considerably decreased at 90 days of curing when the addition was 1%. For the FA-based binders, a small amount of addition, 1% and 2%, decreased the mass loss of UHPC with a similar degree. However, the higher level of 3% addition led to a slight increase in the mass loss of UHPC. It is also noticed that without fiber additions, the mass loss of FA-based UHPC is smaller than that of the slag-based peers whereas the opposite was true when the curing age was more than 7 days. Comparing the Figure 4-2 and Figure 4-3, it is apparent that the mass loss is closely associated with the drying shrinkage evidenced by their similar trend and increasing rate.

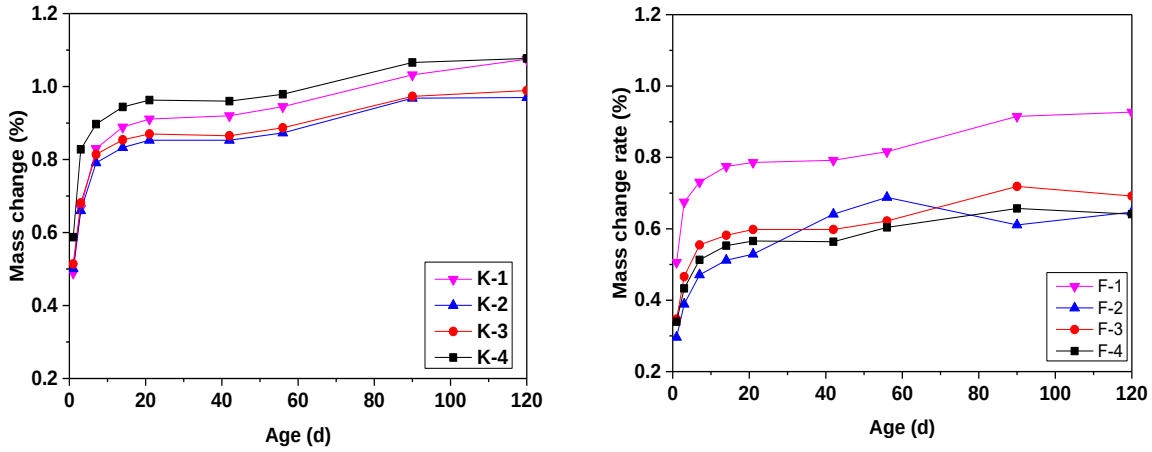


(a) Slag-based UHPC (b) Fly ash-based UHPC

**Figure 4-3.** Effect of steel fiber content on mass loss of UHPC.

### 4.3.3 SEM images of interface between fiber and UHPC matrix

Figure 4-4(a) shows the ESEM images of the sample interface between fibers and binder matrix for the slag-based UHPC with 2% fiber addition after 3 days of curing with a zoomed-in magnitude of 500 times. Figure 4-4(b) is a zoomed-in portion marked with the yellow dash rectangle in Figure 4-4(a) with a 2000-order of magnitude. Figure 4-5(a) is the SEM of the sample for the FA-based UHPC with 2% fiber addition during the early curing stage and Figure 4-5(b) is the corresponding region enlarged by 10,000 times. It is apparent that many small pores were observed on the surface of hydration products irrespective of slag or FA-based binder matrix in the early curing age. Some pores have a

diameter near to or more than 5 μm. This is particular the case for capillary pores between steel fibers and cement binder matrix, with a large volume and some accumulations of big crystals. The phenomenon is due to the hydrophobicity of the steel fiber surface which results in a larger water/cement ratio compared to that of the binder matrix. As a result, the water layer increases in thickness and a reduced ion concentration can be obtained. Under this condition, the ettringite and $Ca(OH)_2$ crystals tend to grow larger without limitation and to orientate in a specific direction, forming a layer rich in crystals. This finally leads to a higher porosity of interface and the contact between C-S-H gel and fiber surface is less like to occur (GARAS et al., 2009). At the same time, the amount of hydrated C-S-H decreases because of the reduced concentration of ions in the interfacial transition zone, making the contact points between C-S-H gel and fiber surface fewer (GARAS et al., 2009). All of the aforementioned reasons make the ITZ between fibers and binder matrix the weakest part in UHPC. The insignificant bonding strength between the fiber and binder matrix because of the weak ITZ results in the limitations of drying shrinkage during the early stage of curing for UHPC with the addition of steel fibers.

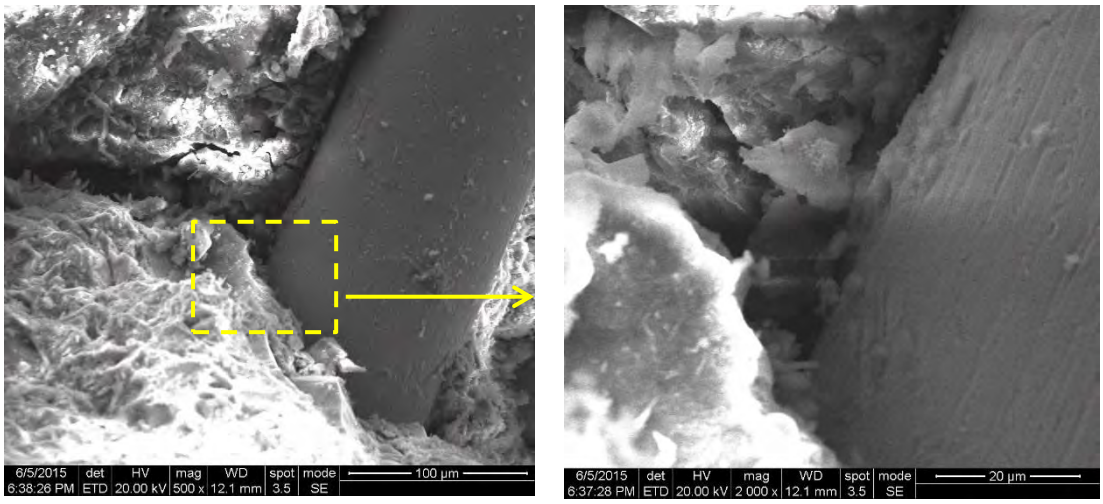


(a) (b)

**Figure 4-4.** SEM images of the slag containing sample with 2% steel fiber at 3 days.

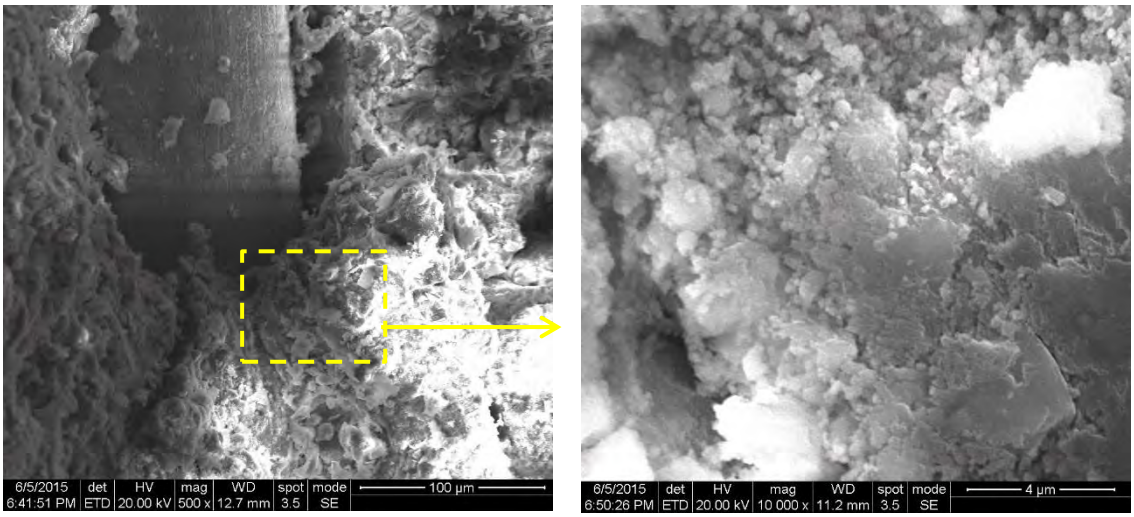


(a) (b)

**Figure 4-5.** SEM images of the fly ash containing sample with 2% steel fiber at 3 days.

Figure 4-6(a) and (b) is the ESEM image showing the morphology of the slag-based UHPC sample with 2% steel fibers after 120 days of curing with a 250-time of enlargement and the corresponding area within the rectangle is enlarged by 8000 times respectively. Figure 4-7(a) shows the SEM images of the FA-based UHPC sample with 2% steel fiber addition after 120 days of curing with Figure 4-7(b) showing the zoomed-in region with a 5000-time enlargement. It can be seen that the surface of steel fibers was covered with some hydration products of OPC which improved the bonding between fibers and binder matrix. With the addition of steel fibers, they can improve the strength, ductility and limit the propagation of cracks. Based on the micro morphologies of the interface between the fibers and binder matrix after 120 days, it is apparent that the ITZ was densified compared to that after 3 days of curing. However, a closer examination of the ITZ with a higher resolution of images implies that there still remained some small gaps and space between fibers and binder matrix even after 120 days of curing regardless of either it was slag or FA-based UHPC. A too much higher steel fiber addition would lead to an adverse effect on limiting the drying shrinkage because of a higher content of ITZ with high porosity between steel fibers and binder matrix.

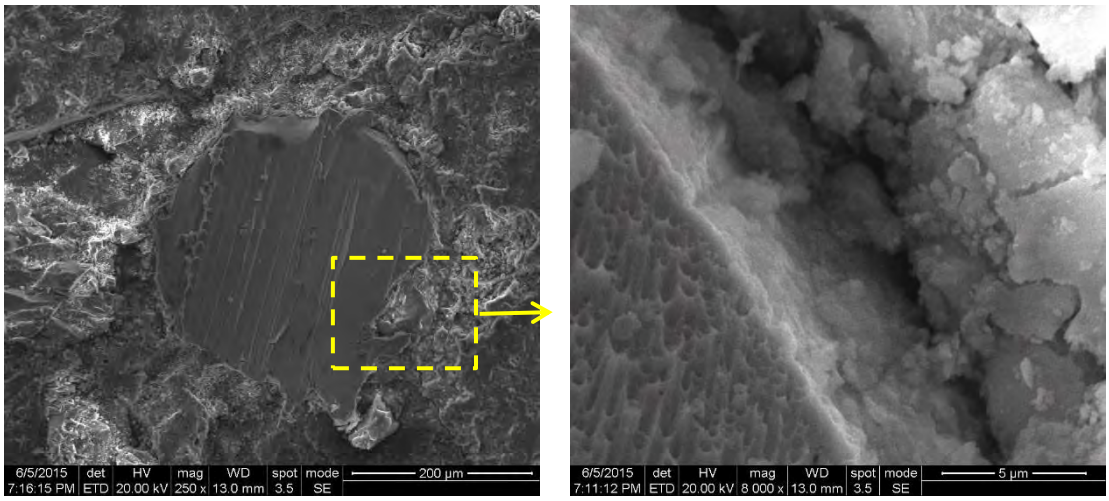


(a) (b)

**Figure 4-6.** SEM images of the slag containing sample with 2% steel fiber at 120 days.

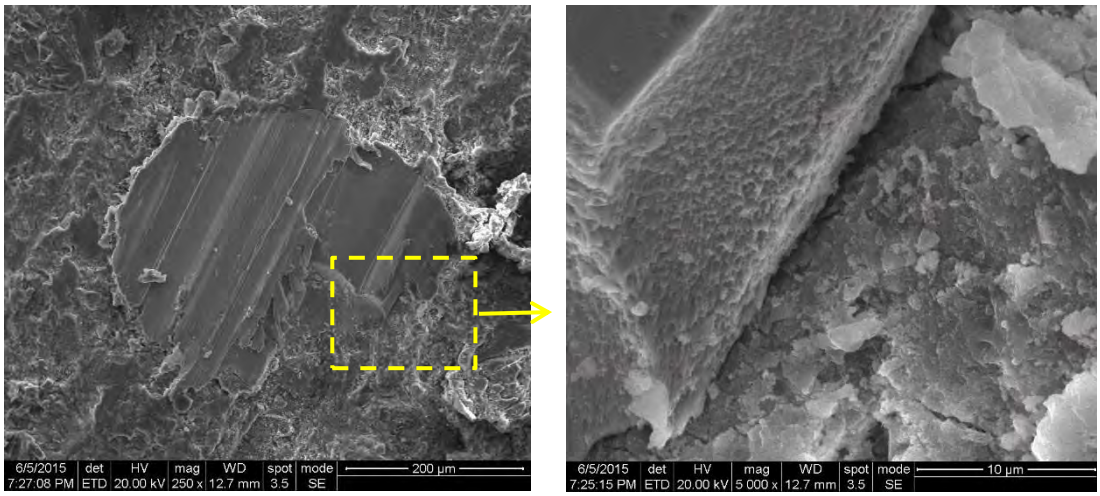


(a) (b)

**Figure 4-7.** SEM images of the fly ash containing sample with 2% steel fiber at 120 days.

## 4.4 Discussion

### 4.4.1 The evolution of drying shrinkage against curing age for UHPC

Guoxing Huang et al. (Wei Sun, 1987) summarized three equations to describe the relationship between drying shrinkage and time, which are shown as follows:

Hyperbolic function: $$X(t) = \frac{t}{a + bt} \quad (4\text{-}3)$$

Logarithmic function: $$X(t) = a + b^0 In(t+1) \quad (4\text{-}4)$$

Exponential function: $X(t) = X(1 - ae^{bt})$ (4-5)

Where X(t) is the shrinkage at time t, and e refers to the natural logarithms, a and b are experimental constants. According to the current studies, Eq. (4-3) can be applied to normal concrete and lightweight concrete and Eq. (4-4) are suitable for FA-based and high strength concrete. Based on the experimental data (the shrinkage curve of UHPC with addition of steel fibers in this study, a formula based on the combined exponential correlation is shown as Eq. (4-6):

$$X(t) = ae^{bt} + ce^{dt} \quad (4\text{-}6)$$

where X is the end point of the shrinkage based on fitting, a,b,c,d are experimental constants as shown in Table 4-5. It shows that composite exponential function Eq. (4-6) is able to describe the relationship between autogenous shrinkage and curing age satisfactorily.

**Table 4-5:** Comparison of experiment data with the calculated results

| No. | a（×10-4） | b（×10-3） | c（×10-4） | d | R2 |
|---|---|---|---|---|---|
| K-1 | 7.155 | 1.97 | -5.45 | -0.177 | 0.957 |
| K-2 | 6.896 | 1.51 | -3.374 | -0.051 4 | 0.790 |
| K-3 | 5.632 | 2.516 | -4.126 | -0.033 8 | 0.979 |
| K-4 | 1.041 | 3.76 | -8.983 | -0.018 | 0.951 |
| F-1 | 7.288 | 2.52 | -5.047 | -0.132 2 | 0.932 |
| F-2 | 6.43 | 2.799 | -4.484 | -0.129 9 | 0.924 |
| F-3 | 3.75 | 2.845 | -3.268 | -0.192 5 | 0.878 |
| F-4 | 5.84 | 2.88 | -3.719 | -0.105 4 | 0.937 |

### 4.4.2 The comparisons between different equations

Up to now, all equations describing the relationship between drying shrinkage and time used in the world for estimation in most of the structural design standard are based on the experiments and semi-empirical equations. The semi-empirical equations were developed based on the diffusion theories. The most representative model overseas is the ACI estimation equation which was set up based on the correction coefficient obtained by calculating the deviations of the experimentally determined influential factors from standard conditions. The drying shrinkage after 7-day humid curing of concrete can be

expressed as:

$$\varepsilon_{sh}(t) = \frac{t}{35+t}\varepsilon_{sh}(u) \tag{4-7}$$

The drying shrinkage after 1 to 3 days of vapor curing can be described as:

$$\varepsilon_{sh}(t) = \frac{t}{55+t}\varepsilon_{sh}(u) \tag{4-8}$$

$$\varepsilon sh\ (\mu) = 780\ \gamma cp \cdot \gamma\lambda \cdot \gamma h \cdot \gamma s \cdot \gamma\varphi \cdot \gamma c \cdot \gamma a \cdot 10\text{-}6\ \text{mm/mm} \tag{4-9}$$

where t is the curing days, γcp、γλ、γh、γs、γφ、γc and γa are the correction coefficients of initial curing conditions, relative humidity, averaged thickness, slump of concrete, the contents of fine aggregates, cement contents and air contents respectively.

Tiemeng Wang(Lixue Wu, 2008) obtained the following drying shrinkage equation based on the experiment results within about 20 years obtained in China:

$$\varepsilon_y(t) = 3.24\times10^{-4}(1-e^{-0.01t})M_1M_2\cdots M_n \tag{4-10}$$

Mn is the correction coefficients under nonstandard conditions, such as cement types, cement grade, water to cement ratio, curing conditions and reinforcements and so forth.

According to the aforementioned equations in this study, the experimental data of drying shrinkage of UHPC with different additions of steel fibers is fitted with ACI equation, the equation proposed by Tiemeng Wang and Eq. (4-6) with the results show in Table 4-6. It is apparent that the correlation coefficient derived from Eq. (4-6) is the highest followed by that derived from ACI calculation equation. The lowest coefficient was seen for the equation developed by Tiemeng Wang.

**Table 4-6:** Regression results for the relationship between drying shrinkage and time of UHPC

| sample | Equation | Regressed Equation | Correlation Coefficient (R2) |
|---|---|---|---|
| K-1 | ACI Equation | y=5.764×10-5x/(1+0.060 31x) | 0.9764 |
| | Wang Equation | y= -7.508×10-4×e(-0.045 83x)+ 8 173×10-4 | 0.9890 |
| | Equation（6） | y=7.922×10-4 e(-0.000 173 9x)-1.026×10-4e(-2.075x) | 0.9886 |
| K-2 | ACI Equation | y=41.81×10-5x/(1+0.043 01x) | 0.9865 |
| | Wang Equation | y=-7.498×10-4×e(-0.035 32x)+8.078×10-4 | 0.9969 |
| | Equation（6） | y=8.385×10-4e(-0.026 45x)-2.103×10-4e(-1.437x) | 0.9969 |

| | | | |
|---|---|---|---|
| K-3 | ACI Equation | y=26.36×10-5x/(1+0.032 51x) | 0.9812 |
| | Wang Equation | y=-6.346×10-4×e(-0.039 73x)+6.992×10-4 | 0.9830 |
| | Equation（6） | y=4.644×10-4e(0.202 1x)-2.93×10-5e(-2.67x) | 0.9906 |
| K-4 | ACI Equation | y=23.12×10-5x/(1+0.031 98x) | 0.9824 |
| | Wang Equation | y=-5.589×10-4×e(-0.023 87x)+6.105 0×10-4 | 0.9853 |
| | Equation（6） | y=4.648×10-4e(0.127x)- -7.261×10-5e(-1.756x) | 0.9870 |
| F-1 | ACI Equation | y=179.1×10-5x/(1+0.124 6x) | 0.9075 |
| | Wang Equation | y=-1.03×10-3×e(-0.375x)+1.409×10-3 | 0.9880 |
| | Equation（6） | y=1.5410×10-4e(-0.045 81x)-3.634×10-4e(-1.296x) | 0.9886 |
| F-2 | ACI Equation | y=176.3×10-4x/(1+0.184x) | 0.8892 |
| | Wang Equation | y=-6.523×10-4×e(0.038 62x)+9.721×10-4 | 0.9836 |
| | Equation（6） | y=8.484×10-4e(0.085 44x)-3.417×10-5e(-2.855x) | 0.9905 |
| F-3 | ACI Equation | y=29.11×10-5x/(1+0.031 2x) | 0.9336 |
| | Wang Equation | y=-7.268×10-4×e(-0.017 17x)+8.520 0×10-4 | 0.9928 |
| | Equation（6） | y=-1.324e(-0.275 6 x)+1.324e(-2.753x) | 0.9946 |
| F-4 | ACI Equation | y=1.976×10-5x/(1+0.021 25x) | 0.9656 |
| | Wang Equation | y=-6.974×10-4×e(-0.016 57 x)+7.708×10-4 | 0.9927 |
| | Equation（6） | y=9.461×10-4e((-0.055 42x)-5.382×10-4e(-0.576 3x) | 0.9960 |

### 4.4.3 UHPC Drying shrinkage mechanism

Drying shrinkage refers to the shrinkage caused by the water loss from cementitious materials due to the lower humidity of the surrounding environment compared to the inner humidity of the cementitious materials. The fully saturated binder matrix is not able to maintain its dimensional stability when exposed to the outside environment with a lower saturated humidity. This is mainly due to the loss of physically bound water which leads to a shrinkage strain. It is usually supposed that the drying shrinkage of concrete is related to the migration of adhesive water in the cement matrix. Therefore, the most probable reason for shrinkage goes to the driving force induced by the difference in relative humidity between the concrete and outside environments and the second reason is the migration of water maintained in the capillary pores (< 50 μm) because of the hydrostatic tension caused by the drying process (Bangham, Fakhoury, & Mohamed, 1932; Bazant & Baweja, 1995).

Compared to autogenous shrinkage, drying shrinkage of concrete can last for a relatively longer time. The increasing rate of drying shrinkage is higher in the early stage of curing than that in the later curing stage. To be specific, the drying shrinkage increases at a relatively high rate within 7 days followed by a gradual decreasing rate in the drying shrinkage development which can be explained by considering the mechanisms. Figure 4-8 shows a typical drying shrinkage curve of traditional cement stone (Bangham et al., 1932). Based on the porous structures and water content status inside, the drying shrinkage is normally separated into two stage: the initial stage (marked as 'AB') during which stage free water in large pores and large capillary pores (radius of pores > 100 nm) is lost first. This only gives rise to a loss in mass for cement stone rather than a shrinkage due to the fact that free water is attached on the microstructure of hydrated phases but without any physical-chemical bonding. When most of the free water is lost, an obvious shrinkage takes place as shown in 'BC' stage if the drying continues. This can be attributed to the compressive stress of the walls of capillary pores produced by the loss of water; with the further decrease in the relative humidity, most of the capillary pores suffer a complete water loss and the capillary pressure changes depending on the water content in the cement stone which reaches the greatest value and then starts to decrease, described as 'CD'. After the complete loss of water in capillary pores, adsorbed water starts to evaporate, the loss of which leads to a reduced opening pressure. This makes the two solid surfaces, i.e. meso-scale crystals, become closer, resulting in the shrinkage stage 'DE'; finally, layer water formed as the single molecule water film is lost from the C-S-H layered structures, which is 'EF' stage in the shrinkage curve. The resistance for the water loss in early stage is less compared to that in the later stage because it is mainly the capillary water that is lost during this stage. Therefore, the drying shrinkage development in the early stage is quicker compared to the later stage.

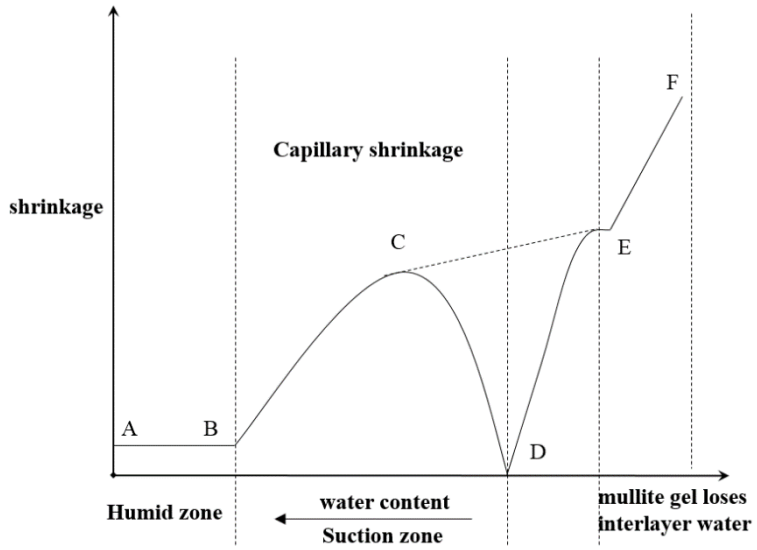


**Figure 4-8.** A typical graph of drying shrinkage of hardened cement paste (Courtial et al., 2013).

Generally speaking, the rate of drying shrinkage for UHPC is relatively high within 14 days of curing followed by a gradual decreasing rate in drying shrinkage until 100 days after which the shrinkage decreased. Besides, concrete with a low water/binder ratio exhibits a large autogenous shrinkage but a small drying shrinkage whereas the concrete with high water/binder ratio has an opposite behavior. In addition, the shrinkage and creep of UHPC with the addition of steel fibers are very small (Courtial et al., 2013). There is a linear correlation between shrinkage and relative humidity. The addition of silica fume can lead to a larger shrinkage compared to the concrete with addition of slag. Moreover, the shrinkage can be reduced by decreasing water/binder ratio or adding steel fibers.

Based on Figure 4-2, the UPHC with FA addition has a smaller drying shrinkage compared to the counterpart with slag addition which indicates that FA has a certain effect on limiting drying shrinkage. This can be due to the delayed moisture loss because of the FA addition which then limits the drying shrinkage. It is reported that concrete with a water/binder ratio at 0.30 and sealed curing conditions, the decreasing rate of relative humidity inside the concrete gradually was reduced when FA addition increased from 15% to 60%. When the addition of FA was larger than 40%, the reduction in the inner relative humidity after 120 days of curing was no more than 13%. In comparison, the oncrete without FA addition experienced a reduction in the relative humidity by more than 20%. With the 60% addition of FA, the inner relative humidity did not start decreasing until

after 7 days of curing (Bouzoubaâ, Zhang, & Malhotra, 2001; Sprince, Korjakins, & Pakrastinsh, 2013; Zheng-wu, Zhen-ping, & Pei-ming, 2004). Rongyan Hui et al. (Concrete shringkage, 1990) found that the drying shrinkage of dam concrete was reduced by about 50% when adding 20% of FA into the dam cement and this reduction was about 90% when the addition was 40%. When using ultra-fine FA, the drying shrinkage can be greatly reduced with an increasing amount of addition and the initiation of cracks was delayed at the same time(P. C. Aitcin, 1986). This can be explained by considering the slow hydration process of FA when mixed with water which means that the effective water/cement ratio is increased, leading to a reduced drying shrinkage of the concrete. It is worth noting that the drying shrinkage may not be reduced when the FA addition is low as Jiang et al.(G. Long, Z. Jiang et al., 2005) found that with an addition of 10%, the drying shrinkage can either be decreased or increased. Additionally, the early-age formation of cracks cannot be avoided by adding FA and it is more likely to suffer from plastic shrinkage and cracking without a proper curing condition (Dan & Mehta, 1988; Gaddam, Inyang, Ogunro, Janardhanam, & Udoeyo, 2009; Hamedanimojarrad, Ray, Thomas, & Vessalas, 2012) .

The effect of slag on the drying shrinkage can be due to its activity. According to the study conducted by Tazawa (Cusson, Daniel, & Hoogeveen, 2008; E. I. Tazawa & S. Miyazawa, 1995) et al., the drying shrinkage of concrete increases as the addition of slag increases when using a type of slag with a specific surface area more than 400 m2/kg. This phenomenon lasts until the addition amount is more than 75% after which a decreasing trend was observed. Within the addition amount ranging between 0-90%, the drying shrinkage decreases with an increasing amount of addition when the slag fineness was 338 m2/kg whereas with the fineness up to 836 m2/kg, the opposite is true for the addition range between 0-60%. Worse still, the drying shrinkage started to occur earlier and it became larger for the long-curing age with an increasing amount of addition (Cui, For, Lecturer, Liang, & Gao, 2011). However, some researchers do not believe that slag can lead to an increased drying shrinkage (B. Wang, Wang, & Ming, 2007). For instance, the concrete manufactured using number 500 finely grinded slag cement displayed a volume increase rather than a drying shrinkage (K. Huang, Min, Mo, & Wang, 2013). In this study, the activity of slag used is relatively higher and exhibits no limiting effect on the drying shrinkage.

The drying shrinkage of concrete can be reduced by adding fibers, especially for steel fibers. It is due to the fact that steel fibers have a relatively large plastic modulus and the bonding strength between the steel fibers and mortar matrix makes them act as a skeleton supporting the concrete matrix when concrete undergoes autogenous shrinkage. Therefore, a reduced shrinkage during early stage of curing was obtained to some extent (A. Noushini, Vessalas, & Samali, 2015). As the curing age proceeds, the plastic modulus of concrete matrix increases, leading to a reduced impact on the shrinkage by steel fibers. On the other hand, there exists an ITZ between steel fibers and concrete matrix which contains a lot of pores. It was confirmed that the porosity in ITZ is 6-10% higher than that of binder matrix according to the quantitative analysis which can be observed with the SEM analysis (A. Turatsinze, H. Farhat, & J. L. Granju, 2003; Z. Wu, Shi, & Khayat, 2016). When the addition of steel fibers reaches a certain point, the limitation effect on the drying shrinkage is weakened as the addition increases. This is attributed to the increased numbers of ITZ areas within which the bonding strength between steel fibers and matrix is low. This explains why the drying shrinkage of UHPC was similar regardless of slag or FA-based when the fiber addition is 2% and 3% in the study.

## 4.5 Conclusion

The effect of amount of steel fiber addition on the shrinkage of UHPC is investigated in the study. Several conclusions are drawn based on the experimental results and related discussions:

(1) UHPC displayed a rapid increase in the drying shrinkage followed by a decreasing rate

(2) It is found that fibers can be used to effectively reduce the drying shrinkage of UPHC. However, it is worth noting that there is little beneficial effect of steel fiber for reducing drying shrinkage when the addition of steel fiber is more than 2%. To be specific, the shrinkage was only reduced by 1.5% for the 3% steel fiber addition of UHPC compared to the UHPC with 2% addition. The reduced shrinkage can be attributed to the interface between steel fibers and concrete matrix whereas this beneficial effect can be limited when the addition of steel fibers surpasses a threshold because of the presence of more interfaces;

(3) A more significant effect for reducing drying shrinkage of UHPC is observed by adding fly ash compared to slag addition which can be explained by considering the drying shrinkage mechanisms of UHPC. The drying shrinkage is mainly induced by the hydrated phases but limited by the unhydrated phases and aggregates. Thus, on the one hand, by replacing the cement with fly ash, the number of hydrated phases decreases leading to a reduced shrinkage. On the other hand, fly ash is also considered as fine aggregate which has a space-filling effect and limit the drying shrinkage at the same time;

(4) The correlation coefficient obtained by using ACI equation to fit the experimental data is lower than that obtained with the equation proposed by Tiemeng Wang et al. The combined exponential equation developed in this study is better at describing the relationship between the drying shrinkage and time for UHPC with the addition of steel fibers compared to the other two equations.

## 4.6 References


P. Acker, Swelling, shrinkage and creep: a mechanical approach to cement hydration, Materials and Structures, 37 (2004) 237-243.

V.Y. Garas, L.F. Kahn, K.E. Kurtis, Short-term tensile creep and shrinkage of ultra-high performance concrete, Cement and Concrete Composites, 31 (2009) 147-152.

Z. Li, Drying shrinkage prediction of paste containing meta-kaolin and ultrafine fly ash for developing ultra-high performance concrete, Materials Today Communications, 6 (2016) 74-80.

R.I. Gilbert, Time effects in concrete structures, 1988.

L. Wu, N. Farzadnia, C. Shi, Z. Zhang, H. Wang, Autogenous shrinkage of high performance concrete: A review, Construction and Building Materials, 149 (2017) 62-75.

B. Barr, S. Hoseinian, M. Beygi, Shrinkage of concrete stored in natural environments, Cement and Concrete Composites, 25 (2003) 19-29.

G. FISCHER, W. Shuxin, Design of engineered cementitious composites (ECC) for processing and workability requirements, Brittle Matrix Composites 7, Elsevier2003, pp. 29-36.

P. Monteiro, Concrete: microstructure, properties, and materials, McGraw-Hill Publishing2006.

H. Chen, W. Wang, J.C. Martin, A.J. Oliphant, P.A. Doerr, J.F. Xu, K.M. DeBorn, C. Chen, L. Sun, Extraction of lignocellulose and synthesis of porous silica nanoparticles from rice husks: a comprehensive utilization of rice husk biomass, ACS Sustainable Chemistry & Engineering, 1 (2012) 254-259.

W. Zhang, M. Zakaria, Y. Hama, Influence of aggregate materials characteristics on the drying shrinkage properties of mortar and concrete, Construction and Building Materials, 49 (2013) 500-510.

J.-C. Chern, Y.-W. Chan, Deformations of concretes made with blast-furnace slag cement and ordinary portland cement, Materials Journal, 86 (1989) 372-382.

R. Khatri, V. Sirivivatnanon, W. Gross, Effect of different supplementary cementitious materials on mechanical properties of high performance concrete, Cement and Concrete Research, 25 (1995) 209-220.

J. Mora-Ruacho, R. Gettu, A. Aguado, Influence of shrinkage-reducing admixtures on the reduction of plastic shrinkage cracking in concrete, Cement and Concrete Research, 39 (2009) 141-146.

D. Bentz, M.R. Geiker, K.K. Hansen, Shrinkage-reducing admixtures and early-age desiccation in cement pastes and mortars, Cement and concrete research, 31 (2001) 1075-1085.

R. Rodden, D. Lange, Feasibility of shrinkage reducing admixtures for concrete runway pavements, (2004).

J. Brooks, X. Jiang, The influence of chemical admixtures on restrained drying shrinkage of concrete, Special Publication, 173 (1997) 249-266.

K.J. Folliard, N.S. Berke, Properties of high-performance concrete containing shrinkage-reducing admixture, Cement and Concrete Research, 27 (1997) 1357-1364.

Y. Dang, J. Qian, Y. Qu, Z. Lin, W. Zhi, D. Qiao, X. Jia, Curing cement concrete by using shrinkage reducing admixture and curing compound, Construction & Building Materials, 48 (2013) 992-997.

Y. Huang, Influence of curing conditions on the drying shrinkage characteristics of cement mortar, Journal of Nanjing University of Technology, 28 (2006) 20-23.

F. Jin, A. Al-Tabbaa, Strength and drying shrinkage of slag paste activated by sodium carbonate and reactive MgO, Construction & Building Materials, 81 (2015) 58-65.

PierreMounanga, KhalidCherkaoui, AbdelhafidKhelidj, MireilleCourtial, M.-N. deNoirfontaine, F. Dunstetter, Extrudable reactive powder concretes: hydration, shrinkage and transfer properties, Revue Franã§aise De Gã©nie Civil, 16 (2012) s99-s114.

S.P. Tarolli, Future of Information Commerce under Contemporary Contract and Copyright Principles, The, Am.u.l.rev, (1997).

C. Shi, Y.L. Mo, High-Performance Construction Materials, 2015.

GARAS, Y. Victor, KAHN, F. Lawrence, KURTIS, E. Kimberly, Short-term tensile creep and shrinkage of ultra-high performance concrete, Cement & Concrete Composites, 31 (2009) 147-152.

K. Koh, G. Ryu, S. Kang, J. Park, S. Kim, Shrinkage Properties of Ultra-High Performance Concrete (UHPC), Advanced Science Letters, 4 (2011) 948-952.

M. Ba, C. Qian, W. Hui, Effects of specimen shape and size on water loss and drying shrinkage of cement-based materials, Journal of Wuhan University of Technology, 28 (2013) 733-740.

A. Cwirzen, V. Penttala, C. Vornanen, Reactive powder based concretes: Mechanical properties, durability and hybrid use with OPC, Cement & Concrete Research, 38 (2008) 1217-1226.

Z. Xian, P. Zhang, W. Zhen, Z. Ling, G. Zeng, C. Zhou, Adsorption of methylene blue onto humic acid-coated Fe 3 O 4 nanoparticles, Colloids & Surfaces A Physicochemical & Engineering Aspects, 435 (2013) 85-90.

P. Chen, Y. Liu, D.I. Mingwei, The effect of Nano-filler on the damping properties of Polyacrylic damping paint, Advanced Materials Research, 183-185 (2011) 2154-2157.

Q. Dai, K. Ng, J. Zhou, E.L. Kreiger, T.M. Ahlborn, Damage investigation of single-edge notched beam tests with normal strength concrete and ultra high performance concrete specimens using acoustic emission techniques, Construction & Building Materials, 31 (2012) 231-242.

BuquanMiao, Jenn‐ChuanChern, Chen‐AnYang, Influences of fiber content on properties of self‐compacting steel fiber reinforced concrete, Journal of the Chinese Institute of Engineers, 26 (2003) 523-530.

Wu Jinfeng, Yu Ligang, Cai Xi, Some bad conditions after the implementation of GB175-2007 General Portland Cement, Cement, (2009) 46-47.

Z.P. Bazant, S. Baweja, Creep and shrinkage prediction model for analysis and design of concrete structures— model B 3, Materials & Structures, 28 (1995) 357-365.

D.H. Bangham, N. Fakhoury, A.F. Mohamed, The Swelling of Charcoal. Part II. Some Factors Controlling the Expansion Caused by Water, Benzene and Pyridine Vapours, Proceedings of the Royal Society of London, 138 (1932) 162-183.

M. Courtial, M.N.D. Noirfontaine, F. Dunstetter, M. Signes-Frehel, P. Mounanga, K. Cherkaoui, A. Khelidj, Effect of polycarboxylate and crushed quartz in UHPC: Microstructural investigation, Construction & Building Materials, 44 (2013) 699-705.

N. Bouzoubaâ, M.H. Zhang, V.M. Malhotra, Mechanical properties and durability of concrete made with high-volume fly ash blended cements using a coarse fly ash, Cement & Concrete Research, 31 (2001) 1393-1402.

J. Zheng-wu, S. Zhen-ping, W. Pei-ming, Self-desiccation Effect of High Performance Concrete, Journal of Wuhan University of Technology-Materials Science, 19 (2004) 82-86.

A. Sprince, A. Korjakins, L. Pakrastinsh, Time-Dependent Behavior of High Performance Fiber-Reinforced Concrete, Advanced Materials Research, 705 (2013) 75-80.

P.C. Aitcin, Concrete structure, properties and materials, Preticehall International, 13 (1986) 499-499.

Long Guangcheng, Jiang Zhengwu, Sun Zhenping, Wang Peiming, Xie Youjun, Study on Self-Drying Effect of Reactive Powder Concrete, Journal of Building Materials, 8 (2005) 7-10.

R. Gaddam, H.I. Inyang, V.O. Ogunro, R. Janardhanam, F.F. Udoeyo, Strength and Leaching Patterns of Heavy Metals from Ash-Amended Flowable Fill Monoliths, 2009.

P. Hamedanimojarrad, A.S. Ray, P.S. Thomas, K. Vessalas, Development of shrinkage resistant microfibre-reinforced cement-based composites, Central European Journal of Engineering, 2 (2012) 289-295.

R. Dan, P.K. Mehta, Compressive strength of low cement/high fly ash concrete, Cement & Concrete Research, 18 (1988) 571-583.

E.I. Tazawa, S. Miyazawa, Influence of cement and admixture on autogenous shrinkage of cement paste, Cement & Concrete Research, 25 (1995) 281-287.

CUSSON, Daniel, HOOGEVEEN, Internal curing of high-performance concrete with pre-soaked fine lightweight aggregate for prevention of autogenous shrinkage cracking, Cement & Concrete Research, 38 (2008) 757-765.

X.L. Cui, C. For, Lecturer, X.W. Liang, D.X. Gao, Loading capacity of high performance concrete shear wall with end columns, Journal of Xian University of Architecture & Technology, 43 (2011) 367-373.

B. Wang, L. Wang, L. Ming, Experimental research on the autogenous shrinkage of MK high performance concrete, Journal of Wuhan University of Technology, 22 (2007) 551-554.

K. Huang, D. Min, L. Mo, Y. Wang, Early age stability of concrete pavement by using hybrid fiber together with MgO expansion agent in high altitude locality, Construction & Building Materials, 48 (2013) 685-690.

A. Noushini, K. Vessalas, B. Samali, Rheological Properties and Compressive Strength Behaviour of Polyvinyl Alcohol Fibre-Reinforced Concrete, Australian Journal of Structural Engineering, 15 (2015) 77-88.

Z. Wu, C. Shi, K.H. Khayat, Influence of silica fume content on microstructure development and bond to steel fiber in ultra-high strength cement-based materials (UHSC), Cement & Concrete Composites, 71 (2016) 97-109.

A. Turatsinze, H. Farhat, J.L. Granju, Influence of autogenous cracking on the durability of repairs by cement-based overlays reinforced with metal fibres, Materials & Structures, 36 (2003) 673-677.

# CHAPTER 5 EFFECTS OF ULTRA-FINE FLY ASH UFA CONTENT ON EARLY AGE SHRINKAGE AND MICROSTRUCTURE DEVELOPMENT OF ULTRA-HIGH STRENGTH CEMENT BASED MATERIALS

Note: this chapter is based on the manuscript entitled "Effects of ultra-fine fly ash (UFA) content on early-age shrinkage and microstructure development of ultra-high strength cement-based materials (UHSC)", by Linmei Wu, Z Zhang and H Wang, published in Proceedings on– the 15th International Congress on the Chemistry of Cement, Prague, Czech Republic, 2019.

**Abstract:** The use of Ultra fine fly ash (UFA) can significantly enhance mechanical properties of concrete given its beneficial filling and pozzolanic effects. In this study, the effect of UFA content on flowability, heat of hydration, mechanical properties and early age shrinkage properties were determined for ultra-high strength cement-based materials (UHSC) containing 0-75% UFA by the mass of binder. Thermal gravimetry (TG) and Fourier transform infrared (FTIR) were used to quantitatively determine the calcium hydroxide (CH) content and pore structure, respectively. The results indicated that the optimal UFA content could be in the range of 15%-30% in terms of flowability, mechanical properties, CH content, porosity, and interfacial bonding properties. The TG analysis revealed that the use of 15%-30% UFA efficiently consumed the CH, transforming it to C-S-H gel. Results show that the addition of 30% UFA significantly improved the early age as well as later age compressive strengths of ordinary and (high volume fly ash) HVFA concretes. All above measured durability properties of HVFA concretes are also improved and in most cases the HVFA concrete containing 30% UFA exhibited superior durability properties than ordinary concrete containing 100% cement. The results also indicate the effectiveness of UFA in producing high packing density and in accelerating the pozzolanic activity to produce more C–S–H gel by consuming calcium hydroxide (CH) in HVFA concretes.

## 5.1 Introduction

Ultra-high strength cement-based material (UHSC) is an advanced material that is characterized by high content of cementitious materials, sand, superplasticizer and/or fibers and absence of coarse aggregate (P Richard & Cheyrezy). The very low water-to-binder ratio and dense microstructure allows its high strength generally over 120 MPa. However, the higher the compressive strength is, the more brittle the matrix becomes. Owing to the use of very fine sand instead of ordinary aggregate, the content of cement in UHSC is as high as 900–1000 kg/m3(Pierre Richard & Cheyrezy, 1995; L. Wu et al., 2017b). In addition, fly ash is an essential ingredient in UHSC.

Application of fly ash concrete for more than ten years history, the concrete mixed with fly ash, not only can partially replace cement, reduce the project cost, but also can improve and enhance the performance of concrete. It has an extreme fineness and a high amorphous silica content. The typical fly ash (FA)-to-cement ratio used is 0.25 regarding the filler effect and pozzolanic effect (E.-H. Yang, Yang, & Li, 2007b). The high cement content with the FA-to-cement ratio of 0.25 leads to a high amount of FA in UHSC mixtures. However, this also causes some disadvantages in the modern construction industry, particularly in developing countries where there are limited resources and significant cost constraints. This provides the motivation for researching other potential materials with similar performances instead of fly ash.

The quantity of fly ash to replace the cement for typical application is limited to 15–20% by mass of the total cementitious material(Bendapudi & Saha, 2011; Supit, Shaikh, & Sarker, 2014). As a by-product of industrial process, the utilization of fly ash has made some progress in addressing the challenges of sustainable construction. In addition, fly ash has pozzolanic activity which is attributed to the presence of $SiO_2$ and $Al_2O_3$(Udoeyo, Inyang, Young, & Oparadu, 2006). It reacts with calcium hydroxide during cement hydration, to form additional Calcium Silicate Hydrate (CSH) and Calcium Aluminate Hydrate (CAH) which are effective in forming denser matrix leading to higher strength and better durability (Bendapudi & Saha, 2011; Malvar & Lenke, 2006; Shaikh & Supit, 2015).

The use of high volume fly ash as partial replacement of cement in concrete has also been studied. The main concern in this regard is whether or not cement can be replaced by fly

ash above the limiting quantity of 15–20% by mass in the concrete. Indeed, the small percentage is beneficial in optimizing the workability and low cost but it may not improve the durability to any considerable extent (Aggarwal, Gupta, & Sachdeva, 2010). On the other hand, due to slow pozzolanic properties of fly ash particles, low early age strength and durability properties are observed (Barbhuiya, Gbagbo, Russell, & Basheer, 2009; Choi, Lee, & Monteiro, 2011). Moreover, the optimization of high volume fly ash has raised many arguments and limitations regardless of the fact that the variation of constituent in fly ash such as alkalis, sulfates, lime and organics may affect the crystallization and slow down the pozzolanic reaction (Bendapudi & Saha, 2011). In order to overcome this deficiency, the incorporation of very small size pozzolanic materials such as silica fume in concrete containing fly ash has also been studied (Bingöl & Tohumcu, 2013; Gesoğlu, Güneyisi, & Özbay, 2009; Nochaiya, Wongkeo, & Chaipanich, 2010).Finer and amorphous materials are expected to accelerate the pozzolanic reaction to improve the early age strength characteristics of mortars and concretes.

Most ultra-fine fly ash (UFA) particles are finer than cement particles, and fly-ash particles will fill in the gap left by cement particles, the physical filling effect thus can improve the strength of concrete(Cheng, Huang, Huang, & Yen, 2011). Low water requirement ratio can reduce the water to binder ratio of blended paste, which is also beneficial for strength and durability. The above two are its physical functions. CH is not only the production of cement hydration, but also the reactant of UFA pozzolanic reaction. So, pozzolanic reaction of UFA can promote the cement hydration, generate more C-S-H gel, contributing to an increased strength and durability of paste or concrete. According to informed researches, Hydration activity of fly ash is low, and the hydration heat evolution of it is always neglected (J. C. Wang & Yan, 2006). And in this study, quantitative analysis on the contribution of UFA and cement in pozzolanic hydration heat were made to determine if it can be neglected.

Extensive research has been done on UHSC, but limited investigations have focused on the enhancement of micro and macro-structure development. In this chapter, the effect of UFA content on properties including flowability, heat of hydration, compressive strengths, and early age shrinkage properties of UHSC were investigated. The results are compared with those obtained from the control sample and the SF modified sample. It provides important implications to improve the durability and mechanical properties of UHSC.

## 5.2 Test program

### 5.2.1 Raw materials

A P.I 42.5 Portland cement complying with the Chinese Standards GB175-2007 was used. Table 5-1 summarizes the main chemical composition and physical properties of the cement. The UFA is manufactured by proprietary separation system that includes selective air classification. The commercially available product typically has a mean particle diameter of about 3 micrometers, with over 90% of the material (by volume) having a particle diameter less than 7 micrometers (as measured by a laser interferometer). Table 5-2 presents the chemical compositions of cement and mineral admixtures. The natural river sand with maximum particle size of 2.36 mm and fineness modulus of 3.0 was from Xiangjiang River. The apparent density and packing density were 2550 kg/m3 and 1570 kg/m3, respectively. A polycarboxylate based superplasticizer (SP) with water-reducing efficiency greater than 30% was used in this study.

**Table 5-1:** Physical properties of cement

| Cement | Density ($kg/m^3$) | 80μm-residue on sieve (%) | Specific surface area ($m^2/kg$) | Setting time(h) | | Flexural Strength (Mpa) | | Compressive Strength (Mpa) | |
|---|---|---|---|---|---|---|---|---|---|
| | | | | Initial | Final | 3d | 28d | 3d | 28d |
| P.I | 3.15 | 0.3 | 380 | 2.5 | 3.4 | 6.4 | 9.0 | 33.0 | 60.0 |

**Table 5-2:** Chemical composition of materials (%)

| Chemical composition | $SiO_2$ | $Al_2O_3$ | $Fe_2O_3$ | CaO | MgO | $K_2O$ | $Na_2O$ | $SO_3$ | LOI |
|---|---|---|---|---|---|---|---|---|---|
| Cement | 25.26 | 6.38 | 4.05 | 64.67 | 2.68 | - | - | 0.94 | 0.9 |
| Silica fume | 90.82 | 1.03 | 1.50 | 0.45 | 0.83 | 0.86 | 0.17 | - | 4.34 |
| Slag | 33.00 | 13.91 | 0.82 | 39.11 | 10.04 | 1.61 | 0.26 | 0.92 | 0.33 |
| UFA | 73.4 | 17.7 | 4.4 | 0.9 | 0.6 | 1.03 | 0.11 | 0.2 | 1.66 |

### 5.2.2 Mixture proportions

Based on the preliminary study, mixture proportion of UHSC with a water-to-binder (w/b) ratio of 0.18 and binder-aggregate ratio of 1.1 was used, as shown in Table 5-3. The SP dosage was fixed at 2% by mass of the binder. For preparation of mixtures, the powder components were dry-mixed at a low speed for 3 min, then water and SP were slowly added. The material was then mixed for 6 min at low speed and 1 min at high speed.

**Table 5-3:** Mixture proportions of UHSC.

| No. | Replacement ratio | Cement (%) | Silica fume (%) | UFA (%) | SP (%) | w/b | binder-aggregate ratio |
|---|---|---|---|---|---|---|---|
| U0 | 0 | 90 | 10 | 0 | 2 | 0.18 | 1：1.1 |
| U1 | 1/6 | 75 | 10 | 15 | 2 | 0.18 | 1：1.1 |
| U2 | 1/3 | 60 | 10 | 30 | 2 | 0.18 | 1：1.1 |
| U3 | 1/2 | 45 | 10 | 45 | 2 | 0.18 | 1：1.1 |
| U4 | 2/3 | 30 | 10 | 60 | 2 | 0.18 | 1：1.1 |
| U5 | 5/6 | 15 | 10 | 75 | 2 | 0.18 | 1：1.1 |

SP*: total mass of liquid-based SP

### 5.2.3 Test procedures

#### 5.2.3.1 **Flowability test**

The flowability of all UHSC mixtures was measured in accordance with the Chinese Standards GB/T 2419-2005. The mixtures were cast into a mini cone mould placed on an automatic jolting table. The mould was lifted vertically and immediately jolted for 25 times (one second for each time). Then two diameters perpendicular to each other were determined and mean value was reported.

#### 5.2.3.2 **Corrugated tube measurement**

Fresh mixtures were filled into corrugated polyethylene tubes with 10 mm inner diameter using a hopper and rodded with a glass rod to eliminate large air bubbles and ensure the mortar in a dense condition. The free ends of tubes were immediately sealed by a stainless-steel cover. Then the gauge head was fixed at a distance of 2 mm to the free end. The lengths were recorded at an interval of 5 min for the first 72 hours. The experiment

was conducted at 20±2 °C and with precision of 0.0001 mm. The autogenous shrinkage was calculated as follows:

$$\varepsilon_{st} = \frac{a_t - a_0}{l_0} \quad (5\text{-}1)$$

where, $\varepsilon_{st}$ is the autogenous shrinkage of concrete at time t (h); $a_t$ is the distance between the sensor head and the steel free head (mm) at time t; $a_0$ is the initial distance between the sensor head and the steel free head (mm); $l_0$ is the original length of the measured part of specimens (mm).

#### 5.2.3.3 **Powder X-ray diffraction analytical methods**

The preparation of samples for XRD was the same as those prepared for TGA. The prepared powders were analyzed by using Philips X-ray diffractometer with CuKα radiation. The samples were step-scanned from 10 to 70° (2θ) at a rate of 5°/min.

#### 5.2.3.4 **Compressive strength test**

Specimens of 40×40×160 $mm^3$ were cast for compressive and flexural strength tests. Three samples of each batch were used. They were demolded 24 h after casting and cured in lime-saturated water until the age of 1, 3, 7, 28, and 91 d. Three-point bending testing was first performed to obtain the flexural strength. Then the six broken specimens with sizes of approximately 40×40×40 $mm^3$ were used to test compressive strength. The mean values of the three (flexural strength) and six samples (compressive strength) were reported.

#### 5.2.3.5 **Micro-hardness measurement**

Micro-indention is based on applying a static load for a known period of time and measuring the response in terms of size of indentation. In this study, a 498 mN load was applied on the samples for 10 s. Points within 0–200 μm distance from the fiber edge was measured. During the indention process, areas with sand were avoided. The micro-hardness or Vickers hardness (HV) was captured during the measurement. The average values of four indentations were reported.

#### 5.2.3.6 **Thermal-gravimetric analyses**

Thermogravimetric (TG) and derivative Thermogravimetric (DTG) analyses were used to quantitatively estimate the amount of hydration products in the UHSC. A Netzsch STA 409 PC equipment was employed. Samples taken from UHSC matrix were put into a vacuum drying chamber to reach constant mass. After that, these dried samples were ground to powder and sieved on a square mesh sieve with diameter of 45 μm. The tested samples up to 10-15 mg, were heated from 0 to 1000°C under nitrogen gas flow at a constant heating rate of 10°C/min. The decomposition of hydration products were observed and quantified (Washburn, 1921). The decomposition of CH is shown as follows:

$$Ca(OH)_2 \xrightarrow{450°C} CaO + H_2O\uparrow \quad (5\text{-}2)$$

According to this equation, the proportion of CH to the residual mass at 1000°C was determined as follows:

$$m = \frac{74 \times m_{loss}}{18 \times m_{remain}} \times 100\% \quad (5\text{-}3)$$

Where m (%) is the proportion of CH content to residual mass; $m_{loss}$ (%) is the mass loss of samples at about 450°C; $m_{remain}$ (%) is the residual mass after heating; 74 and 18 are the molar masses of $Ca(OH)_2$ and $H_2O$, respectively.

#### 5.2.3.7 **Heat of hydration**

The hydration heat was determined using an isothermal calorimeter. About 4 g paste samples was weighed and filled into a glass bottle then placed into TAM Air isothermal calorimeter immediately for measurement of heat of hydration. When the glass bottle was place into TAM Air isothermal calorimeter, the data acquisition system was initiated at the same time to record the output voltage from which the heat flow in the system could be calculated. All measurements were lasted for 2 hours.

### 5.2.4 FTIR spectrum analysis

Powder samples were taken from the split specimen at depths of 0, 5, 10, 15, 20, 25, 30 and 35 mm measured from the edge of the split surface. The IR spectrum of each powder sample mixed with KBr in a proportion of 1:10 was obtained to facilitate quantitative measurement of the depth of carbonation. The background spectrum of the laboratory environment was scanned before the powder sample was scanned. Carbonation is represented by the transformation of the C–O bonds of $CO_2$ into C–O bonds in the $CaCO_3$. Thus, a study of the characteristic peak of the C–O functional group in the wave number range of 1410-1510 $cm^{-1}$ would identify the carbonation in concrete (Collepardi, 2000).

## 5.3 Results and Discussion

### 5.3.1 Effect of UFA content on flowability of fresh UHSC

The variation of mini slump flow of UHSC mixtures with different UFA contents is given in Figure 5-1. From the curves, it is evident that generally, the flow spread increased as the UFA content increased. It is also evident that the addition of UFA up to 75% always increased the flow spread of the cement paste. For instance, the addition of 15%, 30% and 40% UFA increased the flow spread from absolute 200mm to 210mm and 215 mm, respectively. This phenomenon may be explained by the following effects: (1) the slurry effect - the UFA particles, being very fine, tend to move together with the water to form a water-UFA slurry, which has a larger volume than the water itself and therefore would increase the inter-particle spacing between the rough cement grains; and (2) the ball bearing effect - the UFA particles, being perfectly spherical in shape and smooth, would act as ball bearings to reduce the inter-particle friction between the rough cement grains(Kwan & Chen, 2013; L. Wu et al., 2017b).

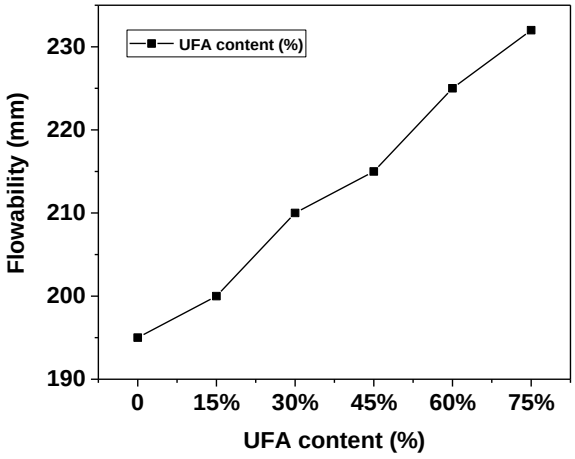


**Figure 5-1.** Effect of UFA Content on Flowability of Fresh UHSC Mixtures.

### 5.3.2 Effect of UFA content on compressive strength of UHSC

At a W/C ratio of 0.18 or lower, the addition of up to 30% UFA significantly increased the strength( Kwan & Chen, 2013), while the addition of 45% or more UFA caused the strength to decrease. However, there are a little different in these compressive strengths. The influences of UFA content on compressive strengths of the UHSC mixture are showed in Figure 5-2. After 7 d, the increase in compressive strength was limited to only 11%. The incorporation of UFA accelerated the early hydration of cement, thus lead to early strength increase. Besides, a significant increase in strength was observed with the increase of UFA replacement from 0 to 30%. However, when UFA exceeded 45%, the strengths tended to decrease. The compressive and flexural strengths of U0 at 28 d were 89.8 and 19.1 MPa, respectively. When 15%, 30%, 45%, and 60% UFA replacement were used, the compressive strength increased by approximately 18%, 16%, 28%, and 8%, respectively, as shown in Figure 5-2 (a). The flexural strength increased by approximately 11%, 15%, 29%, and 9%, respectively.

The addition of 15%-30% UFA decreased the porosity and improved the strength due to its filling effect in addition to the pozzolanic reaction (Vikan & Justnes, 2007). However, a high content of 45% UFA increased plastic viscosity, which could result in air entrapment. Furthermore, high UFA content could significantly increase the risk of micro-cracking due to autogenous shrinkage, which can affect mechanical properties (Lura, Jensen, & Breugel, 2003). The compressive strength increased with the mortar's age and the pozzolanic reaction of fly ash was affected by the components of the mortar. The compressive

strength increased with the mortar's age due to differences in pozzolanic reactivity. The pozzolanic reaction of fly ash was significantly affected by SiO2, Al2O3, and Fe2O3 components, which form the framework of the glass phase, and CaO, MgO, Na2O, and K2O components, which depolymerize the glass structure(Cho, Young Keun, Sang Hwa Jung, 2019).

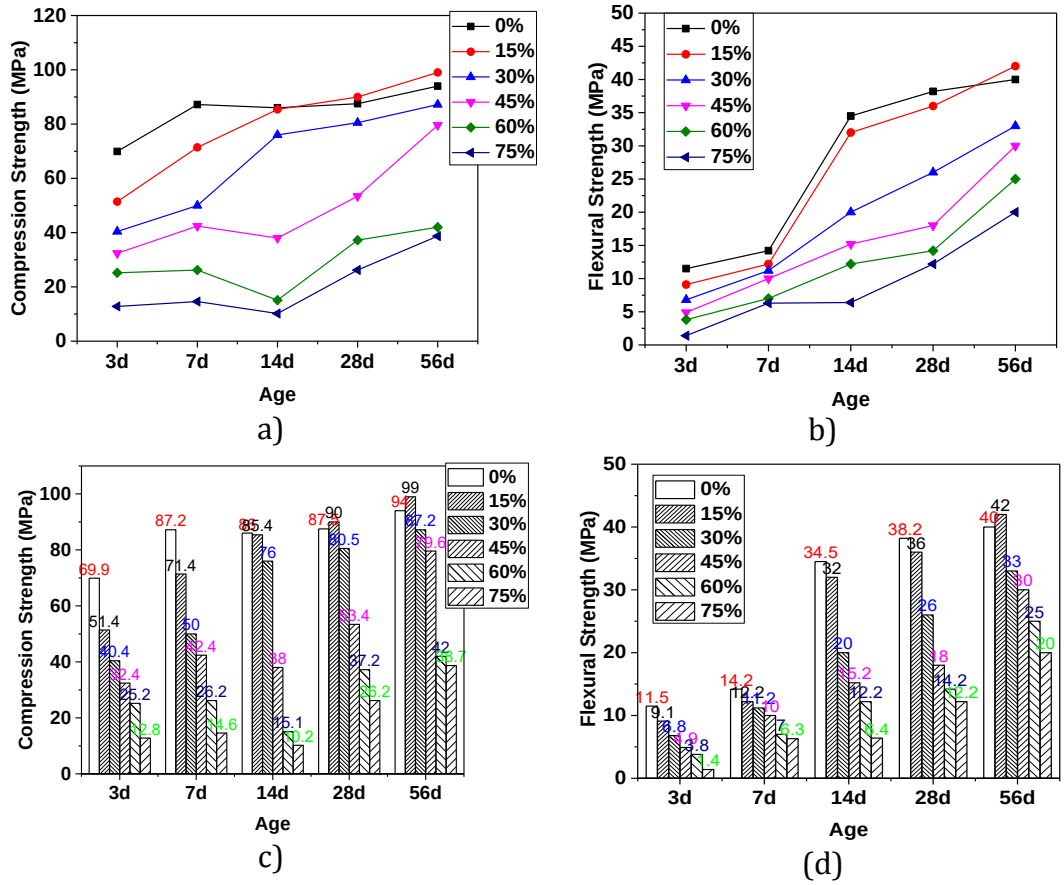


**Figure 5-2.** Effect of UFA Content on mechanical properties of Fresh UHSC.

## 5.3.3 Effect of UFA content on micro hardness of UHSC

The micro-hardness of matrix with different distances to fiber edge is indicated in Figure 5-3. UHSC with 15% UFA had higher micro-hardness than that of the reference batch. This suggested high strength hydration products for UHSCs with UFA.

Figure 5-3 summarizes the micro-hardness results of the UHSC samples that were obtained at different content of UFA. With increase of UFA content, the micro-hardness value of the matrix increased, while the addition of 45% or more UFA caused the micro-

hardness value to decrease. For example, in the NS1.0 sample at 28 d, the micro-hardness of matrix at 40 μm from the surface was 84.1 HV. It increased to 88.6 and 100.5 HV at 80 and 120 μm, respectively. The micro-hardness did not significantly change beyond 120 μm. For the NS1.0 samples at 1 and 7 d, the micro-hardness within distance of 80 μm from the fiber edge was obviously lower than that with far distance.

The micro-hardness increased with prolongation of hydration time. For the NS1.0 sample at 1, 7, and 28 d, the micro-hardness at 80 μm from the fiber edge were 82.9, 85.4, and 96.6 HV, respectively. In addition, the NS1.0 at 28 d showed greater micro-hardness compared to the reference sample NS0. This indicated that the incorporation of 1% nano-SiO2 can enhance the quality of the matrix. It was suggested that bond between fibers and matrix was mainly dominated by adhesion or chemical bond, which is governed by the main hydration product C-S-H with diameter of 10 nm. In addition to the pozzolanic reaction of UFA that resulted in greater volume of C-S-H gel, the UFA acts as nucleus for the precipitation of C-S-H.

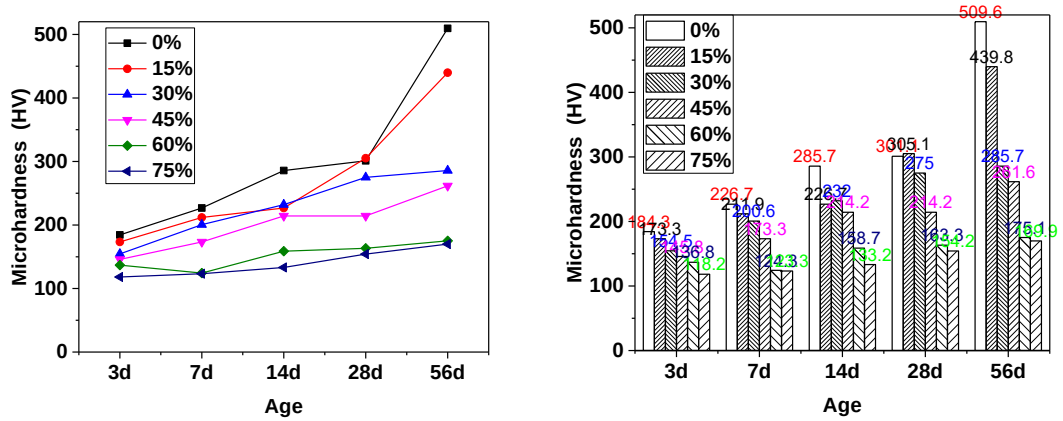


**Figure 5-3.** Effect of UFA Content on micro hardness of UHSC Mixtures.

## 5.3.4 Autogenous shrinkage

Figure 5-4. Shows the effect of UFA content on autogenous shrinkage of UHPC. The autogenous shrinkage increased with the increase of UFA content. Specimens with 25%

and 30% silica fume showed a autogenous shrinkage more than 4000με at 72h, and about 3000με for specimens with 15% and 20% silica fume, while only 2200με for those specimens with 10% silica fume. It was obviously that the autogenous shrinkage of specimens with the 30% silica fume was about twice of that with 10% silica fume. This was consistent with the results in a previous publication.

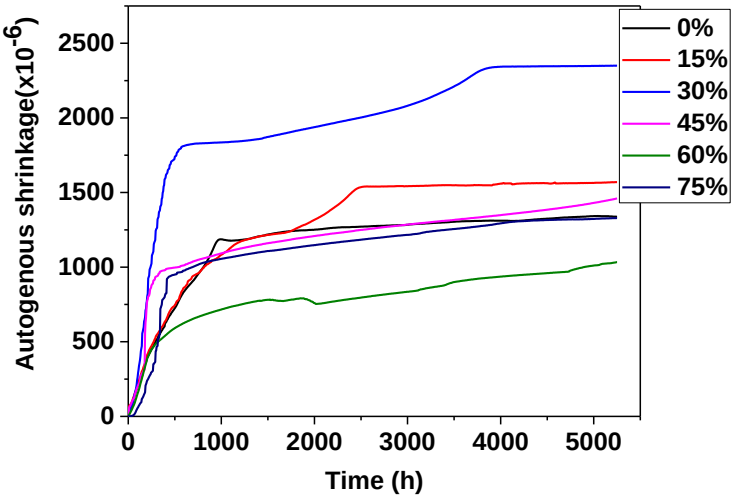


**Figure 5-4.** Effect of UFA Content on autogenous shrinkage of UHSC Mixtures.

### 5.3.5 XRD of UFA

The characteristics of the raw materials based on XRD analysis are shown in Figure 5-5 previous analysis by the authors also showed that ultrafine fly ash is about more amorphous class F fly ash. According to the XRD pattern for the unreacted UFA sample, it is apparent that the main crystalline phases are quartz ($SiO_2$), mullite ($Al_6Si_2O_{13}$), magnetite, hematite ($Fe_2O_3$).

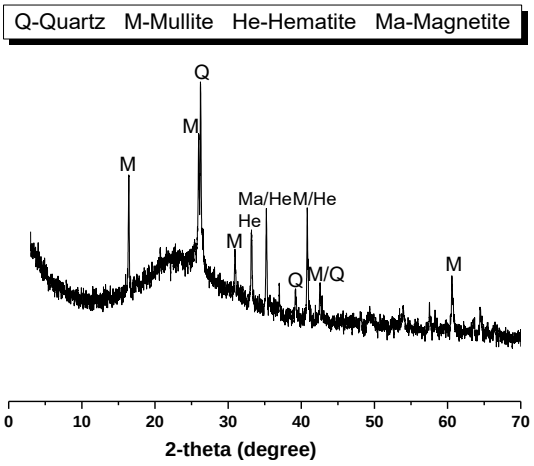


**Figure 5-5.** XRD pattern of UHSC Mixtures.

### 5.3.6 Effect of UFA content on heat of hydration of UHSC

It is clear from the spectrum of the rate of heat evolution that as the content of UFA increases, the height of early rate peak decreases gradually, ranging from 0.0011 W/g when there was no UFA to less than 0.0002 W/g for the content at 45 %. At the same time, the time required to reach the maximum hydration rate was longer with an increase of the UFA amount. Without any UFA addition, the time was around 50 hours whereas this value for the 30% UFA content was more than 60 hours. For the content at 60% and 75 %, there was even no peak during the testing period (0-140 h).

It is clear from the spectrum of the rate of heat evolution that as the content of UFA increases, the height of early rate peak decreases gradually, ranging from 0.0011 W/g when there was no UFA to less than 0.0002 W/g for the content at 45 %. At the same time, the time required to reach the maximum hydration rate was longer with an increase of the UFA amount. Without any UFA addition, the time was around 50 hours whereas this value for the 30% UFA content was more than 60 hours. For the content at 60% and 75 %, there was even no peak during the testing period (0-140 h). The delayed and reduced hydration rate can be explained by considering two effects that UFA have on the cement hydration process. Firstly, the UFA tend to absorb more water due to their high specific surface area (18.5 m2/g). Thus, the available water for the cement hydration was reduced, leading to a reduced and delayed hydration rate. Secondly, the cement content decreased when the UFA content increased. Compared to UFA, normal cement has a higher rate of hydration.

In comparison, however, UFA mainly has a retardation effect on the cement-FA system, especially during the dormant period (Langan, Weng, & Ward, 2002). This result corresponds well with many other studies which show that the inclusion of fly ash led to a decreased degree of hydration (Dale P Bentz, 2014; Poon, Lam, & Wong, 2000; Yoshitake, Wong, Ishida, & Nassif, 2014).

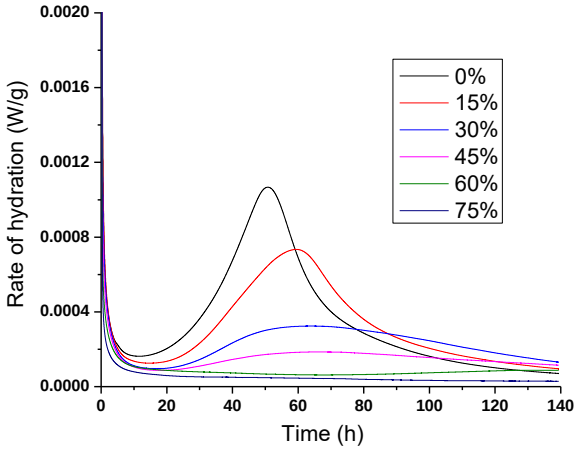


**Figure 5-6.** Effect of UFA Content on rate of hydration of UHSC Mixtures.

### 5.3.7 TIR of UHSC Mixtures

Figure 5-7 shows the effect of UFA Content on FTIR of UHSC U0 and U2. As time proceeded, the peak at around 3420 $cm^{-1}$ which belongs to the OH stretching in water, shifted to higher frequency for U2; whereas for U0, the opposite seemed to occur, shifting from 3447 to 3420 $cm^{-1}$. This contradictory result requires further investigation. What is obvious for both U1 and U2 is the diminishing peaks around 450-480 from 0 to 14-day curing, assigned to the SiO from $SiO_4$. Another band locating at around 1110-1120 cm-1 decreased sharply from 0-day to 14-day with a slight shift towards higher frequency, 1119 to 1220 and 1120 to 1130 for U0 and U2 respectively.

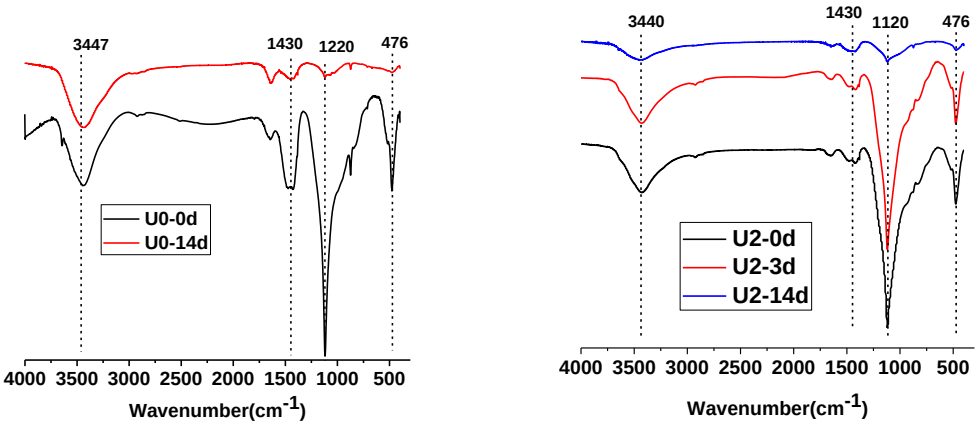


(a) (b)

**Figure 5-7.** Effect of UFA Content on FTIR of U0 and U2.

Figure 5-8 shows the effect of UFA Content on FTIR of UHSC Mixtures. The broad band centered at ~3440-3450 $cm^{-1}$ is observed in all cases and is difficult to interpret in this case. Thus, this information is not discussed in detail in this study. There is little difference in the peaks centered at 475±3 $cm^{-1}$ irrespectively of 0 day or 14-day curing. This is also the case for the peak located around 1120±5 $cm^{-1}$. It is worth pointing that the wavenumber at around 475 and 1120 for U3 (45% UFA content) displayed the greatest peak among all samples.

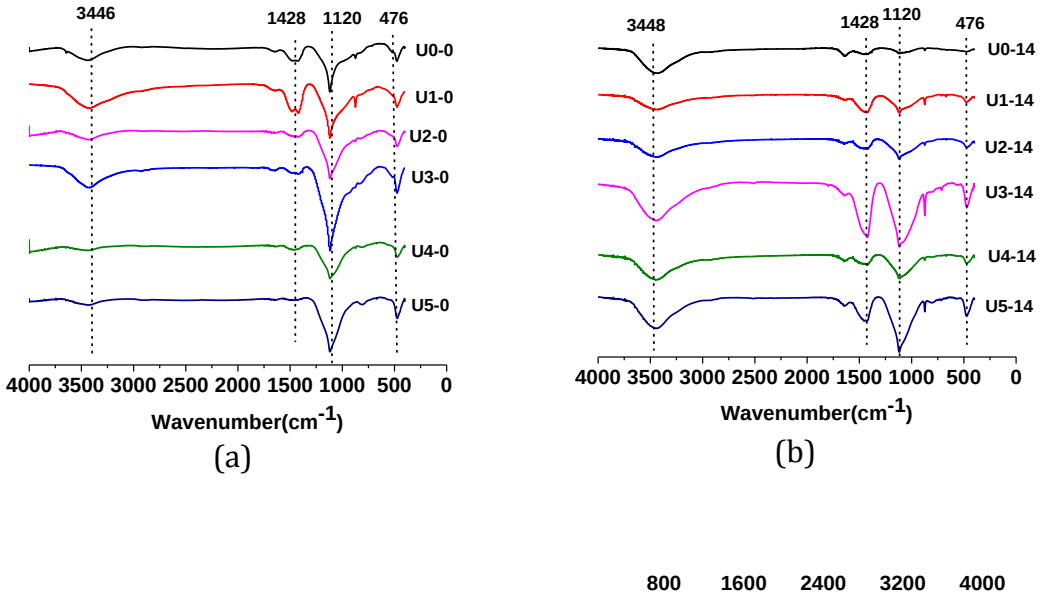


(a) (b)

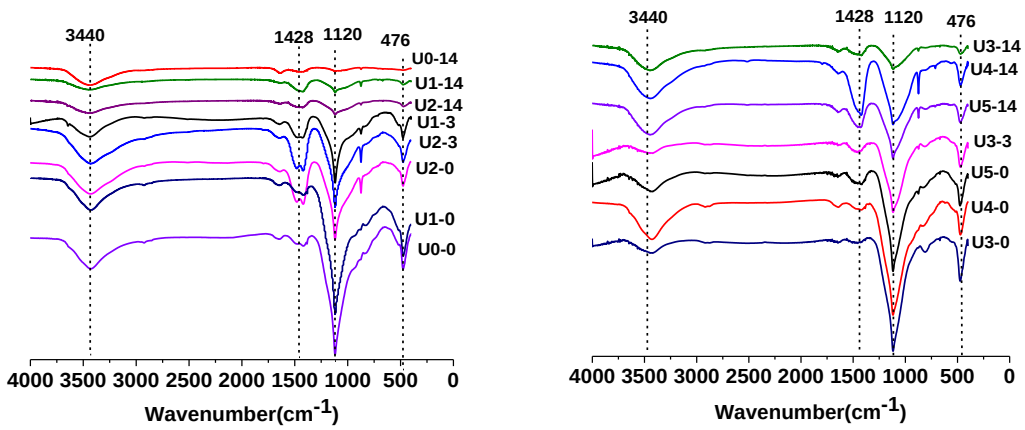


(c) (d)

**Figure 5-8.** Effect of UFA Content on FTIR of UHSC Mixtures.

### 5.3.8 SEM of UHSC Mixtures

Figure 5-9 (a and b) illustrates the SEM images of UFA, It is apparent that UFA particles are finer than the normal fly ash particles which explains why UFA exhibit a higher reactivity during hydration process. This is significantly finer than typical FA as demonstrated in figure.

Figure 5-9 (c and d) illustrates the SEM images of the surface and surface layers, Figure 5-9 (e and f) illustrates the SEM images of the surface and surface layers. The formation of calcite is detected on surface as well as internal layers near the surface of the specimens. The micrographs show that the samples with 15% UFA obtained a more compact and densified microstructure after 7 days of curing compared to that of samples with 30% and 45% UFA addition. This can be explained by considering the effect of fly ash on hydration process: fly ash can delay the hydration reactions which results in a more porous microstructure. After 28-day curing time, fewer pores were observed for all mixes irrespective of addition levels of UFA because of the continuous formation of hydration products making the binder matrix more compact. However, it is obvious that the sample with 15% UFA had a denser matrix in comparison to other two binders although the difference was not as prominent as that for 7-day curing. The SEM results correspond well with the compressive strengths after 7 days and 28 days of curing accordingly. The sample with 15% UFA showed the highest compressive strength among all samples with different UFA contents. It is also worth noting that after 7-day curing, there were more un-reacted

fly ash particles observed in the binder matrix compared to after 28-day of curing which again confirmed the delayed fly ash reaction evolution.

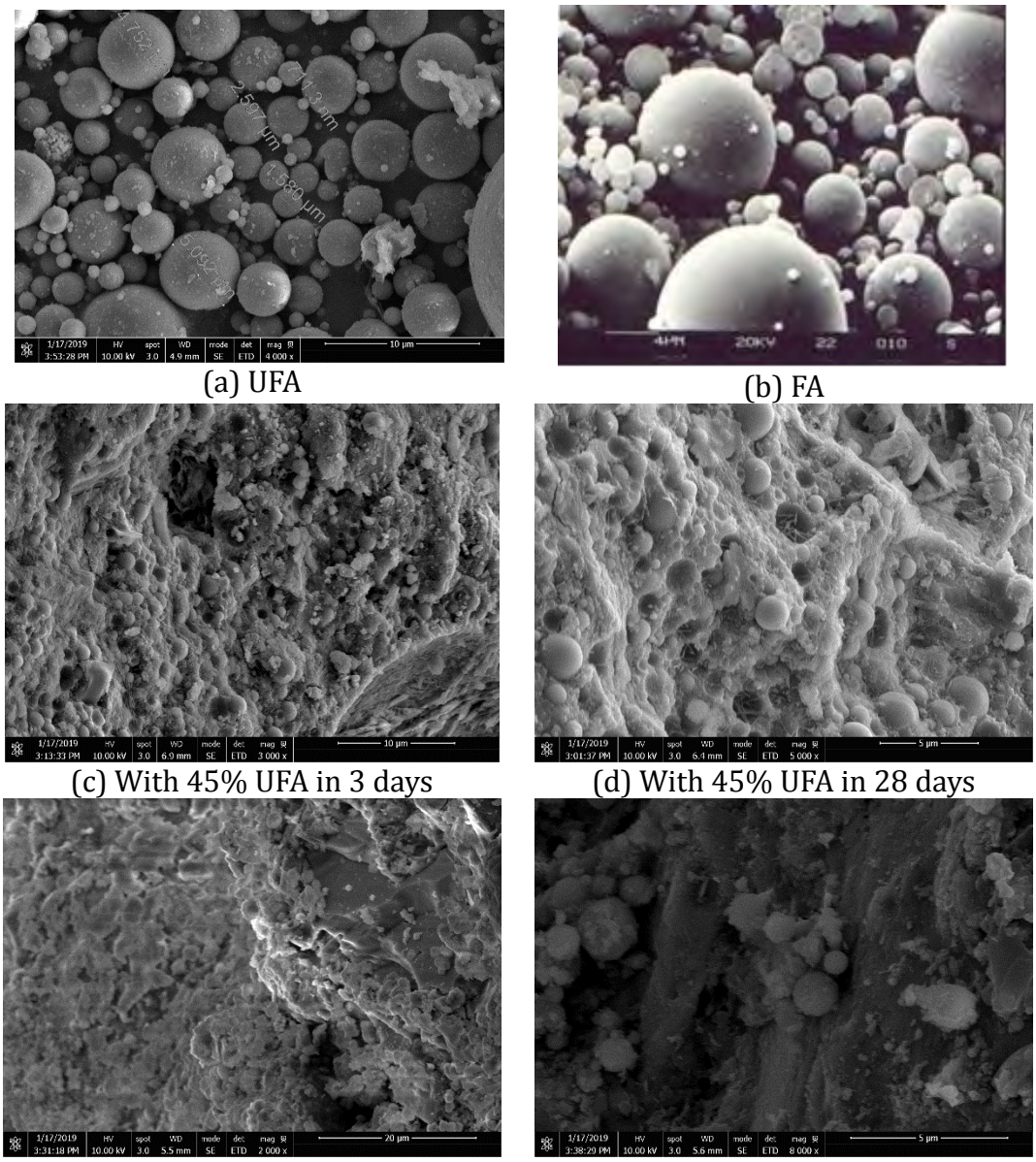

(a) UFA (b) FA

(c) With 45% UFA in 3 days (d) With 45% UFA in 28 days

(e) With 15% UFA in 3 days (f) With 15% UFA in 28 days

**Figure 5-9.** SEM images of UHSC mixtures specimen.

## 5.4 Conclusion

Based on the results from this study, the following conclusions can be drawn:

(1) Due to the accelerated hydration of cement by UFA the compressive and flexural strengths of UHSC containing UFA were significantly enhanced at early age up to 7 d. After

7 d, about 11% increase in strengths was obtained. The compressive and flexural strengths of UHSC samples with 30% UFA at 28 d were 28% and 29% higher than those of the reference sample, respectively. However, when 30% UFA was replaced, strengths decreased due to reduced workability and entrapment of air bubbles.

(2) The concrete containing 30 % UFA yielded the highest compressive strength at all ages. The early age compressive strength of HVFA concretes is also improved due to addition of 30% UFA. Most significant improvement of about 200% is observed in HVFA concrete containing 52% fly ash and 8% UFA at 3 days.

## 5.5 References


P. Richard, M. Cheyrezy, Reactive Powder Concrete with high ductility and 200-800 MPa compressive strength, Metha, PK (edition) Concrete Technology Past Present and Future, SP.

P. Richard, M. Cheyrezy, Composition of reactive powder concretes, Cement and concrete research, 25 (1995) 1501-1511.

L. Wu, N. Farzadnia, C. Shi, Z. Zhang, H. Wang, Autogenous shrinkage of high performance concrete: a review, Construction and Building Materials, 149 (2017) 62-75.

E.-H. Yang, Y. Yang, V.C. Li, Use of high volumes of fly ash to improve ECC mechanical properties and material greenness, ACI materials journal, 104 (2007) 620.

S.W. Supit, F.U. Shaikh, P.K. Sarker, Effect of ultrafine fly ash on mechanical properties of high volume fly ash mortar, Construction and building materials, 51 (2014) 278-286.

S.C.K. Bendapudi, P. Saha, Contribution of fly ash to the properties of mortar and concrete, Int J Earth Sci Eng, 4 (2011) 1017-1023.

F.F. Udoeyo, H. Inyang, D.T. Young, E.E. Oparadu, Potential of wood waste ash as an additive in concrete, Journal of materials in civil engineering, 18 (2006) 605-611.

L.J. Malvar, L.R. Lenke, Efficiency of fly ash in mitigating alkali-silica reaction based on chemical composition, ACI materials journal, 103 (2006) 319.

F.U. Shaikh, S.W. Supit, Compressive strength and durability properties of high volume fly ash (HVFA) concretes containing ultrafine fly ash (UFFA), Construction and building materials, 82 (2015) 192-205.

V. Aggarwal, S. Gupta, S. Sachdeva, Concrete durability through high volume fly ash concrete (HVFC) a literature review, International Journal of Engineering Science and Technology, 2 (2010) 4473-4477.

S. Barbhuiya, J. Gbagbo, M. Russell, P. Basheer, Properties of fly ash concrete modified with

S.J. Choi, S.S. Lee, P.J. Monteiro, Effect of fly ash fineness on temperature rise, setting, and strength development of mortar, Journal of Materials in Civil Engineering, 24 (2011) 499-505.

T. Nochaiya, W. Wongkeo, A. Chaipanich, Utilization of fly ash with silica fume and properties of Portland cement–fly ash–silica fume concrete, Fuel, 89 (2010) 768-774.

M. Gesoğlu, E. Güneyisi, E. Özbay, Properties of self-compacting concretes made with binary, ternary, and quaternary cementitious blends of fly ash, blast furnace slag, and silica fume, Construction & Building Materials, 23 (2009) 1847-1854.

A.F. Bingöl, İ. Tohumcu, Effects of different curing regimes on the compressive strength properties of self compacting concrete incorporating fly ash and silica fume, Materials & Design, 51 (2013) 12-18.

A.S. Cheng, Y.L. Huang, C.H. Huang, T. Yen, Effects of Fly Ash Particle Sizes on the Compressive Strength and Fracture Toughness of High Performance Concrete, Advanced Materials Research, 284-286 (2011) 5.

J.C. Wang, P.Y. Yan, Influence of initial casting temperature and dosage of fly ash on hydration heat evolution of concrete under adiabatic condition, Journal of Thermal Analysis & Calorimetry, 85 (2006) 755-760.

E.W. Washburn, Note on a method of determining the distribution of pore sizes in a porous material, Proceedings of the National Academy of Sciences, 7 (1921) 115-116.

M. Collepardi, Ordinary and long-term durability of reinforced concrete structures, Canmet/aci International Conference on Durability of Concrete, 2000.

A. Kwan, J. Chen, Adding fly ash microsphere to improve packing density, flowability and strength of cement paste, Powder technology, 234 (2013) 19-25.

H. Vikan, H. Justnes, Rheology of cementitious paste with silica fume or limestone, Cement & Concrete Research, 37 (2007) 1512-1517.

P. Lura, O.M. Jensen, K.V. Breugel, Autogenous shrinkage in high-performance cement paste:

B. Langan, K. Weng, M. Ward, Effect of silica fume and fly ash on heat of hydration of Portland cement, Cement and Concrete research, 32 (2002) 1045-1051.

C. Poon, L. Lam, Y. Wong, A study on high strength concrete prepared with large volumes of low calcium fly ash, Cement and Concrete Research, 30 (2000) 447-455.

I. Yoshitake, H. Wong, T. Ishida, A.Y. Nassif, Thermal stress of high volume fly-ash (HVFA) concrete made with limestone aggregate, Construction and Building Materials, 71 (2014) 216-225.

D.P. Bentz, Activation energies of high-volume fly ash ternary blends: hydration and setting, Cement and Concrete Composites, 53 (2014) 214-223.

# CHAPTER 6 MICROSTRUCTURE DEVELOPMENT OF ULTRA-HIGH PERFORMANCE CONCRETE AFTER LONG TERM EXPOSURE TO DIFFERENT CONDITIONS

Note: this chapter is based on the manuscript entitled "Carbonation and chloride ingression of ultra-high performance concrete (UHPC) after long-term exposure to different conditions", by Linmei Wu, Z Zhang and H Wang, submitted in journal of **Construction and Building Materials**.

**Abstract:** In UHPC mixes, the hydration degree of cement paste is low under the conditions of extreme-low W/B. The utilization of supplementary cementitious materials (SCMs) fly ash, slag and silica fume to partially replace the cement not only decreases un-hydrated cement but also improves this reaction at late age. In this study, carbonation and chloride ingression in UHPC after exposure to three different conditions: water, seawater, and outdoor for a duration of 1080 days, were studied to examine the effects of SCMs on the long-term durability. The results indicated that the optimal steel fiber content is 2% when considering flowability, mechanical properties, CH content and porosity. The UHPC specimens exposed to seawater at 1080 d also efficiently consumed CH. TGA/DTG results indicated that the CH was consumed with the formation of $CaCO_3$ (calcite) due to the carbonation effect at outdoor conditions whereas for the water and seawater immersion conditions, the CH was transformed into other reaction products including $Mg(OH)_2$ and ettringite. Moreover, seawater and water conditions led to a decrease of C-S-H content, which was particularly evident after 28 day. Fibre addition improved the performance of fly ash based UHPC, while it had little impact on the slag-based counterpart. Because of a denser microstructure evidenced by diffusion coefficient and porous characteristics, slag based samples. XRD and SEM analysis implies that for the sample exposed to outdoor and seawater condition based UHPC underwent less deterioration compared to fly ash (FA) containing UHPCs, more calcite was formed than the water condition. To compare the seawater and outdoor exposures, the surface layer of the sample immersed in seawater had some brucite and calcite as well as Friedel's salt and sulfoaluminates. However, for outdoor condition, the surface pH dropped due to the penetration of $CO_2$ into the binder neutralizing the pore solution. As time passed, more large-sized and smallsized pores formed in the seawater because of the expanding effect induced by ettringite, whereas for

outdoor environments, more medium-sized pores were produced due to the formation of calcites.

## 6.1 Introduction

The need to address the aging of today's infrastructures presents engineers and designers with a unique opportunity to redefine the methods and materials with which new civil projects are undertaken. Engineers must look to new innovations, considering resilience to natural hazards, efficiency in design, and sustainability of materials while cultivating new structural concepts. Ultra-high performance concrete (UHPC) is one such innovation(L. Wu, Farzadnia, Shi, Zhang, & Wang, 2017a). UHPC as a new class of cementitious materials that have exceptional mechanical and durability characteristics(C. Shi, Wang, Wu, & Wu, 2015a). Since last thirty years, ultra-high performance concrete (UHPC) has become more and more popular material in civil engineering. However, there was speculation that the long-term performance of UHPC may be negatively affected by the exposure to different conditions due to the abundant amount of unhydrated cementitious particles in the matrix(L. Wu et al., 2017a; Yingzi Yang, Yang, & Li, 2011). In the marina, water and outdoor environment, physical and chemical reaction were occasion on the UHPC structure.

Carbonation is known as a neutralizing process, a chemical reaction of $Ca(OH)_2$ and calcium–silicate–hydrate (C–S–H) with $CO_2$ to form $CaCO_3$ and water (G. Kim et al., 2016). Carbonation reduces the hydroxide concentration in the pore solution, destroying the passivity of the steel fiber (Taylor-Lange, Juenger, & Siegel, 2013).The traditional way of determining the depth of carbonation is to spray phenolphthalein indicator onto the surface of a freshly split concrete prism. Several reports have discussed the deterioration of carbonated concrete, proposing a formula to describe carbonation (C.-F. Chang & Chen, 2006; Papadakis, 2000; Saetta, Schrefler, & Vitaliani, 1993). In addition, corrosion of UHPC is of great concern because it is the most widespread cause of degradation in reinforced concrete structures. Initially, steel embedded in concrete is naturally protected from corrosion by the alkalinity of its pore solution (12.5 and higher) (Ahmad, 2003; Bertolini, Elsener, Pedeferri, Redaelli, & Polder, 2013; Poupard, L'hostis, Catinaud, & Petre-Lazar,

2006) . This high alkalinity enables the formation of a passive film on the rebar surface which prevents the development of an active corrosion process. However, this passive state can be inhibited by the destruction of the protective film due to the penetration of aggressive ions (chlorides) or an acidification of the environment in the vicinity of the rebar (carbonation). In the marine environment, steel corrosion is the natural result of the chloride penetration in concrete cover. Even UHPC are much more densified compared to normal concretes, there are still lots of small pores, and the corrosion may also happen in UHPC, but little research has been conducted about it.

For conventional concretes, a similar trend of durability is reported but at higher magnitudes especially when exposed to aggressive conditions (Nanukuttan et al., 2015; M. Santhanam & Otieno, 2016; Thomas, 2016). It is due in large part to the diffusion of external ions into the matrix which could adversely affect it because of the carbonation (in outdoor conditions) or chloride ingression (in seawater). On the contrary, several researches on the durability of UHPC demonstrated low permeability against diffusion of external agents into the matrix. In the study by Alkaysi et al. (A. Mo, El-Tawil, Liu, & Hansen, 2016), the air void content and the total charge pass were as low as 5.8% and 89 coulombs , respectively, for the UHPC specimens with 1.5% fiber. Yu et al. (R. Yu, P. Spiesz, & H. J. H. Brouwers, 2014) reported the porosity was about 3% for the limestone incorporated UHPC, which is in agreement with the study (Abbas, Soliman, & Nehdi, 2015). In another study by Tafraoui et al. (Tafraoui, Escadeillas, & Vidal, 2016a), the gas permeability of UHPC and chloride diffusion coefficient were reported to be lower than $1.5\times10^{-19}m^2$ and $1.7\times10^{-14}(m^2/s)$, respectively. The superior durability of UHPC is mostly related to the high packing density and low porosity induced by low water-to-binder ratio, and pozzolanic reactivity of supplementary cementitious materials incorporated in the matrix (C. Shi, Wu, Xiao et al., 2015b; D. Wang et al., 2015).

A lot of research has been carried out on UHPC property and microstructure, but most of them focused on the short term performances with just normal curing conditions. However, very limited has been reported in the literature about the long-term performance of the UHPC, especially when the UHPC specimens were subjected to different exposure conditions (water, seawater and outdoor). In this chapter, long-term behavior of ultra-high performance concrete maintained in water, seawater, and outdoor conditions for up to 1080 days was investigated. Outdoor condition imitates the natural

environment which mainly focused on the nature carbonation of long term. In comparison, seawater condition simulates the marine environment, focusing on the relationship between corrosion depth and the properties of UHPCs.

## 6.2 Experimental program

### 6.2.1 Raw materials

Portland cement P.I 42.5, complying with the Chinese Standards GB175-2007 was used. Table 6-1 summarizes the physical properties of the cement. Fly ash and ground furnace slag were used to partially replace cement in the concrete mixture, with the specific surface area of 427 $m^2$/kg and 446 $m^2$/kg, respectively. Silica fume with 63% particle size of 0.1-0.5 μm and specific surface area of 18500 $m^2$/kg was used. Table 6-2 shows the chemical properties of cement, fly ash and slag. Natural river sand with a fineness modulus of 3.0 was used. Particles with size greater than 2.36 mm were removed by sieving. The straight steel fiber with diameter of 0.2 mm and length of 13 mm was used. A polycarboxylene based super plasticizer (SP) was used. Its water-reducing capacity was greater than 30%. The dosage of SP in the all mixture was 2% by the mass of cementitious materials.

**Table 6-1:** Physical properties of Portland cement P.I 42.5.

| Density ($kg/m^3$) | 80 μm-residue on sieve (%) | Specific surface area ($m^2$/kg) | Setting time(h) | | Flexural Strength (MPa) | | Compressive Strength (MPa) | |
|---|---|---|---|---|---|---|---|---|
| | | | Initial | Final | 3d | 28d | 3d | 28d |
| 3.15 | 0.3 | 380 | 2.5 | 3.4 | 6.4 | 9.0 | 33.0 | 60.0 |

**Table 6-2:** Chemical composition of cementitious materials (weight %), LOI is loss on ignition.

| Chemical composition | $SiO_2$ | $Al_2O_3$ | $Fe_2O_3$ | CaO | MgO | $K_2O$ | $Na_2O$ | $SO_3$ | LOI |
|---|---|---|---|---|---|---|---|---|---|
| Cement | 25.26 | 6.38 | 4.05 | 64.67 | 2.68 | - | - | 0.94 | 0.9 |
| Silica fume | 90.82 | 1.03 | 1.50 | 0.45 | 0.83 | 0.86 | 0.17 | - | 4.34 |
| Slag | 33.00 | 13.91 | 0.82 | 39.11 | 10.04 | 1.61 | 0.26 | 0.92 | 0.33 |
| Fly ash | 54.29 | 32.55 | 5.53 | 1.34 | 2.56 | 1.34 | 0.49 | 0.35 | 1.55 |

### 6.2.2 Mixture proportions

The mixture proportions of UHPCs were designed based on a previous study (C. Shi, Wang et al., 2015a). In brief, the w/b of 0.18 and binder-to-aggregate ratio of 1:1.1 were selected and kept constant throughout the study. The SP was used at 2% by mass ratio of the binder. Steel fiber contents were 0, 1%, 2%, and 3% of the concrete by volume. Table 6-3 shows the mixture proportions of UHPCs based on mass of ingredients.

**Table 6-3:** Mixture proportions of UHPCs.

| No. | w/b | Mass of ingredients (kg/m$^3$) | | | | | | | |
|---|---|---|---|---|---|---|---|---|---|
| | | Water | Cement | Silica fume | Slag | Fly Ash | SP* | Sand | Fiber |
| K0 | 0.18 | 164 | 550 | 200 | 250 | 0 | 20 | 1100 | 0.0 |
| K1 | 0.18 | 164 | 550 | 200 | 250 | 0 | 20 | 1100 | 78.5 |
| K2 | 0.18 | 164 | 550 | 200 | 250 | 0 | 20 | 1100 | 157.0 |
| K3 | 0.18 | 164 | 550 | 200 | 250 | 0 | 20 | 1100 | 235.5 |
| F0 | 0.18 | 164 | 550 | 200 | 0 | 250 | 20 | 1100 | 0.0 |
| F1 | 0.18 | 164 | 550 | 200 | 0 | 250 | 20 | 1100 | 78.5 |
| F2 | 0.18 | 164 | 550 | 200 | 0 | 250 | 20 | 1100 | 157.0 |
| F3 | 0.18 | 164 | 550 | 200 | 0 | 250 | 20 | 1100 | 235.5 |

*SP means the total mass of liquid-based SP.

### 6.2.3 Mixing procedure and specimen preparation

In the mixing procedure, dry powders, including cement, silica fume, slag or fly ash, and natural river sand, were first mixed for 3 min in a high-speed drum mixer. Then, water and superplasticizer were added and mixed for 6 min at low speed. Afterwards, steel fibers were added through passing a sieve with the size of 5 mm and mixed for another 6 min until the mixtures were uniformly distributed. UHPC mixtures were then cast into molds and vibrated to consolidate the mixtures. The specimens were demolded after one 1 day and then cured in water at the temperature of 20±3°C for 28 days. The properties of hardened concrete such as compressive strength and initial length were measured at 28 d before exposure to different conditions. Figure 6-1 illustrates the mixing and specimen preparation procedure.

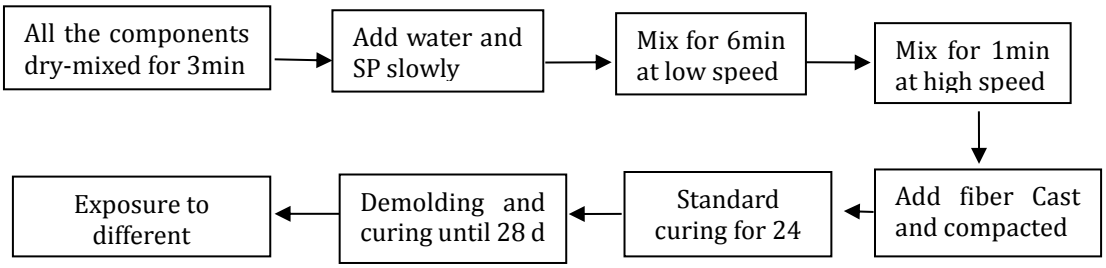


**Figure 6-1.** The mixing and preparation procedure of UHPC specimens.

The UHPC is a very dense and impermeable composite and previous studies have shown that the ingression of chloride into the matrix and the carbonation depth is minimal compared to normal strength concrete. Hence, to explain the long-term performance of the specimens, samples were taken from a 5 mm surface layer by slicer (Figure 6-2) with the maximum exposure duration (esp. in outdoor conditions).

**Figure 6-2.** Slicer.

### 6.2.4 Exposure conditions

UHPC specimens were exposed to three conditions for a duration of 1080 days as shown below:

(1) **Outdoor.** Specimens were exposed to the natural outdoor conditions in Changsha. Specimens were placed facing south at a 45° inclination. Figure 6-3 illustrates mean values of the temperature and humidity in Changsha, China. The curing temperature and humidity changed according to the local weather with a

minimum temperature of -1°C and relative humidity of 76% and a maximum temperature of 33°C and relative humidity of 86% during the exposure period.

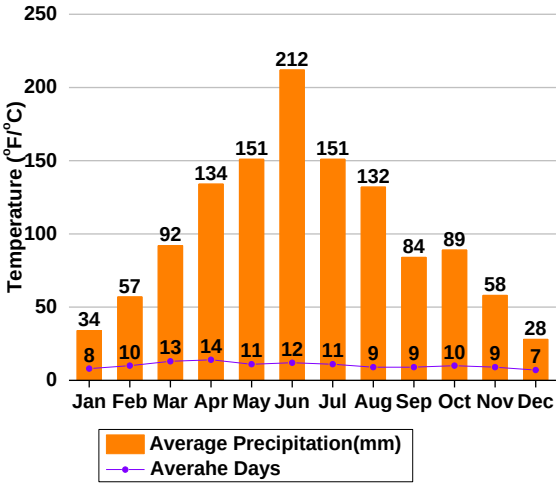


**Figure 6-3.** Mean values of temperature and humidity change of Changsha during the exposure time.

(2) **Tap water.** The UHPC specimens were immersed in the normal tap water, no lime was used.

(3) **Seawater.** According to the composition of a natural seawater in the Gulf of China (NS) and the artificial seawater as specified by ASTM D-14 (AS1) (as shown in Table 6-4), an artificial seawater (AS2) was prepared for the use of this study. Given the long-time process of corrosion, the concentration of AS2 was elevated to accelerate the corrosion process.

After the curing scheme, the specimens were exposed to the three conditions from day zero (0), which denotes the first day of exposure. Water and seawater in storage tanks were refreshed every three weeks.

**Table 6-4:** The compositions of the natural seawater in the Gulf of China (NS), the ASTM D-14 specified artificial seawater (AS1) and the artificial seawater used in this study (AS2) (g/L).

| Chemical | NaCl | $Na_2SO_4$ | $MgCl_2$ | $MgCl_2{\cdot}6H_2O$ | $MgSO_4{\cdot}7H_2O$ | $CaSO_4{\cdot}2H_2O$ | $CaC1_2$ | $CaCO_3$ | KCl |
|---|---|---|---|---|---|---|---|---|---|
| NS | 21.0 | - | 2.54 | - | 1.54 | 2.43 | - | 0.1 | - |
| AS1 | 24.5 | 4.1 | - | 2.54 | - | - | 1.2 | - | 0.1 |
| AS2 | 25.0 | 10.0 | 12.7 | 7 | - | - | - | - | 0.1 |

### 6.2.5 Testing methods

#### 6.2.5.1 **Flowability**

The fresh UHPC mixtures were filled into a conical mold in the form of a frustum. Then it was automatically vibrated for 25 times on a flow table. Two diameters perpendicular to each other were determined. The mean value of the two measurements was recorded as the mini slump flow.

#### 6.2.5.2 **Test of depth of colorless region using phenolphthalein indicator**

The test specimens were taken out of the outdoor and seawater exposure after 1080 days and split in a tensile splitting test. After splitting the concrete specimens, the freshly split surface was cleaned and sprayed with a phenolphthalein pH indicator. The indicator used was a phenolphthalein 1% ethanol solution with 1 g phenolphthalein and 90 ml 95.0 V/V% ethanol diluted in water to 100 ml (Fukushima, Yoshizaki, Tomosawa, & Takahashi, 1998). Carbonation depth is assessed using a solution of phenolphthalein indicator that appears pink in contact with alkaline concrete with pH values in excess of 9 and colourless at lower levels of pH. The test is most commonly carried out by spraying the indicator on freshly exposed surfaces of concrete broken from the structure or on split cores. Hence there may be corrosion in the zone ahead of the front defined by the indicator. In general the change in pH occurs in this zone which is only a few millimetres ahead and the phenolphthalein method provides a good indication of the location of the depassivation front, the test is covered by BS EN 14630(B. EN, 2006).

#### 6.2.5.3 **Thermogravimetric analysis (TGA)**

TGA was performed using a Netzsch STA 409 PC equipment to qualitatively determine the changes of chemical phases in specimens in different conditions at exposure ages of 60 and 1080 days. The tested powder samples of selected mixtures were weighed (10 mg) and heated from room temperature to 1000°C in a nitrogen atmosphere at a heating rate of 10°C/min.

#### 6.2.5.4 **Scanning electron microscopy (SEM)**

Scanning electron microscopy (SEM) was employed to study the microstructure of UHPC. SEM samples were taken from freshly crushed specimens, cut into small fragments and soaked in ethanol prior to testing, to stop the hydration of cement. Subsequently, the samples were dried at 65°C and sputtered with gold before observation using ION SPUTTER E-1045.

#### 6.2.5.5 **Powder X-ray diffraction analytical methods**

The preparation of samples for XRD was the same as those prepared for TGA. The prepared powders were analyzed by using Philips X-ray diffractometer with CuKα radiation. The samples were step-scanned from 10 to 70° (2θ) at a rate of 5°/min.

#### 6.2.5.6 **Pore structure measurement**

Mercury intrusion porosimetry (MIP) is considered as the most commonly used pore structure characterization technique for cement-based materials. This technique is based on the principle that mercury, a typical non-wetting liquid, can only intrude a porous material if a certain pressure is applied on the measured samples. The samples were broken into 3.5-5.0 mm pieces and soaked in acetone to stop further hydration. Then they were dried at 60°C in oven for 24 h before examination. The experiments were carried out under low pressure of 0.2758 MPa and high pressure of 413.7 MPa, respectively. A glass tube with the specimen and mercury in was subsequently placed in a low and high pressure analysis port. Full-scan auto mode was selected with contacted angle and surface tension of 140$^{o}$ and 480 mN/m respectively. The intrusion mercury volume was recorded at each pressure point.

#### 6.2.5.7 **Nitrogen adsorption and desorption (NAD) analysis**

NAD analyses were conducted with the gas volumetric analyzer Quantachrome Instruments QuadraSorb Station 1. The ground cement paste powders were preheated at 60℃ for 24 h under vacuum condition to eliminate the influence of free water.

## 6.3 Results and discussion

### 6.3.1 Effect of steel fiber content on flowability of fresh UHPC

Figure 6-4 shows the flowability of the mixtures with different contents of fibers. It is observed that, for K0 and F0 mixtures without steel fibers, the slump flowability was higher than 200 mm. With the incorporation of 3% steel fiber, the slump flowability decreased to 140 and 150 mm, respectively. Moreover, the slump flowability of fly ash containing mixture is higher than slag containing mixture, which is due to the ball bearing effect of fly ash (NetAnswer).

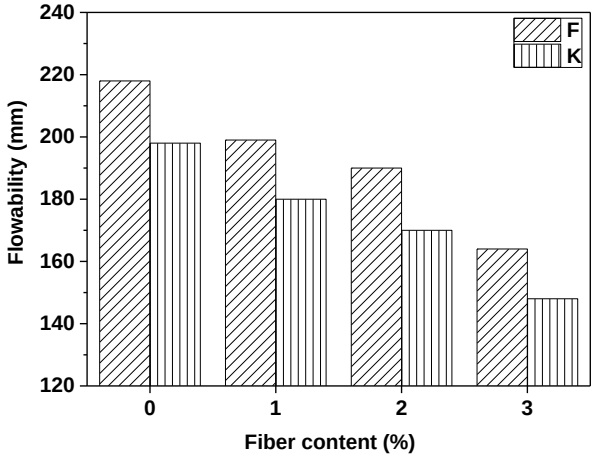


**Figure 6-4.** Effect of steel fiber contents on flowability of slag containing (K) and fly ash containing (F) UHPC mixtures.

### 6.3.2 Carbonation degree of UHPC

Figure 6-5 presents the mean depth of the region of colorless phenolphthalein "*Xp*". In the noncarbonated part of the specimen, where the UHPC porous solution was still highly alkaline, a purple-red color was obtained. In the carbonated part of the specimen exposed to seawater where the alkalinity of concrete is reduced, no coloration occurred. The average depth "*Xp*" of the colorless phenolphthalein region was measured from three points, perpendicular to the two edges of the split face, both immediately after spraying the indicator

For the sample in seawater condition, almost no uncolored area was measured. After immersion in outdoor condition for 1080 days, the UHPC sample displayed a depth at about 0.1mm due to carbonation (Figure 6-5). These two different results indicate that for outdoor immersion, some $CO^{2-}$ penetrated the binder matrix and neutralized the pH of the pore systems by depleting the $OH^-$. In contrast, in seawater conditions, mainly it's the ion exchange that dominates the decalcification reactions. To be specific, $Ca^{2+}$ was replaced by $Mg^{2+}$ and reacts with $SO_4^{2-}$ to form ettringite leading to a huge consumption of Ca rather than $OH^-$.

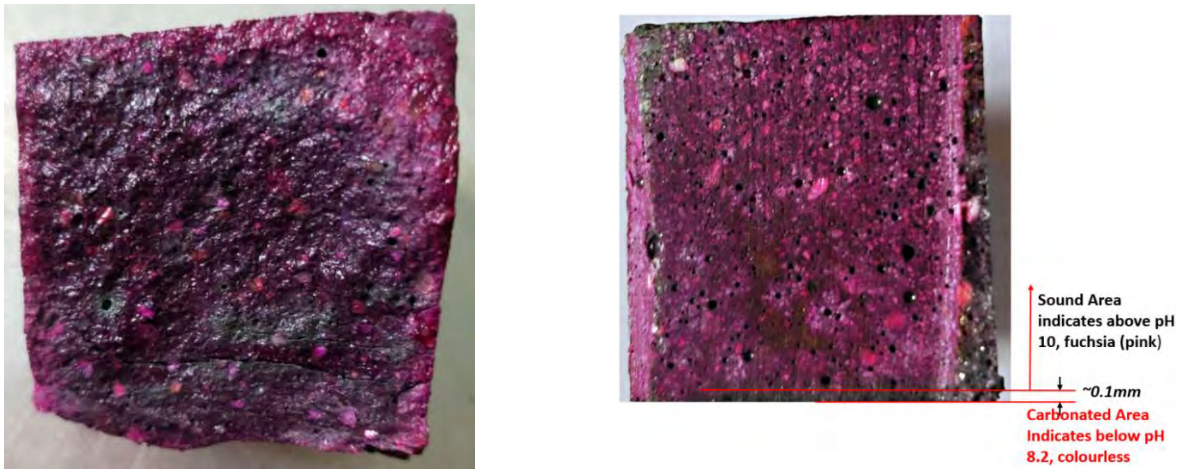


(a) Seawater 1080d (b) Outdoors 1080d

**Figure 6-5.** Sectional colour image of UHPCs sprayed with a phenolphthalein solution.

### 6.3.3 TG/DTG analyses

Figure 6-6 shows the TG/DTG curves of the samples immersed in different environments for 28 days. The effects of various environments on the binder phases of Fly-ash based F0 UHPC is presented. In outdoors, more $Ca(OH)_2$ and $CaCO_3$ left. (The endothermal peaks at the four temperature ranges, from low to high temperature in order, are due to the dehydration of C-S-H and ettringite as well as evaporable water in pore systems, dehydroxylation of CH, and decomposition of $CaCO_3$, respectively.) The hydration of C-S-H, ettringite and AFm phases are linked with the peaks up to 400°C, the second peak belong to the dehydration of calcium hydroxide ranging between 450°C to 500°C and the third one between 500 °C to 800 °C is assigned to the decarbonation of calcium carbonate (Alarcon-Ruiz, Platret, Massieu, & Ehrlacher, 2005). For the first peak, it was obvious that

the samples subjected to outdoor condition obtained a higher peak with the intensity much stronger than the other two conditions. In DTG curve, the peak is almost 0.35 (%/min) whereas the peaks for the other two are only at about 0.18 (%/min). This indicates that the sample in the outdoor condition had much more C-S-H and other phases and most hydrated phases disappeared for the sample exposed to water and seawater. The largest peak assigned to calcium hydroxide and the least one belonging to the decomposition of calcium carbonates also imply that the samples exposed to outdoor condition experienced fewer changes in phases compared to other two conditions.

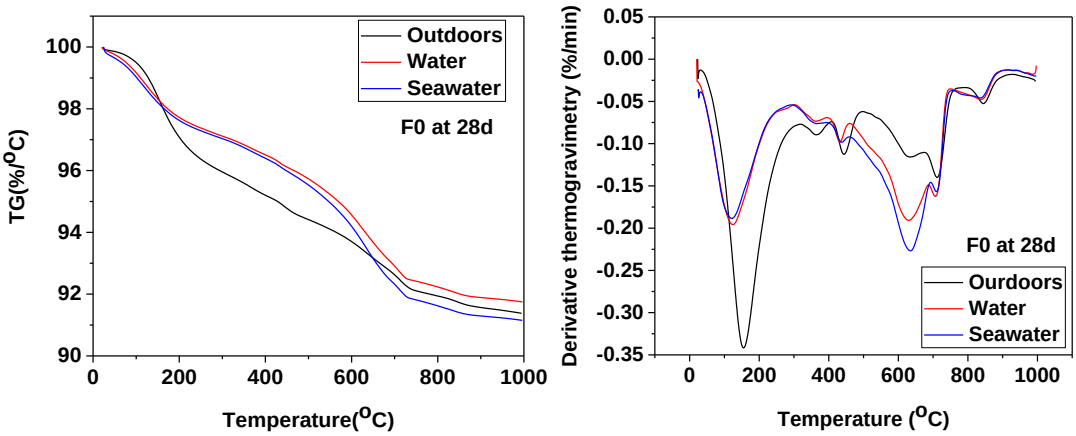


**Figure 6-6.** TG and DTG curves of UHPCs exposure to different environment after 28 d.

Figure 6-7 shows the TG and DTG curves phase change of outdoors, water and seawater at 360 and 1080 d .The hydration products in hardened concrete are calcium silicate hydrate (C-S-H) with endothermal peak at approximately 80-90°C, ettringite with endothermal peak around 130°C, calcium hydroxide (CH) with an endothermal peak in the range of 450-550°C, and calcium carbonate with endothermal peak in the range of 600-700°C. The peak assigned to the decarbonation of carbonates for the sample in the outdoors was more significant than the other two peaks indicating that the samples had larger amount of calcite. This also is in line with the obviously smaller peak which belongs to the dehydration of calcium hydroxide at about 460-470 °C. This can be explained by considering the fact that due to the carbonation effect induced by $CO_2$, some calcium hydroxides were transformed to calcium carbonates. The greatest mass loss at about 100 °C is associated with the evaporation of free water and dehydration of loosely bonded water in C-S-H gel. The samples immersed in seawater underwent the largest mass loss,

implying that water is less tightly bonded compared to the other two conditions. Therefore, the exposure towards seawater led to a great loss of C-S-H gel which can be attributed to the reaction between C-S-H gel and different ions in seawater, especially sulfates. It is already known that sulfate can react with $Ca^{2+}$ leading to the dissolution of CH and decalcification of C-S-H. This is also in consistent with the small peak, corresponding to the dehydroxylation of CH for seawater since some CH reacts with various ion species in the seawater, such as $Mg^{2+}$ and sulfates, as in the following equation:

$$Ca(OH)_2\ (s) \rightarrow Ca^{2+}\ (aq) + 2OH^-\ (aq)$$

$$Mg^{2+} + SO_4^{2-} + Ca^{2+}\ (aq) + 2OH^-\ (aq)\ CaO{\cdot}Al_2O_3{\cdot}CaSO_4{\cdot}18H_2O$$

$$\rightarrow Mg(OH)_2\ (Brucite) + 3CaO{\cdot}Al_2O_3{\cdot}3CaSO_4{\cdot}32H_2O\ (Ettringite)$$

$$MgSO_4\ (aq) + Ca(OH)_2(aq) + CaO{\cdot}Al_2O_3{\cdot}CaSO_4{\cdot}18H_2O$$

$$\rightarrow Mg(OH)_2(Brucite) + 3CaO{\cdot}Al_2O_3{\cdot}3CaSO_4{\cdot}32H_2O(Ettringite) \qquad (6\text{-}1)$$

Compared to the other conditions, the sample in water had more CH and less calcite with more tightly bonded water. This implies that the water immersion condition is the least aggressive environment compared to outdoor and seawater.

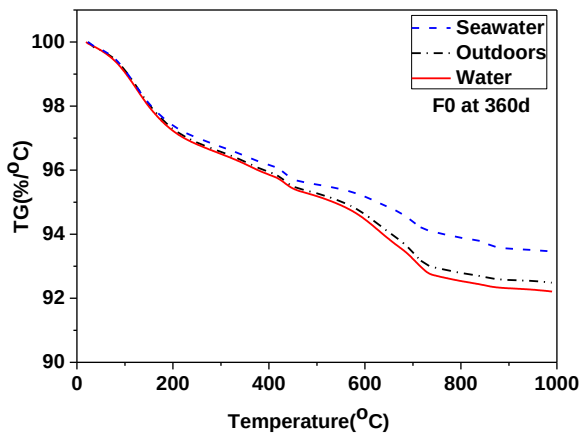


(a) TGA of F0 for 360d

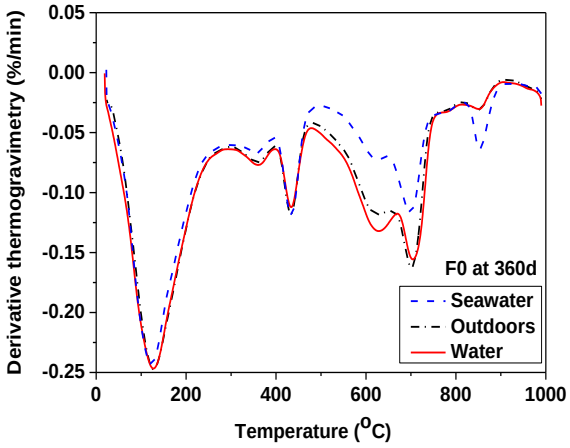


(b) DTG of F0 for 360d

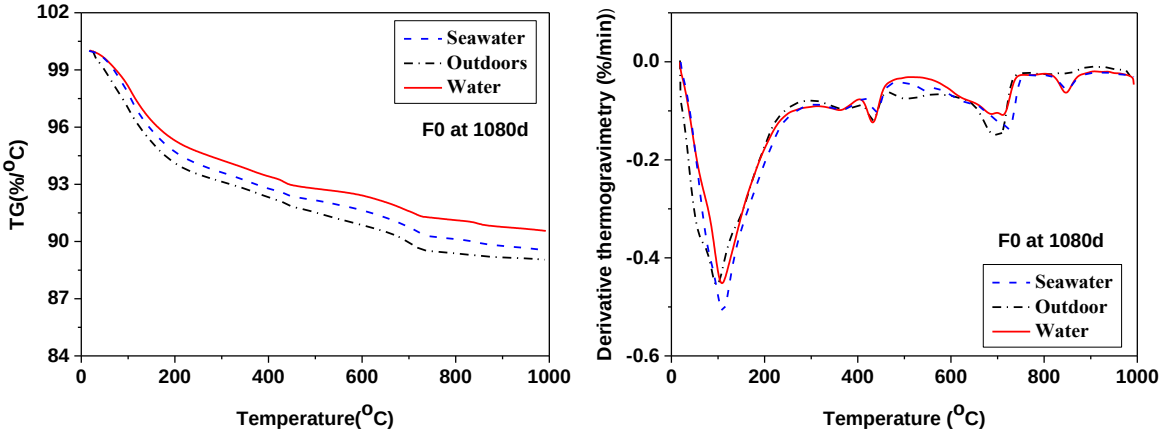


(C)TGA of F0 for 1080d (d) DTG of F0 for 1080d

**Figure 6-7.** TGA curves of UHPCs after exposure to different conditions after 360d and 1080d.

Figure 6-8 shows the effects of steel fiber contents on TG and DTG curves of UHSC exposed to outdoors and seawater after 90 d and 1080d 28 d. The peaks at around 730 °C indicates the decarbonation of calcium carbonates, i.e. calcite. Thus, the larger mass loss for Fly ash-based samples (F0 and F2) indicates a larger amount of calcite which is attributed to more ingress of $CO_2$ into the sample. This is due to a higher porosity and greater pore diameter of the sample. With easier access into the porous systems, more carbonates penetrated the binder matrix and thus leading to higher amount of calcite. $CO_2$ also resulted in the decalcification from C-S-H gel and more water from C-S-H gel was released out and less tightly bounded. Thus, it is seen that the peak at around 120 °C, assigned to the amount of evaporable water in the binder system was also larger.

Compared to the samples without fiber additions, the samples with fibres (F2, K2) suffered less from both the mass loss due to water evaporation and decarbonation of calcite as well as the dehydroxylation of CH. This is contributed to the improved porous system where less $CO_2$ were present in the porous networks, and thus less calcite and free bonded water were formed.

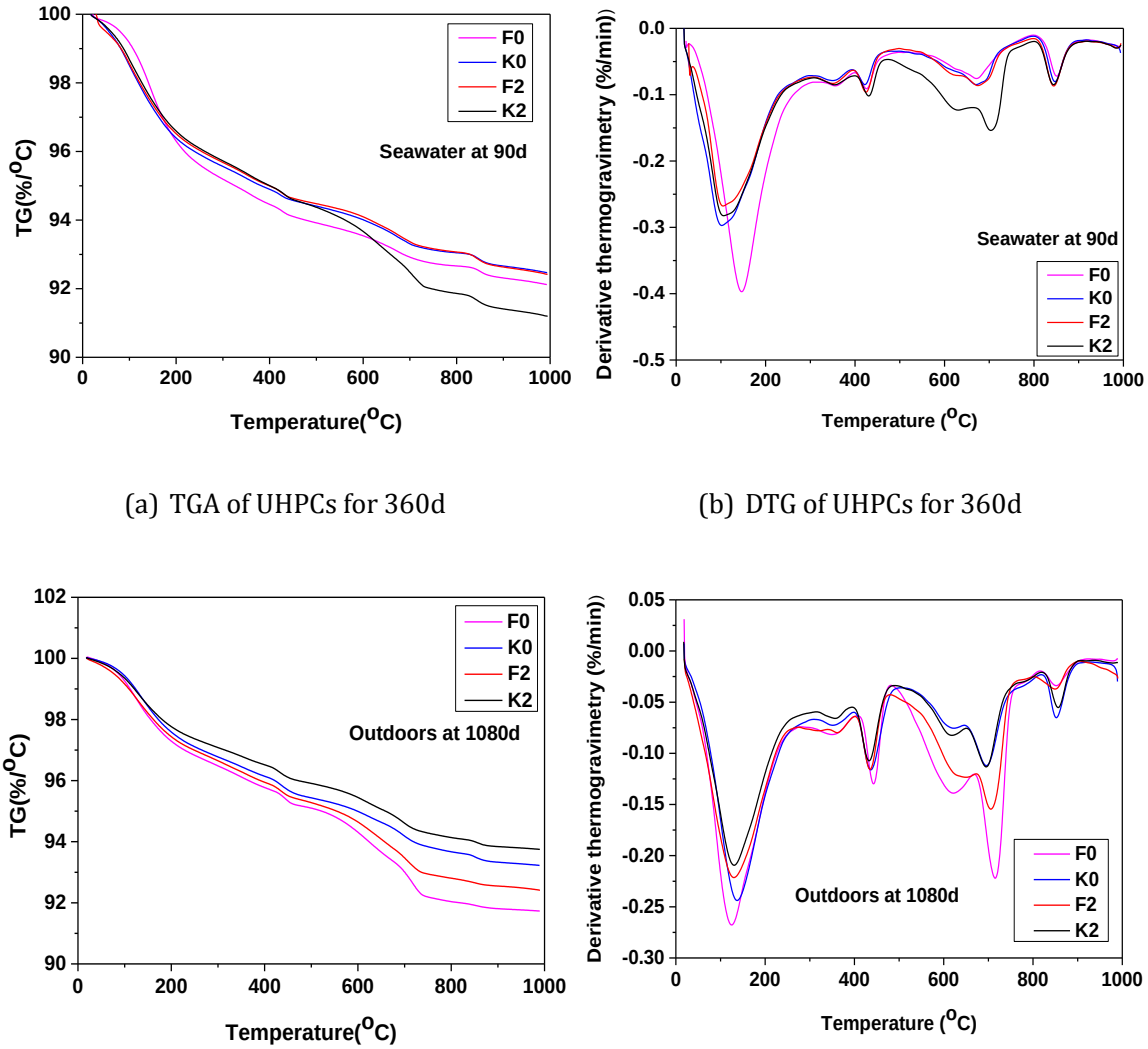


(a) TGA of UHPCs for 360d

(b) DTG of UHPCs for 360d

(c) TGA of UHPCs for 1080d

(d) DTG of UHPCs for 1080d

**Figure 6-8.** TGA curves of UHPCs with steel fiber after exposure to different conditions after 90d and 1080d.

Figure 6-9 shows TGA curves and the contents of CH and $CaCO_3$ for slag containing and fly ash containing specimens without fibers. As can be seen, the decomposition peaks of calcium hydroxide and $CaCO_3$ were detected at ~180 ℃ and ~780°C ℃, respectively. In general, the results show low amount of CH in the surface layers, which can confirm either consumption of CH by slag and fly ash through pozzolanic reactions [9-10] or another reaction mechanism such as leach-out. As the specimens subjected to the TG analysis contained no fibers, the conventional penetration mechanism due to surface corrosion of fibers is considered as least probable. In outdoor conditions, more carbonates were formed with the greatest amount of CH left as the CH can only be assumed by $CO_2$. However,

for the exposure condition in seawater and water, the leaching effect of CH in both conditions and the reactions between different ions in the seawater and CH led to the greatest depletion of CH. The largest mass loss around 100℃ indicates that the outdoor samples had the largest amount of evaporable water indicating that C-S-H gel in the system was preserved better compared to other circumstances.

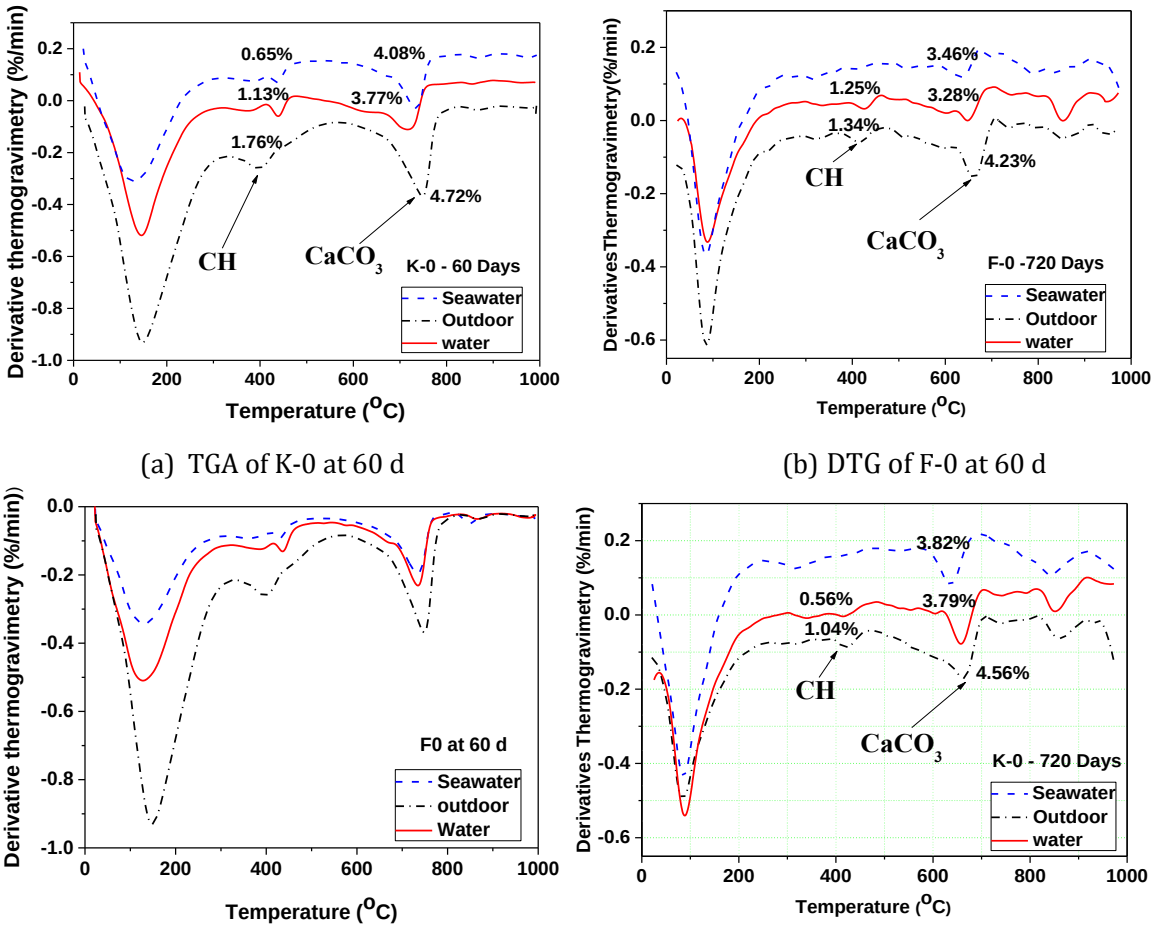


(a) TGA of K-0 at 60 d

(b) DTG of F-0 at 60 d

(c) TGA of K-0 at 720 d

(d) DTG of F-0 at 720 d

**Figure 6-9.** TGA curves of UHPCs after exposure to different conditions.

## 6.3.4 CH content

Figure 6-10 shows the CH content of UHPC samples at different ages. The samples exposed to outdoor condition had the greatest amount of CH left, indicating that carbonation effect has less negative impact on the consumption of CH compared to the seawater and water condition. This can be explained by considering that for seawater and water conditions, $Mg^{2+}$, $SO_4^{2-}$ can react with $OH^-$ and $Ca^{2+}$ respectively, leading to the formation of brucite, i.e. $Mg(OH)_2$ and ettringite.

For the sample with fibre addition K2, the CH content after 1080 days of exposure was larger compared to the corresponding sample K0 without fibre. This was apparent for K0 and K2 whereas not the case for F0 and F2. Moreover, it can be seen from the comparison between. K2 and K0 have lower porosity and smaller pore diameter compared to F2 and F0. a much higher reaction consumption rate towards CH compared to $CO_2$.

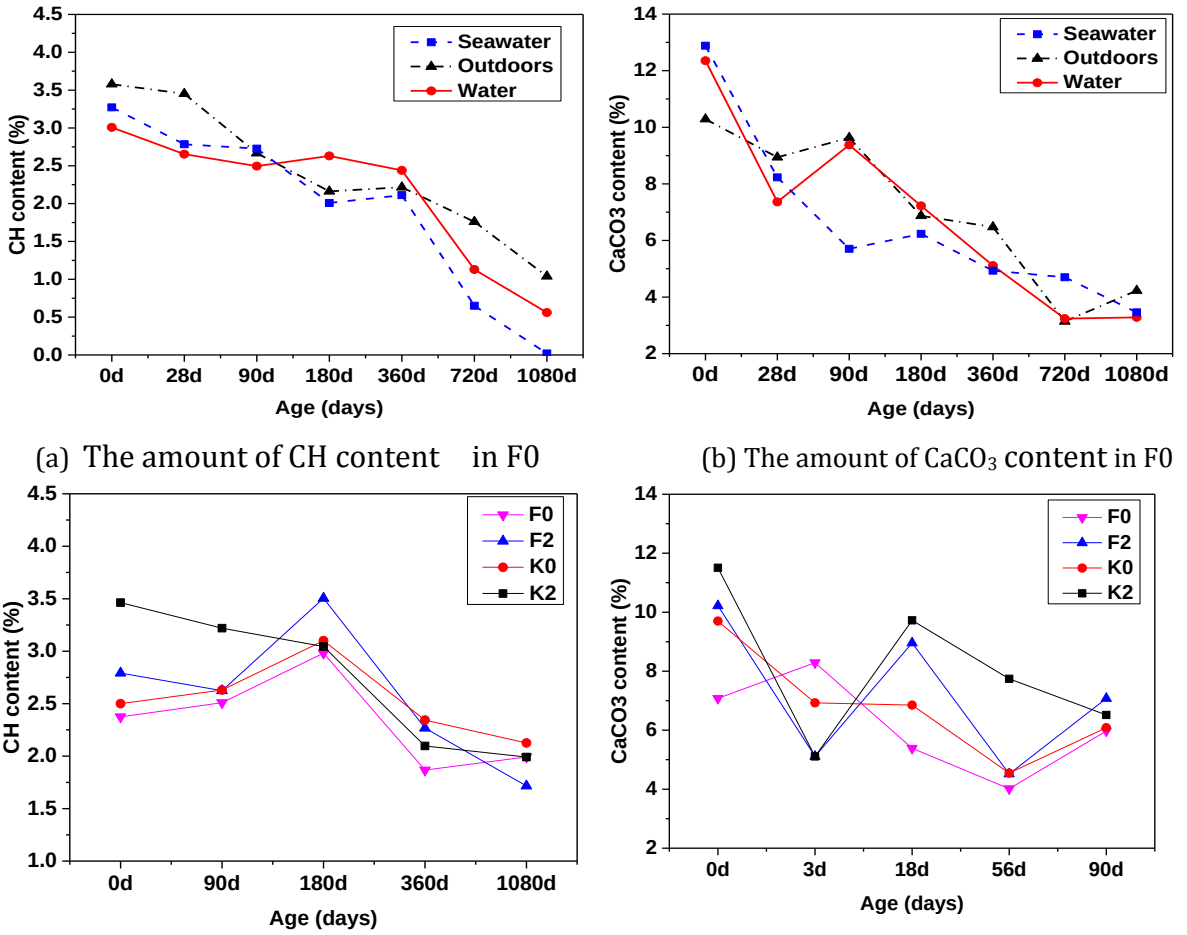


(a) The amount of CH content in F0

(b) The amount of $CaCO_3$ content in F0

(c) The amount of CH content in seawater

(d) The amount of $CaCO_3$ content in seawater

**Figure 6-10.** Amount of CH formed in UHPC samples with age.

### 6.3.5 Analysis of XRDA test results

The carbonation can be also through conventional carbonation as long-term exposure may also cause surface corrosion (as specially observed in seawater specimens but also probable in high humidity of outdoor conditions in Changsha), which can provide pathway for infiltration of $CO_2$. The discussion is revised accordingly and both hypothesis; leach out and conventional carbonation are discussed. Besides, the details of the TGA test is added to the revised manuscript to solidify the judgment. Furthermore, in parallel with TGA

analysis, the XRD test was conducted on the same powder sample previously, albeit, authors did not used in the previously submitted manuscript to avoid redundancy. In the revised manuscript the XRD patterns are also added to support the results.

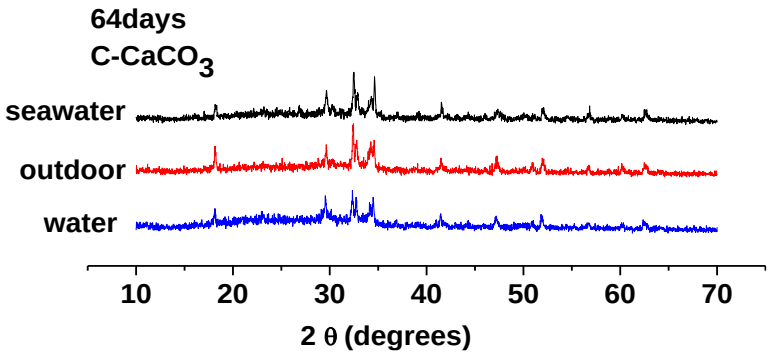


(a) XRD patterns of F-0 after exposure to different conditions at 64 d

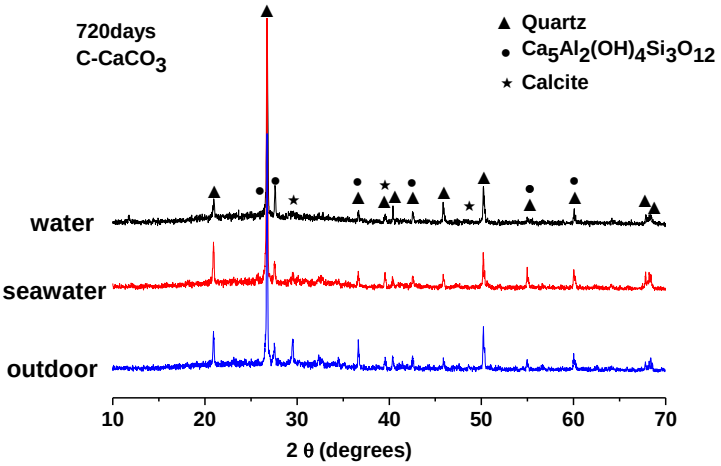


(b) XRD patterns of F-0 after exposure to different conditions at 720d

**Figure 6-11.** XRD patterns of F-0 after exposure to different conditions.

Figure 6-11 is XRD patterns of F-0 after exposure to different condition. The results reveal that as the exposure prolongs to 1080 days, the amount of CH is decreased in all specimens, though, at different rates, which is along with increase in the content of $CaCO_3$. The $CaCO_3$ content is the highest in the specimens exposed to the outdoor condition followed by those immersed in seawater. The XRD patterns from the surface layers also confirm the relative higher contents of $CaCO_3$ in the specimens exposed to the seawater and outdoor conditions.

## 6.3.6 Pore structure characteristics

### 6.3.6.1 Mercury intrusion porosimetry (MIP) results analysis

Table 6-5 is the MIP results of UHPC. Figure 6-12 is the Effects of different environment on porosity and pore size distribution of UHPCs. For the samples immersed in the seawater for different durations, the pore volume changed over exposure period, which was obvious after 180 days. The 28-day and 90-day results indicate that most of the pores are in a range between 20-100 nm, whereas after 180 days the dimeter of the pores increased significantly. After 1080-day of exposure, the diameter of many pores was greater than 100 μm. It is also noteworthy that the volume of small-sized pores (< 20 nm) also increased at the same time indicating that some medium-sized pores were filled by the reaction products and thus the pore size decreased accordingly. The rapid changes in the pore sizes with an increase in the volume of both large pores (>100 μm) and small pores (<50 nm) suggests that there was a considerable accumulation of the amount of reaction products, such as ettringite, in the porous networks after 180 days of immersion. This is also consistent with the SEM results in which ettringite was observed after 1080 days.

When the F0 samples immersed in the three conditions, it is obvious that when exposed to the outdoor environment, most of the pores had a dimeter between 20 and 100 nm with the volume up to 67.5 % and the most probable diameter at 22.8 nm as shown in Figure 6-12. However, there were more small-sized pores (<20 nm) and larger pores (>100 nm) when exposed to the water and seawater conditions. The most probable diameter for the water and seawater condition was 13.3 and 14.2 nm respectively. In addition, there were also some pores ranging between 20 and 50 μm, which was especially the case for the samples submerged in water. This can be explained by considering the possible reaction products formed during the process: in outdoor conditions, the products are mainly calcite with a molar volume at 31.20 $cm^3$/mol, whereas one of the reaction products ettringite due to the immersion in seawater has a molar volume at 710.32 $cm^3$/mol. This significant volume increase of ettringite led to the growth in the pore size.

**Table 6-5:** MIP results of UHPC.

| No | total volume ($cm^3/g$) | The most probable pore (nm) | mean diameter (nm) | Median pore diameter (nm) | Pore size distribution (%) | | |
|---|---|---|---|---|---|---|---|
| | | | | | <20nm | 20-100nm | >100nm |
| Water1080d | 0.081 | 13.3 | 21.7 | 21.7 | 46.5 | 23.4 | 30.0 |
| Seawater1080d | 0.09 | 14.2 | 17.4 | 17.3 | 59.3 | 21.1 | 19.6 |
| Outdoors1080d | 0.124 | 31.5 | 37.0 | 38.0 | 8.5 | 67.5 | 19.6 |
| Seawater90d | 0.134 | 20.8 | 24.0 | 24.5 | 37.4 | 41.5 | 21.1 |
| Seawater28d | 0.146 | 22.8 | 36.3 | 38.0 | 17.5 | 47.1 | 35.6 |

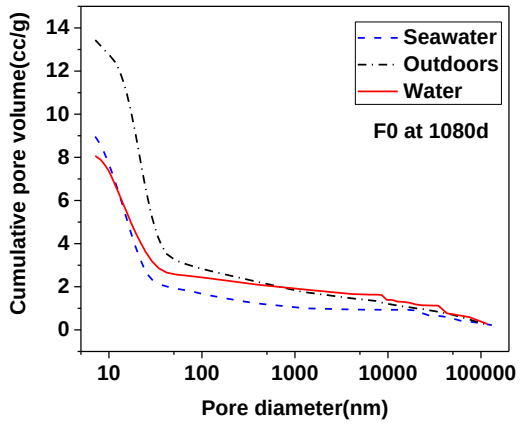


(a) Cumulative pore volume of F0 at 1080d

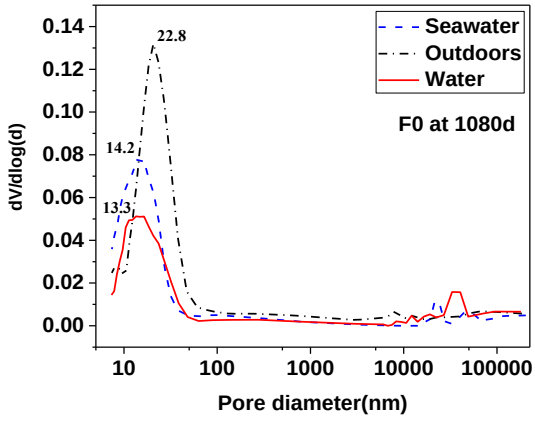


(b) Pore size distributions of F0 at 1080d

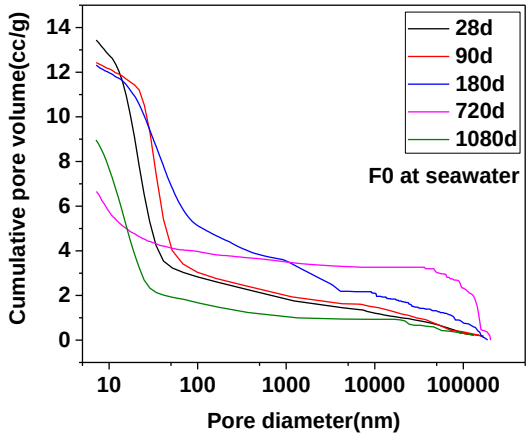


(c) Cumulative pore volume of F0 / seawater

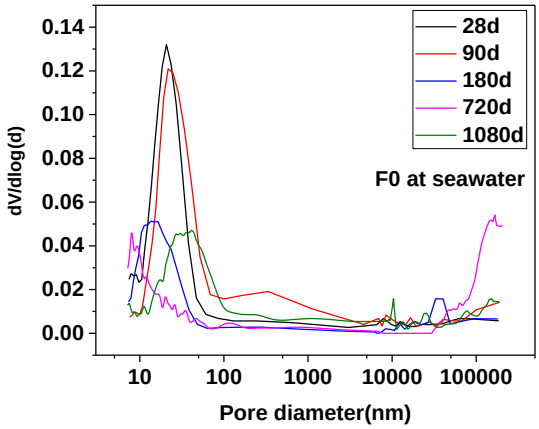


(d) Pore size distributions of F0 / seawater

**Figure 6-12.** Effects of different environment on porosity and pore size distribution of UHPCs.

### 6.3.6.2 **Nitrogen adsorption and desorption (NAD) results analysis**

Figure 6-13 plots the pore analysis of K0 and F0, respectively after 1080-day immersion in seawater. Table 6-6 is the characteristic properties of UHPC specimens. The porosities of the two mixtures fall within the range of reported for UHPC (Abbas et al., 2015; Abdulkareem, Fraj, Bouasker, & Khelidj, 2018; N. K. Lee, Koh, Kim, & Ryu, 2018) . The results from NAD pore structure analysis show that the slag containing and fly ash containing specimens both have low porosity, which means a potential of extremely slow $CO_2$ infiltration to the matrix.

The obtained results tend to indicated pervious, low quality mixes not up to the standards for UHPC, with significant exchanges with surrounding liquids or water vapor.

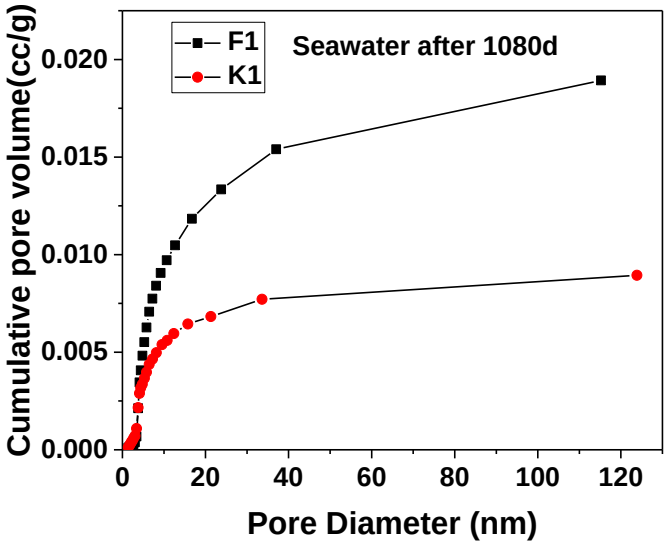


(a) Cumulative pore volume of UHPCs exposure at seawater

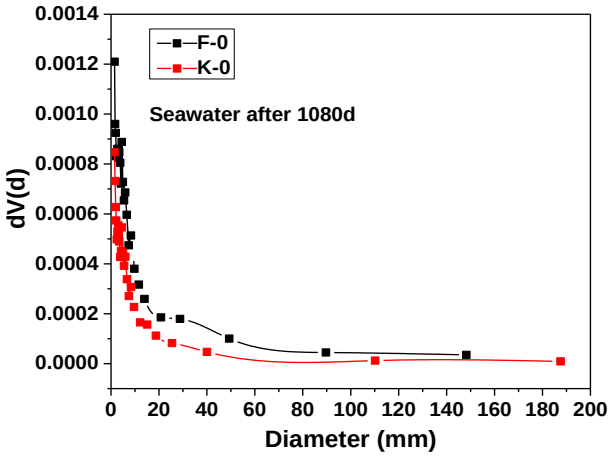


(b) Pore size distributions of UHPCs exposure at seawater

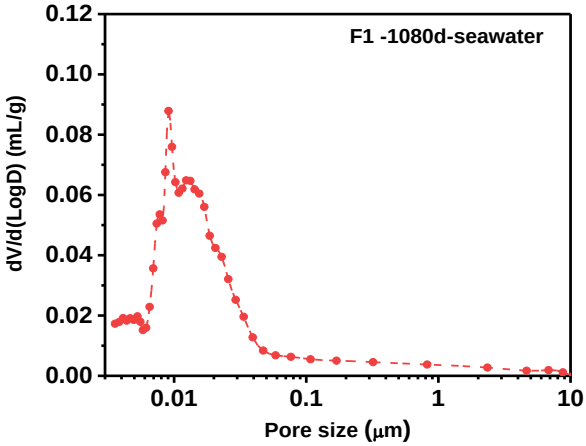


(c) micro-cumulative pore size of F1 exposure at seawater

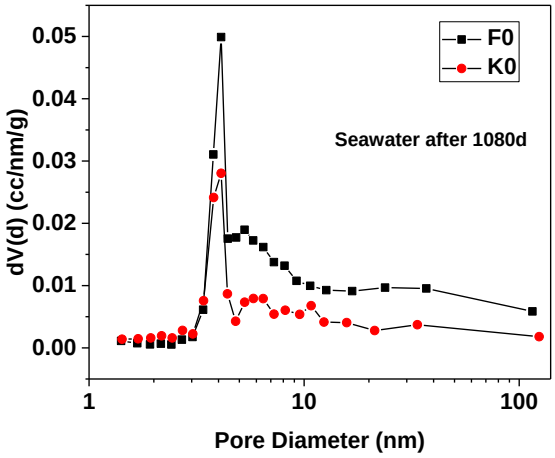


(d) Cumulative pore volume of UHPCs without steel fiber exposure at seawater

**Figure 6-13.** The pore analysis of K0 and F0, respectively after 1080-day immersion in seawater.

**Table 6-6:** Characteristic properties of UHPC specimens.

| UHPC | Compressive strength (MPa, fiber content 2%) | Chloride diffusivity coefficient ($m^2/s$) | Water absorption in vacuum (%) | Total pore volume (cc/g) | Average pore Diameter (nm) |
|---|---|---|---|---|---|
| K | 130 | $1.3\times10^{-13}$ | 1.5 | 0.0087 | 7.62 |
| F | 120 | $2.6\times10^{-13}$ | 1.8 | 0.0181 | 10.96 |

### 6.3.7 SEM/EDX

Figure 6-14 (a and b) illustrates the SEM images of the surface and surface layers (in powder form) of the seawater exposed specimens, respectively. The formation of brucite on the surface and co-existence of brucite and calcite in a few micrometers from the surface of the specimens are observed. The same findings were reported by Palin et al. (Palin, Wiktor, & Jonkers, 2015). The formation of expansive phases as well as surface corrosion can explain the expansion of UHPC specimens in seawater. Santhanam et al. (Manu Santhanam, Cohen, & Olek, 2006b) reported the deposit of ettringite in a region close to the surface of the conventional concrete specimens in seawater followed by some cracks but at a higher depth comparing to this study. Also, formation of a brucite layer and a small deposit of a mixture of chloroaluminate (possibly Friedel's salt) and sulfoaluminates were noticed (Z. Shi et al., 2017). Similar observations were reported by Brown and Badger (Brown & Badger, 2000) and Brown and Doer (Brown & Doerr, 2000).

Figure 6-14 (c and d) illustrates the SEM images of the surface and surface layers (in powder form) of specimens exposed to outdoor conditions. The formation of calcite is detected on surface as well as internal layers near the surface of the specimens. However, in previous studies on carbonation of UHPC with a short-term exposure, the diffusion of $CO_2$ into the matrix is reported to be zero due to the impermeable matrix of the UHPC (Tafraoui, Escadeillas, & Vidal, 2016b). The formation of $CaCO_3$ on the surface layers of the UHPC can be related to the long-term exposure to outdoor conditions by which surface corrosion can provide pathway for $CO_2$ to infiltrate into the surface layers. However, the preliminary test on specimens using Phenolphthalein alcohol solution as the indicator is unable to measure the extent of carbonation due to the very dense matrix of specimens.

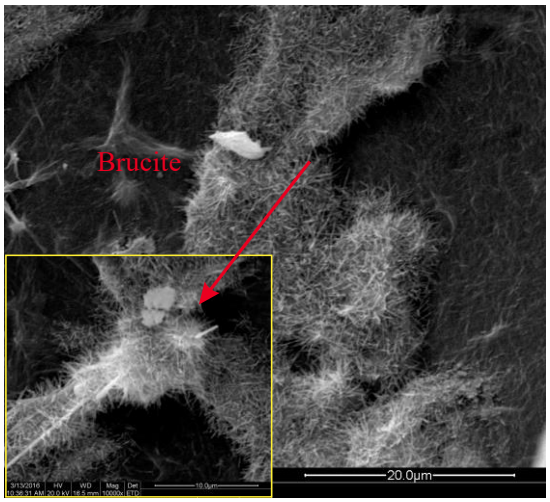


(a) surface of K-0 exposed to seawater at 1080 d

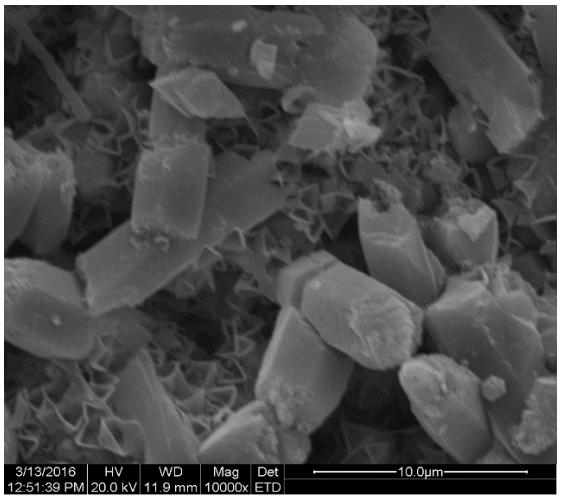


(b) 0.5 mm internal layer (ground) part

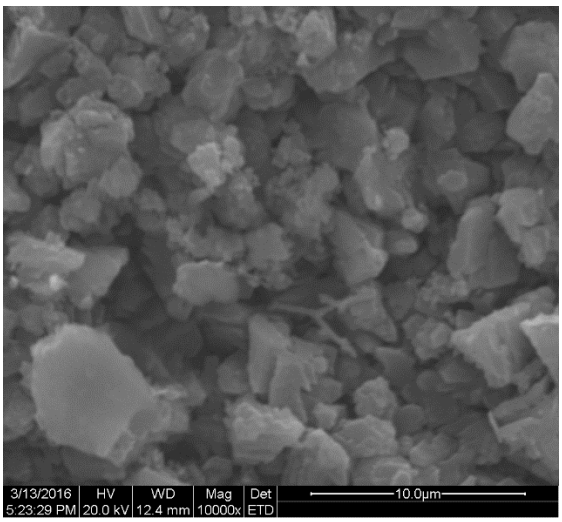


(c) surface of F-0 exposed to outdoor conditions at 1080 d

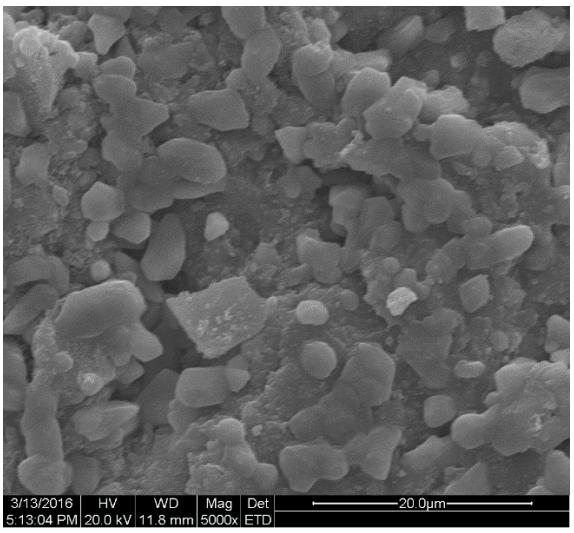


(d) 0.5 mm internal layer (ground) part

**Figure 6-14.** SEM images of specimens after exposure.

Figure 6-15 shows the surface and internal fibers in specimens exposed to seawater after 1080 days. As seen, the inner fibers are protected from the corrosion, while surface corrosion is apparent. The surface corrosion of fibers is also reported in a previous study (Balouch, Forth, & Granju, 2010). However, the surface corrosion alone cannot be responsible for the low strength development of the specimens exposed to seawater as the internal fibers were maintained unaffected, however, development of associated micro cracks on the surface can provide path for the external agents to further diffuse in the surface layers.

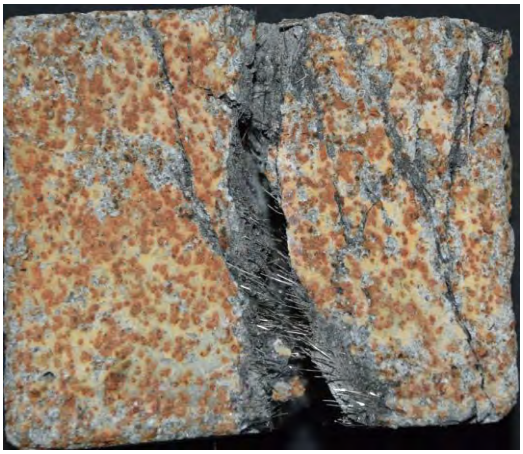

(a) F4 exposure at seawater after 1080d

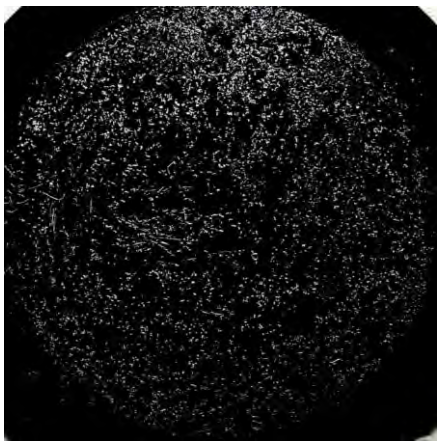

(b) fiber distribution of F3

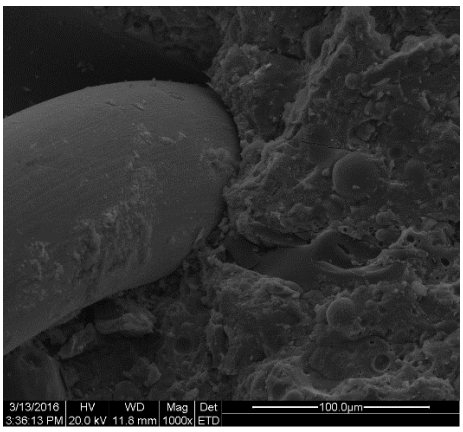


(c) SEM of F3 seawater

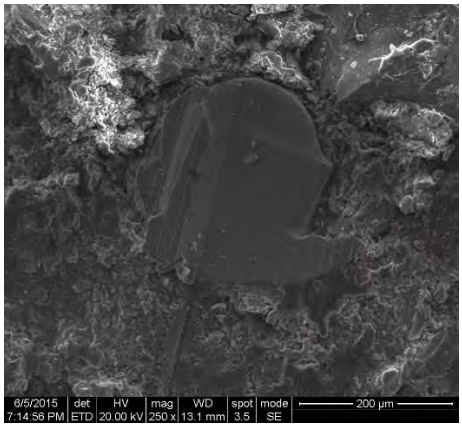


(d) SEM of F3 seawater

**Figure 6-15.** Surface appearance and internal fibers of specimen F-3 exposed to seawater after 1080 days.

## 6.4 Conclusion

Based on the results from this study, the following conclusions can be drawn:

(1) Due to the ball effect of fly ash, the flowability of UHPCs containing fly ash were better than UHPCs containing slag. With the increase of the content of steel fiber, the flowability of fresh UHPCs decreased, cause the Elastic Modulus and physical effect of steel fiber.

(2) TG/DTG analyses indicated that UHPC specimens exposed to seawater at 1080 d also efficiently consumed the CH. The TGA/DTG results indicated that $Ca(OH)_2$ was consumed with the formation of $CaCO_3$ (calcite) due to the carbonation effect in outdoor conditions

whereas for the water and seawater immersion conditions, the $Ca(OH)_2$ was transformed into other reaction products including $Mg(OH)_2$ and ettringite. Moreover, seawater and water condition led to a loss of C-S-H gel, which was especially the case after 28 day of immersion.

(3) XRD and SEM analysis implies that for the sample exposed to outdoor and seawater condition based UHPC underwent less deterioration compared to FA containing UHPCs, more calcite was formed than the water condition. To compare the seawater and outdoor exposures, the surface layer of the sample immersed in seawater had some brucite and calcite as well as Friedel's salt and sulfoaluminates. However, for outdoor condition, the surface pH dropped due to the penetration of $CO_2$ into the binder neutralizing the pore solution. As time passed, more large-sized and small sized pores formed in the seawater because of the expanding effect induced by ettringite, whereas for outdoor environments, more medium-sized pores were produced due to the formation of calcites.

(4) Fiber addition improved the performance of fly ash (FA) based UHPC, while it had little impact on the slag-based counterpart. Because of a denser microstructure evidenced by diffusion coefficient and porous characteristics, slag based samples.

## 6.5 References

L. Wu, N. Farzadnia, C. Shi, Z. Zhang, H. Wang, Autogenous shrinkage of high performance concrete: A review, Construction & Building Materials, 149 (2017) 62-75.

C. Shi, D. Wang, L. Wu, Z. Wu, The hydration and microstructure of ultra high-strength concrete with cement–silica fume–slag binder, Cement & Concrete Composites, 61 (2015) 44-52.

Y. Yang, E.H. Yang, V.C. Li, Autogenous healing of engineered cementitious composites at early age, Cement & Concrete Research, 41 (2011) 176-183.

G. Kim, J.Y. Kim, K.E. Kurtis, L.J. Jacobs, Y.L. Pape, M. Guimaraes, Quantitative evaluation of carbonation in concrete using nonlinear ultrasound, Materials & Structures, 49 (2016) 399-409.

S.C. Taylor-Lange, M.C.G. Juenger, J.A. Siegel, Impact of cement renders on airborne ozone and carbon dioxide concentrations, Atmospheric Environment, 70 (2013) 263-266.

C.-F. Chang, J.-W. Chen, The experimental investigation of concrete carbonation depth, Cement and Concrete Research, 36 (2006) 1760-1767.

V.G. Papadakis, Effect of supplementary cementing materials on concrete resistance against carbonation and chloride ingress, Cement and concrete research, 30 (2000) 291-299.

A.V. Saetta, B.A. Schrefler, R.V. Vitaliani, The carbonation of concrete and the mechanism of moisture, heat and carbon dioxide flow through porous materials, Cement and Concrete Research, 23 (1993) 761-772.

O. Poupard, V. L'hostis, S. Catinaud, I. Petre-Lazar, Corrosion damage diagnosis of a reinforced concrete beam after 40 years natural exposure in marine environment, Cement and concrete research, 36 (2006) 504-520.

S. Ahmad, Reinforcement corrosion in concrete structures, its monitoring and service life prediction—a review, Cement and concrete composites, 25 (2003) 459-471.

L. Bertolini, B. Elsener, P. Pedeferri, E. Redaelli, R.B. Polder, Corrosion of steel in concrete: prevention, diagnosis, repair, John Wiley & Sons2013.

S.V. Nanukuttan, P.A.M. Basheer, W.J. Mccarter, L. Tang, N. Holmes, T.M. Chrisp, G. Starrs, B. Magee, The performance of concrete exposed to marine environments: Predictive modelling and use of laboratory/on site test methods, Construction & Building Materials, 93 (2015) 831-840.

M. Thomas, 6 – The durability of concrete for marine construction : Materials and properties, Marine Concrete Structures, (2016) 151-170.

M. Santhanam, M. Otieno, Deterioration of concrete in the marine environment, 2016.

A. Mo, S. El-Tawil, Z. Liu, W. Hansen, Effects of silica powder and cement type on durability of ultra high performance concrete (UHPC), Cement & Concrete Composites, 66 (2016) 47-56.

R. Yu, P. Spiesz, H.J.H. Brouwers, Effect of nano-silica on the hydration and microstructure development of Ultra-High Performance Concrete (UHPC) with a low binder amount, Construction & Building Materials, 65 (2014) 140-150.

S. Abbas, A.M. Soliman, M.L. Nehdi, Exploring mechanical and durability properties of ultra-high performance concrete incorporating various steel fiber lengths and dosages, Construction & Building Materials, 75 (2015) 429-441.

A. Tafraoui, G. Escadeillas, T. Vidal, Durability of the Ultra High Performances Concrete containing metakaolin, Construction & Building Materials, 112 (2016) 980-987.

D. Wang, C. Shi, Z. Wu, J. Xiao, Z. Huang, Z. Fang, A review on ultra high performance concrete: Part II. Hydration, microstructure and properties, Construction & Building Materials, 96 (2015) 368-377.

C. Shi, Z. Wu, J. Xiao, D. Wang, Z. Huang, Z. Fang, A review on ultra high performance concrete: Part I. Raw materials and mixture design, Construction & Building Materials, 101 (2015) 741-751.

T. Fukushima, Y. Yoshizaki, F. Tomosawa, K. Takahashi, RELATIONSHIP BETWEEN NEUTRALIZATION DEPTH AND CONCENTRATION DISTRIBUTION OF $CACO_3$-$CA(OH)_2$ IN CARBONATED CONCRETE, Recent Advances in Concrete Technology, 1998.

B. EN, 14630, 2006. Products and systems for the protection and repair of concrete structures. Test methods. Determination of carbonation depth in hardened concrete by the phenolphthalein method, British Standard, (2006).

NetAnswer, Effect of fly ash gradation on workability, strength and durability of Portland cement fly ash mortars, Materials & Structures.

L. Alarcon-Ruiz, G. Platret, E. Massieu, A. Ehrlacher, The use of thermal analysis in assessing the effect of temperature on a cement paste, Cement and Concrete Research, 35 (2005) 609-613.

O.M. Abdulkareem, A.B. Fraj, M. Bouasker, A. Khelidj, Effect of chemical and thermal activation on the microstructural and mechanical properties of more sustainable UHPC, Construction & Building Materials, 169 (2018) 567-577.

N.K. Lee, K. Koh, M.O. Kim, G. Ryu, Uncovering the role of micro silica in hydration of ultra-high performance concrete (UHPC), Cement and Concrete Research, 104 (2018) 68-79.

D. Palin, V. Wiktor, H.M. Jonkers, Autogenous healing of marine exposed concrete: Characterization and quantification through visual crack closure, Cement & Concrete Research, 73 (2015) 17-24.

M. Santhanam, M. Cohen, J. Olek, Differentiating seawater and groundwater sulfate attack in Portland cement mortars, Cement & Concrete Research, 36 (2006) 2132-2137.

Z. Shi, M.R. Geiker, B. Lothenbach, K. De Weerdt, S.F. Garzón, K. Enemark-Rasmussen, J. Skibsted, Friedel's salt profiles from thermogravimetric analysis and thermodynamic modelling of Portland cement-based mortars exposed to sodium chloride solution, Cement and Concrete Composites, 78 (2017) 73-83.

P.W. Brown, S. Badger, The distributions of bound sulfates and chlorides in concrete subjected to mixed NaCl, MgSO 4 , Na 2 SO 4 attack, Cement & Concrete Research, 30 (2000) 1535-1542.

P.W. Brown, A. Doerr, Chemical changes in concrete due to the ingress of aggressive species, Cement & Concrete Research, 30 (2000) 411-418.

A. Tafraoui, G. Escadeillas, T. Vidal, Durability of the ultra high performances concrete containing metakaolin, Construction and Building Materials, 112 (2016) 980-987.

S. Balouch, J. Forth, J.-L. Granju, Surface corrosion of steel fibre reinforced concrete, Cement and Concrete Research, 40 (2010) 410-414.

# CHAPTER 7 LONG-TERM PERFORMANCE OF ULTRA-HIGH PERFORMANCE CONCRETE (UHPC) UNDER DIFFERENT EXPOSURE CONDITIONS

Note: this chapter is based on the manuscript entitled “Long-term performance of ultra-high performance concrete (UHPC) under different exposure conditions”, by Linmei Wu, Z Zhang and H Wang, submitted in journal of **Construction and Building Materials.**

**Abstract**: The low hydration extent of cement particles in UHPC under the conditions of extremely low W/B can be altered by the incorporation supplementary cementitious materials (SCMs) and fibers in a long-term of view, which may affect their performances when exposed to different conditions. This study investigated the effects of slag, fly ash, and fiber contents on long-term strength development, dimensional stability, and mass change in three exposure conditions: water, seawater, and outdoor, for a duration of 720 days. Thermogravimetric analysis (TGA), X-ray diffractometry (XRD) and scanning electron stereoscopy (SEM) were applied to examine the hydration phases during this exposure period. The results showed that the specimens in water and outdoor conditions experienced a shrinking behavior, while in contrast, the specimens exposed to seawater expanded slightly with a higher rate of mass gain. The compressive strength of specimens under seawater and outdoor expose conditions were lower than those in water and the main hindering mechanism to strength development was the shortage of calcium hydroxide from the matrix, which led to lower reaction extent of SCMs.

**Key Words:** UHPC; Long-term performance; Compressive strength; Dimensional stability; Mass change

## 7.1 Introduction

Ultra-high performance concrete (UHPC) is a composite material with improved static and dynamic mechanical properties comparing to conventional concretes; and excellent durability, which has the most promising function in marine structures, as well as in

infrastructures (Paul Acker & Behloul, 2004; Schmidt & Fehling, 2005). Numerous studies of UHPC have reported their durability performances. The chloride ingression and carbonation have been proven to be extremely low in the UHPC, due to dense and impermeable matrix (D. Wang et al., 2015). In a study by Safeer Abbas et al. (Abbas et al., 2015), no deterioration in mechanical properties of UHPC was observed after various severe exposures to chloride ions. Tafraoui et al. (Tafraoui et al., 2016a) showed that the gas permeability of UHPC and chloride diffusion coefficient were lower than $1.5\times10^{-19}m^2$ and $1.7\times10^{-14}(m^2/s)$, respectively. A study by Piérard et al. (Julie, Dooms, & Cauberg, 2012) showed a carbonation depth of only 1.5 to 2.0 mm after a one year of exposure to a 1-percent $CO_2$ atmosphere. Although studies have shown that UHPC is resistant to harsh environments, the examinations were mostly limited to the short-term performances. There is limited reporting their long-term performances, particularly under different exposure conditions. It is known that exposure conditions, as external factor, can led to substantially different behavior of concretes. In a study by Islam et al. (Islam, Islam, Mondal, & Islam, 2009), up to 22% reduction in compressive strength was reported in conventional concrete specimens exposed to seawater with a duration of 12 month. Formation of expansive phases as well as leachable compounds were considered as the main reasons for the strength deterioration in the conventional slag concrete. It was reported that seawater infiltrated the matrix and reacted with the hydrated products of cement and slag forming ettringite and the Friedel's salt by which the micro cracks propagated and the bond between hydrated product and aggregate particles loosened; the concrete gradually became porous due to leaching action of the newly formed compounds which further decreased the compressive strength (Islam et al., 2009). It is reported that HPC for marine structure is durable and the chloride diffusion coefficient is just 1/10~1/15 compare with normal concrete(Leng, Feng, & Lu, 2000). However, chloride ions penetrate into the HPC used in Hong Kong-Zhuhai-Macao Bridge, especially when steel fiber is used in HPC, seawater is corrosive to the interfacial between the concrete and fiber (Pengsheng, Shengnian, & Jianbo XIONG, 2017). The addition of steel fiber could prevent steels from corrosion. However, after concrete cracks, for any mix design of concrete, the steel corrosion would accelerate under the seawater conditions (Aıtcin, 2003). So when the external condition becomes worse such as marine environment or outdoors, the durability of UHPC is affected.

On the other hand, unlike in conventional concretes, which are mixed at a regular water-to-cement ratio (w/c = 0.32-0.5), UHPC usually consists of extremely low water-to-cementitious materials ratio (w/c = 0.14-0.24) and high contents of superplasticizer. At the conditions of ultra-low w/c, abundant amounts of un-hydrated cementitious materials in the matrix (C. Shi, Wang et al., 2015b) (Manzi, Mazzotti, & Bignozzi, 2013) may affect the long-term performance of UHPC. Due to ongoing hydration, it has a retrieving effect on physicochemical properties of UHPC, also known as "autogenous/self-healing" (Mihashi & Nishiwaki, 2012; M. Wu, Johannesson, & Geiker, 2012). Recently, hydro-chemo-mechanical and micromechanical modellings have been proposed to represent these healing capacity of UHPC (Davies & Jefferson, 2017; Hilloulin, Grondin, Matallah, & Loukili, 2014). However, when SCMs (slag and fly ash etc.) are incorporated in UHPC, the hydration process and healing capacity at later ages might be alternated due to the lack of sufficient $Ca(OH)_2$. when the slag is be used as SCMs, it can help to consume CH(P.-K. Chang & Hou, 2003), the self-healing of HPC decreased in the long term. There was a decrease in sorptivity (water absorption) with age for HPC with fly ash in it. Fly ash was less pronounced in improving the sorptivity after 44 days(Elahi, Basheer, Nanukuttan, & Khan, 2010), when the fly ash is used as SCMs, it will affect the durability of HPC.

Given the application environments of UHPC, usually rigid or corrosive, the long-term performance and the durability, rather than the high strength, are the most concerned (required) characteristics. Hence, a comprehensive understanding on the long-term performance of UHPC exposed to different conditions is critical. This chapter studies the long-term behavior of different SCM-containing UHPCs exposed to water, seawater, and outdoor conditions for a duration of 720 days, by investigating the changes in compressive strength, dimensional stability and mass change. To better understand the results obtained at macro level, thermogravimetric analysis (TGA), X-ray diffraction (XRD), and scanning electron microscopy (SEM) were conducted to examine the phase change and microstructure of UHPCs after long-term exposure.

## 7.2 Experimental program

### 7.2.1 Raw materials

Portland cement P.I 42.5, complying with the Chinese Standard GB175-2007 was used. Table 7-1 summarizes the physical properties of the cement. Fly ash and ground blast furnace slag, with the specific surface areas of 427 $m^2$/kg and 446 $m^2$/kg, respectively, were used to partially replace cement in the concrete mixture. Silica fume with 63% particles between 0.1 to 0.5 μm (diameter) and specific surface area of 18500 $m^2$/kg was used. Table 7-2 shows the chemical composition of cement, silica fume, fly ash and slag. The natural river sand with maximum particle size of 2.36 mm and fineness modulus of 3.0 was applied to cast UHPC specimens. It had a specific weight and bulk density of 2550 kg/$m^3$ and 1570 kg/$m^3$, respectively. The straight steel fiber with diameter of 0.2 mm and length of 13 mm was used. A polycarboxylate based super-plasticizer (SP) with a solid content of 21% was applied to adjust to desirable workability.

**Table 7-1:** Physical properties of Portland cement P.I 42.5.

| Density (g/$cm^3$) | 80 μm-residue on sieve (%) | Specific surface area ($m^2$/kg) | Setting time (h) | | Flexural strength (MPa) | | Compressive strength (MPa) | |
|---|---|---|---|---|---|---|---|---|
| | | | Initial | Final | 3 d | 28 d | 3 d | 28 d |
| 3.15 | 0.3 | 380 | 2.5 | 3.4 | 6.4 | 9.0 | 33.0 | 60.0 |

**Table 7-2:** Chemical composition of cementitious materials (weight %), LOI is loss on ignition.

| Chemical composition | $SiO_2$ | $Al_2O_3$ | $Fe_2O_3$ | CaO | MgO | $K_2O$ | $Na_2O$ | $SO_3$ | LOI |
|---|---|---|---|---|---|---|---|---|---|
| Cement | 25.26 | 6.38 | 4.05 | 64.67 | 2.68 | - | - | 0.94 | 0.9 |
| Silica fume | 90.82 | 1.03 | 1.50 | 0.45 | 0.83 | 0.86 | 0.17 | - | 4.34 |
| Slag | 33.00 | 13.91 | 0.82 | 39.11 | 10.04 | 1.61 | 0.26 | 0.92 | 0.33 |
| Fly ash | 54.29 | 32.55 | 5.53 | 1.34 | 2.56 | 1.34 | 0.49 | 0.35 | 1.55 |

### 7.2.2 Mixture proportions

The mixture proportions of UHPCs were designed based on a previous study (C. Shi, Wang et al., 2015a). In brief, the w/b of 0.18 and binder-to-aggregate ratio of 1.1 were selected and kept constant throughout the study. The SP was used at 2% by the mass of the binder.

Steel fiber contents were 0, 1%, 2%, and 3% by the volume of concrete. Table 7-3 shows the mixture proportion of UHPC based on mass of ingredients.

**Table 7-3:** Mixture proportions of UHPCs.

| No. | w/b | Mass of ingredients (kg/m$^3$) | | | | | | | |
|---|---|---|---|---|---|---|---|---|---|
| | | Water | Cement | Silica fume | Slag | Fly Ash | SP* | Sand | Fiber |
| K0 | 0.18 | 164 | 550 | 200 | 250 | 0 | 20 | 1100 | 0.0 |
| K1 | 0.18 | 164 | 550 | 200 | 250 | 0 | 20 | 1100 | 78.5 |
| K2 | 0.18 | 164 | 550 | 200 | 250 | 0 | 20 | 1100 | 157.0 |
| K3 | 0.18 | 164 | 550 | 200 | 250 | 0 | 20 | 1100 | 235.5 |
| F0 | 0.18 | 164 | 550 | 200 | 0 | 250 | 20 | 1100 | 0.0 |
| F1 | 0.18 | 164 | 550 | 200 | 0 | 250 | 20 | 1100 | 78.5 |
| F2 | 0.18 | 164 | 550 | 200 | 0 | 250 | 20 | 1100 | 157.0 |
| F3 | 0.18 | 164 | 550 | 200 | 0 | 250 | 20 | 1100 | 235.5 |

*SP means total mass of liquid-based SP.

### 7.2.3 Mixing procedures and specimen preparation

In mixing, dry powders, including cement, silica fume, slag or fly ash, and natural river sand, were firstly dry mixed for 3 min in a high-speed drum mixer. Then, water and superplasticizer were added and mixed for 6 min at low speed. Afterwards, steel fiber was added through passing a sieve with size of 5 mm and mixed for another 6 min until the mixtures were homogeneous. The obtained UHPC mixtures were then cast into molds and vibrated for consolidation. The cubic specimen size for the compressive strength test was 40 × 40 × 40 mm$^3$. The specimen size for long-term dimension stability test was 75 × 75 × 275 mm$^3$.The specimens were demolded 1 day after casting and then cured in lime saturated water at the temperature of 20 ± 2°C for 28 days. Then the properties of the hardened concrete such as compressive strength and initial length were measured before exposure to different conditions.

### 7.2.4 Exposure conditions

UHPC specimens were exposed to three conditions for a duration of 720 days.

(4) **Outdoor.** Specimens were exposed to the natural outdoor conditions in Changsha. Specimens were placed facing south at a 45° inclination. Figure 7-1 illustrates mean values of the temperature and humidity in Changsha, China. The curing

temperature and humidity changed according to the local weather with a minimum temperature of -1°C and relative humidity of 76% and a maximum temperature of 33°C and relative humidity of 86% during the exposure period.

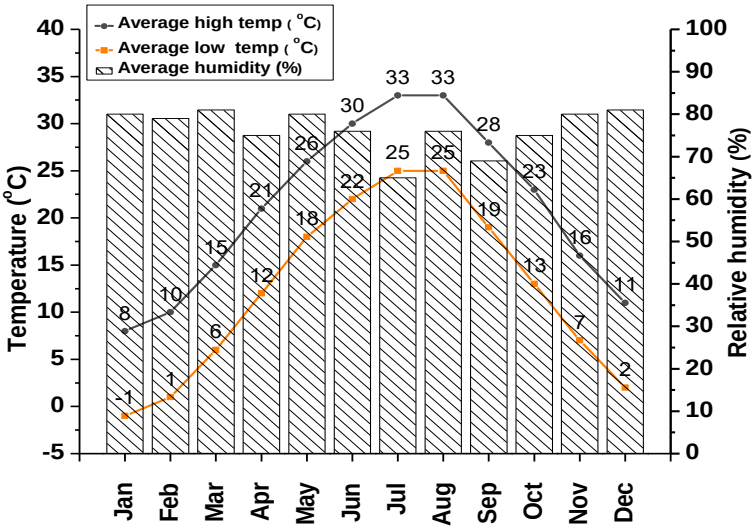


**Figure 7-1.** Mean values of temperature and humidity change of Changsha during the exposure time.

(5) **Tap water.** The UHPC specimens were immersed in the normal tap water, no lime was used.

(6) **Seawater.** According to the composition of a natural seawater in the Gulf of China (NS) and the artificial seawater as specified by ASTM D-14 (AS1) (as shown in Table 7-4), an artificial seawater (AS2) was prepared for the use of this study. Given the long-time process of corrosion, the concentration of AS2 was elevated to accelerate the corrosion process.

After the curing scheme (put the specimens were demolded 1 day after casting and then cured in lime saturated water at the temperature of 20 ± 2°C for 28 days), the specimens were exposed to the three conditions from day zero (0), which denotes the first day of exposure. Water and seawater in storage tanks were refreshed every three weeks.

**Table 7-4:** The compositions of the natural seawater in the Gulf of China (NS), the ASTM D-14 specified artificial seawater (AS1) and the artificial seawater used in this study (AS2) (g/L).

| Chemical | NaCl | $Na_2SO_4$ | $MgCl_2$ | $MgCl_2{\cdot}6H_2O$ | $MgSO_4{\cdot}7H_2O$ | $CaSO_4{\cdot}2H_2O$ | $CaC1_2$ | $CaCO_3$ | KCl |
|---|---|---|---|---|---|---|---|---|---|
| NS | 21.0 | - | 2.54 | - | 1.54 | 2.43 | - | 0.1 | - |
| AS1 | 24.5 | 4.1 | - | 2.54 | - | - | 1.2 | - | 0.1 |
| AS2 | 25.0 | 10.0 | 12.7 | 7 | - | - | - | - | 0.1 |

## 7.3 Testing methods

### 7.3.1 Workability

The fresh mortar was filled into a mini cone placed on an automatic jump table as described in Chinese standard of GB2419-2005. The mini cone has an upper diameter of 70 mm, a lower diameter of 100 mm, and a height of 60 mm. After mini cone was vertically lifted, the mortar was vibrated automatically for 25 times. Two diameters perpendicular to each other were then determined and mean value was reported.

### 7.3.2 Compressive strength

At exposure ages of 1, 7, 28, 56, 90, 120, 216, 448, 630, and 720 days, the compressive strengths of the specimens were tested according to EN 196-1 (T. EN, 2005). At least three specimens were tested at each age to obtain the average strength.

### 7.3.3 Nitrogen adsorption and desorption (NAD) analysis

NAD analyses were conducted with the gas volumetric analyzer Quantachrome Instruments QuadraSorb Station 1. The ground cement paste powders were preheated at 60℃ for 24 h under vacuum condition to eliminate the influence of free water.

### 7.3.4 Dimensional stability

The long-term dimensional stability was monitored based on the length change of the specimens according to Chinese standard GBJ82-85. The two measuring heads were embedded in the two sides of each specimen. The measurements were carried out at

exposure ages of 1, 7, 28, 56, 90, 120, 216, 448, 630 and 720 days. The length was measured by a digital micrometer (BC-300) and calculated by Eq. (7-1):

$$\varepsilon_{st}^{'} = \frac{L_0 - L_t}{L_b} \tag{7-1}$$

Where $\varepsilon'_{st}$ is the length change index of concrete at $t$ days;

$L_b$ is the standard length of specimen, which is the length of concrete subtracted the two times of the embedded depth of the measuring heads;

$L_t$ is the measured length at $t$ days;

$L_0$ is the initial reading of the specimen.

The reported result was the mean value of the length change of three specimens calculated accurate to $1\times10^{-6}$.

### 7.3.5 Mass change

The mass change was recorded concomitantly to the length change measurements. The mass was measured by electronic balance and mass change ratio was calculated by Eq. (7-2):

$$\varepsilon = \frac{m_0 - m_t}{m_0} \tag{7-2}$$

Where $m_0$ is the initial weight of the specimens after 28 days of standard curing (day 0); and $m_t$ is the weight of specimens at measured day $t$ after exposure.

### 7.3.6 Thermogravimetric analysis (TGA)

Thermogravimetric analysis was performed using a Netzsch STA 409 PC equipment to quantitatively determine the changes of mineral phases in UHPC under different conditions at exposure ages of 60 and 720 days. The samples were taken from the surface layer (2 mm) of the side with maximum exposure (esp. in outdoor conditions) using a Small CNC lathe microtome (Model C000057). The tested powder samples of selected mixtures were weighed (10 mg) and heated from room temperature to 1000°C in a nitrogen atmosphere at 10°C/min. Derivative thermogravimetry was used to estimate the extent of carbonation on the surface layers of the specimens after exposure to different conditions.

### 7.3.7 X-ray diffractometry (XRD)

The preparation of samples for XRD was the same as those prepared for TGA. The prepared powders were analyzed by using Philips X-ray diffractometer with CuKα radiation. The samples were step-scanned from 10 to 70° (2θ) at a rate of 5°/min.

### 7.3.8 Scanning electron microscopy (SEM)

Scanning electron microscopy (SEM) was employed to study the microstructure of UHPC. SEM samples were taken from freshly broken specimens, cut into small fragments and soaked in ethanol prior to testing, to stop the hydration of cement. Subsequently, the samples were dried at 65°C and sputtered with gold before analyzing using ION SPUTTER E-1045.

## 7.4 Experimental results

### 7.4.1 Workability

Figure 7–2 shows the workability of the mixtures with different contents of fibers. It is observed that, for K0 and F0 mixtures without steel fibers, the slump flowability is higher than 200 mm. With the incorporation of 3% steel fiber, the slump flowability decreases to 140 and 150 mm, respectively. Moreover, the slump flowability of fly ash containing mixture is higher than slag containing mixture, which is due to the ball bearing effect of fly ash (NetAnswer).

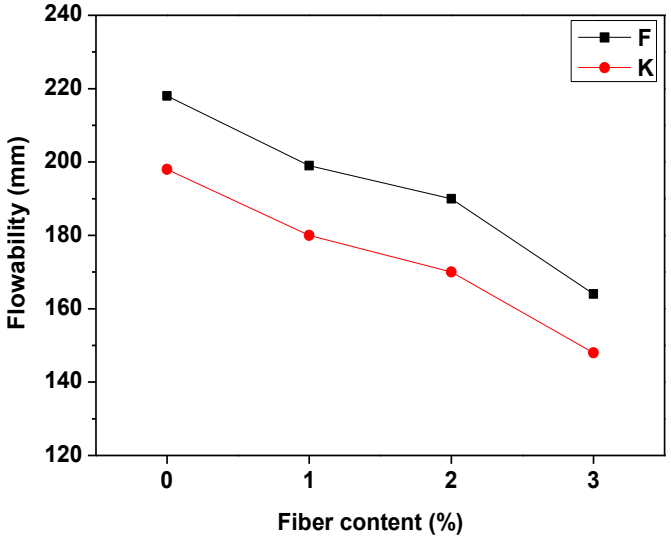


**Figure 7-2.** Effect of steel fiber contents on flowability of slag containing (K) and fly ash containing (F) UHPC mixtures.

## 7.4.2 Porosity

Figure 7-3 plots the pore analysis of K0 and F0, respectively. The porosities of the two mixtures fall within the range of reported for UHPC (Abbas et al., 2015; Abdulkareem et al., 2018; N. K. Lee et al., 2018) . The results from NAD pore structure analysis show that the slag containing and fly ash containing specimens both have low porosity, which means a potential of extremely slow $CO_2$ infiltration to the matrix.

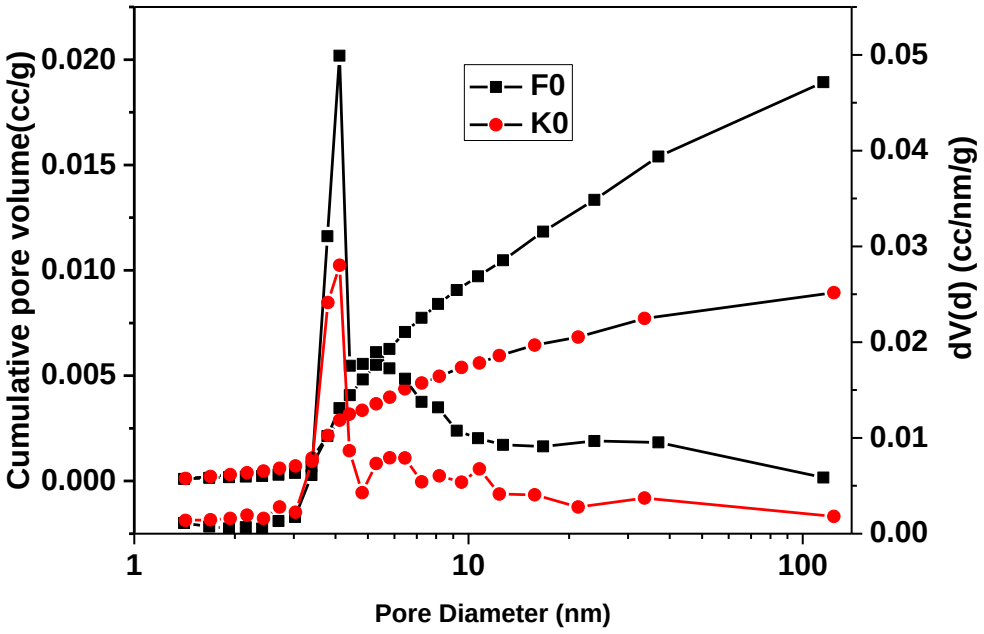

**Figure 7-3.** Cumulative pore volume and Pore size distributions in K0 and F0 as calculated by the BJH method with desorption data.

### 7.4.3 Compressive strength development

Figure 7-4 shows the compressive strength development of the UHPC specimens subjected to the three exposure conditions over a period of 720 days. The results illustrate a distinct trend for the strength development after exposure to water, seawater and outdoor conditions. The specimens in water obtain higher strength, while the strength increase is less in those exposed to outdoor conditions. On the contrary, the specimens in seawater experienced slight decrease in strength at the initial days, followed by a strength gain at later ages after 56 days.

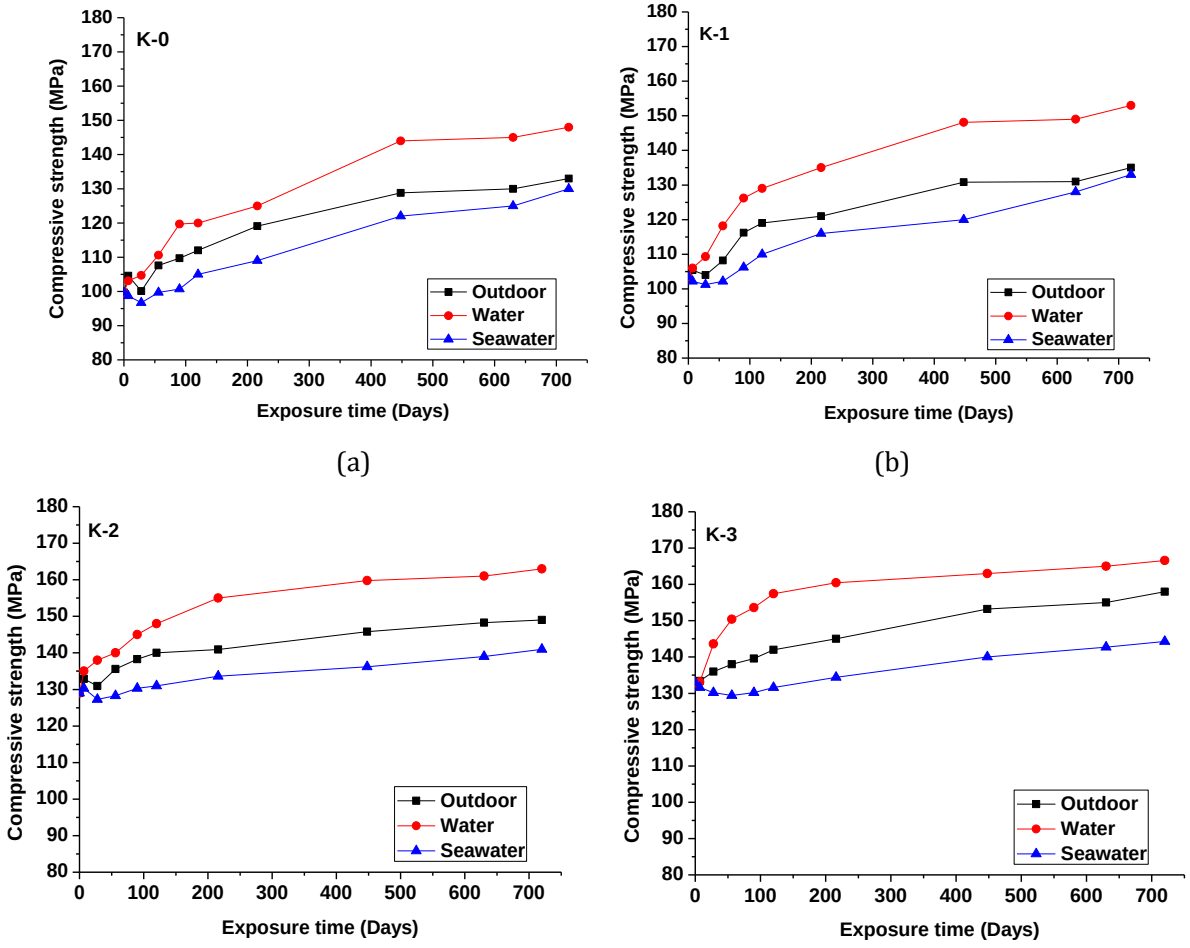

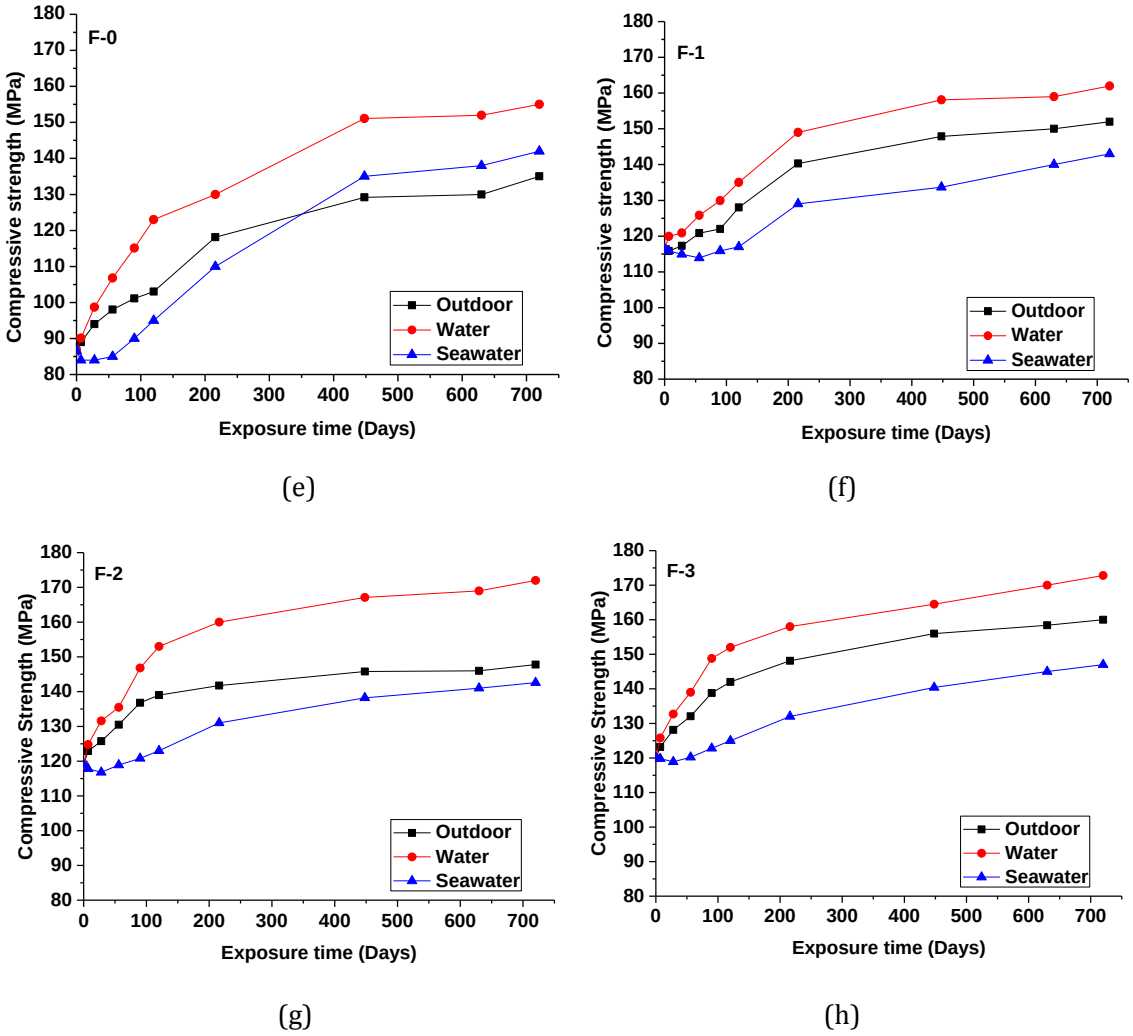


**Figure 7-4.** Compressive strength development of UHPCs under the three exposure conditions.

Figure 7-4 (a-d) illustrate the compressive strengths of slag containing UHPCs with 0, 1, 2, and 3% fiber addition under the three exposure conditions. The strength development continues in the testing period. In ages earlier than 216 days, the strength development is more remarkable for all specimens, especially for K-3 specimens immersed in water. This can be attributed to the increased bond strength at the interface of fibers as the strength of the matrix, which continuously being condensed as later pozzolanic reaction undergoes(Habel et al., 2006; Wille, Naaman, El-Tawil, & Parra-Montesinos, 2012). Extensive studies indicated that the incorporation of steel fiber significantly increased the mechanical properties of UHPC, such as compressive strength, flexural strength and ductility (Hoang & Fehling, 2017; Simões et al., 2017). Wu et al. (Z. Wu, C. Shi, & K. H.

Khayat, 2016) showed that formation of higher and stronger hydration products in the vicinity of fibers and the refinement of the interfacial zone of fiber-matrix in UHPC. The strength loss of K-0, K-1, K-2 and K-3 at 28 days under outdoor conditions (compared to the initial strength at day 0) is probably due to the drying shrinkage of samples, as being taken out from the saturated lime water. However, as steel fiber content is increased to 3%, the negative effect of drying shrinkage on strength is controlled.

The strength development rate at early ages is comparatively lower in the specimens exposed to the outdoor conditions. The negative effect of slag incorporation on carbonation of conventional concrete is reported by Gruyaert et al.(Gruyaert, Heede, & Belie, 2013). The authors in [29] showed that gas permeability of the mixtures increased with the increase of slag content and the carbonation reaction led to coarsening of the pore structure under $CO_2$ exposure conditions. However, previous studies have confirmed very low $CO_2$ penetration of UHPC (NetAnswer). It is noted that exposure to seawater decreases the early age strength and hinders the ultimate strength growth in all the specimens. The ultimate strengths of slag-containing UHPC specimens increase by ~25% after 720 days of exposure. The increased ratios of strength in water and outdoor exposures are as high as ~45% and ~30%, respectively. Although the increase under seawater exposure conditions is relatively lower, compared to the loss of strength of conventional concretes under seawater conditions, the UHPC exhibit better resistance in a long-term view.

Figure 7-4 (e-h) shows the effect of exposure conditions on fly ash containing UHPC specimens. The strength increases consistently during the exposure time to water. This strength development characteristic is related to the well-known filler and pozzolanic effect of fly ash, which serves better at later ages due to its slow pozzolanic reactivity (Bouzoubaa, Zhang, Malhotra, & Golden, 1999; De Weerdt et al., 2011; Deschner et al., 2012). Zhao et al. (Y. Zhao, Gong, & Zhao, 2017) reported that fly ash has less contribution to compressive strength of high performance concrete comparing that of slag, which is in a good agreement with the result of this study at day 0. In this study, although the initial strengths of the fly ash containing specimens at day 0 are lower, the ultimate compressive strengths are comparable to those of slag containing specimens after 720 days of exposure. It is noted that unlike the slag containing specimens, there is no initial strength loss for

the fly ash containing specimens when immersed samples are taken out of the lime water. This is due to the better

The exposure to outdoor and seawater conditions reduces the strength development rates. The beneficial effect of fly ash on long-term performance of the conventional concrete is well documented (Ahmaruzzaman, 2010). Chalee and Jaturapitakkul (Chalee & Jaturapitakkul, 2008) reported that the compressive strength of the conventional concrete containing fly ash is maintained higher than that of cement based concrete after exposure to marine environments for a duration of 21 years. Moffatt et al. (Moffatt, Thomas, & Fahim, 2017) also reported similar findings; the concretes with fly ash exhibited higher strength at later ages than those controls without fly ash after 24 years of exposure to the marine environment. The improved performance of the fly ash containing concrete is related to the refined pore structure as well the depleted calcium hydroxide content due to the pozzolanic effect of fly ash. In this study, the addition of fibers provided similar enhancement of strength to that of the slag containing specimens.

### 7.4.4 Dimensional stability

Figure 7-5 shows the length changes of UHPC specimens exposed to outdoor, water and seawater conditions. The length change is less pronounced for specimens in water and seawater than those exposed to the outdoor conditions. On the other hand, it is observed that the length change is in the form of shrinkage in the specimens exposed to outdoor and water, while an expansion is observed in the specimens exposed to seawater. In all exposure conditions, the stabilizing effect of fibers is apparent. In general, using fibers in UHPC results in increased strain capacity and energy absorption by controlling expansion and crack propagation (D. Y. Yoo & Banthia, 2016).

Figure 7-5 (a-b) illustrates the length changes of UHPC specimens in the form of shrinkage when exposed to the outdoor conditions. The shrinkage is severe for both K-0 and F-0 specimens as the exposure duration prolonged to 720 days. However, the addition of fibers restricts the shrinkage by up to 78% and 83% for slag containing and fly ash containing UHPC specimens, respectively. The restricting effect is lower when only 1%

fiber is used in the mixture. Wioletta et al. (Raczkiewicz, 2017) showed that the addition of 1% steel fibers reduced the total shrinkage of tested specimens by more than 26% in the period of one year. They also reported that the incorporation of 1% steel fiber stabilized the length change in the first 80 days of outdoor exposure. In the present study, the length change is generally stabilized at ages later than 150 days. During almost the same age, the strengths reach the highest, which shows a direct relationship between the length change and strength development, which is reported elsewhere (J. Brooks, 2005). On the other hand, it is observed that slag containing specimens showed almost 24% higher length change than those with fly ash. For conventional concrete, Shariq et al.(Shariq, Prasad, & Abbas, 2016) reported that the concrete with slag exhibited higher shrinkage strain than that of the plain concrete. Slag particles absorb more water than cement, which in a low w/b concrete with insufficient free water can lead to a higher amount of capillary pressure formed in the cement matrix, and results in more severe shrinkage of concrete (Hooton, Stanish, & Prusinski, 2009). On the other hand, the lower activity of the fly ash comparing to that of slag, increases its filling effect and decreases the tortuosity of the system and hence hinders that drying out process (Y. Zhao et al., 2017).

Figure 7-5 (c and d) shows the lengths of UHPC specimens are maintained well in water. Although the same shrinking trend is observed for specimens immersed in water, the change ratio is much lower than those exposed to the outdoor conditions. For example, the length changes of K-0 and F-0 in water are 90%, and 88 % lower than those under outdoor conditions, respectively. The addition of fibers also decreased the length change of specimens but at a lower rate than those exposed to the outdoor conditions. Furthermore, the incorporation of slag and fly ash has a negligible effect on the shrinking behavior of the specimens immersed in water. Similar to the outdoor exposure, a rapid increase is observed in the length during the first 150 days, with a more gradual increase afterwards. The specimens in water have a more stable behavior in the long run than those exposed to the outdoor conditions.

Unlike the former two series of exposures, UHPC specimens in seawater (Figure 7-5 (e-f)) show expansive trend with a magnitude almost like those immersed in water. However, the incorporation of slag causes more expansion compared to that of fly ash. The results show that expansion of K-0 is 11% higher than that of F-0 at 720 days. Addition of 2 and

3% fibers also showes to be more effective in slag containing specimens where 80% and 84% reduction are observed in long run (720 days), respectively. The expansion is more rapid in the first 200 days and becomes more gradual especially in the fly ash containing specimens as the exposure elongated. Santhanam et al.(Manu Santhanam, Cohen, & Olek, 2006a) also reported an expansion of 1.2% in mortars immersed in seawater for a duration of 32 weeks. They related the expansion to the formation of ettringite after 12 weeks of immersion. The quantity of brucite also fluctuated between 2 and 3%; all phase changes were concomitant with the reduction in calcium hydroxide. The expanding behavior of conventional concrete is also reported in other researches, which is related to the formation of Friedel's salt and ettringite due to ingression of chloride and sulfates in the matrix (P. Mehta, 1999; Nagataki & Gomi, 1998; YaoZhong, 1993). Ghazy and Bassuoni (Ghazy & Bassuoni, 2017) reported up to 1% expansion of concrete specimens after 540 days of exposure to different salts. They found that the combination of $MgCl_2$ and $CaCl_2$ (which resembles seawater) had more expansive effect on the specimens than $NaCl_2$ alone. Their results showed a complex mechanism of damage by penetrated $MgCl_2$, by which $Mg^{2+}$ and $Cl^-$ ions caused instability in the pore solution due to the reduction of pH. This process decomposed calcium hydroxide and released $OH^-$ ions to balance the pH of the solution. Increasing the concentration of $Mg^{2+}$ and $OH^-$ ions within the surface of the specimen formed brucite, while $Cl^-$ ions were bound temporarily by the aluminate phases forming Friedel's salt. Furthermore, the presence of high concentration of $Cl^-$ ions led to the formation of porous calcium-silicate-hydrate (C-S-H), due to the leaching of $Ca^{2+}$ ions and formation of soluble $CaCl_2$. As a result, the leaching of $Ca^{2+}$ ions from C-S-H increased the penetration of $Mg^{2+}$ ions into the cement gel, changing it to non-cementitious magnesium-silicate-hydrate (M-S-H).

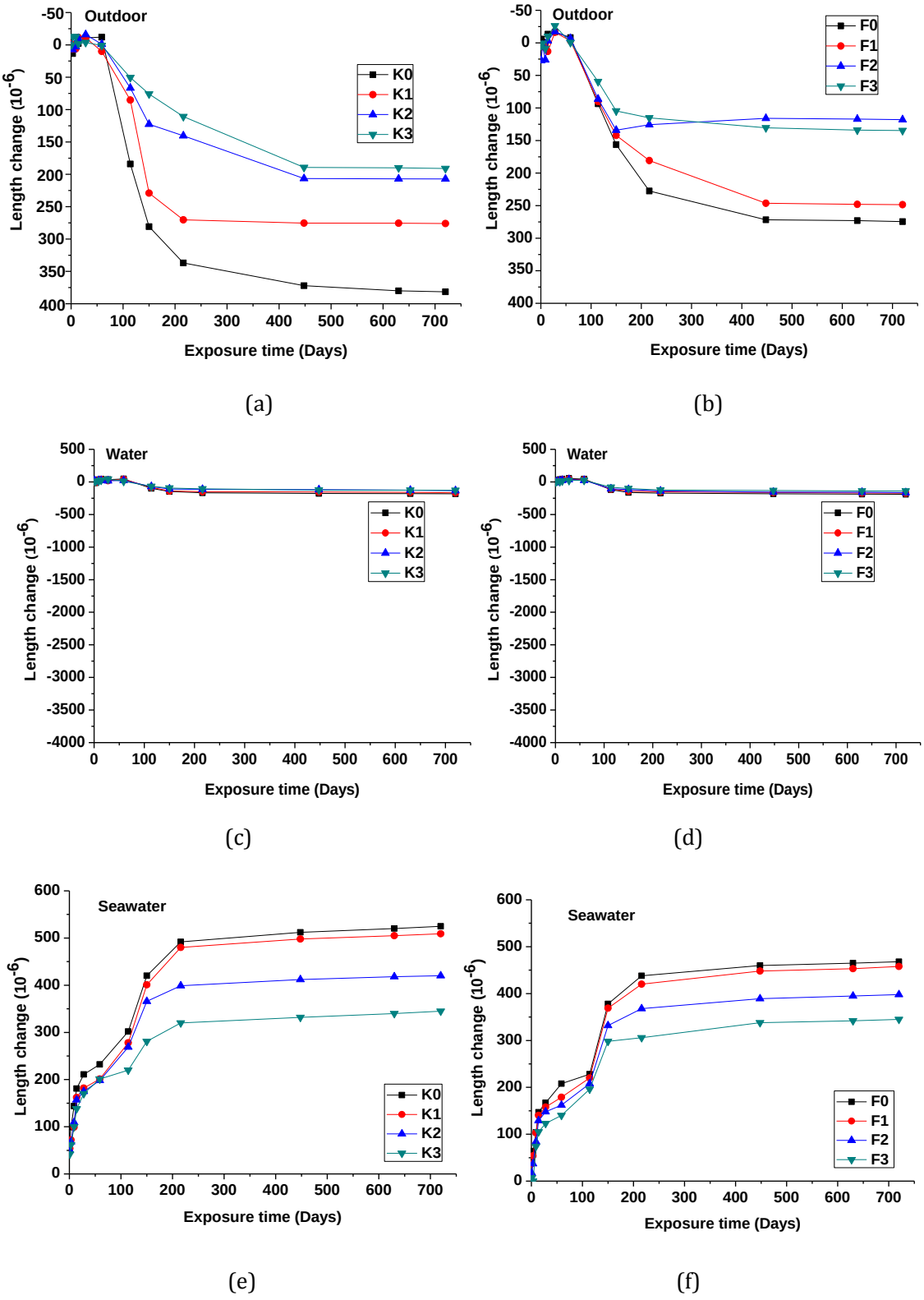


**Figure 7-5.** Length change of UHPCs under different exposure conditions: (a), (c), (e) slag containing UHPC specimens; (b), (d), (f) fly ash containing UHPC specimens.

### 7.4.5 Mass change

Figure 7-6 shows the mass change for the specimens exposed to the three conditions. The results reveal that the changes in the length of the UHPC specimens are concurrent with their mass gain over exposure time, which can be related to the progressive hydration of cementitious binder (Soliman, 2011). However, mass gain has dissimilar increase rates in the slag containing and fly ash containing UHPC specimens when seawater exposure conditions are applied. The increase in the mass is the least in the specimens exposed to outdoor in all UHPC specimens, initiating with a rapid increase at the early ages, with a steady growth along the exposure duration. Comparatively, the mass gain is higher for those specimens immersed in water where up to 0.7% increase is observed in all specimens during the first 150 days with a more gradual increase as the exposure proceeding. The seawater exposed specimen exhibit a rapid mass gain continues to 216 days, up to 1% increase in mass. Santhanam et al. (Manu Santhanam et al., 2006a) reported up to 3% increase in the mass of mortars with w/b of 0.485 after 21 weeks of immersion in seawater. There is a sudden change in the mass initiating at 12 weeks which is attributed to the formation of ettringite after 12 weeks and an increase in the amount of brucite between 12 and 21 weeks, based on thermogravimetric analysis. They also reported a complete consumption of calcium hydroxide with the presence of infiltrated seawater in the matrix. As in carbonation due to outdoor exposure, the depletion of CH along with formation of $CaCO_3$ is reported to bring about up to 11% in volume increase and 35% increase of mass of conventional concrete (Ceukelaire & Nieuwenburg, 1993).
The results here are conclusive that the mass gain in the UHPC specimens exposed to different conditions are much smaller than those in conventional concrete reported earlier (2-12% based on exposure time, specimen size and w/b (M. F. Ba, Qian, & Wang, 2013; Bissonnette, Pierre, & Pigeon, 1999)). However, the incorporation of fly ash and slag has a remarkable influence on the mass gain of specimens exposed to seawater, unlike those maintained in water and outdoor conditions. It should be stated that the mass gain in the specimen immersed in water is in the form of shrinkage while for the seawater exposed specimens, the mass gain caused the expansion. Considering the impermeable property of UHPC matrix, a different mechanism from that of conventional strength concrete is expected.

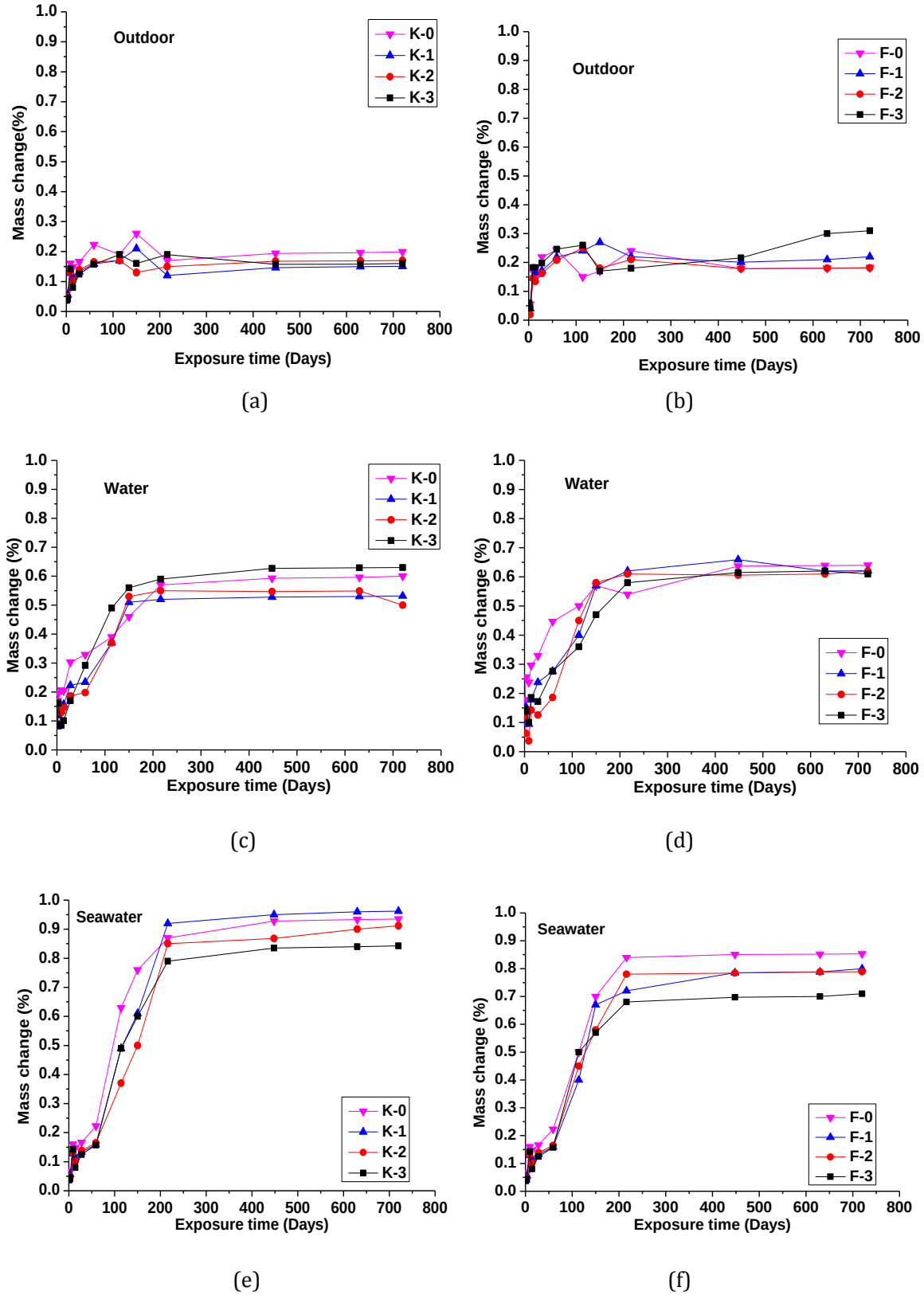


**Figure 7-6.** Mass change of UHPCs under different exposure conditions: (a), (c), (e) slag containing UHPC specimens; (b), (d), (f) fly ash containing UHPC specimens.

## 7.5 Discussion

The results showed that UHPC demonstrated different performances in water, seawater, and outdoor conditions. In general, the UHPC in water gained higher strength in a duration of 720 days, which is concurrent with shrinkage and mass gain. The strength development is more remarkable at later ages for fly ash containing UHPCs and at earlier ages for slag containing UHPCs. However, no significant difference is observed in terms of length change and mass gain. For the specimens exposed to the outdoor conditions, the strength development is at a lower rate comparing to those immersed in water; and less mass gain is noticed. However, their length changes are up to ten times more than those immersed in water. For seawater exposed specimens, a different trend is observed, and the specimens show an expansive behavior. The strength gain is hindered, and a higher mass gain is recorded. The incorporation of fly ash and slag had almost similar effects on specimens when exposed to water and outdoor conditions but differed for those immersed in seawater. On the other hand, the inclusion of fibers especially at higher contents restricts the length change and increases the compressive strength.

For conventional concretes, a similar trend of durability is reported but at higher magnitudes especially when exposed to aggressive conditions (Nanukuttan et al., 2015; M. Santhanam & Otieno, 2016; Thomas, 2016). The reason is mostly related to the diffusion of external ions into the matrix which could adversely affect it due to carbonation (in outdoor conditions) or chloride ingression (in seawater). On the contrary, several researches on the durability of UHPC demonstrated low permeability against diffusion of external agents into the matrix. In the study by Alkaysi et al. (A. Mo et al., 2016), the air void content and the total charge pass were as low as 5.8% and 89 coulombs , respectively, in the UHPC specimens with 1.5% fiber. Yu et al. (R. Yu et al., 2014) reported the porosity was about 3% for the limestone incorporated UHPC, which is in agreement with (Abbas et al., 2015). In another study by Tafraoui et al. (Tafraoui et al., 2016a), the gas permeability of UHPC and chloride diffusion coefficient were reported to be lower than $1.5\times10^{-19}m^2$ and $1.7\times10^{-14}(m^2/s)$, respectively. The superior durability of UHPC is mostly related to the high packing density, low water-to-binder ratio, low porosity and pozzolanic reactivity of supplementary cementitious materials incorporated in the matrix (C. Shi, Wu, Xiao et al., 2015b; D. Wang et al., 2015).

Taking the dense matrix of UHPC into account, the recorded changes in the compressive strength, mass and length of the UHPC specimens in this study needed further study through chemical and microstructural analyses as the diffusion of external agents into the matrix is least probable. In general, two mechanisms can be used to explain the long-term performance of the UHPC specimens in this study. Firstly, limited diffusion of the external agents into the surface layers of specimens can be expected as the exposure time lasts for about 2 years. Figure 7-7 shows the surface and internal fibers in specimens exposed to seawater after 720 days. As seen, the inner fibers are protected from the corrosion, while surface corrosion is apparent. The surface corrosion of fibers is also reported in a previous study (Balouch et al., 2010). However, the surface corrosion alone cannot be responsible for the low strength development of the specimens exposed to seawater as the internal fibers were maintained unaffected, however, development of associated microcracks on the surface can provide path for the external agents to further diffuse in the surface layers. Figure 7-8 (a and b) illustrates the SEM images of the surface and surface layers (in powder form) of the seawater exposed specimens, respectively. The formation of brucite on the surface and co-existence of brucite and calcite in a few micrometers from the surface of the specimens are observed. The same findings were reported by Palin et al. (Palin et al., 2015). The formation of expansive phases as well as surface corrosion can explain the expansion of UHPC specimens in seawater. Santhanam et al. (Manu Santhanam et al., 2006b) reported the deposit of ettringite in a region close to the surface of the conventional concrete specimens in seawater followed by some cracks but at a higher depth comparing to this study. Also, formation of a brucite layer and a small deposit of a mixture of chloroaluminate (possibly Friedel's salt) and sulfoaluminate were noticed [60]. Similar observations were reported by Brown and Badger (Brown & Badger, 2000) and Brown and Doer (Brown & Doerr, 2000).

Figure 7-8 (c and d) illustrates the SEM images of the surface and surface layers (in powder form) of specimens exposed to outdoor conditions. The formation of calcite is detected on surface as well as internal layers near the surface of the specimens. However, in previous studies on carbonation of UHPC in a short-term exposure, the diffusion of $CO_2$ into the matrix is reported to be zero due to the impermeable matrix of the UHPC (Tafraoui et al., 2016b). The formation of $CaCO_3$ on the surface layers of the UHPC can be related to

the long-term exposure to outdoor conditions by which surface corrosion can provide pathway for $CO_2$ to infiltrate into the surface layers. However, the preliminary test on specimens using Phenolphthalein alcohol solution is unable to measure the extent of carbonation due to the very dense matrix of specimens. Therefore, TGA and XRD analyses were performed at selected ages to elaborate the extent of intrusion of aggressive agents.

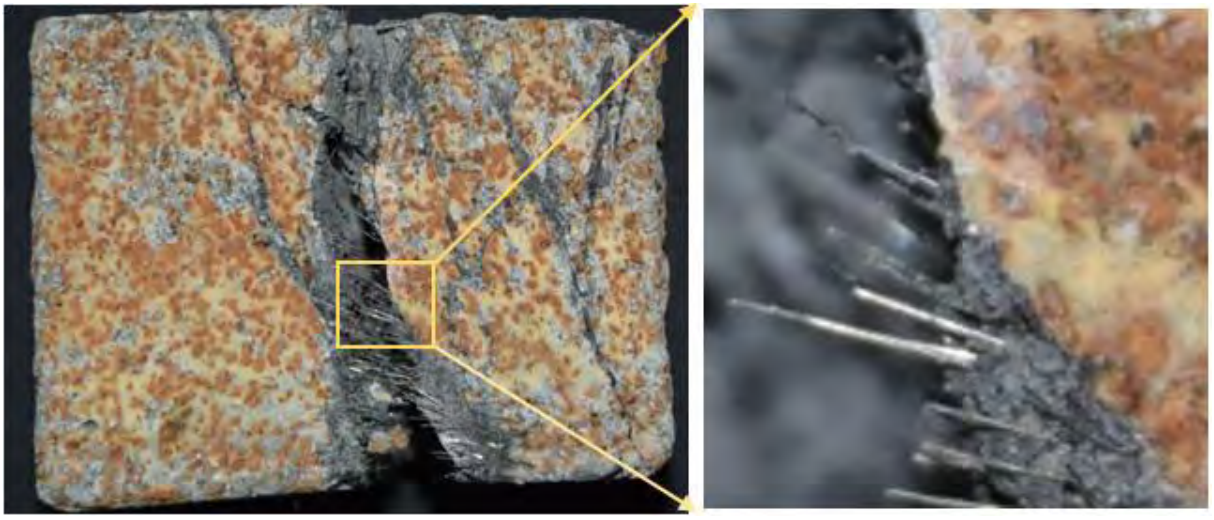

Surface corrosion Internal fibers

**Figure 7-7.** Surface appearance and internal fibers of specimen F-3 exposed to seawater after 720 days.

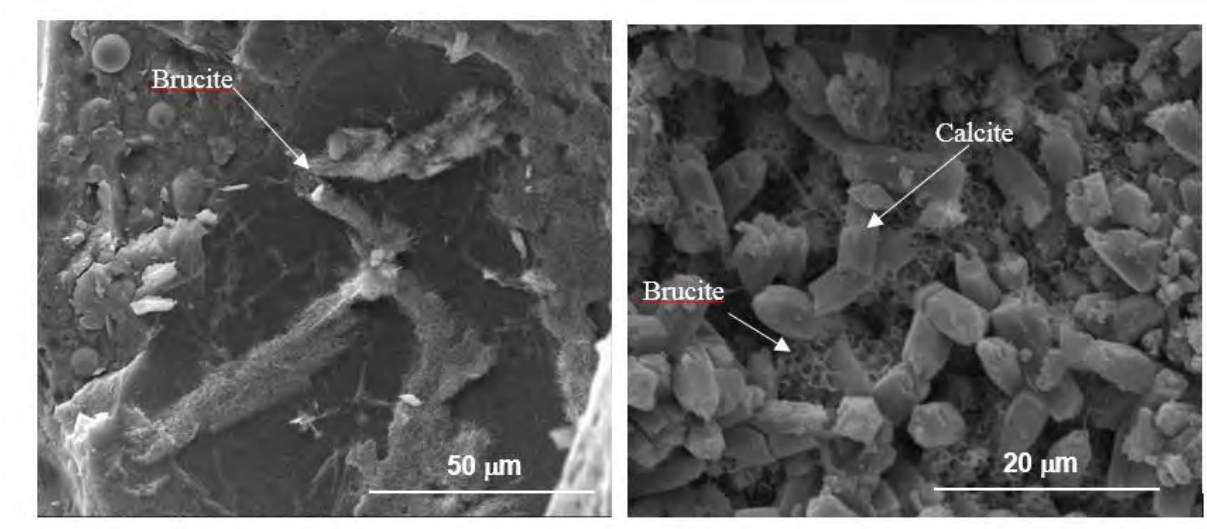


(a) surface of K-0 exposed to seawater at 720 d (b) 0.5 mm internal layer (ground) part

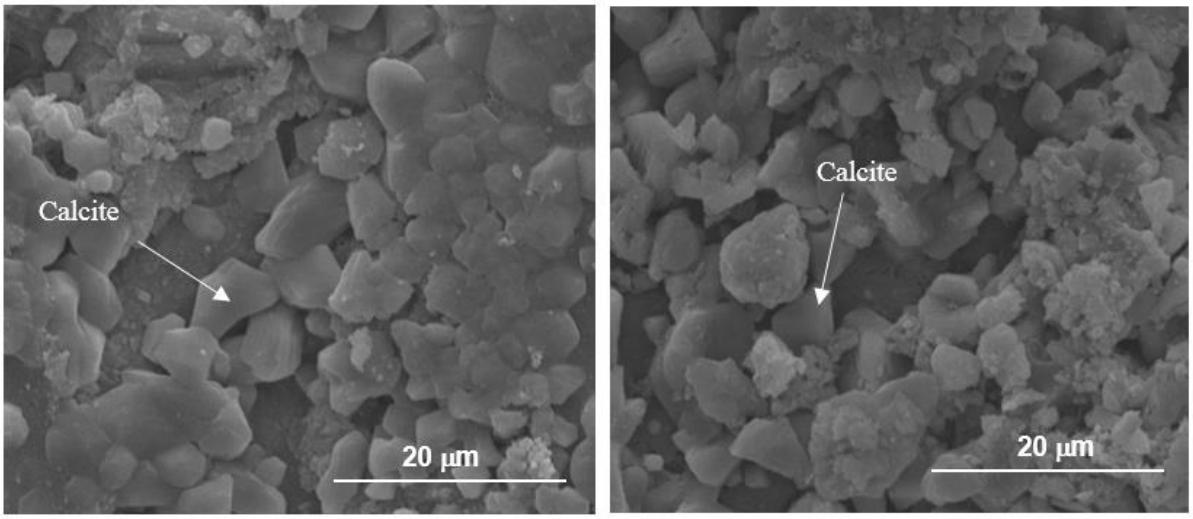


c) surface of F-0 exposed to outdoor conditions at 720 d

d ) 0.5 mm internal layer (ground) part

**Figure 7-8.** SEM images of specimens after exposure.

Figure 7-9 shows TGA curves and the contents of CH and $CaCO_3$ for slag containing and fly ash containing specimens without fibers. As can be seen, the decomposition peaks of calcium hydroxide and $CaCO_3$ were detected at ~180°C and ~780°C, respectively. In general, the results show low amount of CH in the surface layers, which can confirm either consumption of CH by slag and fly ash through pozzolanic reactions [9-10] or another reaction mechanism such as leach-out. As the specimens subjected to the TG analysis contained no fibers, the conventional penetration mechanism due to surface corrosion of fibers is considered as least probable.

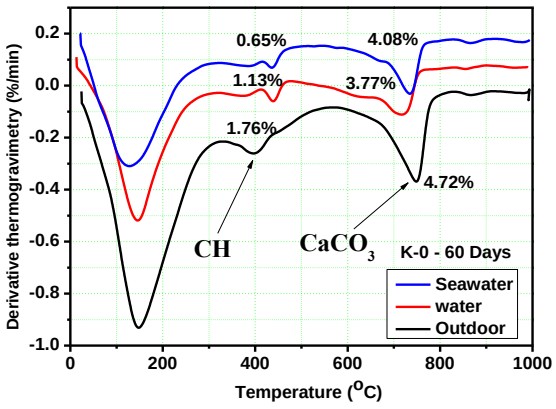


(a) K-0 at 60 d

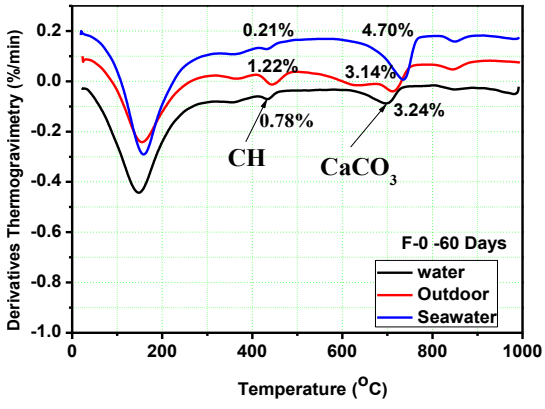


(b) F-0 at 60 d

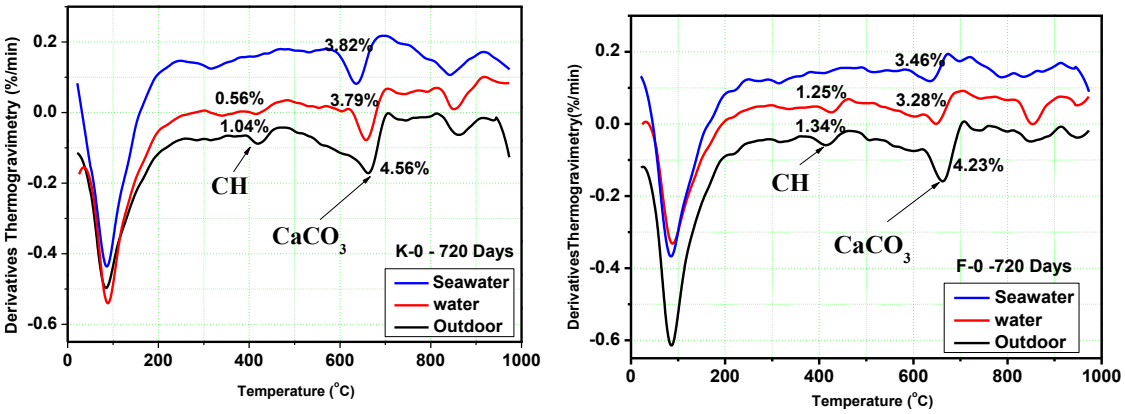


(c) K-0 at 720 d (d) F-0 at 720 d

**Figure 7-9.** TGA curves of UHPCs after exposure to different conditions.

The results reveal that as the exposure prolongs to 720 days, the amount of CH is decreased in all specimens, though, at different rates, which is along with increase in the content of $CaCO_3$. The $CaCO_3$ content is the highest in the specimens exposed to the outdoor condition followed by those immersed in seawater. The XRD patterns from the surface layers also confirm the relative higher contents of $CaCO_3$ in the specimens exposed to the seawater and outdoor conditions.

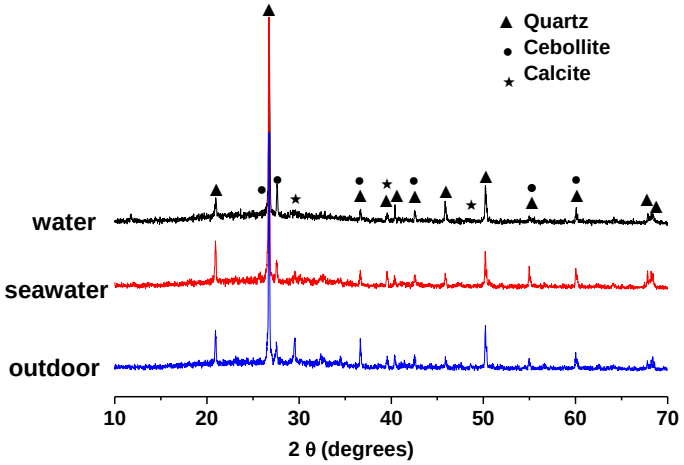


**Figure 7-10.** XRD patterns of F-0 after exposure to different conditions at 720 d.

As the mixture compositions in each series (K-0 and F-0) are the same, it can be concluded that the variation of CH content in specimens after different exposure is due to a factor other than pozzolanic reactions. It is probably dominated by the influence of exposure conditions. The interaction of aggressive ions and the CH can be mainly dominated by the leach out of CH, which was also reported in studies by Carde and François [64] and Heukamp (Carde & François, 1997; Heukamp, 2003). They argued that at the contact of cement-based materials with water, ionic transfer occurs between external water and

soluble matrix. The ionic transfer breaks the chemical equilibrium of the medium and hydrates, so the equilibrium will be restored as long as dissolution or precipitation of hydrates are possible (Matite & Moranville, 1997; Revertegat, Richet, & Gegout, 1992). The calcium hydroxide is the first mineral to be dissolved, followed by progressive decalcification of C-S-H. As for fiber reinforced specimens, it may also be safe to state that the dominant mechanism is the leach-out of CH into the outside environment as surface corrosion can be uniform in all specimens owing to the similar contents of fiber used.

Assuming the dominant role of leach-out, the TGA results show that the CH leaching rate from the matrix varied in different exposure conditions. The rate is at the highest for the specimens exposed to seawater. The mechanism, therefore, can be explained as follows: the rate of leaching is the highest in seawater as the leached CH reacted with chemical constituents in seawater; causing a concentration gradient in the pore solution at the vicinity of the exposed surface, which promoted further leaching (Tasong, Lynsdale, & Cripps, 1999). For examples, the cation ions like $Mg^{2+}$ combine with $SO_4^{2-}$ in seawater can react with CH and calcium monosulfoaluminate hydrate to promote formation of brucite and ettringite, as in the following equation:

$$MgSO_4+Ca(OH)_2+CaO\cdot Al_2O_3\cdot CaSO_4\cdot 18H_2O \rightarrow Mg(OH)_2(\text{Brucite})+3CaO\cdot Al_2O_3\cdot 3CaSO_4\cdot 32H_2O$$

( Ettringite) (7-3)

Formation of brucite continues until $Ca(OH)_2$ is completely depleted in the solution. Soluble carbonates in seawater can further react with CH to form calcite on the surface of the concrete (Morse, Mucci, & Millero, 1980). This can increase the concentration gradient in seawater and hence increase the leaching. It should be noted that in the test setup of this study seawater is refreshed in the tank every 3 weeks so the concentration gradient is maintained throughout the exposure period which enhance the leaching process. In outdoor exposed specimens, the reduction in CH is also observed but at a rate much lower than those in seawater, however, the $CaCO_3$ formation is more pronounced as seen from the TGA curves and XRD patterns. In a consideration of the low to zero penetration in the UHPC (Andrade, Frias, & Aarup, 1996; Piérard, Julie, & Cauberg, 2012), it can be stated that formation of $CaCO_3$ is a result of the reaction of $CO_2$ in the environment with the surface CH rather than infiltration of $CO_2$ into the matrix. The formation of $CaCO_3$ can fill the pores on the surface of the UHPC specimens. As can be seen for Figure 7-10, the CH

contents of specimens exposed to the outdoor condition is the highest one, while the eminent peaks of $CaCO_3$ are also detected, showing the hindering effect of calcite crystallization. Muller et al. (Müller, 2010) reported that carbonation completely filled microcracks. The filling effect of carbonation on the surface layer can also promote the hydration of the cementitious binder by reducing the drying out of the matrix and contribute to further strength gain over time. Besides, the stabilization of changes in mass and length at about 150 days can be related to the filled surface porosity, which could reduce the interaction of CH and external agents and contributed to formation of a closed system reducing changes in mass and length. In this case, the carbonated surface can act like a shield to improve the internal curing and improving the dimensional stability. Similar systems were used by Shi et. al. (Pan, Shi, Jia, Zhang, & Wu, 2015) as in $CO_2$ surface treatment. The remarkable strength development of specimens in the outdoor condition can be attributed to this mechanism. However, in the UHPC specimens with fly ash, the amount of leaching CH and the carbonation rate is less than that of slag containing concrete, which may be related to more gradual hydration process in presence of fly ash. Fly ash reacts with calcium hydroxide in a pozzolanic reaction to produce C-(A)-S-H, which can refine the pore structure and improve the mechanical properties and the impermeability of the matrix (Gebler & Klieger, 1986). In this study, the CH content is the highest for specimens in water, which may also be related to the blockage of the pores but by hydration products at the vicinity of the surface owing to hydration of the adjacent unhydrated particles and water. The filled-out pores can hinder the CH leach-out into the water and contribute to higher strength gain in the specimens.

Overall, the leaching of CH from specimens exposed to seawater and those maintained in the outdoor conditions along with limited diffusion of the external agents into the matrix in fiber reinforced specimens can explain the lower strength gain over the exposure time. For the specimens in water, the maintained calcium hydroxide can react with slag or fly ash to form C-S-H and further strengthen the matrix (Madhavi, Raju, & Mathur, 2014). The higher shrinkage rate in outdoor specimens can also be corresponded to the accumulated carbonation shrinkage resulted from both mechanisms which brought about mass gain as well. On the contrary, the formation of expansive phases on the surface of specimens in seawater such as brucite, calcite as well as the surface corrosion lead to the highest recorded mass and length after the long-term exposure.

## 7.6 Conclusion

This study investigated the effect of supplementary cementitious materials, namely, slag and fly ash, as well as steel fiber content on the long-term performance of UHPC in water, seawater and outdoor conditions for a duration of 720 days. The results from compressive strength, dimensional stability and mass change showed distinct behaviors of the UHPC specimens after exposed to the three different conditions.

- In general, the compressive strength of UHPC specimens in water kept increasing in the period of 720 days. The strength development is more remarkable at later ages for fly ash containing UHPC and at earlier ages for slag containing UHPC. For the specimens exposed to the outdoor condition, the strength development is at a lower rate comparing to those immersed in water. On the contrary, the strength gain is hindered in seawater exposed specimens. The use of steel fibers, especially at 2 and 3% contents increases the strength.
- The length change is in the form of shrinkage in specimens exposed to the outdoor condition, while an expanding trend is observed for the specimens in seawater. The specimens in water show the best dimensional stability. The incorporation of slag and fly ash is not a key influencing the dimensional stability, while increase in the fiber contents contributes to more stable behavior of the UHPC in terms of length change.
- The exposure conditions also affect the mass change for both slag and fly ash containing specimens over time, albeit, it was significantly lower than those recorded for the conventional concrete reported in the literature. The mass gain is the highest in seawater exposed specimens followed by those kept in water. The specimens exposed to the outdoor conditions have the lowest change in mass in which up to only 0.2% is recorded. Neither fiber content nor incorporation of slag/fly have significant effect on the mass gain during the exposure duration.
- The slow diffusion of external agents into the surface layers and the CH leach-out are two possible mechanisms responsible for the distinct long-term performance of the UHPC specimens exposed to three different conditions. However, results of TGA and XRD on specimens without fibers show that CH leach-out should be the dominant mechanism. TGA curves shows that the CH content in seawater exposed specimens is detected to be the lowest at 60 and 720 days. As the comparison is

made in the specimens of the same mixture composition, it is concluded that the CH leached out from the matrix varied due to the difference in exposure conditions.

## 7.7 References


P. Acker, M. Behloul, Ductal® technology: A large spectrum of properties, a wide range of applications, Proc. of the Int. Symp. on UHPC Kassel, Germany, 2004, pp. 11-23.

M. Schmidt, E. Fehling, Ultra-High-Performance Concrete: Research, Development and Application in Europe, Seventh International Symposium on the Utilization of High-Strength/High-Performance Concrete, ACI SP-288, American Concrete Institute, 1 & 2 (2005).

D. Wang, C. Shi, Z. Wu, J. Xiao, Z. Huang, Z. Fang, A review on ultra high performance concrete: Part II. Hydration, microstructure and properties, Construction & Building Materials, 96 (2015) 368-377.

S. Abbas, A.M. Soliman, M.L. Nehdi, Exploring mechanical and durability properties of ultra-high performance concrete incorporating various steel fiber lengths and dosages, Construction & Building Materials, 75 (2015) 429-441.

A. Tafraoui, G. Escadeillas, T. Vidal, Durability of the Ultra High Performances Concrete containing metakaolin, Construction & Building Materials, 112 (2016) 980-987.

P. Julie, B. Dooms, N. Cauberg, Evaluation of durability parameters of UHPC using accelerated lab tests, Proceedings of the 3rd International Symposium on UHPC and Nanotechnology for High Performance Construction MaterialsKassel, Germany, 2012, pp. 371-376.

M.M. Islam, M.S. Islam, B.C. Mondal, M.R. Islam, Strength behavior of concrete using slag with cement in sea water environment, J Civ Eng, (2009).

F. Leng, N. Feng, X. Lu, An experimental study on the properties of resistance to diffusion of chloride ions of fly ash and blast furnace slag concrete, Cement and Concrete Research, 30 (2000) 989-992.

W. Pengsheng, W. Shengnian, Z.F. Jianbo XIONG, A Comprehensive Cost Analysis Related to Anti-corrosion Design and Total Life Cycle of Coastal Engineering Constructions Assigned for Different Length of Service Life, Corrosion Science and Protetion Technology, 30 (2017) 99-104.

P. Aıtcin, The durability characteristics of high performance concrete: a review, Cement and concrete composites, 25 (2003) 409-420.

S. Manzi, C. Mazzotti, M. Bignozzi, Short and long-term behavior of structural concrete with recycled concrete aggregate, Cement and Concrete Composites, 37 (2013) 312-318.

H. Mihashi, T. Nishiwaki, Development of Engineered Self-Healing and Self-Repairing Concrete-State-of-the-Art Report, ACT, 10 (2012) 170-184.

M. Wu, B. Johannesson, M. Geiker, A review: Self-healing in cementitious materials and engineered cementitious composite as a self-healing material, Construction & Building Materials, 28 (2012) 571-583.

B. Hilloulin, F. Grondin, M. Matallah, A. Loukili, Modelling of autogenous healing in ultra high performance concrete, Cement & Concrete Research, 61-62 (2014) 64-70.

R. Davies, A. Jefferson, Micromechanical modelling of self-healing cementitious materials, International Journal of Solids & Structures, (2017).

P.-K. Chang, W.-M. Hou, A study on the hydration properties of high performance slag concrete analyzed by SRA, Cement and Concrete Research, 33 (2003) 183-189.

A. Elahi, P. Basheer, S. Nanukuttan, Q. Khan, Mechanical and durability properties of high performance concretes containing supplementary cementitious materials, Construction and Building Materials, 24 (2010) 292-299.

C. Shi, D. Wang, L. Wu, Z. Wu, The hydration and microstructure of ultra high-strength concrete with cement–silica fume–slag binder, Cement & Concrete Composites, 61 (2015) 44-52.

T. EN, 196-1. Methods of testing cement–Part 1: Determination of strength, European Committee for standardization, 26 (2005).

NetAnswer, Effect of fly ash gradation on workability, strength and durability of Portland cement fly ash mortars, Materials & Structures.

O.M. Abdulkareem, A.B. Fraj, M. Bouasker, A. Khelidj, Effect of chemical and thermal activation on the microstructural and mechanical properties of more sustainable UHPC, Construction & Building Materials, 169 (2018) 567-577.

N.K. Lee, K. Koh, M.O. Kim, G. Ryu, Uncovering the role of micro silica in hydration of ultra-high performance concrete (UHPC), Cement and Concrete Research, 104 (2018) 68-79.

K. Habel, M. Viviani, E. Denarié, E. Brühwiler, Development of the mechanical properties of an ultra-high performance fiber reinforced concrete (UHPFRC), Cement and Concrete Research, 36 (2006) 1362-1370.

K. Wille, A.E. Naaman, S. El-Tawil, G.J. Parra-Montesinos, Ultra-high performance concrete and fiber reinforced concrete: achieving strength and ductility without heat curing, Materials and structures, 45 (2012) 309-324.

A.L. Hoang, E. Fehling, Influence of steel fiber content and aspect ratio on the uniaxial tensile and compressive behavior of ultra high performance concrete, Construction & Building Materials, 153 (2017) 790-806.

T. Simões, C. Octávio, J. Valença, H. Costa, D. Dias-Da-Costa, E. Júlio, Influence of concrete strength and steel fibre geometry on the fibre/matrix interface, Composites Part B Engineering, 122 (2017).

Z. Wu, C. Shi, K.H. Khayat, Influence of silica fume content on microstructure development and bond to steel fiber in ultra-high strength cement-based materials (UHSC), Cement & Concrete Composites, 71 (2016) 97-109.

E. Gruyaert, P.V.D. Heede, N.D. Belie, Carbonation of slag concrete: Effect of the cement replacement level and curing on the carbonation coefficient – Effect of carbonation on the pore structure, Cement & Concrete Composites, 35 (2013) 39-48.

NetAnswer, Long term carbonation of UHPC, Materials & Structures.

N. Bouzoubaa, M.-H. Zhang, V. Malhotra, D.M. Golden, Blended fly ash cements a review, Materials Journal, 96 (1999) 641-650.

K. De Weerdt, M.B. Haha, G. Le Saout, K.O. Kjellsen, H. Justnes, B. Lothenbach, Hydration mechanisms of ternary Portland cements containing limestone powder and fly ash, Cement and Concrete Research, 41 (2011) 279-291.

F. Deschner, F. Winnefeld, B. Lothenbach, S. Seufert, P. Schwesig, S. Dittrich, F. Goetz-Neunhoeffer, J. Neubauer, Hydration of Portland cement with high replacement by siliceous fly ash, Cement and Concrete Research, 42 (2012) 1389-1400.

Y. Zhao, J. Gong, S. Zhao, Experimental study on shrinkage of HPC containing fly ash and ground granulated blast-furnace slag, Construction & Building Materials, 155 (2017) 145-153.

M. Ahmaruzzaman, A review on the utilization of fly ash, Progress in energy and combustion science, 36 (2010) 327-363.

W. Chalee, C. Jaturapitakkul, Long Term Performance of Fly Ash Concrete in Marine Environment, The Eighth ISOPE Pacific/Asia Offshore Mechanics Symposium, International Society of Offshore and Polar Engineers, 2008.

E.G. Moffatt, M.D.A. Thomas, A. Fahim, Performance of high-volume fly ash concrete in marine environment, Cement & Concrete Research, (2017).

D.Y. Yoo, N. Banthia, Mechanical properties of ultra-high-performance fiber-reinforced concrete: A review, Cement & Concrete Composites, 73 (2016) 267-280.

W. Raczkiewicz, The effect of micro-reinforcement steel fibers addition on the size of the shrinkage of concrete and corrosion process of the main reinforcement bars, Procedia Engineering, 195 (2017) 155-162.

J. Brooks, 30-year creep and shrinkage of concrete, Magazine of concrete research, 57 (2005) 545-556.

M. Shariq, J. Prasad, H. Abbas, Creep and drying shrinkage of concrete containing GGBFS, Cement and Concrete Composites, 68 (2016) 35-45.

R.D. Hooton, K. Stanish, J. Prusinski, The effect of ground granulated blast furnace slag (slag cement) on the drying shrinkage of concrete–a critical review of the literature, Slag Cement Concrete, (2009) 79-94.

M. Santhanam, M. Cohen, J. Olek, Differentiating seawater and groundwater sulfate attack in Portland cement mortars, Cement and Concrete Research, 36 (2006) 2132-2137.

S. Nagataki, H. Gomi, Expansive admixtures (mainly ettringite), Cement and concrete composites, 20 (1998) 163-170.

P. Mehta, Sulfate attack in marine environment, American Ceramic Society, Inc, Materials Science of Concrete: Sulfate Attack Mechanisms(USA), (1999) 295-299.

X. YaoZhong, RECENT PROGRESS IN CEMENT CHEMISTRY——NOTES ON THE 9TH INTERNATIONAL CONGRESS ON THE CHEMISTRY OF CEMENT [J], Journal of The Chinese Ceramic Society, 6 (1993) 014.

A. Ghazy, M.T. Bassuoni, Resistance of concrete to different exposures with chloride-based salts, Cement & Concrete Research, 101 (2017) 144-158.

A.M. Soliman, Early-age shrinkage of ultra high-performance concrete: mitigation and compensating mechanisms, (2011).

L.D. Ceukelaire, D.V. Nieuwenburg, Accelerated carbonation of a blast-furnace cement concrete, Cement & Concrete Research, 23 (1993) 442-452.

B.T. Bissonnette, P. Pierre, M. Pigeon, Influence of key parameters on drying shrinkage of cementitious materials, Cement & Concrete Research, 29 (1999) 1655-1662.

M.F. Ba, C.X. Qian, H. Wang, Effects of specimen shape and size on water loss and drying shrinkage of cement-based materials, J Wuhan Univ Technol, 28 (2013) 733-740.

S.V. Nanukuttan, P.A.M. Basheer, W.J. Mccarter, L. Tang, N. Holmes, T.M. Chrisp, G. Starrs, B. Magee, The performance of concrete exposed to marine environments: Predictive modelling and use of laboratory/on site test methods, Construction & Building Materials, 93 (2015) 831-840.

M. Thomas, 6 – The durability of concrete for marine construction : Materials and properties, Marine Concrete Structures, (2016) 151-170.

M. Santhanam, M. Otieno, Deterioration of concrete in the marine environment, 2016.

A. Mo, S. El-Tawil, Z. Liu, W. Hansen, Effects of silica powder and cement type on durability of ultra high performance concrete (UHPC), Cement & Concrete Composites, 66 (2016) 47-56.

R. Yu, P. Spiesz, H.J.H. Brouwers, Effect of nano-silica on the hydration and microstructure development of Ultra-High Performance Concrete (UHPC) with a low binder amount, Construction & Building Materials, 65 (2014) 140-150.

C. Shi, Z. Wu, J. Xiao, D. Wang, Z. Huang, Z. Fang, A review on ultra high performance concrete: Part I. Raw materials and mixture design, Construction & Building Materials, 101 (2015) 741-751.

S. Balouch, J. Forth, J.-L. Granju, Surface corrosion of steel fibre reinforced concrete, Cement and Concrete Research, 40 (2010) 410-414.

D. Palin, V. Wiktor, H.M. Jonkers, Autogenous healing of marine exposed concrete: Characterization and quantification through visual crack closure, Cement & Concrete Research, 73 (2015) 17-24.

M. Santhanam, M. Cohen, J. Olek, Differentiating seawater and groundwater sulfate attack in Portland cement mortars, Cement & Concrete Research, 36 (2006) 2132-2137.

P.W. Brown, S. Badger, The distributions of bound sulfates and chlorides in concrete subjected to mixed NaCl, MgSO 4 , Na 2 SO 4 attack, Cement & Concrete Research, 30 (2000) 1535-1542.

P.W. Brown, A. Doerr, Chemical changes in concrete due to the ingress of aggressive species, Cement & Concrete Research, 30 (2000) 411-418.

A. Tafraoui, G. Escadeillas, T. Vidal, Durability of the ultra high performances concrete containing metakaolin, Construction and Building Materials, 112 (2016) 980-987.

C. Carde, R. François, Effect of the leaching of calcium hydroxide from cement paste on mechanical and physical properties, Cement and Concrete Research, 27 (1997) 539-550.

F.H. Heukamp, Chemomechanics of calcium leaching of cement-based materials at different scales: The role of CH-dissolution and CSH degradation on strength and durability performance of materials and structures, Massachusetts Institute of Technology, 2003.

E. Revertegat, C. Richet, P. Gegout, Effect of pH on the durability of cement pastes, Cement and Concrete Research, 22 (1992) 259-272.

V. Matite, M. Moranville, The leaching of the reactive powder concretes: results on transfer properties, MRS Online Proceedings Library Archive, 503 (1997).

W.A. Tasong, C.J. Lynsdale, J.C. Cripps, Aggregate-cement paste interface: Part I. Influence of aggregate geochemistry, Cement and Concrete Research, 29 (1999) 1019-1025.

J.W. Morse, A. Mucci, F.J. Millero, The solubility of calcite and aragonite in seawater of 35%. salinity at 25 C and atmospheric pressure, Geochimica et Cosmochimica Acta, 44 (1980) 85-94.

Piérard, B.D. Julie, N. Cauberg, Evaluation of durability parameters of UHPC using accelerated lab tests, the 3rd International Symposium on UHPC and Nanotechnology for High Performance Construction MaterialsKassel, Germany, 2012, pp. 371-376.

M.C. Andrade, M. Frias, B. Aarup, Durability of ultra-high strength concrete: compact reinforced composite, BHP96 Fourth International Symposium on Utilization of High-Strength/High-Performance Concrete 1996, pp. 29-31.

C. Müller, Durability of Ultra-High Performance Concrete (UHPC), the Third International fib Congress and Exhibition Incorporating the PCI Annual

Convention and National Bridge Conference, Compact Disc, Washington, DC, 2010, pp. 135.

X. Pan, C. Shi, L. Jia, J. Zhang, L. Wu, Effect of inorganic surface treatment on air permeability of cement-based materials, Journal of Materials in Civil Engineering, 28 (2015) 04015145.

S.H. Gebler, P. Klieger, Effect of fly ash on the durability of air-entrained concrete, Special Publication, 91 (1986) 483-520.

T.C. Madhavi, L.S. Raju, D. Mathur, Durabilty and strength properties of high volume fly ash concrete, Journal of Civil Engineering Research, 4 (2014) 7-11.

# CHAPTER 8 CONCLUSIONS AND FUTURE WORK

## 8.1 General discussion

The aim of this thesis was to conduct fundamental research on the early-age shrinkage and long-term stability of UHPC, their micromechanics, formation kinetics and stability, to ensure highly durable products. Based on systematic experimental studies on setting and hardening process, microstructure development, deformation, increase of toughness, constitutive relationships and durability, it clarified the mechanisms of setting and hardening, the features of microstructure development, and the relationships between microstructure and macro-properties of UHPC. The effects of fibres on toughness of UHPC will be explained. Based on the migration of chloride ion in UHPC, the requirements for cover design of rebar reinforced UHPC structure in marine environments was be proposed. The research works included understanding UFA physics and chemistry and their effects on the UHPC early age hydration reactivity, investigating the effects of slag, fly ash, and fiber contents on long-term strength development, dimensional stability, and mass change in three exposure conditions: water, seawater, and outdoor, for a duration of hydration and microstructure development. The research was provide scientific base for production and application of UHPC in Australia.

The first key outcome of this research was the discovery the effect of supplementary cementitious materials, namely, slag and fly ash, as well as steel fiber content on the long-term performance of UHPC in water, seawater and outdoor conditions for a duration of 1080 days. The results from compressive strength, dimensional stability and mass change showed distinct behaviors of the UHPC specimens after exposed to the three different conditions. The results from compressive strength, dimensional stability and mass change showed distinct behaviors of the UHPC specimens after exposed to the three different conditions. The second key outcome is as the discovery of the importance of fly ash particle physics in UHPC, which answered a set of questions concerning which UFA is most suitable and why, and understood the micromechanism of autogenous shrinkage and drying shrinkage from pore structure, mechanical, moisture lose and chemical stability.

## 8.2 Conclusions

Based on the results from this study, the following conclusions can be drawn:

In chapter 2, Autogenous shrinkage is an unavoidable volume reduction due to the self-desiccation of concrete, especially when low water-to-cement ratio is applied. Capillary tension theory well explicates the autogenous mechanism in concrete. This theory can elaborate the accentuated influence of low water-to-cement ratio and SCMs in autogenous shrinkage of HPC as they remarkably affect the pore structure, relative humidity, self-stress, degree of hydration, and interface structure. Although some studies have addressed the effects of pore structure and relative humidity in particular on autogenous shrinkage, the role of self-stress, degree of hydration and interface structure are mostly discussed through influence of cement, SCMs, aggregates, and etc. The utilization of low temperature and spherical shape cement can properly reduce autogenous shrinkage. Appropriate contents of fly ash can inhibit autogenous shrinkage of concrete, while silica fume increases autogenous shrinkage. The effect of slag on autogenous shrinkage, though, depends on its fineness. The impact of steel fiber is associated with the content; low amount of steel fibers can restrain the autogenous shrinkage of concrete, while excessive contents increase cohesiveness and decrease workability of high performance concrete, which can lead to furthered autogenous shrinkage.

In chapter 3 reports the effects of steel fibre on the autogenous shrinkage of UHPC was evaluated by using ring tests and corrugated tube method under plastic film sealed conditions. The results indicated that the development of autogenous shrinkage of UHPC was mainly during the first 24 hours. The autogenous shrinkage of UHPC is significant reduced by adding steel fibre. The optimal fibre content was found to be 3% where UHPC exhibited highest strength (107 MPa at 3 day) and lowest autogenous shrinkage (750×10-6μm at 3 day, which was only 30% of that of the specimens without steel fibre).

In chapter 4 reports the study of the influence of steel fibers on drying shrinkage of ultra-high performance concrete (UHPC) at fiber volume content of 0%, 1%, 2% and 3%, temperature of 20 ± 2°C and relative humidity of 50 ± 5%. The results showed that during the first 7 days, the drying shrinkage rate of UHPC was very fast, while after 7 days it gradually decreased. The interfacial bonding of steel fiber and the physical properties of

steel fiber can effectively reduce the drying shrinkage. However, when the steel fiber exceeds an optimal volume, the effect of steel fiber on drying shrinkage can decrease. Compared with the steel fiber content at 2%, the drying shrinkage of the UHPC with 3% steel fiber was decreased by only 1.5%. The reason is that the increase in the steel fiber leads to an increase in the interface layer, the interface transition zone is usually more porous than the matrix, which easily leads to shrinkage, and consequently reducing the beneficial effect of steel fiber on drying shrinkage control. It was also found that the inhibition of fly ash on the drying shrinkage of UHPC was higher than slag. The experiment also tested the classic dry shrinkage models: the ACI model and the Wang Tiemeng model. Based on the two models and the experimental fitting, a new mathematical model (a combined index model) has been proposed. The results showed that the combined index model fitted better than the two models mentioned above.

In chapter 5 is about the Effects of ultra-fine fly ash (UFA) content on early-age shrinkage and microstructure development of ultra-high strength cement-based materials (UHSC). Due to the accelerated hydration of cement by UFA the compressive and flexural strengths of UHSC containing UFA were significantly enhanced at early age up to 7 d. After 7 d, about 11% increase in strengths was obtained. The compressive and flexural strengths of UHSC samples with 20% silica fume at 91 d were 28% and 29% higher than those of the reference sample, respectively. However, when 25% silica fume was replaced, strengths decreased due to reduced workability and entrapment of air bubbles.

In chapter 6 and 7 is about the long term hydration mechanisms and microstructure development of UHPC, Due to the ball effect of fly ash, the flowability of UHPCs containing fly ash were better than UHPCs containing slag. With the increase of the content of steel fiber, the flowability of fresh UHPCs decreased, cause the Elastic Modulus and physical effect of steel fiber. TG/DTG analyses indicated that UHPC specimens exposed to seawater at 1080 d also efficiently consumed the CH. The TGA/DTG results indicated that $Ca(OH)_2$ was consumed with the formation of $CaCO_3$ (calcite) due to the carbonation effect in outdoor conditions whereas for the water and seawater immersion conditions, the $Ca(OH)_2$ was transformed into other reaction products including $Mg(OH)_2$ and ettringite. Moreover, seawater and water condition led to a loss of C-S-H gel, which was especially the case after 28 day of immersion. Fiber addition improved the performance of fly ash (FA) based UHPC, while it had little impact on the slag-based counterpart. Because of a

denser microstructure evidenced by diffusion coefficient and porous characteristics, slag based samples.

In general, the compressive strength of UHPC specimens in water kept increasing in the period of 1080 days. The strength development is more remarkable at later ages for fly ash containing UHPC and at earlier ages for slag containing UHPC. For the specimens exposed to the outdoor condition, the strength development is at a lower rate comparing to those immersed in water. On the contrary, the strength gain is hindered in seawater exposed specimens. The use of steel fibres, especially at 2 and 3% contents increases the strength. The length change is in the form of shrinkage in specimens exposed to the outdoor condition, while an expanding trend is observed for the specimens in seawater. The specimens in water show the best dimensional stability. The incorporation of slag and fly ash is not a key influencing the dimensional stability, while increase in the fiber contents contributes to more stable behaviour of the UHPC in terms of length change. The exposure conditions also affect the mass change for both slag and fly ash containing specimens over time, albeit, it was significantly lower than those recorded for the conventional concrete reported in the literature. The mass gain is the highest in seawater exposed specimens followed by those kept in water. The specimens exposed to the outdoor conditions have the lowest change in mass in which up to only 0.2% is recorded. Neither fiber content nor incorporation of slag/fly have significant effect on the mass gain during the exposure duration. The slow diffusion of external agents into the surface layers and the CH leach-out are two possible mechanisms responsible for the distinct long-term performance of the UHPC specimens exposed to three different conditions. However, results of TGA and XRD on specimens without fibers show that CH leach-out should be the dominant mechanism. TGA curves shows that the CH content in seawater exposed specimens is detected to be the lowest at 60 and 720 days. As the comparison is made in the specimens of the same mixture composition, it is concluded that the CH leached out from the matrix varied due to the difference in exposure conditions.

## 8.3 Future work

This research was try to understand the hydration mechanisms and microstructure development of UHPC with a wide range of densities and strengths under laboratory conditions. In the research two important issues were noted: the high shrinkage of UHPC and modelling of hydration based on UHPC. The following aspects of the efforts also need to be carried out:

(1) The definition of shrinkage is not entirely unified, and the established test methods also lack uniform standards, which restricts the further development of this field.

(2) The effect of supplementary cementitious materials on shrinkage deformation behaviour is still controversial, and its mechanism shows absence of an in-depth study.

(3) Researches mostly intend for a single shrinkage behaviour, but ignore the connection between various shrinkage mechanisms, which is difficult to grasp the characteristics of shrinkage and deformation of concrete.

(4) The researches on mechanism of autogenous shrinkage are mainly limited to the capillary theory, and some factors have not been taken into account, such as temperature and the type of supplementary cementitious materials. Moreover, effects of mixing content on shrinkage strain rate and ultimate shrinkage value are also unclear. Simultaneously, the influence mechanism of internal curing agents on autogenous shrinkage should be further reconnoitred.

(5) As the UHPC is a complex multi-phase material, the structure can change because of hydration heat and different components used. Therefore, the multiscale homogenous approach should take the time scale, scholastic and the chemical admixtures into account. The multiscale XFEM can describe the multiple phase materials and track the dynamic boundary of inclusion (like aggregate, C-S-H gel, fiber) with level set method and can be applied instead of FEM.

# References


Abbas, S., Soliman, A. M., & Nehdi, M. L. (2015). Exploring mechanical and durability properties of ultra-high performance concrete incorporating various steel fiber lengths and dosages. *Construction & Building Materials, 75*, 429-441.

Abdulkareem, O. M., Fraj, A. B., Bouasker, M., & Khelidj, A. (2018). Effect of chemical and thermal activation on the microstructural and mechanical properties of more sustainable UHPC. *Construction & Building Materials, 169*, 567-577.

Acker, P. (2004). Swelling, shrinkage and creep: a mechanical approach to cement hydration. *Materials and structures, 37*(4), 237-243.

Acker, P., & Behloul, M. (2004). *Ductal® technology: A large spectrum of properties, a wide range of applications.* Paper presented at the Proc. of the Int. Symp. on UHPC Kassel, Germany.

Aftcin, P.-C., Bédard, C., Plumat, M. S. M., & Haddad, G. (1984). Very high strength cement for very high strength concrete. *MRS Online Proceedings Library Archive, 42*.

Aggarwal, V., Gupta, S., & Sachdeva, S. (2010). Concrete durability through high volume fly ash concrete (HVFC) a literature review. *International Journal of Engineering Science and Technology, 2*(9), 4473-4477.

Ahmad, S. (2003). Reinforcement corrosion in concrete structures, its monitoring and service life prediction—a review. *Cement and Concrete Composites, 25*(4-5), 459-471.

Ahmaruzzaman, M. (2010). A review on the utilization of fly ash. *Progress in energy and combustion science, 36*(3), 327-363.

Aitcin, P. (1999). *17 AUTOGENOUS SHRINKAGE MEASUREMENT.* Paper presented at the Autogenous shrinkage of concrete: proceedings of the international workshop, organised by JCI (Japan Concrete Institute), Hiroshima, June 13-14, 1998.

Aıtcin, P. (2003). The durability characteristics of high performance concrete: a review. *Cement and Concrete Composites, 25*(4), 409-420.

Aitcin, P. C. (1986). Concrete structure, properties and materials. *Preticehall International, 13*(4), 499-499.

Aïtcin, P. C. (2003). The durability characteristics of high performance concrete: a review. *Cement and Concrete Composites, 25*(4–5), 409-420. doi:http://doi.org/10.1016/S0958-9465(02)00081-1

Alaee, F. J. (2002). *Retrofitting of concrete structures using high performance fibre reinforced cementitious composite (HPFRCC).* Cardiff University.

Alarcon-Ruiz, L., Platret, G., Massieu, E., & Ehrlacher, A. (2005). The use of thermal analysis in assessing the effect of temperature on a cement paste. *Cement and Concrete Research, 35*(3), 609-613. doi:https://doi.org/10.1016/j.cemconres.2004.06.015

Aldahdooh, M., Bunnori, N. M., & Johari, M. M. (2013). Evaluation of ultra-high-performance-fiber reinforced concrete binder content using the response surface method. *Materials & Design, 52*, 957-965.

Aldred, J. M., Holland, T. C., Morgan, D. R., Roy, D. M., Bury, M. A., Hooton, R. D., . . . Jaber, T. M. (2006). Guide for the use of silica fume in concrete. *Reported by ACI–American Concrete Institute–Committee, 234*.

Andrade, M. C., Frias, M., & Aarup, B. (1996). *Durability of ultra-high strength concrete: compact reinforced composite*. Paper presented at the BHP96 Fourth International Symposium on Utilization of High-Strength/High-Performance Concrete

Andreasen, A., & Andersen, J. (1930). About the Relationship between Density and Particle Spacing in Products Made of Loose Particles: Kolloid.

Attiogbe, E. K., Weiss, W., & See, H. T. (2004). *A look at the stress rate versus time of cracking relationship observed in the restrained ring test.* Paper presented at the The Advances in Concrete Through Science and Engineering, a Rilem International Conference.

Ba, M., Qian, C., & Hui, W. (2013). Effects of specimen shape and size on water loss and drying shrinkage of cement-based materials. *Journal of Wuhan University of Technology, 28*(4), 733-740.

Ba, M. F., Qian, C. X., & Wang, H. (2013). Effects of specimen shape and size on water loss and drying shrinkage of cement-based materials. *Journal of Wuhan University of Technology-Materials Science Edition, 28*(4), 733-740.

Balouch, S., Forth, J., & Granju, J.-L. (2010). Surface corrosion of steel fibre reinforced concrete. *Cement and Concrete Research, 40*(3), 410-414.

Bangham, D. H., Fakhoury, N., & Mohamed, A. F. (1932). The Swelling of Charcoal. Part II. Some Factors Controlling the Expansion Caused by Water, Benzene and Pyridine Vapours. *Proceedings of the Royal Society of London, 138*(834), 162-183.

Bao, Y., Meng, W., Chen, Y., Chen, G., & Khayat, K. H. (2015). Measuring mortar shrinkage and cracking by pulse pre-pump Brillouin optical time domain analysis with a single optical fiber. *Materials Letters, 145*, 344-346.

Barbhuiya, S., Gbagbo, J., Russell, M., & Basheer, P. (2009). Properties of fly ash concrete modified with hydrated lime and silica fume. *Construction and Building Materials, 23*(10), 3233-3239.

Bărbos, G. A. (2016). Long-term Behavior of Ultra–High Performance Concrete (UHPC) Bended Beams. *Procedia Technology, 22*, 203-210.

Barr, B., Hoseinian, S., & Beygi, M. (2003). Shrinkage of concrete stored in natural environments. *Cement and Concrete Composites, 25*(1), 19-29.

Bazant, Z. P., & Baweja, S. (1995). Creep and shrinkage prediction model for analysis and design of concrete structures— model B 3. *Materials & Structures, 28*(6), 357-365.

Beltzung, F., & Wittmann, F. (2002). Influence of cement composition on endogenous shrinkage. *Self-desiccation and Its Importance in Concrete Technology. Report TVBM3104. ISBN, 573185343*, 113-126.

Bendapudi, S. C. K., & Saha, P. (2011). Contribution of fly ash to the properties of mortar and concrete. *Int J Earth Sci Eng, 4*(06), 1017-1023.

Bentur, A., Igarashi, S.-i., & Kovler, K. (2001). Prevention of autogenous shrinkage in high-strength concrete by internal curing using wet lightweight aggregates. *Cement and Concrete Research, 31*(11), 1587-1591.

Bentz, D., Geiker, M. R., & Hansen, K. K. (2001). Shrinkage-reducing admixtures and early-age desiccation in cement pastes and mortars. *Cement and Concrete Research, 31*(7), 1075-1085.

Bentz, D. P. (2008). A review of early-age properties of cement-based materials. *Cement and Concrete Research, 38*(2), 196-204.

Bentz, D. P. (2014). Activation energies of high-volume fly ash ternary blends: hydration and setting. *Cement and Concrete Composites, 53*, 214-223.

Bentz, D. P., Garboczi, E. J., Haecker, C. J., & Jensen, O. M. (1999). Effects of cement particle size distribution on performance properties of Portland cement-based materials. *Cement and Concrete Research, 29*(10), 1663-1671.

Bentz, D. P., Geiker, M. R., & Hansen, K. K. (2001). Shrinkage-reducing admixtures and early-age desiccation in cement pastes and mortars. *Cement and Concrete Research, 31*(7), 1075-1085.

Bentz, D. P., & Haecker, C. J. (1999). An argument for using coarse cements in high-performance concretes. *Cement and Concrete Research, 29*(4), 615-618. doi:http://doi.org/10.1016/S0008-8846(98)00201-4

Bentz, D. P., & Peltz, M. A. (2008). Reducing thermal and autogenous shrinkage contributions to early-age cracking. *ACI Materials Journal, 105*(4), 414.

Bertolini, L., Elsener, B., Pedeferri, P., Redaelli, E., & Polder, R. B. (2013). *Corrosion of steel in concrete: prevention, diagnosis, repair*: John Wiley & Sons.

Bingöl, A. F., & Tohumcu, İ. (2013). Effects of different curing regimes on the compressive strength properties of self compacting concrete incorporating fly ash and silica fume. *Materials & Design, 51*(5), 12-18.

Bissonnette, B. T., Pierre, P., & Pigeon, M. (1999). Influence of key parameters on drying shrinkage of cementitious materials. *Cement & Concrete Research, 29*(10), 1655-1662.

Blais, P. Y., & Couture, M. (1999a). PRECAST, PRESTRESSED PEDESTRIAN BRIDGE-WORLD'S FIRST REACTIVE POWDER CONCRETE BRIDGE. *PCI journal, 44*(5).

Blais, P. Y., & Couture, M. (1999b). Precast, prestressed pedestrian bridge: World's first Reactive Powder Concrete structure. *PCI journal, 44*(5), 60-71.

Bonneau, O., Poulin, C., Dugat, M., & Tcin, P.-C. A. (1996). Reactive powder concretes: from theory to practice. *Concrete International, 18*(4), 47-49.

Bonneau, O., Vernet, C., Moranville, M., & Aïtcin, P.-C. (2000). Characterization of the granular packing and percolation threshold of reactive powder concrete. *Cement and Concrete Research, 30*(12), 1861-1867.

Bouzoubaa, N., Zhang, M.-H., Malhotra, V., & Golden, D. M. (1999). Blended fly ash cements a review. *Materials Journal, 96*(6), 641-650.

Bouzoubaâ, N., Zhang, M. H., & Malhotra, V. M. (2001). Mechanical properties and durability of concrete made with high-volume fly ash blended cements using a coarse fly ash. *Cement & Concrete Research, 31*(10), 1393-1402.

Brooks, J. (2005). 30-year creep and shrinkage of concrete. *Magazine of Concrete Research, 57*(9), 545-556.

Brooks, J., & Jiang, X. (1997). The influence of chemical admixtures on restrained drying shrinkage of concrete. *Special Publication, 173*, 249-266.

Brooks, J. J. (2015). 6 - Shrinkage of Concrete *Concrete and Masonry Movements* (pp. 137-185): Butterworth-Heinemann.

Brown, P. W., & Badger, S. (2000). The distributions of bound sulfates and chlorides in concrete subjected to mixed NaCl, MgSO 4 , Na 2 SO 4 attack. *Cement & Concrete Research, 30*(10), 1535-1542.

Brown, P. W., & Doerr, A. (2000). Chemical changes in concrete due to the ingress of aggressive species. *Cement & Concrete Research, 30*(3), 411-418.

Bullard, J. W., Jennings, H. M., Livingston, R. A., Nonat, A., Scherer, G. W., Schweitzer, J. S., . . . Thomas, J. J. (2011). Mechanisms of cement hydration. *Cement and Concrete Research, 41*(12), 1208-1223.

Bullock, R. E., & Foltz, S. D. (1995). *REMR Management Systems-Navigation and Reservoir Structures, Condition Rating Procedures for Concrete in Gravity Dams, Retaining Walls, and Spillways*. Retrieved from

BuquanMiao, Jenn‐ChuanChern, & Chen‐AnYang. (2003). Influences of fiber content on properties of self‐compacting steel fiber reinforced concrete. *Journal of the Chinese Institute of Engineers, 26*(4), 523-530.

Burrows, R., Kepler, W., Hurcomb, D., Schaffer, J., & Sellers, J. (2004). Three simple tests for selecting low-crack cement. *Cement and Concrete Composites, 26*(5), 509-519.

Burrows, R. W. (1998). *The visible and invisible cracking of concrete*.

Carde, C., & François, R. (1997). Effect of the leaching of calcium hydroxide from cement paste on mechanical and physical properties. *Cement and Concrete Research, 27*(4), 539-550.

Ceukelaire, L. D., & Nieuwenburg, D. V. (1993). Accelerated carbonation of a blast-furnace cement concrete. *Cement & Concrete Research, 23*(2), 442-452.

Chalee, W., & Jaturapitakkul, C. (2008). *Long Term Performance of Fly Ash Concrete in Marine Environment.* Paper presented at the The Eighth ISOPE Pacific/Asia Offshore Mechanics Symposium.

Chang, C.-F., & Chen, J.-W. (2006). The experimental investigation of concrete carbonation depth. *Cement and Concrete Research, 36*(9), 1760-1767.

Chang, P.-K., & Hou, W.-M. (2003). A study on the hydration properties of high performance slag concrete analyzed by SRA. *Cement and Concrete Research, 33*(2), 183-189.

Chen, H., Wang, W., Martin, J. C., Oliphant, A. J., Doerr, P. A., Xu, J. F., . . . Sun, L. (2012). Extraction of lignocellulose and synthesis of porous silica nanoparticles from rice husks: a comprehensive utilization of rice husk biomass. *ACS Sustainable Chemistry & Engineering, 1*(2), 254-259.

Chen, P., Liu, Y., & Mingwei, D. I. (2011). The effect of Nano-filler on the damping properties of Polyacrylic damping paint. *Advanced Materials Research, 183-185*, 2154-2157.

Cheng, A. S., Huang, Y. L., Huang, C. H., & Yen, T. (2011). Effects of Fly Ash Particle Sizes on the Compressive Strength and Fracture Toughness of High Performance Concrete. *Advanced Materials Research, 284-286*, 5.

Chern, J.-C., & Chan, Y.-W. (1989). Deformations of concretes made with blast-furnace slag cement and ordinary portland cement. *Materials Journal, 86*(4), 372-382.

Cheyrezy, M., Maret, V., & Frouin, L. (1995). Microstructural analysis of RPC (reactive powder concrete). *Cement and Concrete Research, 25*(7), 1491-1500.

Choi, S. J., Lee, S. S., & Monteiro, P. J. (2011). Effect of fly ash fineness on temperature rise, setting, and strength development of mortar. *Journal of Materials in Civil Engineering, 24*(5), 499-505.

Collepardi, M. (2000). *ORDINARY AND LONG-TERM DURABILITY OF REINFORCED CONCRETE STRUCTURES.* Paper presented at the Canmet/aci International Conference on Durability of Concrete.

Courtial, M., Noirfontaine, M. N. D., Dunstetter, F., Signes-Frehel, M., Mounanga, P., Cherkaoui, K., & Khelidj, A. (2013). Effect of polycarboxylate and crushed quartz in

UHPC: Microstructural investigation. *Construction & Building Materials, 44*(7), 699-705.

Craeye, B., Geirnaert, M., & De Schutter, G. (2011). Super absorbing polymers as an internal curing agent for mitigation of early-age cracking of high-performance concrete bridge decks. *Construction and Building Materials, 25*(1), 1-13.

Cui, X. L., For, C., Lecturer, Liang, X. W., & Gao, D. X. (2011). Loading capacity of high performance concrete shear wall with end columns. *Journal of Xian University of Architecture & Technology, 43*(3), 367-373.

CUSSON, Daniel, & HOOGEVEEN. (2008). Internal curing of high-performance concrete with pre-soaked fine lightweight aggregate for prevention of autogenous shrinkage cracking. *Cement & Concrete Research, 38*(6), 757-765.

Cwirzen, A., Penttala, V., & Vornanen, C. (2008). Reactive powder based concretes: Mechanical properties, durability and hybrid use with OPC. *Cement & Concrete Research, 38*(10), 1217-1226.

Dai, Q., Ng, K., Zhou, J., Kreiger, E. L., & Ahlborn, T. M. (2012). Damage investigation of single-edge notched beam tests with normal strength concrete and ultra high performance concrete specimens using acoustic emission techniques. *Construction & Building Materials, 31*(6), 231-242.

Damidot, D., Lothenbach, B., Herfort, D., & Glasser, F. (2011). Thermodynamics and cement science. *Cement and Concrete Research, 41*(7), 679-695.

Dan, R., & Mehta, P. K. (1988). Compressive strength of low cement/high fly ash concrete. *Cement & Concrete Research, 18*(4), 571-583.

Dang, Y., Qian, J., Qu, Y., Lin, Z., Zhi, W., Qiao, D., & Jia, X. (2013). Curing cement concrete by using shrinkage reducing admixture and curing compound. *Construction & Building Materials, 48*(11), 992-997.

Dauriac, C. (1997). Special concrete may give steel stiff competition. *The Seattle Daily Journal of Commerce*.

Davies, R., & Jefferson, A. (2017). Micromechanical modelling of self-healing cementitious materials. *International Journal of Solids & Structures*.

De Weerdt, K., Haha, M. B., Le Saout, G., Kjellsen, K. O., Justnes, H., & Lothenbach, B. (2011). Hydration mechanisms of ternary Portland cements containing limestone powder and fly ash. *Cement and Concrete Research, 41*(3), 279-291.

Deschner, F., Winnefeld, F., Lothenbach, B., Seufert, S., Schwesig, P., Dittrich, S., . . . Neubauer, J. (2012). Hydration of Portland cement with high replacement by siliceous fly ash. *Cement and Concrete Research, 42*(10), 1389-1400.

Dowd, W. (1999). *Reactive powder concrete: ultra-high performance cement based composite.* Paper presented at the United States: Construction Innovation Forum.

El-Dieb, A. (2007). Self-curing concrete: Water retention, hydration and moisture transport. *Construction and Building Materials, 21*(6), 1282-1287.

El-Dieb, A. S. (2009). Mechanical, durability and microstructural characteristics of ultra-high-strength self-compacting concrete incorporating steel fibers. *Materials & Design, 30*(10), 4286-4292.

Elahi, A., Basheer, P., Nanukuttan, S., & Khan, Q. (2010). Mechanical and durability properties of high performance concretes containing supplementary cementitious materials. *Construction and Building Materials, 24*(3), 292-299.

EN, B. (2006). 14630, 2006. Products and systems for the protection and repair of concrete structures. Test methods. Determination of carbonation depth in hardened concrete by the phenolphthalein method. *British Standard*.

EN, T. (2005). 196-1. Methods of testing cement–Part 1: Determination of strength. *European Committee for standardization, 26*.

Fehling, E., Schmidt, M., Walraven, J., Leutbecher, T., & Fröhlich, S. (2014). *Ultra-high performance concrete UHPC: Fundamentals, design, examples*: John Wiley & Sons.

Feylessoufi, A., Crespin, M., Dion, P., Bergaya, F., Van Damme, H., & Richard, P. (1997). Controlled rate thermal treatment of reactive powder concretes. *Advanced cement based materials, 6*(1), 21-27.

FISCHER, G., & Shuxin, W. (2003). Design of engineered cementitious composites (ECC) for processing and workability requirements *Brittle Matrix Composites 7* (pp. 29-36): Elsevier.

Fisher, L. R., & Israelachvili, J. N. (1981). Experimental studies on the applicability of the Kelvin equation to highly curved concave menisci. *Journal of colloid and Interface Science, 80*(2), 528-541.

Folliard, K. J., & Berke, N. S. (1997). Properties of high-performance concrete containing shrinkage-reducing admixture. *Cement and Concrete Research, 27*(9), 1357-1364.

Fowler, D. W. (1999). Polymers in concrete: a vision for the 21st century. *Cement and Concrete Composites, 21*(5-6), 449-452.

Frías, M., la Villa, R. V., Rojas, M., Medina, C., & Juan Valdés, A. (2012). Scientific aspects of kaolinite based coal mining wastes in pozzolan/Ca $(OH)_2$ system. *Journal of the American Ceramic Society, 95*(1), 386-391.

Fukushima, T., Yoshizaki, Y., Tomosawa, F., & Takahashi, K. (1998). *RELATIONSHIP BETWEEN NEUTRALIZATION DEPTH AND CONCENTRATION DISTRIBUTION OF $CACO_3$-$CA(OH)_2$ IN CARBONATED CONCRETE.* Paper presented at the Recent Advances in Concrete Technology.

Gaddam, R., Inyang, H. I., Ogunro, V. O., Janardhanam, R., & Udoeyo, F. F. (2009). *Strength and Leaching Patterns of Heavy Metals from Ash-Amended Flowable Fill Monoliths*.

GARAS, Victor, Y., KAHN, Lawrence, F., KURTIS, & Kimberly, E. (2009). Short-term tensile creep and shrinkage of ultra-high performance concrete. *Cement & Concrete Composites, 31*(3), 147-152.

Garas, V., Kurtis, K., & Kahn, L. (2012). Creep of UHPC in tension and compression: effect of thermal treatment. *Cement and Concrete Composites, 34*(4), 493-502.

Garas, V. Y., Kahn, L. F., & Kurtis, K. E. (2009). Short-term tensile creep and shrinkage of ultra-high performance concrete. *Cement and Concrete Composites, 31*(3), 147-152.

Gdoutos, M. K., Shah, S., & Dattatraya, D. (2003). *Relationships between engineering characteristics and material properties of high strength-high performance concrete.* Paper presented at the Role of Concrete In Sustainable Development: Proceedings of the International Symposium dedicated to Professor Surendra Shah, Northwestern University, USA held on 3–4 September 2003 at the University of Dundee, Scotland, UK.

Gebler, S. H., & Klieger, P. (1986). Effect of fly ash on the durability of air-entrained concrete. *Special Publication, 91*, 483-520.

Gesoğlu, M., Güneyisi, E., & Özbay, E. (2009). Properties of self-compacting concretes made with binary, ternary, and quaternary cementitious blends of fly ash, blast furnace slag, and silica fume. *Construction & Building Materials, 23*(5), 1847-1854.

Ghafari, E., Costa, H., Júlio, E., Portugal, A., & Durães, L. (2014). The effect of nanosilica addition on flowability, strength and transport properties of ultra high performance concrete. *Materials & Design, 59*, 1-9.

Ghafari, E., Ghahari, S. A., Costa, H., Júlio, E., Portugal, A., & Durães, L. (2016). Effect of supplementary cementitious materials on autogenous shrinkage of ultra-high performance concrete. *Construction and Building Materials, 127*, 43-48. doi:http://doi.org/10.1016/j.conbuildmat.2016.09.123

Ghazy, A., & Bassuoni, M. T. (2017). Resistance of concrete to different exposures with chloride-based salts. *Cement & Concrete Research, 101*, 144-158.

Gilbert, R. I. (1988). *Time effects in concrete structures*.

Gonzalez-Corominas, A., & Etxeberria, M. (2016). Effects of using recycled concrete aggregates on the shrinkage of high performance concrete. *Construction and Building Materials, 115*, 32-41.

Grasley, Z. C., & Lange, D. A. (2007). Thermal dilation and internal relative humidity of hardened cement paste. *Materials and structures, 40*(3), 311-317.

Grasley, Z. C., Lange, D. A., & D'Ambrosia, M. D. (2006). Internal relative humidity and drying stress gradients in concrete. *Materials and structures, 39*(9), 901-909.

Gruyaert, E., Heede, P. V. D., & Belie, N. D. (2013). Carbonation of slag concrete: Effect of the cement replacement level and curing on the carbonation coefficient – Effect of carbonation on the pore structure. *Cement & Concrete Composites, 35*(1), 39-48.

Güneyisi, E., Gesoğlu, M., & Özturan, T. (2004). Properties of rubberized concretes containing silica fume. *Cement and Concrete Research, 34*(12), 2309-2317.

Guoxing Huang, R. H. (1990). *The shrinkage of concrete* China railway publishing house.

Habel, K., Viviani, M., Denarié, E., & Brühwiler, E. (2006). Development of the mechanical properties of an ultra-high performance fiber reinforced concrete (UHPFRC). *Cement and Concrete Research, 36*(7), 1362-1370.

Hamedanimojarrad, P., Ray, A. S., Thomas, P. S., & Vessalas, K. (2012). Development of shrinkage resistant microfibre-reinforced cement-based composites. *Central European Journal of Engineering, 2*(2), 289-295.

Hassan, A., Jones, S., & Mahmud, G. (2012). Experimental test methods to determine the uniaxial tensile and compressive behaviour of ultra high performance fibre reinforced concrete (UHPFRC). *Construction and Building Materials, 37*, 874-882.

Heukamp, F. H. (2003). *Chemomechanics of calcium leaching of cement-based materials at different scales: The role of CH-dissolution and CSH degradation on strength and durability performance of materials and structures.* Massachusetts Institute of Technology.

Hilloulin, B., Grondin, F., Matallah, M., & Loukili, A. (2014). Modelling of autogenous healing in ultra high performance concrete. *Cement & Concrete Research, 61-62*(61-62), 64-70.

Hoang, A. L., & Fehling, E. (2017). Influence of steel fiber content and aspect ratio on the uniaxial tensile and compressive behavior of ultra high performance concrete. *Construction & Building Materials, 153*, 790-806.

Holt, E. (2005). Contribution of mixture design to chemical and autogenous shrinkage of concrete at early ages. *Cement and Concrete Research, 35*(3), 464-472. doi:http://doi.org/10.1016/j.cemconres.2004.05.009

Hooton, R. D., Stanish, K., & Prusinski, J. (2009). The effect of ground granulated blast furnace slag (slag cement) on the drying shrinkage of concrete–a critical review of the literature. *Slag Cement Concrete*, 79-94.

Hu, Z., Shi, C., Cao, Z., Ou, Z., Wang, D., Wu, Z., & He, L. (2013). A review on testing methods for autogenous shrinkage measurement of cement-based materials. *Journal of Sustainable Cement-Based Materials, 2*(2), 161-171.

Huang, K., Deng, M., Mo, L., & Wang, Y. (2013). Early age stability of concrete pavement by using hybrid fiber together with MgO expansion agent in high altitude locality. *Construction and Building Materials, 48*, 685-690.

Huang, K., Min, D., Mo, L., & Wang, Y. (2013). Early age stability of concrete pavement by using hybrid fiber together with MgO expansion agent in high altitude locality. *Construction & Building Materials, 48*(19), 685-690.

Huang, Y. (2006). Influence of curing conditions on the drying shrinkage characteristics of cement mortar. *Journal of Nanjing University of Technology, 28*(3), 20-23.

Huy, Q. (2013). *Modelling properties of cement paste from microstructure: porosity, mechanical properties, creep and shrinkage.* ÉCOLE POLYTECHNIQUE FÉDÉRALE DE LAUSANNE.

Igarashi, S.-i., Bentur, A., & Kovler, K. (2000). Autogenous shrinkage and induced restraining stresses in high-strength concretes. *Cement and Concrete Research, 30*(11), 1701-1707. doi:http://doi.org/10.1016/S0008-8846(00)00399-9

Islam, M. M., Islam, M. S., Mondal, B. C., & Islam, M. R. (2009). Strength behavior of concrete using slag with cement in sea water environment. *J Civ Eng*.

Itim, A., Ezziane, K., & Kadri, E.-H. (2011). Compressive strength and shrinkage of mortar containing various amounts of mineral additions. *Construction and Building Materials, 25*(8), 3603-3609. doi:http://doi.org/10.1016/j.conbuildmat.2011.03.055

Jensen, O. M., & Hansen, P. F. (1995). Autogenous relative humidity change in silica fume-modified cement paste. *Advances in Cement Research, 7*(25), 33-38.

Jensen, O. M., & Hansen, P. F. (2001). Water-entrained cement-based materials: I. Principles and theoretical background. *Cement and Concrete Research, 31*(4), 647-654.

Jensen, O. M., & Hansen, P. F. (2002). Water-entrained cement-based materials: II. Experimental observations. *Cement and Concrete Research, 32*(6), 973-978.

Ji, T., Zhang, B.-b., Zhuang, Y.-Z., & Wu, H.-C. (2015). Effect of Lightweight Aggregate on Early-Age Autogenous Shrinkage of Concrete. *ACI Materials Journal, 112*(3).

Jiajun, Y., Shuguang, H., Fazhou, W., Yufei, Z., & Zhichao, L. (2006). Effect of pre-wetted light-weight aggregate on internal relative humidity and autogenous shrinkage of concrete. *Journal of Wuhan University of Technology-Mater. Sci. Ed., 21*(1), 134-137.

Jiang, C., Yang, Y., Wang, Y., Zhou, Y., & Ma, C. (2014). Autogenous shrinkage of high performance concrete containing mineral admixtures under different curing temperatures. *Construction and Building Materials, 61*, 260-269.

Jiang, Z., Sun, Z., & Wang, P. (2005). Autogenous relative humidity change and autogenous shrinkage of high-performance cement pastes. *Cement and Concrete Research, 35*(8), 1539-1545. doi:http://doi.org/10.1016/j.cemconres.2004.06.028

Jiang, Z., Sun, Z., & Wang, P. (2006). Internal relative humidity distribution in high-performance cement paste due to moisture diffusion and self-desiccation. *Cement and Concrete Research, 36*(2), 320-325.

Jin, F., & Al-Tabbaa, A. (2015). Strength and drying shrinkage of slag paste activated by sodium carbonate and reactive MgO. *Construction & Building Materials, 81*, 58-65.

Jinchang, P., & Ronggui, L. (2016). Improvement of performance of ultra-high performance concrete based composite material added with nano materials. *Frattura ed Integrit Strutturale*(36), 130.

Julie, P., Dooms, B., & Cauberg, N. (2012). *Evaluation of durability parameters of UHPC using accelerated lab tests*. Paper presented at the Proceedings of the 3rd International Symposium on UHPC and Nanotechnology for High Performance Construction Materials, Kassel, Germany.

Kaufmann, J., Winnefeld, F., & Hesselbarth, D. (2004). Effect of the addition of ultrafine cement and short fiber reinforcement on shrinkage, rheological and mechanical properties of Portland cement pastes. *Cement and Concrete Composites, 26*(5), 541-549.

Kawashima, S., & Shah, S. P. (2011). Early-age autogenous and drying shrinkage behavior of cellulose fiber-reinforced cementitious materials. *Cement and Concrete Composites, 33*(2), 201-208.

Kazemi Kamyab, M. (2013). Autogenous Shrinkage and Hydration Kinetics of SH-UHPFRC under Moderate to Low Temperature Curing Conditions.

Khatri, R., Sirivivatnanon, V., & Gross, W. (1995). Effect of different supplementary cementitious materials on mechanical properties of high performance concrete. *Cement and Concrete Research, 25*(1), 209-220.

Kim, G., Kim, J. Y., Kurtis, K. E., Jacobs, L. J., Pape, Y. L., & Guimaraes, M. (2016). Quantitative evaluation of carbonation in concrete using nonlinear ultrasound. *Materials & Structures, 49*(1-2), 399-409.

Kim, J.-K., & Lee, C.-S. (1999). Moisture diffusion of concrete considering self-desiccation at early ages. *Cement and Concrete Research, 29*(12), 1921-1927.

Koh, K., Ryu, G., Kang, S., Park, J., & Kim, S. (2011). Shrinkage Properties of Ultra-High Performance Concrete (UHPC). *Advanced Science Letters, 4*(3), 948-952.

Kohno, K., Okamoto, T., Isikawa, Y., Sibata, T., & Mori, H. (1999). Effects of artificial lightweight aggregate on autogenous shrinkage of concrete. *Cement and Concrete Research, 29*(4), 611-614.

Kong, X.-m., Zhang, Z.-l., & Lu, Z.-c. (2015). Effect of pre-soaked superabsorbent polymer on shrinkage of high-strength concrete. *Materials and structures, 48*(9), 2741-2758.

Korpa, A., Kowald, T., & Trettin, R. (2009). Phase development in normal and ultra high performance cementitious systems by quantitative X-ray analysis and thermoanalytical methods. *Cement and Concrete Research, 39*(2), 69-76.

Kwan, A., & Chen, J. (2013). Adding fly ash microsphere to improve packing density, flowability and strength of cement paste. *Powder Technology, 234*, 19-25.

Langan, B., Weng, K., & Ward, M. (2002). Effect of silica fume and fly ash on heat of hydration of Portland cement. *Cement and Concrete Research, 32*(7), 1045-1051.

Lee, H., Lee, K., & Kim, B. (2003). Autogenous shrinkage of high-performance concrete containing fly ash. *Magazine of Concrete Research, 55*(6), 507-515.

Lee, K. M., Lee, H. K., Lee, S. H., & Kim, G. Y. (2006). Autogenous shrinkage of concrete containing granulated blast-furnace slag. *Cement and Concrete Research, 36*(7), 1279-1285. doi:http://doi.org/10.1016/j.cemconres.2006.01.005

Lee, N. K., Koh, K., Kim, M. O., & Ryu, G. (2018). Uncovering the role of micro silica in hydration of ultra-high performance concrete (UHPC). *Cement and Concrete Research, 104*, 68-79.

Leng, F., Feng, N., & Lu, X. (2000). An experimental study on the properties of resistance to diffusion of chloride ions of fly ash and blast furnace slag concrete. *Cement and Concrete Research, 30*(6), 989-992.

Li, Y., Bao, J., & Guo, Y. (2010). The relationship between autogenous shrinkage and pore structure of cement paste with mineral admixtures. *Construction and Building Materials, 24*(10), 1855-1860.

Li, Y., & Li, J. (2014). Capillary tension theory for prediction of early autogenous shrinkage of self-consolidating concrete. *Construction and Building Materials, 53*, 511-516.

Li, Z. (2016). Drying shrinkage prediction of paste containing meta-kaolin and ultrafine fly ash for developing ultra-high performance concrete. *Materials Today Communications, 6*, 74-80.

Liu, B., Xie, Y., Zhou, S., & Yuan, Q. (2000). Influence of ultrafine fly ash composite on the fluidity and compressive strength of concrete. *Cement and Concrete Research, 30*(9), 1489-1493.

Liu, J., Shi, C., Ma, X., Khayat, K. H., Zhang, J., & Wang, D. (2017). An overview on the effect of internal curing on shrinkage of high performance cement-based materials. *Construction and Building Materials, 146*, 702-712. doi:https://doi.org/10.1016/j.conbuildmat.2017.04.154

Long, G. (2003). *The composites, structures, and properties of reactive powder concrete.* Ph. D. Thesis, Tongji University, China.

Lothenbach, B., Scrivener, K., & Hooton, R. (2011). Supplementary cementitious materials. *Cement and Concrete Research, 41*(12), 1244-1256.

Loukili, A., Khelidj, A., & Richard, P. (1999). Hydration kinetics, change of relative humidity, and autogenous shrinkage of ultra-high-strength concrete. *Cement and Concrete Research, 29*(4), 577-584.

Lura, P. (2003). *Autogenous deformation and internal curing of concrete.* TU Delft, Delft University of Technology.

Lura, P., Jensen, O. M., & Breugel, K. V. (2003). Autogenous shrinkage in high-performance cement paste: An evaluation of basic mechanisms. *Cement & Concrete Research, 33*(2), 223-232.

Lura, P., Jensen, O. M., & van Breugel, K. (2003). Autogenous shrinkage in high-performance cement paste: an evaluation of basic mechanisms. *Cement and Concrete Research, 33*(2), 223-232.

Lura, P., Pease, B., Mazzotta, G. B., Rajabipour, F., & Weiss, J. (2007). Influence of shrinkage-reducing admixtures on development of plastic shrinkage cracks. *ACI Materials Journal, 104*(2), 187.

Madhavi, T. C., Raju, L. S., & Mathur, D. (2014). Durabilty and strength properties of high volume fly ash concrete. *Journal of Civil Engineering Research, 4*(2A), 7-11.

Malhotra, V. (2002). High-performance high-volume fly ash concrete. *Concrete International, 24*(7), 30-34.

Malvar, L. J., & Lenke, L. R. (2006). Efficiency of fly ash in mitigating alkali-silica reaction based on chemical composition. *ACI Materials Journal, 103*(5), 319.

Manzi, S., Mazzotti, C., & Bignozzi, M. (2013). Short and long-term behavior of structural concrete with recycled concrete aggregate. *Cement and Concrete Composites, 37*, 312-318.

Maruyama, I., & Teramoto, A. (2013). Temperature dependence of autogenous shrinkage of silica fume cement pastes with a very low water–binder ratio. *Cement and Concrete Research, 50*, 41-50. doi:http://doi.org/10.1016/j.cemconres.2013.03.017

Matite, V., & Moranville, M. (1997). The leaching of the reactive powder concretes: results on transfer properties. *MRS Online Proceedings Library Archive, 503*.

Mazloom, M., Ramezanianpour, A., & Brooks, J. (2004). Effect of silica fume on mechanical properties of high-strength concrete. *Cement and Concrete Composites, 26*(4), 347-357.

Mazzoli, A., Monosi, S., & Plescia, E. S. (2015). Evaluation of the early-age-shrinkage of Fiber Reinforced Concrete (FRC) using image analysis methods. *Construction and Building Materials, 101*, 596-601.

McDermott, M. K., Chen, T., Williams, C. M., Markley, K. M., & Payne, G. F. (2004). Mechanical properties of biomimetic tissue adhesive based on the microbial transglutaminase-catalyzed crosslinking of gelatin. *Biomacromolecules, 5*(4), 1270-1279.

Meddah, M. S., Suzuki, M., & Sato, R. (2011). Influence of a combination of expansive and shrinkage-reducing admixture on autogenous deformation and self-stress of silica fume high-performance concrete. *Construction and Building Materials, 25*(1), 239-250.

Meddah, M. S., & Tagnit-Hamou, A. (2009). Pore structure of concrete with mineral admixtures and its effect on self-desiccation shrinkage. *ACI Mater J, 106*(3), 241-250.

Mehta, P. (1999). Sulfate attack in marine environment. *American Ceramic Society, Inc, Materials Science of Concrete: Sulfate Attack Mechanisms(USA)*, 295-299.

Mehta, P. K. (1986). Concrete. Structure, properties and materials.

Mehta, P. K., & Burrows, R. W. (2001). Building durable structures in the 21 st century. *Indian Concrete Journal, 75*(7), 437-443.

mejlhede Jensen, O., & Freiesleben Hansen, P. (1996). Autogenous deformation and change of the relative humidity in silica fume-modified cement paste. *ACI Materials Journal, 93*(6), 539-543.

Miao, B., Chern, J. C., & Yang, C. A. (2003). Influences of fiber content on properties of self‐compacting steel fiber reinforced concrete. *Journal of the Chinese Institute of Engineers, 26*(4), 523-530.

Mihashi, H., & Nishiwaki, T. (2012). Development of Engineered Self-Healing and Self-Repairing Concrete-State-of-the-Art Report. *ACT, 10*(5), 170-184.

Mo, A., El-Tawil, S., Liu, Z., & Hansen, W. (2016). Effects of silica powder and cement type on durability of ultra high performance concrete (UHPC). *Cement & Concrete Composites, 66*, 47-56.

Mo, L., Deng, M., & Wang, A. (2012). Effects of MgO-based expansive additive on compensating the shrinkage of cement paste under non-wet curing conditions. *Cement and Concrete Composites, 34*(3), 377-383.

Moffatt, E. G., Thomas, M. D. A., & Fahim, A. (2017). Performance of high-volume fly ash concrete in marine environment. *Cement & Concrete Research*.

Monteiro, P. (2006). *Concrete: microstructure, properties, and materials*: McGraw-Hill Publishing.

Mora-Ruacho, J., Gettu, R., & Aguado, A. (2009). Influence of shrinkage-reducing admixtures on the reduction of plastic shrinkage cracking in concrete. *Cement and Concrete Research, 39*(3), 141-146.

Morse, J. W., Mucci, A., & Millero, F. J. (1980). The solubility of calcite and aragonite in seawater of 35%. salinity at 25 C and atmospheric pressure. *Geochimica et Cosmochimica Acta, 44*(1), 85-94.

Mounanga, P., Khelidj, A., Loukili, A., & Baroghel-Bouny, V. (2004). Predicting Ca $(OH)_2$ content and chemical shrinkage of hydrating cement pastes using analytical approach. *Cement and Concrete Research, 34*(2), 255-265.

Müller, C. (2010, May 29–June 2). *Durability of Ultra-High Performance Concrete (UHPC).* Paper presented at the the Third International fib Congress and Exhibition Incorporating the PCI Annual

Convention and National Bridge Conference, Washington, DC.

Nagataki, S., & Gomi, H. (1998). Expansive admixtures (mainly ettringite). *Cement and Concrete Composites, 20*(2-3), 163-170.

Nanukuttan, S. V., Basheer, P. A. M., Mccarter, W. J., Tang, L., Holmes, N., Chrisp, T. M., . . . Magee, B. (2015). The performance of concrete exposed to marine environments: Predictive modelling and use of laboratory/on site test methods. *Construction & Building Materials, 93*(19), 831-840.

NetAnswer. Effect of fly ash gradation on workability, strength and durability of Portland cement fly ash mortars. *Materials & Structures*.

NetAnswer. Long term carbonation of UHPC. *Materials & Structures*.

Neto, A. A. M., Cincotto, M. A., & Repette, W. (2008). Drying and autogenous shrinkage of pastes and mortars with activated slag cement. *Cement and Concrete Research, 38*(4), 565-574.

Nevell, T. P., & Zeronian, S. H. (1985). Cellulose chemistry and its applications.

Ng, K. M., Tam, C. M., & Tam, V. W. (2010). Studying the production process and mechanical properties of reactive powder concrete: a Hong Kong study. *Magazine of Concrete Research, 62*(9), 647-654.

Nochaiya, T., Wongkeo, W., & Chaipanich, A. (2010). Utilization of fly ash with silica fume and properties of Portland cement–fly ash–silica fume concrete. *Fuel, 89*(3), 768-774.

Noushini, A., Vessalas, K., Arabian, G., & Samali, B. (2014). Drying shrinkage behaviour of fibre reinforced concrete incorporating polyvinyl alcohol fibres and fly ash. *Advances in Civil Engineering, 2014*.

Noushini, A., Vessalas, K., & Samali, B. (2015). Rheological Properties and Compressive Strength Behaviour of Polyvinyl Alcohol Fibre-Reinforced Concrete. *Australian Journal of Structural Engineering, 15*(1), 77-88.

Odler, I. (1998). Hydration, setting and hardening of Portland cement. *LEA's Chemistry of Cement and Concrete, 4*, 241-297.

Oliveira, M. J., Ribeiro, A. B., & Branco, F. G. (2014). Combined effect of expansive and shrinkage reducing admixtures to control autogenous shrinkage in self-compacting concrete. *Construction and Building Materials, 52*, 267-275.

Paillere, A. M., Buil, M., & Serrano, J. (1989). Effect of fiber addition on the autogenous shrinkage of silica fume. *Materials Journal, 86*(2), 139-144.

Pakravan, H. R., Latifi, M., & Jamshidi, M. (2017). Hybrid short fiber reinforcement system in concrete: A review. *Construction and Building Materials, 142*, 280-294. doi:http://doi.org/10.1016/j.conbuildmat.2017.03.059

Palin, D., Wiktor, V., & Jonkers, H. M. (2015). Autogenous healing of marine exposed concrete: Characterization and quantification through visual crack closure. *Cement & Concrete Research, 73*, 17-24.

Pan, X., Shi, C., Jia, L., Zhang, J., & Wu, L. (2015). Effect of inorganic surface treatment on air permeability of cement-based materials. *Journal of Materials in Civil Engineering, 28*(3), 04015145.

Pang, L. F., Ruan, S. Y., & Cai, Y. T. (2011). *Effects of internal curing by super absorbent polymer on shrinkage of concrete.* Paper presented at the Key Engineering Materials.

Papadakis, V. G. (2000). Effect of supplementary cementing materials on concrete resistance against carbonation and chloride ingress. *Cement and Concrete Research, 30*(2), 291-299.

Park, S. H., Kim, D. J., Ryu, G. S., & Koh, K. T. (2012). Tensile behavior of ultra high performance hybrid fiber reinforced concrete. *Cement and Concrete Composites, 34*(2), 172-184.

Pei, H., Li, Z., Zhang, B., & Ma, H. (2014). Multipoint measurement of early age shrinkage in low w/c ratio mortars by using fiber Bragg gratings. *Materials Letters, 131*, 370-372.

Pengsheng, W., Shengnian, W., & Jianbo XIONG, Z. F. (2017). A Comprehensive Cost Analysis Related to Anti-corrosion Design and Total Life Cycle of Coastal Engineering Constructions Assigned for Different Length of Service Life. *Corrosion Science and Protetion Technology, 30*(1), 99-104.

Persson, B. (1998). Experimental studies on shrinkage of high-performance concrete. *Cement and Concrete Research, 28*(7), 1023-1036.

Persson, B. (2002). Eight-year exploration of shrinkage in high-performance concrete. *Cement and Concrete Research, 32*(8), 1229-1237.

Philippot, S., Masse, S., Zanni, H., Nieto, P., Maret, V., & Cheyrezy, M. (1996). 29Si NMR study of hydration and pozzolanic reactions in reactive powder concrete (RPC). *Magnetic resonance imaging, 14*(7-8), 891-893.

Piérard, Julie, B. D., & Cauberg, N. (2012). *Evaluation of durability parameters of UHPC using accelerated lab tests.* Paper presented at the the 3rd International Symposium on UHPC and Nanotechnology for High Performance Construction Materials, Kassel, Germany.

Piérard, J., Dooms, B., & Cauberg, N. (2012). *Evaluation of durability parameters of UHPC using accelerated lab tests.* Paper presented at the Proceedings of the 3rd International Symposium on UHPC and Nanotechnology for High Performance Construction Materials, Kassel, Germany.

PierreMounanga, KhalidCherkaoui, AbdelhafidKhelidj, MireilleCourtial, deNoirfontaine, M.-N., & Dunstetter, F. (2012). Extrudable reactive powder concretes: hydration, shrinkage and transfer properties. *Revue Franã§aise De Gã©nie Civil, 16*(sup1), s99-s114.

Poon, C., Lam, L., & Wong, Y. (2000). A study on high strength concrete prepared with large volumes of low calcium fly ash. *Cement and Concrete Research, 30*(3), 447-455.

Potgieter-Vermaak, S., Potgieter, J., Kruger, R., Spolnik, Z., & Van Grieken, R. (2005). A characterisation of the surface properties of an ultra fine fly ash (UFFA) used in the polymer industry. *Fuel, 84*(18), 2295-2300.

Poupard, O., L'hostis, V., Catinaud, S., & Petre-Lazar, I. (2006). Corrosion damage diagnosis of a reinforced concrete beam after 40 years natural exposure in marine environment. *Cement and Concrete Research, 36*(3), 504-520.

Raczkiewicz, W. (2017). The effect of micro-reinforcement steel fibers addition on the size of the shrinkage of concrete and corrosion process of the main reinforcement bars. *Procedia Engineering, 195*, 155-162.

Ramachandran, V. S. (1996). *Concrete admixtures handbook: properties, science and technology*: William Andrew.

Ramezanianpour, A. A. (2014). Fly ash *Cement replacement materials* (pp. 47-156): Springer.

Rao, G. (1998). Influence of silica fume replacement of cement on expansion and drying shrinkage. *Cement and Concrete Research, 28*(10), 1505-1509.

Rao, G. A. (2001). Long-term drying shrinkage of mortar—influence of silica fume and size of fine aggregate. *Cement and Concrete Research, 31*(2), 171-175.

Revertegat, E., Richet, C., & Gegout, P. (1992). Effect of pH on the durability of cement pastes. *Cement and Concrete Research, 22*(2-3), 259-272.

Richard, P., & Cheyrezy, M. Reactive Powder Concrete with high ductility and 200-800 MPa compressive strength, Metha, PK (edition) Concrete Technology Past Present and Future: SP.

Richard, P., & Cheyrezy, M. (1995). Composition of reactive powder concretes. *Cement and Concrete Research, 25*(7), 1501-1511.

Rip, A., & Kemp, R. (1998). Technological change. *Human choice and climate change, 2*(2), 327-399.

Rodden, R., & Lange, D. (2004). Feasibility of shrinkage reducing admixtures for concrete runway pavements.

Rongbing, B., & Jian, S. (2005). Synthesis and evaluation of shrinkage-reducing admixture for cementitious materials. *Cement and Concrete Research, 35*(3), 445-448.

Rossi, P. (2013). Influence of fibre geometry and matrix maturity on the mechanical performance of ultra high-performance cement-based composites. *Cement and Concrete Composites, 37*, 246-248.

Saetta, A. V., Schrefler, B. A., & Vitaliani, R. V. (1993). The carbonation of concrete and the mechanism of moisture, heat and carbon dioxide flow through porous materials. *Cement and Concrete Research, 23*(4), 761-772.

Santhanam, M., Cohen, M., & Olek, J. (2006a). Differentiating seawater and groundwater sulfate attack in Portland cement mortars. *Cement and Concrete Research, 36*(12), 2132-2137.

Santhanam, M., Cohen, M., & Olek, J. (2006b). Differentiating seawater and groundwater sulfate attack in Portland cement mortars. *Cement & Concrete Research, 36*(12), 2132-2137.

Santhanam, M., & Otieno, M. (2016). *Deterioration of concrete in the marine environment*.

Sayari, A., Yang, Y., Kruk, M., & Jaroniec, M. (1999). Expanding the pore size of MCM-41 silicas: use of amines as expanders in direct synthesis and postsynthesis procedures. *The Journal of Physical Chemistry B, 103*(18), 3651-3658.

Schachinger, I., Hilbig, H., Stengel, T., & Fehling, E. (2008). *Effect of curing temperature at an early age on the long-term strength development of UHPC.* Paper presented at the 2nd International Symposium on Ultra High Performance Concrete.

Schlitter, J., Bentz, D., & Weiss, W. (2013). Quantifying stress development and remaining stress capacity in restrained, internally cured mortars. *ACI Materials Journal, 110*(1), 3.

Schmidt, M., & Fehling, E. (2005). Ultra-High-Performance Concrete: Research, Development and Application in Europe. *Seventh International Symposium on the Utilization of High-Strength/High-Performance Concrete, ACI SP-288, American Concrete Institute, 1 & 2*.

Schrefler, B. A., Majorana, C. E., Khoury, G. A., & Gawin, D. (2002). Thermo-hydro-mechanical modelling of high performance concrete at high temperatures. *Engineering Computations, 19*(7), 787-819.

Shaikh, F. U., & Supit, S. W. (2015). Compressive strength and durability properties of high volume fly ash (HVFA) concretes containing ultrafine fly ash (UFFA). *Construction and Building Materials, 82*, 192-205.

Shariq, M., Prasad, J., & Abbas, H. (2016). Creep and drying shrinkage of concrete containing GGBFS. *Cement and Concrete Composites, 68*, 35-45.

Shi, C., & Mo, Y. L. (2015). *High-Performance Construction Materials*.

Shi, C., Wang, D., Wu, L., & Wu, Z. (2015a). The hydration and microstructure of ultra high-strength concrete with cement–silica fume–slag binder. *Cement & Concrete Composites, 61*, 44-52.

Shi, C., Wang, D., Wu, L., & Wu, Z. (2015b). The hydration and microstructure of ultra high-strength concrete with cement–silica fume–slag binder. *Cement and Concrete Composites, 61*, 44-52.

Shi, C., Wu, X., & Tang, M. (1991). Hydration of alkali-slag cements at 150 C. *Cement and Concrete Research, 21*(1), 91-100.

Shi, C., Wu, Z., Lv, K., & Wu, L. (2015). A review on mixture design methods for self-compacting concrete. *Construction and Building Materials, 84*, 387-398.

Shi, C., Wu, Z., Wang, D., & Wu, L. (2014). *Design and properties of ultra high performance concrete.* Paper presented at the Proceedings of the First International Conference on Construction Materials and Structures in Johannesburg, IOS Press EbooNs.

Shi, C., Wu, Z., Xiao, J., Wang, D., Huang, Z., & Fang, Z. (2015a). A review on ultra high performance concrete: Part I. Raw materials and mixture design. *Construction and Building Materials, 101*, 741-751.

Shi, C., Wu, Z., Xiao, J., Wang, D., Huang, Z., & Fang, Z. (2015b). A review on ultra high performance concrete: Part I. Raw materials and mixture design. *Construction & Building Materials, 101*, 741-751.

Shi, Z., Geiker, M. R., Lothenbach, B., De Weerdt, K., Garzón, S. F., Enemark-Rasmussen, K., & Skibsted, J. (2017). Friedel's salt profiles from thermogravimetric analysis and thermodynamic modelling of Portland cement-based mortars exposed to sodium chloride solution. *Cement and Concrete Composites, 78*, 73-83.

Simões, T., Octávio, C., Valença, J., Costa, H., Dias-Da-Costa, D., & Júlio, E. (2017). Influence of concrete strength and steel fibre geometry on the fibre/matrix interface. *Composites Part B Engineering, 122*.

Smith, J., Cusatis, G., Pelessone, D., Landis, E., O'Daniel, J., & Baylot, J. (2014). Discrete modeling of ultra-high-performance concrete with application to projectile penetration. *International Journal of Impact Engineering, 65*, 13-32.

Soliman, A. M. (2011). Early-age shrinkage of ultra high-performance concrete: mitigation and compensating mechanisms.

Sprince, A., Korjakins, A., & Pakrastinsh, L. (2013). Time-Dependent Behavior of High Performance Fiber-Reinforced Concrete. *Advanced Materials Research, 705*, 75-80.

Su, Y., Li, J., Wu, C., Wu, P., & Li, Z.-X. (2016). Effects of steel fibres on dynamic strength of UHPC. *Construction and Building Materials, 114*, 708-718.

Subramaniam, K. V., Gromotka, R., Shah, S. P., Obla, K., & Hill, R. (2005). Influence of ultrafine fly ash on the early age response and the shrinkage cracking potential of concrete. *Journal of Materials in Civil Engineering, 17*(1), 45-53.

Supit, S. W., Shaikh, F. U., & Sarker, P. K. (2014). Effect of ultrafine fly ash on mechanical properties of high volume fly ash mortar. *Construction and Building Materials, 51*, 278-286.

Tafraoui, A., Escadeillas, G., & Vidal, T. (2016a). Durability of the Ultra High Performances Concrete containing metakaolin. *Construction & Building Materials, 112*, 980-987.

Tafraoui, A., Escadeillas, G., & Vidal, T. (2016b). Durability of the ultra high performances concrete containing metakaolin. *Construction and Building Materials, 112*, 980-987.

Tam, C. M., Tam, V. W., & Ng, K. M. (2012). Assessing drying shrinkage and water permeability of reactive powder concrete produced in Hong Kong. *Construction and Building Materials, 26*(1), 79-89.

Tarolli, S. P. (1997). Future of Information Commerce under Contemporary Contract and Copyright Principles, The. *Am.u.l.rev*(5).

Tasong, W. A., Lynsdale, C. J., & Cripps, J. C. (1999). Aggregate-cement paste interface: Part I. Influence of aggregate geochemistry. *Cement and Concrete Research, 29*(7), 1019-1025.

Taylor-Lange, S. C., Juenger, M. C. G., & Siegel, J. A. (2013). Impact of cement renders on airborne ozone and carbon dioxide concentrations. *Atmospheric Environment, 70*(2), 263-266.

Tazawa, E.-i. (1999). *Autogenous shrinkage of concrete*: CRC Press.

Tazawa, E.-i., & Miyazawa, S. (1995). Influence of cement and admixture on autogenous shrinkage of cement paste. *Cement and Concrete Research, 25*(2), 281-287.

Tazawa, E. (1996). Technical committee report on Autogenous shrinkage. *Proceedings of JCI, 18*, 29-38.

Tazawa, E., & Miyazawa, S. (1997). Influence of constituents and composition on autogenous shrinkage of cementitious materials. *Magazine of Concrete Research, 49*(178), 15-22.

Tazawa, E. I., & Miyazawa, S. (1995). Influence of cement and admixture on autogenous shrinkage of cement paste. *Cement & Concrete Research, 25*(2), 281-287.

Termkhajornkit, P., Nawa, T., Nakai, M., & Saito, T. (2005). Effect of fly ash on autogenous shrinkage. *Cement and Concrete Research, 35*(3), 473-482. doi:10.1016/j.cemconres.2004.07.010

Thomas, M. (2016). 6 – The durability of concrete for marine construction : Materials and properties. *Marine Concrete Structures*, 151-170.

Toledo Filho, R. D., Ghavami, K., Sanjuán, M. A., & England, G. L. (2005). Free, restrained and drying shrinkage of cement mortar composites reinforced with vegetable fibres. *Cement and Concrete Composites, 27*(5), 537-546.

Turatsinze, A., Farhat, H., & Granju, J.-L. (2003). Influence of autogenous cracking on the durability of repairs by cement-based overlays reinforced with metal fibres. *Materials and Structures, 36*(10), 673-677.

Turatsinze, A., Farhat, H., & Granju, J. L. (2003). Influence of autogenous cracking on the durability of repairs by cement-based overlays reinforced with metal fibres. *Materials & Structures, 36*(10), 673-677.

Turcry, P., Loukili, A., Barcelo, L., & Casabonne, J. M. (2002). Can the maturity concept be used to separate the autogenous shrinkage and thermal deformation of a cement paste at early age? *Cement and Concrete Research, 32*(9), 1443-1450.

Udoeyo, F. F., Inyang, H., Young, D. T., & Oparadu, E. E. (2006). Potential of wood waste ash as an additive in concrete. *Journal of Materials in Civil Engineering, 18*(4), 605-611.

Van Breugel, K., & Van Tuan, N. (2015). *Autogenous Shrinkage of HPC and Ways to Mitigate it* (Vol. 629): Trans Tech Publ.

Van Damme, H. (2018). Concrete material science: past, present, and future innovations. *Cement and Concrete Research, 112*, 5-24.

Van den Heede, P., & De Belie, N. (2012). Environmental impact and life cycle assessment (LCA) of traditional and 'green'concretes: literature review and theoretical calculations. *Cement and Concrete Composites, 34*(4), 431-442.

Van Tuan, N., Ye, G., Van Breugel, K., & Copuroglu, O. (2011). Hydration and microstructure of ultra high performance concrete incorporating rice husk ash. *Cement and Concrete Research, 41*(11), 1104-1111.

Vikan, H., & Justnes, H. (2007). Rheology of cementitious paste with silica fume or limestone. *Cement & Concrete Research, 37*(11), 1512-1517.

Wang, B., Wang, L., & Ming, L. (2007). Experimental research on the autogenous shrinkage of MK high performance concrete. *Journal of Wuhan University of Technology, 22*(3), 551-554.

Wang, C., Yang, C., Liu, F., Wan, C., & Pu, X. (2012). Preparation of ultra-high performance concrete with common technology and materials. *Cement and Concrete Composites, 34*(4), 538-544.

Wang, D., Shi, C., Wu, Z., Wu, L., Xiang, S., & Pan, X. (2016). Effects of nanomaterials on hardening of cement–silica fume–fly ash-based ultra-high-strength concrete. *Adv. Cem. Res, 28*(9), 555-566.

Wang, D., Shi, C., Wu, Z., Xiao, J., Huang, Z., & Fang, Z. (2015). A review on ultra high performance concrete: Part II. Hydration, microstructure and properties. *Construction & Building Materials, 96*, 368-377.

Wang, F., Zhou, Y., Peng, B., Liu, Z., & Hu, S. (2009). Autogenous shrinkage of concrete with super-absorbent polymer. *ACI Materials Journal, 106*(2), 123.

Wang, J. C., & Yan, P. Y. (2006). Influence of initial casting temperature and dosage of fly ash on hydration heat evolution of concrete under adiabatic condition. *Journal of Thermal Analysis & Calorimetry, 85*(3), 755-760.

Washburn, E. W. (1921). Note on a method of determining the distribution of pore sizes in a porous material. *Proceedings of the National Academy of Sciences, 7*(4), 115-116.

Wille, K., Naaman, A. E., El-Tawil, S., & Parra-Montesinos, G. J. (2012). Ultra-high performance concrete and fiber reinforced concrete: achieving strength and ductility without heat curing. *Materials and structures, 45*(3), 309-324.

Wong, A. C. L., Childs, P. A., Berndt, R., Macken, T., Peng, G.-D., & Gowripalan, N. (2007). Simultaneous measurement of shrinkage and temperature of reactive powder concrete at early-age using fibre Bragg grating sensors. *Cement and Concrete Composites, 29*(6), 490-497. doi:http://doi.org/10.1016/j.cemconcomp.2007.02.003

Wu, L., Farzadnia, N., Shi, C., Zhang, Z., & Wang, H. (2017a). Autogenous shrinkage of high performance concrete: A review. *Construction & Building Materials, 149*, 62-75.

Wu, L., Farzadnia, N., Shi, C., Zhang, Z., & Wang, H. (2017b). Autogenous shrinkage of high performance concrete: a review. *Construction and Building Materials, 149*, 62-75.

Wu, L., Liu, P., Shi, C., Zhang, Z., Bui, T. Q., & Jiao, D. (2016). Edge-based smoothed extended finite element method for dynamic fracture analysis. *Applied Mathematical Modelling, 40*(19-20), 8564-8579.

Wu, L., Liu, P., Zhang, Z., Zhu, D., & Wang, H. (2018). Multiscale modeling for high-performance concrete: a review. *International Journal for Multiscale Computational Engineering, 16*(3).

Wu, M., Johannesson, B., & Geiker, M. (2012). A review: Self-healing in cementitious materials and engineered cementitious composite as a self-healing material. *Construction & Building Materials, 28*(1), 571-583.

Wu, Z., Shi, C., He, W., & Wu, L. (2016). Effects of steel fiber content and shape on mechanical properties of ultra high performance concrete. *Construction and Building Materials, 103*, 8-14.

Wu, Z., Shi, C., & Khayat, K. H. (2016). Influence of silica fume content on microstructure development and bond to steel fiber in ultra-high strength cement-based materials (UHSC). *Cement & Concrete Composites, 71*, 97-109.

Xian, Z., Zhang, P., Zhen, W., Ling, Z., Zeng, G., & Zhou, C. (2013). Adsorption of methylene blue onto humic acid-coated Fe 3 O 4 nanoparticles. *Colloids & Surfaces A Physicochemical & Engineering Aspects, 435*(9), 85-90.

XIANG, S., SHI, C., WU, L., & CHONG, L. (2015). Synthesis of Polycarboxylate with Different Comb Structures and It's Influence on Properties of Fresh Cement Pastes. *Journal of The Chinese Ceramic Society*(5), 5.

Yang, C., Lai, J., & Xu, S. (2012). Study on Preparing Ecological Reactive Powder Concrete Using Solid Waste. *Wuhan Ligong Daxue Xuebao(Journal of Wuhan University of Technology), 34*(2), 9-12.

Yang, E.-H., Yang, Y., & Li, V. C. (2007a). Use of high volumes of fly ash to improve ECC mechanical properties and material greenness. *ACI Materials Journal, 104*(6), 620-628.

Yang, E.-H., Yang, Y., & Li, V. C. (2007b). Use of high volumes of fly ash to improve ECC mechanical properties and material greenness. *ACI Materials Journal, 104*(6), 620.

Yang, I. H., Joh, C., & Kim, B.-S. (2010). Structural behavior of ultra high performance concrete beams subjected to bending. *Engineering Structures, 32*(11), 3478-3487.

Yang, Q. (1999). Inner relative humidity and degree of saturation in high-performance concrete stored in water or salt solution for 2 years. *Cement and Concrete Research, 29*(1), 45-53.

Yang, Y., Sato, R., & Kawai, K. (2005). Autogenous shrinkage of high-strength concrete containing silica fume under drying at early ages. *Cement and Concrete Research, 35*(3), 449-456. doi:http://doi.org/10.1016/j.cemconres.2004.06.006

Yang, Y., Yang, E. H., & Li, V. C. (2011). Autogenous healing of engineered cementitious composites at early age. *Cement & Concrete Research, 41*(2), 176-183.

YaoZhong, X. (1993). RECENT PROGRESS IN CEMENT CHEMISTRY——NOTES ON THE 9TH INTERNATIONAL CONGRESS ON THE CHEMISTRY OF CEMENT [J]. *Journal of The Chinese Ceramic Society, 6*, 014.

Yazıcı, H., Yardımcı, M. Y., Aydın, S., & Karabulut, A. Ş. (2009). Mechanical properties of reactive powder concrete containing mineral admixtures under different curing regimes. *Construction and Building Materials, 23*(3), 1223-1231.

Yazıcı, H., Yiğiter, H., Karabulut, A. Ş., & Baradan, B. (2008). Utilization of fly ash and ground granulated blast furnace slag as an alternative silica source in reactive powder concrete. *Fuel, 87*(12), 2401-2407.

Ye, H., & Radlińska, A. (2016). A review and comparative study of existing shrinkage prediction models for portland and non-portland cementitious materials. *Advances in Materials Science and Engineering, 2016*.

Yoo, D.-Y., Banthia, N., & Yoon, Y.-S. (2015). Effectiveness of shrinkage-reducing admixture in reducing autogenous shrinkage stress of ultra-high-performance fiber-reinforced concrete. *Cement and Concrete Composites, 64*, 27-36.

Yoo, D.-Y., Kang, S.-T., Lee, J.-H., & Yoon, Y.-S. (2013). Effect of shrinkage reducing admixture on tensile and flexural behaviors of UHPFRC considering fiber distribution characteristics. *Cement and Concrete Research, 54*, 180-190.

Yoo, D. Y., & Banthia, N. (2016). Mechanical properties of ultra-high-performance fiber-reinforced concrete: A review. *Cement & Concrete Composites, 73*, 267-280.

Yoshitake, I., Wong, H., Ishida, T., & Nassif, A. Y. (2014). Thermal stress of high volume fly-ash (HVFA) concrete made with limestone aggregate. *Construction and Building Materials, 71*, 216-225.

Yu, R., Spiesz, P., & Brouwers, H. (2014). Effect of nano-silica on the hydration and microstructure development of Ultra-High Performance Concrete (UHPC) with a low binder amount. *Construction and Building Materials, 65*, 140-150.

Yu, R., Spiesz, P., & Brouwers, H. (2014). Mix design and properties assessment of ultra-high performance fibre reinforced concrete (UHPFRC). *Cement and Concrete Research, 56*, 29-39.

Yu, R., Spiesz, P., & Brouwers, H. J. H. (2014). Effect of nano-silica on the hydration and microstructure development of Ultra-High Performance Concrete (UHPC) with a low binder amount. *Construction & Building Materials, 65*(9), 140-150.

Zanni, H., Cheyrezy, M., Maret, V., Philippot, S., & Nieto, P. (1996). Investigation of hydration and pozzolanic reaction in reactive powder concrete (RPC) using 29Si NMR. *Cement and Concrete Research, 26*(1), 93-100.

Zhang, J., Gao, Y., & Wang, Z. (2013). Evaluation of shrinkage induced cracking performance of low shrinkage engineered cementitious composite by ring tests. *Composites Part B: Engineering, 52*, 21-29.

Zhang, J., & Zhao, Y. (2016). The mechanical properties and microstructure of ultra-high-performance concrete containing various supplementary cementitious materials. *Journal of Sustainable Cement-Based Materials*, 1-13.

Zhang, M., Tam, C., & Leow, M. (2003). Effect of water-to-cementitious materials ratio and silica fume on the autogenous shrinkage of concrete. *Cement and Concrete Research, 33*(10), 1687-1694.

Zhang, W., Zakaria, M., & Hama, Y. (2013). Influence of aggregate materials characteristics on the drying shrinkage properties of mortar and concrete. *Construction and Building Materials, 49*, 500-510.

Zhao, D. F., Liu, M., & Zhang, S. J. (2014). *Review on Relationships of Temperature History, Fatigue Damage and Microstructure Evolution Mechanism of Concrete.* Paper presented at the Applied Mechanics and Materials.

Zhao, Y., Gong, J., & Zhao, S. (2017). Experimental study on shrinkage of HPC containing fly ash and ground granulated blast-furnace slag. *Construction & Building Materials, 155*, 145-153.

Zheng-wu, J., Zhen-ping, S., & Pei-ming, W. (2004). Self-desiccation Effect of High Performance Concrete. *Journal of Wuhan University of Technology-Materials Science, 19*(4), 82-86.

Junchao Yu, Qingxin Zhao (2013). Effect of steel fiber on creep properties of concrete. Journal of the Chinese Ceramic Society, 41 (8), 1087-1093.

Liu Jiaping, Tian Qian, & Tang Mingshu. (2006). Effects of Expansion Agents and Shrinkage Reducers on Shrinkage and Cracking of High Performance Concrete. Journal of Southeast University (Natural Science Edition), 36, 195-197.

Shi Caijun, Tong Baihui, & He Fuqiang. (2011). ASTM Cement Mortar and Concrete Ring-type Restricted Shrinkage Cracking Test Standard.

Wu Xueli. (2008). Research on prediction model of concrete strength and dry shrinkage. Chinese Academy of Building Sciences.

Wu Linmei, Shi Caijun, Zhang Zuhua, & Wang Hao. (2018). Effect of Steel Fiber on Dry Shrinkage of Ultra High Performance Concrete. Materials Review, 31 (23), 58-65.

Wu Jinfeng, Yu Ligang, & Cai Xi. (2009). Some bad conditions after the implementation of GB175-2007 "General Portland Cement". Cement (3), 46-47.

Sun Wei. (1987). Study on the Interface of Steel Fiber Reinforced Concrete. Concrete and Cement Products, 2, 3-7.

Sun Jiaying, Luan Feng, & Zhang Yu. (2000). Effect of mesh polypropylene fibers on durability of high performance concrete. Journal of the Chinese Ceramic Society (z1).

Li Shujin, Qian Hongping, & Xu Yicheng. (2014). Study on Early Shrinkage and Crack Resistance of Fiber Self-Compacting Concrete. Bulletin of the Chinese Ceramic Society, 33 (12), 3140-3144.

Lin Hongbin. (2011). Preparation and performance of steel fiber self-compacting high-strength concrete. Chongqing University. Concrete shrinkage. (1990).

Wang Chong, Pu Xincheng, Chen Ke, Liu Fang, Wu Jianhua, & Peng Xiaoqin. (2008). Testing of Hydration Process of Cement Paste Materials with Ultra Low Water-Binder Ratio. Journal of Materials Science and Engineering, 26 (6), 852-857.

Tian Qian. (2006). Study on shrinkage and mechanism of cement-based materials with low water-to-binder ratio and large amount of mineral admixtures [D]. Nanjing: Southeast University.

Qi Ling. (1996). Some mechanical properties of the interface in concrete. Journal of Guangxi University of Technology, 7 (1), 26-30.

Zhengwu Jiang, Zhenping Sun, & Peiming Wang (2003). Research on the Relative Humidity Change of High Performance Concrete. Journal of the Chinese Ceramic Society, 31 (8), 770-773.

Jian Shouwei, Kong Wei, Ma Baoguo, & Zhang Ludong. (2014). Effect of fiber on early plastic shrinkage of thin-layer mortar. Materials Review, 28 (22), 109-113.

Ma Xinwei, Li Xueying, & Jiao Hejun. (2009). Research on the application of superabsorbent polymers in mortar and concrete. Journal of Wuhan University of Technology (2).

Long Guangcheng, Jiang Zhengwu, Sun Zhenping, Wang Peiming, & Xie Youjun. (2005). Self-drying effect of reactive powder concrete. Journal of Building Materials, 8 (1), 7-10.

# Appendix

## *A1. The bending failure morphology of the UHPC samples*

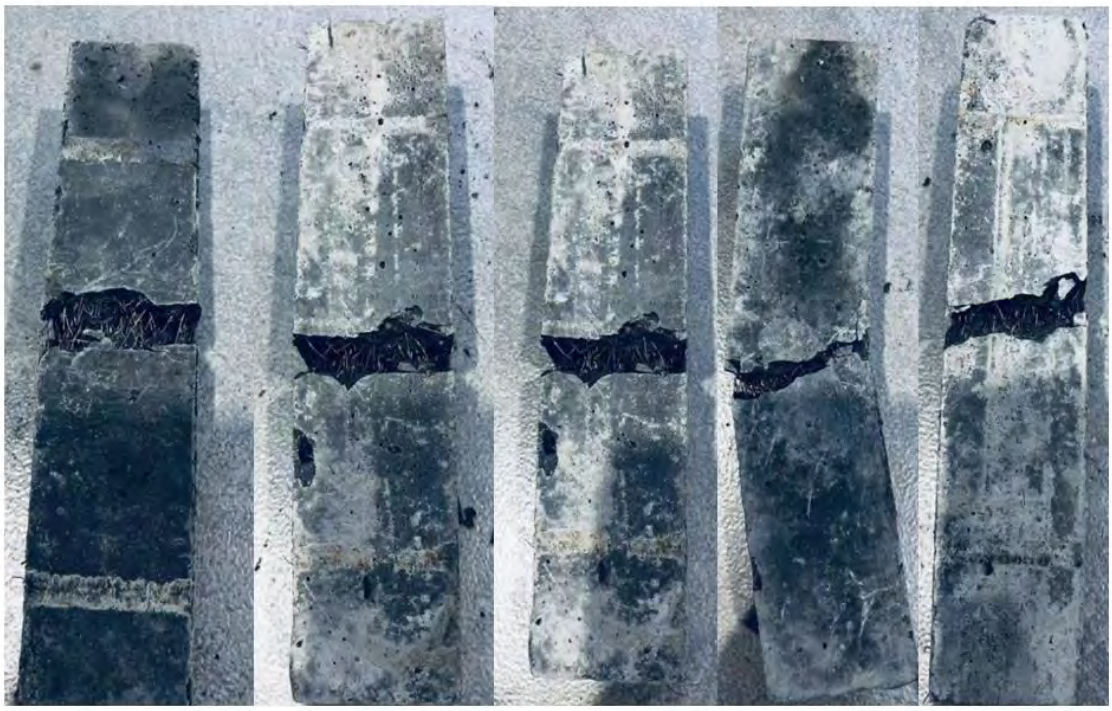


## *A2. Three point bending load displacement curve of slag containing UHPC*

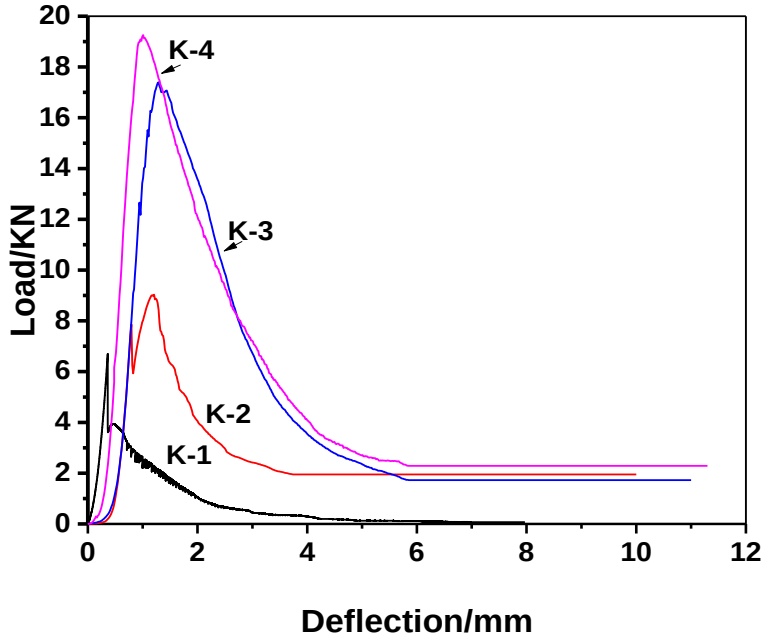

## *A3. Three point bending load displacement curve of fly ash containing UHPC*

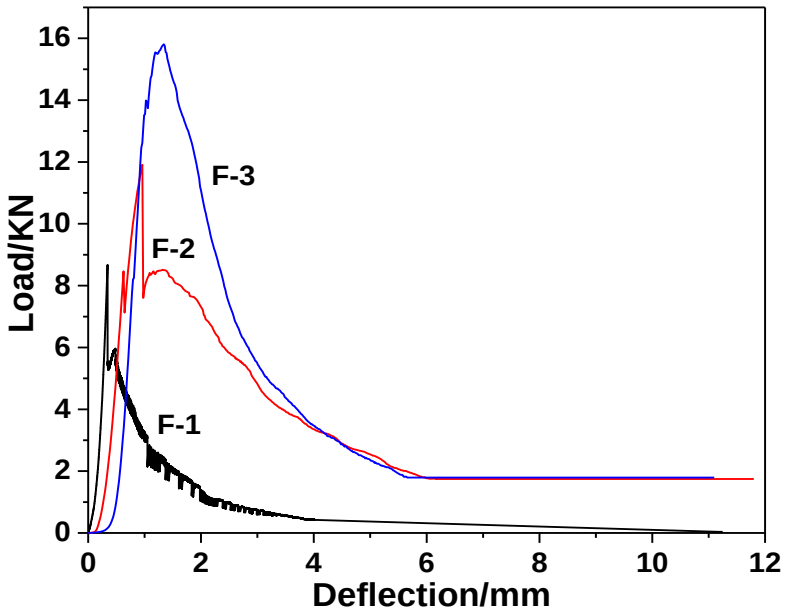


## *A4. Steel fibres (3%) distribution of the sample F4*

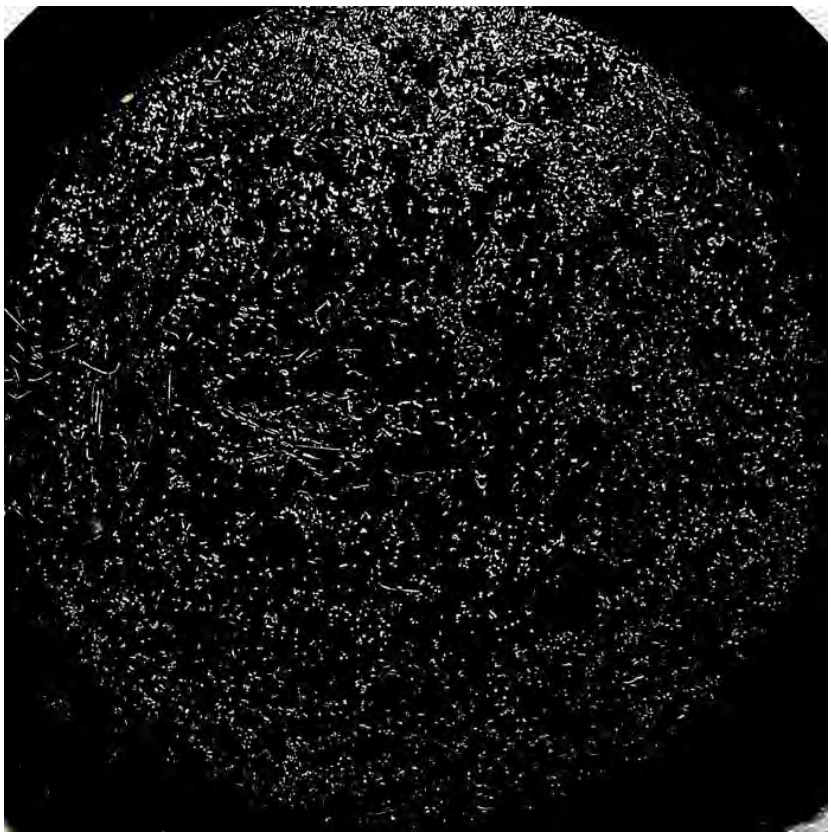

## *A5. SEM of the UHPC samples*

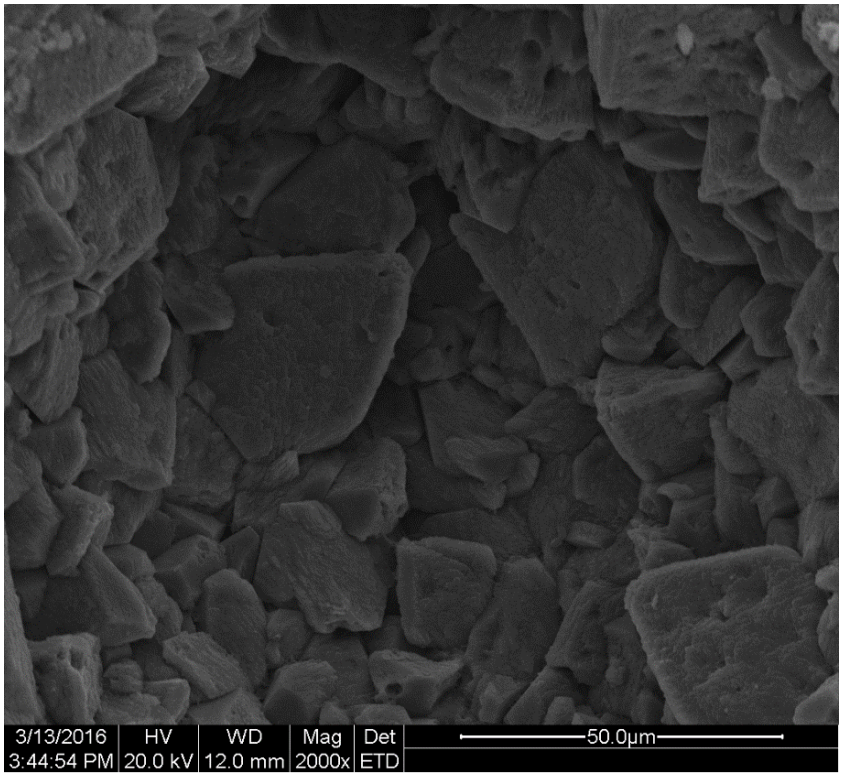


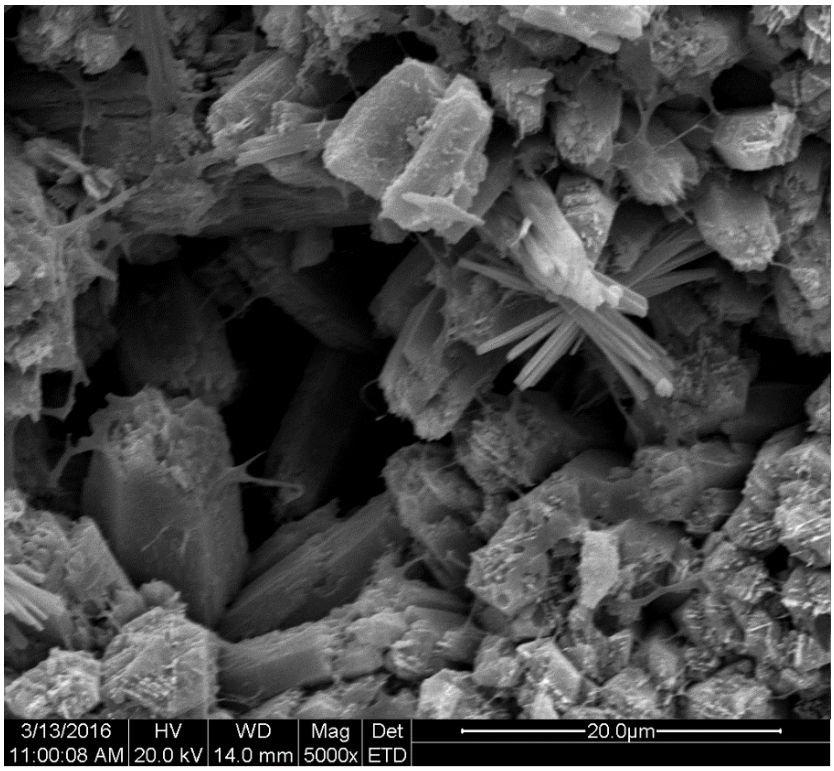

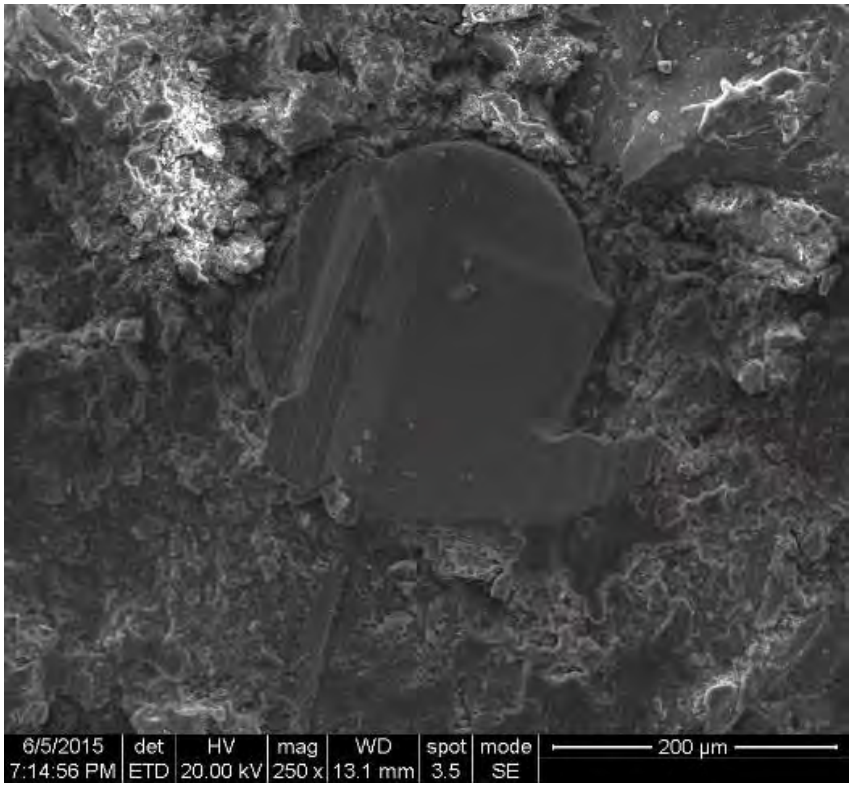
6/5/2015 | det | HV | mag | WD | spot | mode | 200 µm
7:14:56 PM | ETD | 20.00 kV | 250 x | 13.1 mm | 3.5 | SE

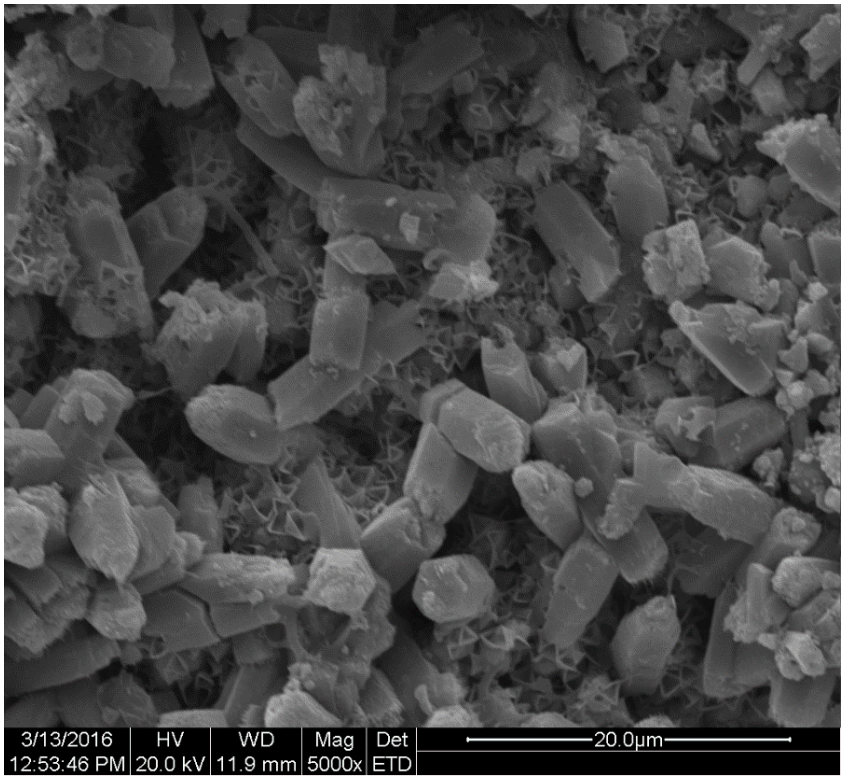
3/13/2016 | HV | WD | Mag | Det | 20.0µm
12:53:46 PM | 20.0 kV | 11.9 mm | 5000x | ETD